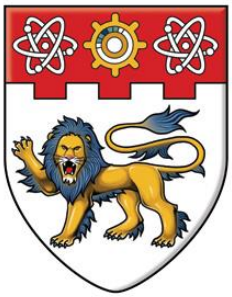

NANYANG TECHNOLOGICAL UNIVERSITY

THE STUDY OF HALOGEN BONDING INDUCED REACTION

HE WEI

SCHOOL OF PHYSICAL AND MATHEMATICAL SCIENCES

2016

The study of halogen bonding induced reaction

He Wei

School of Physical and Mathematical Sciences

A thesis submitted to the Nanyang Technological University
in partial fulfillment of the requirement for the degree of
Doctor of Philosophy

2016

ACKNOWLEDGMENTS

First of all, I would like to express my greatest respect and gratitude to my supervisor, Professor Tan Choon Hong, for the strong support he has given me during my Ph.D. study. His patience and insightful advice have been extremely valuable for me in both my research and future career.

I am also grateful to my friends in the TCH lab for their valuable suggestions and assistance, particularly Chin Kek Foo, Dr. Teng Bo, Wang Yang, Ge Yiceng, Yao Zhen, Jiang Huan, Ban Xu, Cui Xiyang, Zhang Xin, Ye Xinyi, Wang Tianxiang, Dr. Wong Hui Lin Valerie, Dr. Cao Weidi, Dong Shen, Song Zhijian, Dr. Yuan Mingjun and Dr. Wang Chao, Dr. Zong Lili, Dr. Han Manyi. My appreciation is also extended to friends who have helped me in both research and life: Dr. Rao Wei Dong, Tan Yu Jia, Zhang Yue Xia, Zhang Yuanyuan, Bai Linyi, Wu Bin and Dr. Lim Yee Hwee.

I would also like to thank the CBC technical support staff: Dr. Li Yongxin, Dr. Ganguly Rakesh and Ms. Goh Ee Ling for their assistance with common laboratory instruments.

The financial support provided by Nanyang Technological University in the form of a research scholarship is also gratefully acknowledged.

Most importantly, I would like to thank my family. To my beautiful wife, Li Xue, I am grateful for her continued love and support through the many ups and downs in my life and for affording me the most precious gift of all, our child Ziang. I am also thankful towards my parents for their support throughout my Ph.D. study.

ABSTRACT

As a classic non-covalent bond interaction, halogen bonding is well studied in material sciences and crystal engineering, and its application in catalysis has attracted research attention in these years. A brief introduction of the properties of halogen bonding is described in the first chapter of this thesis. Due to the high directionality and high energy characteristics, halogen bonding has been widely used in crystal engineering, material science and even in the biological system. Based on these unique properties, an introduction to the background of halogen bond and recent development in catalysis is presented, which forms the basis for our proposed research design.

We synthesized a series of novel halogen bond donors, and the structure and evidence of the presence of halogen bonding was proved by X-ray, ITC and NMR studies. The results of these halogen bond donors is presented in Chapter 2. In the next two chapters, these novel halogen bond donors were used as catalysts in the hydrogen transfer reduction of C=N bond compounds with Hantzsch ester and the [3+2] cycloaddition. In these two reactions, the C=N and the carbonyl compound were activated by halogen bond donor through halogen bonding, and product was obtained in good yield. The interaction between the substrate with halogen bond donor was confirmed by using NMR study and ITC.

Table of Contents

PUBLICATIONS

1. **He, W.**; Ge, Y. C.; Tan, C.-H.* Halogen Bonding Induced Hydrogen Transfer Reaction of C=N Bond with Hantzsch Ester.

   Org. Lett. **2014**, *16*, 3244 - 3247.

2. Wu, K. K.; **He, W.**; Sun, C. L.; Yu, Z. K. * Bimetallic Pt–Sn/γ-Al_2O_3 catalyzed b-alkylation of secondary alcohols with primary alcohols under solvent-free conditions

   Tetrahedron Lett. **2016**, *57*, 4017–4020 (co-first author)

3. Wu, K. K.†; **He, W.** †; Sun, C. L.; Yu, Z. K. * Scalable Synthesis of Secondary and Tertiary Amines by Heterogeneous Pt-Sn/γ-Al_2O_3 Catalyzed N-Alkylation of Amines with Alcohols

   Tetrahedron **2016**, *72*, 5816-5821. (co-first author)

4. **He, W.**; Wang, L. D.; Sun, C. L.; Wu, K. K.; He, S. B.; Chen, J. P.; W, P.; Yu, Z. K.* Pt-Sn/γ-Al_2O_3 Catalyzed Highly Efficient Direct Synthesis of Secondary and Tertiary Amines and Imines.

   Chem. Eur. J. **2011**, *17*, 13308-13317.

5. **He, W.**; He, S. B.; Sun, C. L.; Wu, K. K.; Wang, L. D.; Yu, Z. K.* Heterogeneous Bimetallic Pt-Sn/γ-Al_2O_3 Catalyzed N-Alkylation of Amines: Efficient Synthesis of Secondary and Tertiary Amines.

   Chin. J. Catal. **2012**, *33*, 717-722.

6. **He, W.**; Tan, C. -H.* Halogen Bonding Induced [3+2] Cyclo-Addition Reaction.

   Manuscript in preparation.

7. **He, W.**; Tan, C. -H.* Carbon dioxide Reduction with Thiol Catalyzed by Organo Base

   Manuscript in preparation.

ABBREVIATIONS

Ac	acetate
AIBN	2,2'-azo *bis*isobutyronitrile
Am	amyl (*n*-pentyl)
Boc	*Tert*-butyloxycarbonyl
BQ	benzoquinone
Bu	butyl
Bn	benzyl
Bz	benzoyl
Cbz	benzyloxycarbonyl
DABCO	1,4−diazabicyclo[2.2.2]octane
DBU	1,8−diazabicyclo[5.4.0]undec-7-ene
DCM	dichloromethane
DDQ	2,3−dichloro−5,6−dicyano−1,4−benzoquinone
DIBAL	diisobutylaluminum hydride
DMA	*N*, *N*−dimethylacetamide
DMAP	4−dimethylaminopyridine
DME	1,2−dimethoxyethane
DMF	dimethylformamide
DMSO	dimethylsulfoxide
Equiv.	equivalent
ESI	electrospray ionization
GC	gas chromatography
HRMS	high−resolution mass spectrometry

HPLC	high performance liquid chromatography
HWE	Horner−Wadsworth−Emmons
IBX	*o*−iodoxybenzoic acid
IPA	isopropyl alcohol
^{i}Pr	isopropyl
KHMDS	potassium bis(trimethylsilyl)amide
LAH	lithium aluminum hydride
LDA	lithium diisopropylamide
LiHMDS	Lithium hexamethyldisilazide
Mes	mesityl
MOM	methoxymethyl
Ms	mesyl (methanesulfonyl)
NBS	*N*−bromosuccinimide
NMO	*N*−methylmorpholine oxide
OAc	acetate
OTf	trifluoromethanesulfonate
PCC	pyridinium chlorochromate
PDC	pyridinium dichromate
Piv	pivaloyl
TBAI	Tetra-(*n*-butyl) ammonium iodide
TBAB	tetra-(*n*-butyl) ammonium bromide
TBS	*tert*-butyldimethylsilyl
TLC	thin layer chromatography
TMS	trimethylsilyl

α	alpha
β	beta
γ	gamma
μ	micro
π	pi
η	eta
ω	omega
σ	sigma

COMPOUND NUMBERING SCHEME

Compound	Structure	
C1	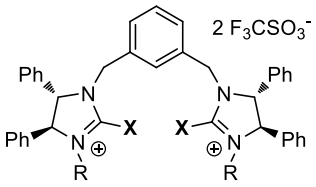	**C1**, X = I, R = CH_3
C2		**C2**, X = H, R = CH_3
C7		**C7**, X = I, R = *n*-Bu
C3	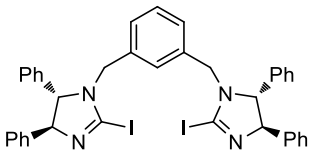	
C4	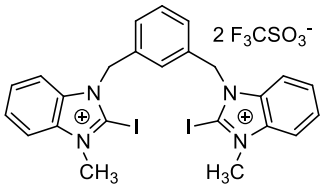	
C5	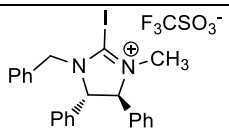	
C6	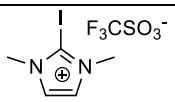	
C8	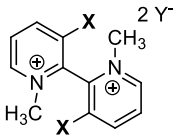	**C8**, X = I, Y^- = $F_3CSO_3^-$
C9		**C9**, X = I; Y^- = Cl^-
C10		**C10**, X = I; Y^- = BF_4^-
C13		**C13**, X = H; Y^- = $F_3CSO_3^-$
C11	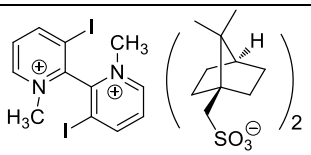	
C12	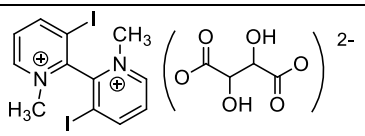	

C14

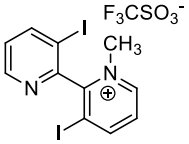

C15

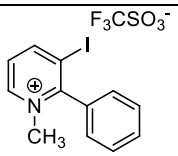

C16

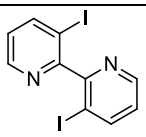

C17

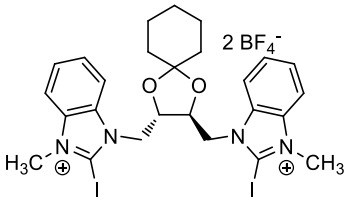

C18

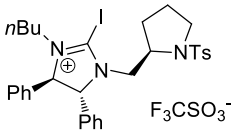

C19

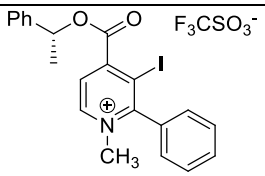

1a-i

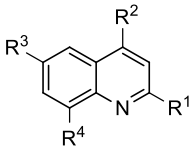

1a, R^1 = H, R^2 = H, R^3 = H, R^4 = H

1b, R^1 = CH_3, R^2 = H, R^3 = H, R^4 = H

1c, R^1 = H, R^2 = CH_3, R^3 = H, R^4 = H

1d, R^1 = Ph, R^2 = H, R^3 = H, R^4 = H

1e, R^1 = 4-MeO-C_6H_4, R^2 = H, R^3 = H, R^4 = H

1f, R^1 = Ph, R^2 = H, R^3 = Br, R^4 = H

1g, R^1 = Ph, R^2 = H, R^3 = NO_2, R^4 = H

1h, R^1 = Ph, R^2 = H, R^3 = CH_3, R^4 = H

1i, R^1 = CH_3, R^2 = H, R^3 = H, R^4 = OH

1j	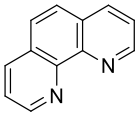	
2a-g	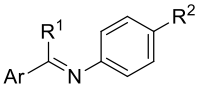	**2a**, R^1 = H, R^2 = H, Ar = Ph **2b**, R^1 = H, R^2 = H, Ar = 4-ClC_6H_4 **2c**, R^1 = H, R^2 = H, Ar = 4-MeC_6H_4 **2d**, R^1 = H, R^2 = H, Ar = NaphthylC_6H_4 **2e**, R^1 = H, R^2 = CH_3, Ar = 4-$NO_2C_6H_4$ **2f**, R^1 = H, R^2 = NO_2, Ar = 4-$NO_2C_6H_4$ **2g**, R^1 = CH_3, R^2 = H, Ar = Ph
3a, 3b	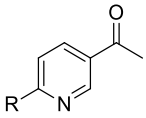	**3a**, R = H **3b**, R = CH_3
4a-i	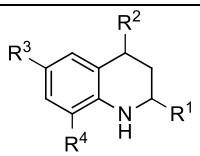	**4a**, R^1 = H, R^2 = H, R^3 = H, R^4 = H **4b**, R^1 = CH_3, R^2 = H, R^3 = H, R^4 = H **4c**, R^1 = H, R^2 = CH_3, R^3 = H, R^4 = H **4d**, R^1 = Ph, R^2 = H, R^3 = H, R^4 = H **4e**, R^1 = 4-MeO-C_6H_4, R^2 = H, R^3 = H, R^4 = H **4f**, R^1 = Ph, R^2 = H, R^3 = Br, R^4 = H **4g**, R^1 = Ph, R^2 = H, R^3 = NO_2, R^4 = H **4h**, R^1 = Ph, R^2 = H, R^3 = CH_3, R^4 = H **4i**, R^1 = CH_3, R^2 = H, R^3 = H, R^4 = OH
4j	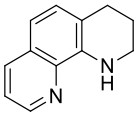	
4k, 4l	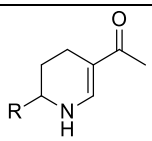	**4k**, R = H **4l**, R = CH_3

5a-g	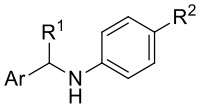	**5a**, R^1 = H, R^2 = H, Ar = Ph **5b**, R^1 = H, R^2 = H, Ar = 4-ClC_6H_4 **5c**, R^1 = H, R^2 = H, Ar = 4-MeC_6H_4 **5d**, R^1 = H, R^2 = H, Ar = NaphthylC_6H_4 **5e**, R^1 = H, R^2 = CH_3, Ar = 4-$NO_2C_6H_4$ **5f**, R^1 = H, R^2 = NO_2, Ar = 4-$NO_2C_6H_4$ **5g**, R^1 = CH_3, R^2 = H, Ar = Ph
6a-h	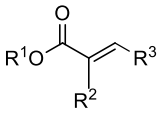	**6a**, R^1 = Et, R^2 = CH_3, R^3 = H **6b**, R^1 = CH_3, R^2 = H, R^3 = H **6c**, R^1 = Et, R^2 = H, R^3 = H **6d**, R^1 = *t*Bu, R^2 = H, R^3 = H **6e**, R^1 = Ph, R^2 = H, R^3 = H **6f**, R^1 = $CHCH_2$, R^2 = H, R^3 = H **6g**, R^1 = *t*Bu, R^2 = H, R^3 = CH_3 **6h**, R^1 = CH_3, R^2 = H, R^3 = Ph
7a, 7b	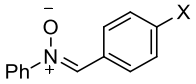	**7a**, X = H **7b**, X =F
8a-m	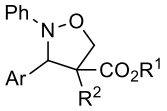	**8a**, R^1 = Et, R^2 = CH_3, Ar = Ph **8b**, R^1 = CH_3, R^2 = H, Ar = Ph **8c**, R^1 = Et, R^2 = H, Ar = Ph **8d**, R^1 = *t*Bu, R^2 = H, Ar = Ph **8e**, R^1 = Ph, R^2 = H, Ar = Ph **8f**, R^1 = $CHCH_2$, R^2 = H, Ar = Ph **8i**, R^1 = Et, R^2 = CH_3, Ar = 4-FC_6H_4 **8j**, R^1 = Me, R^2 = H, Ar = 4-FC_6H_4

8k, R^1 = Et, R^2 = H, Ar = 4-FC_6H_4

8l, R^1 = *t*Bu, R^2 = H, Ar = 4-FC_6H_4

8m, R^1 = $CHCH_2$, R^2 = H, Ar = 4-FC_6H_4

Chapter 1

Introduction

1.1 Introduction

Halogen bonding is the non-covalent interaction that occurs between a halogen atom (Lewis acid) and a Lewis base.[1] As shown in the Figure 1.1, halogen bonding contains two parts, where D refers to an electron-rich species, and is also termed a halogen bond acceptor. Halogen bond acceptors can be seen as Lewis bases, and they usually contain N, O or X atom, which can donate the lone pair to the donor.

Hydrogen bonding: D---H—A

Halogen bonding: D---X—A

Figure 1.1 Halogen and hydrogen bonding.

On the other hand, A refers to an electron-poor species that can act as a halogen bond donor in X-A. This non-covalent interaction was conclusively revealed by Hassel through X-ray crystallographic studies of dihalogen molecules with Lewis bases (Figure 1.2).[2]

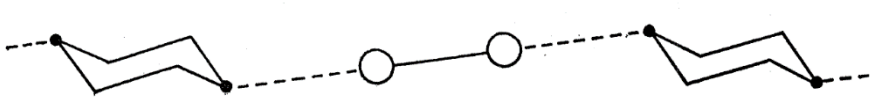

Figure 1.2 Linear chains in the 1:1 adduct of 1,4-dioxane and bromine.

Investigations of halogen adducts commenced in Oslo in the early 1950s, where chemists used X-ray crystallography to study the adduct formed between 1,4-dioxane and bromine. The most striking feature of the resulting crystal structure (Figure 1.2) is the alternating dioxane and bromine molecules in a linear -O-Br-Br-O- arrangement, which when combined together, formed an “endless” chain running in a specific direction. Surprisingly, the direction of this “endless” chain is approximately that of the “equatorial direction in cyclohexane”, and this highly directional property proved to be a unique nature of halogen bonding in future studies.[3] The distance between the oxygen and the bromine atom in the dioxane-bromine adduct is around 2.7 Å and this value is much larger than the sum of the covalent radii of the

oxygen and bromine atoms. However, this distance is shorter than the sum of the corresponding van der Waals radii 3.4 Å. Hence, this observation provides conclusive evidence to support the non-covalent nature of the halogen bonding interaction between these two atoms. For the formation of similar crystalline 1:1 adducts of dioxane and chlorine, or of dioxane and iodine, "polymerization" of simple complexes into "endless" chains, as observed in crystalline dioxane-bromine compound, was also observed.

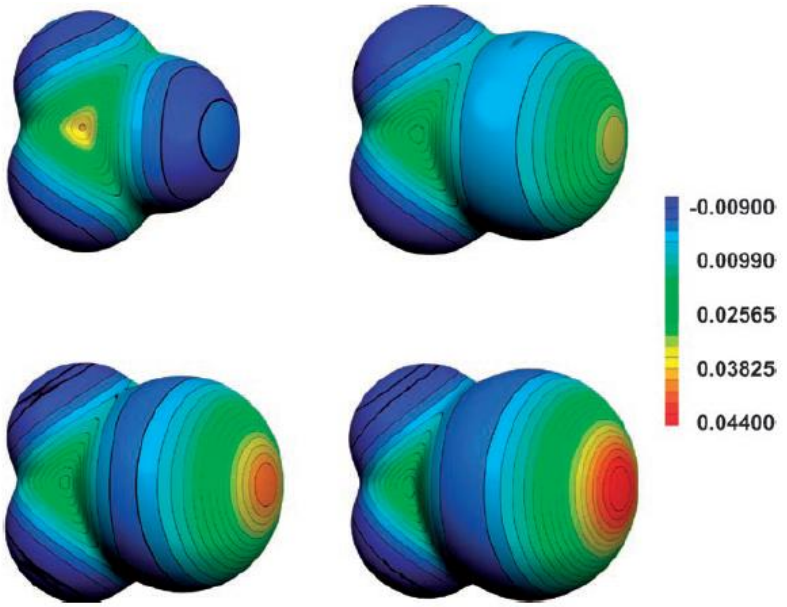

Figure 1.3 The molecular electrostatic potential (in Hartrees) at the isodensity surface with 0.001 electrons $Bohr^{-3}$: CF_4 (top left), CF_3Cl (top right), CF_3Br (bottom left), CF_3I (bottom right).

Through theoretical and experimental studies, it has been demonstrated that the electron density is anisotropically distributed around the halogen atoms in halides. In covalently bonded halogen atoms, a region of positive electrostatic potential is present, and the direction is along the covalent bond. This "σ hole" disposes the lone pair, which is closer towards the halogen atom, and accounts for the orientation of the halogen bonds (Figure 1.3).[4]

The bonding nature of halogen bond results in the D···X distances being shorter than the sum of the van der Waals radii of the corresponding atoms. Due to the electron donating effect from D (halogen bond acceptor) to the anti-bonding X-A orbital, the bond length of the

covalent X-A bond is lengthened during the formation of a halogen bond. At the same time, by increasing the electron-withdrawing effect of the neighboring groups in species A, the magnitude of the electropositive potential on the halogen increases accordingly. Therefore, the strength of the halogen bond can be fine-tuned by modifying the substituents on the carbon skeleton.

The strength of the interaction involved in halogen bond formation varies in intensity across a range of 10 to 200 kJ mol^{-1}, which is within the range of most of the non-covalent interactions, such as weak Cl···Cl interaction between chlorocarbons to the very strong $I^-\cdots I_2$ interaction in I_3^- species. In fact, the remarkable strength of some halogen bonds allows them to prevail over analogous hydrogen-bonding recognition processes.

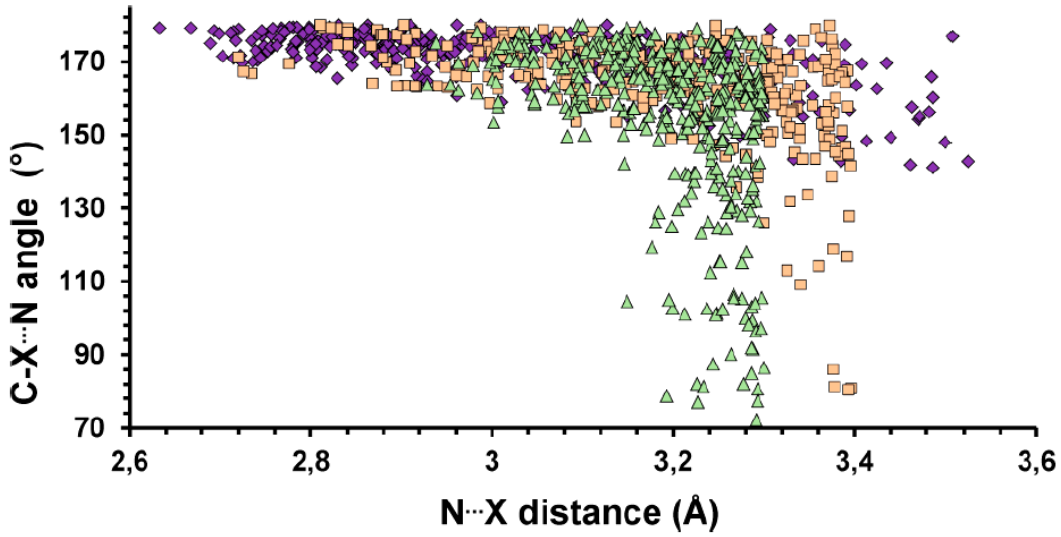

Figure 1.4 Scatterplot derived from a CSD search reporting the C– X···N angle (°) versus the X···N distance (Å) for crystal structures containing X···N contacts. Color code: blue rhombuses, I···N contacts; pink squares, Br···N contacts; green triangles, Cl···N contacts. Only error-free and nonpolymeric structures containing single-bonded I, Br, or Cl atoms and showing no disorder with R < 0.05 are considered.

As mentioned, halogen bonding is a highly directional interaction, and this phenomenon is more pronounced than that in hydrogen bonding. In addition, shorter interactions are generally more directional than longer ones.[3] The directionality of the halogen bond is due to the fact that during the formation of the halogen bond, the nucleophile enters the halogen atom

σ-hole, which is narrowly confined to the R−X covalent bond axis, and the R−X···Y angle between the covalent and noncovalent bonds around the halogen is approximately 180°.[5] Figure 1.4 shows the CSD (version 5.35) scatterplots of intermolecular C−X···N interaction versus X···N distance (X = I, Br, and Cl). It is evident that short and strong halogen bond are more directional than the long and weak ones, and by reducing the polarizability of the halogen bond donor, the linearity slightly decreases (mean values for the C−X···N angle are 171.4° for I, 164.1° for Br, and 154.6° for Cl). This trend is general and has also been observed when XB acceptor sites other than nitrogen is used. The direction of this non-covalent bond is along the C-X bond axis of the XB donor and the axis of the lone pair of electrons of the Lewis base in the XB acceptor. The angle between covalent and non-covalent bond around the corresponding halogen atom, such as X in D···X-A interaction, is almost 180°.

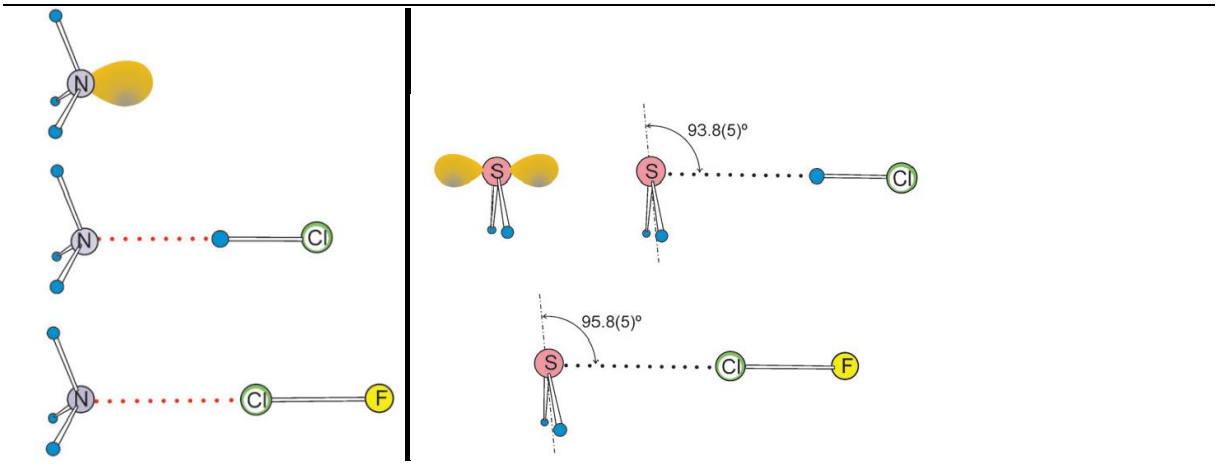

Figure 1.5 (Left) Experimentally determined geometries of the hydrogen bonded complex $H_3N\cdots HCl$ and its halogen-bonded analogue $H_3N\cdots ClF$ (both drawn to scale) with a non-bonding electron-pair (n-pair) model of NH_3. The n-pair electron distribution is drawn in the exaggerated style. (Right) The experimentally determined geometries of $H_2S\cdots HCl$ and $H_2S\cdots ClF$ drawn to scale. A n-pair model of H_2S is shown for comparison. (ref: H_2S with ClF bond angle_acie,1999,38,264)

As shown in the Figure 1.5, ammonia acts as a halogen bond acceptor, and a halogen bonding interaction is formed with ClF, which is a halogen bond donor. This halogen bond between the nitrogen atom with the chlorine atom is along the direction of the lone pair of nitrogen atom and chloride atom, which is similar to the hydrogen bond that can be formed between NH_3 and HCl. The angle of the halogen bond involving the Cl-F covalent bond is

around 180 °. In the case of H_2S and ClF, the direction of the halogen bond formed between the sulfur and chloride atoms is along the lone pair of both atoms, and the angle of the halogen bond with S-H bond is around 96°. Most importantly, the unique highly directional nature of the halogen bond highlights the potential of applying it in catalysis, which is similar to the case with hydrogen bonds.

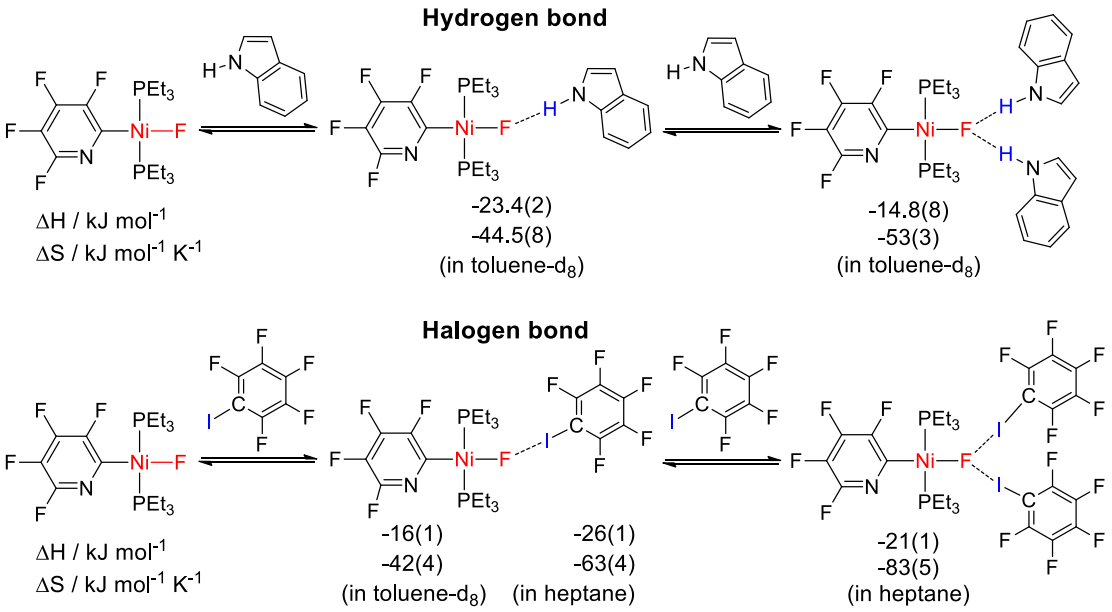

Figure 1.6 Comparison of enthalpies and entropies of formation of N--H/F--Ni hydrogen bonds and C--I/F--Ni halogen bonds as determined by NMR titration in solution.

The energy of the halogen bond interaction is usually stronger than the corresponding hydrogen bond. In 2008, Lee Brammer and co-workers reported the formation of a supramolecular structure involving metal and halogen bond interaction (Figure 1.6).[5f] These metal complexes contain a fluorine atom which is coordinated with the metal (Ni), which can be seen as an ideal hydrogen bond donor and halogen bond acceptor, respectively. When involved in interactions with the corresponding hydrogen bond acceptor or the halogen bond donor, the energy of these interactions can be measured. The authors compared the energy of halogen bond and the corresponding hydrogen bond, and found that the energy involved in the halogen bond is much higher than that in hydrogen bonding interaction. Therefore, the

higher energy of the halogen bond may confer distinct advantages over hydrogen bonding interactions, particularly in catalytic reactions that are traditionally challenging to carry out.

1.2 Halogen bond donors and acceptors

Halogen bond consists of two moieties, the halogen bond donor and acceptor, which act as a pair of Lewis acid and base. Most of the research concerning halogen bonding focuses primarily on the development of unique donors or acceptors,[5d] and investigates the interaction between them. The basic properties and findings based on previous studies[4] are herein summarized and presented. First, the comparison of the strength of halogen bond donor with similar moieties is important for the study of halogen bonding interaction. As shown in Figure 1.3, in this classic halogen bond donor model, the electrostatic potential remains negative around the fluorine atoms, whereas an area of positive charge emerges for chlorine, bromine, and iodine atoms. This area is surrounded by an electro-neutral ring and extends to a negatively charged belt. In general, the positive potential along the C-X bond direction increases in the order: C-F < C-Cl < C-Br < C-I, which corresponds with the polarizability of halogen atom. Hence, most of halogen bond donors contain iodine or bromine atom as the active site. On the other hand, the strength of the halogen bond increases as the electron-withdrawing nature of the atom, or moiety, bound to a given halogen increases. For a given halogen bond donor, the strength of the halogen bond decreases according to the hybridization order of the neighboring carbon: C(sp)-X > C(sp^2)-X > C(sp^3)-X, with halo-alkynes being particularly good halogen bond donors.[5]

Haloarenes are also good halogen bond donors and the theory holds true for haloheteroarenes, due to the electron-withdrawing effect of the heteroatom: the heteroarene is more electron-deficient than normal arenes. Additionally, the halogen atom becomes an even better donor.[6] The most successful example using this effect is the interesting molecular

conductors used to control the packing of bromo- and iodo-substituted tetrathiafulvalene derivatives.

For the halogen bond acceptor, typical organic compounds containing nitrogen atoms (such as amine and pyridine derivatives) form stronger halogen bonds than standard oxygen and sulfur compounds (such as ethers, alcohols, and thioethers) because of the more nucleophilic lone pair of electron in nitrogen.[7c,d] The relative effectiveness of the oxygen and sulfur atoms as halogen bond acceptor sites typically depends on the nature of the halogen bond donor. Although the pairings predicted by the HSAB theory are favored, a general order of XB acceptors or donors according to their strength cannot be made.

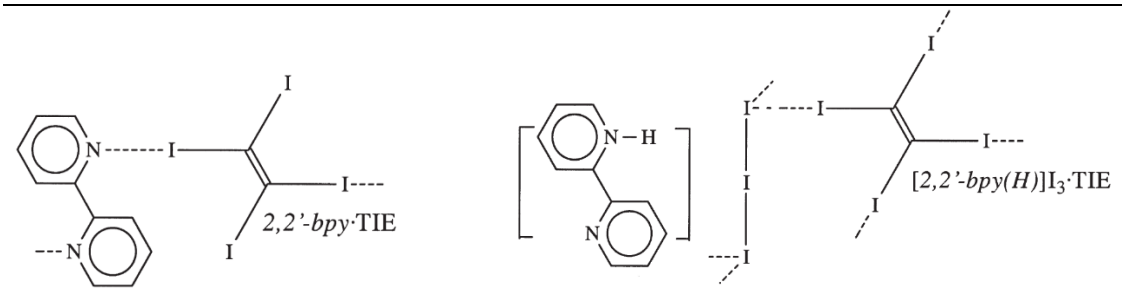

Figure 1.7 (Left) Halogen bonding between N atom of bispyridine with I atom; (Right) Halogen bond between I_3^- anion with I atom.

Anions are usually better halogen bond acceptors than neutral species,[8] which demonstrates the great potential of halogen bond in anion coordination chemistry. The more dissociated the anion pair, the stronger the bonding interaction formed between the halogen bond donor and the anion. Most of the known halogen bonded adducts are formed from halide anions, with iodide and fluoride anions being the most and the least frequently occurring halogen bond acceptors respectively. On the other hand, polyhalides, such as $[I_3]^-$, $[Br_3]^-$, $[ICl_2]^-$, $[CN]^-$ and $[SCN]^-$ can function as halogen bond acceptors.[9] For example, in Figure 1.7 (left), a classic halogen bond interaction is formed between tetraiodoethylene and bipyridine through the iodine and nitrogen atoms. A stronger halogen bond was however formed between I_3^- anion with tetraiodoethylene through interacting with the two iodine

atoms in presence of the mixture of I_3^- and bipyridine, in which interaction with the anionic I_3^- is preferred (Figure 1.7, right). The solvation energies of the starting anions and the adducts, as well as the strength of the resultant halogen bond greatly affect the association process, and the relative influence of the two parameters is different in solution and in the solid state. Based on an understanding of the properties of halogen bond donor and acceptor, combined with an in-depth study of catalysis, suitable donors and acceptors for catalytic reactions can be designed.

1.3 Halogen bonding application in crystal engineering

Non-covalent interactions, being selective, directional, and strongly attractive, can induce the self-assembly of predictable supra-molecular aggregates, hence can be applied in the crystal engineering.[10] For the most common example, the hydrogen bonding interaction is used to design the corresponding molecular as the building block of the crystal. Besides driving the self-assembly of aggregates joined by extensive networks of hydrogen bonds,[11] the hydrogen-bonded dimers can be used as sticky sites that compel molecules to associate together.

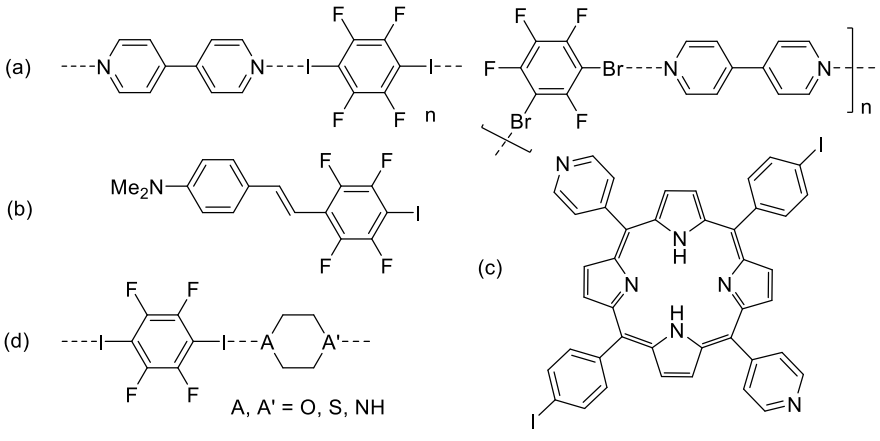

Figure 1.8 Application of halogen-bonding in crystal engineering.

In terms of energy and high directionality nature, halogen bonding is very similar to hydrogen bond, and has also been widely applied in crystal engineering and materials

chemistry. Halogen atoms, in which the σ hole is augmented by electron-withdrawing neighboring groups, act as halogen bond donors and can effectively function as the "sticky sites" that direct molecular association. This is the case for polyhalocarbons, which frequently behave as reliable tectons. Due to the directionality of halogen bonding, the design and construction of supra-molecular architecture can be realized.

In the 1990s, the impact of halogen bonding was gradually seen in research fields which required control of intermolecular recognition and self-assembly processes.[12] In particular, applications of halogen bonding were found in crystal engineering and supramolecular chemistry.[13] These processes are generally under thermodynamic control, which are reversible under experimental conditions, until the assembly with halogen bond is formed under the most thermodynamically favorable state. In 2008, a number of studies[13g,h] reported the supramolecular architectures formed by iodo- and bromo-perfluorocarbons with neutral or anionic electron donors, and can be used as versatile building block in crystal engineering (Figure 1.8).

As mentioned earlier, halogen bonds tend to be linear and are formed along the C-X bond axis of the halogen bond donor and axis of the lone pair of electrons of the heteroatom in the halogen bond acceptor. Guided by this property, the structure of the crystal can be designed and fine-tuned by changing the related donors and acceptors. Generally, different types of crystals with 1D, 2D and 3D architectures can be formed through a combination of multi-site donors and acceptors.

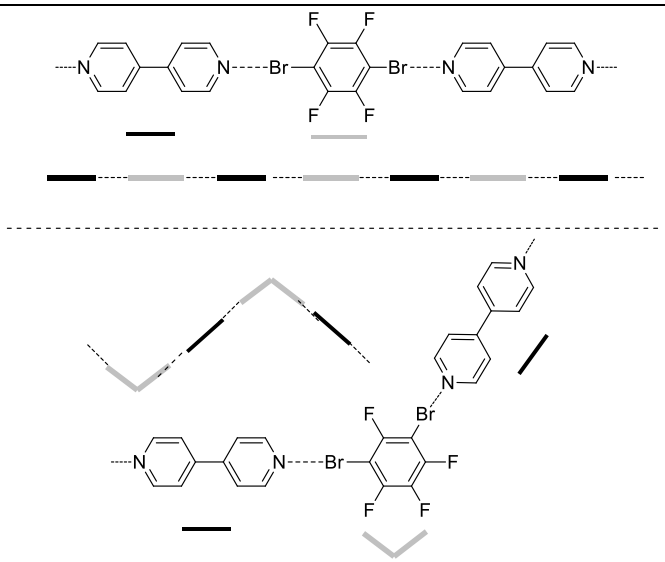

Figure 1.9 (Top) Linear and (Bottom) herringbone infinite chains formed by the self-assembly of bidentate XB donors and acceptors.

As shown in Figure 1.9, 1,4-dibromo-tetrafluoro benzene and 1,3-dibromo-tetrafluoro benzene can act as two-site halogen bond donors and interact with another two-site acceptor, such as 4,4'-bipyridine. When the axes of the donor and acceptor sites are parallel and coaxial, linear polymers are formed, which correspond to 1D structure.[14] Due to the different directionality of the related donor, the final structure of the polymer is different, which forms the basic strategy of modifying the properties of the polymer. Hence, when one or both of the interactive moieties are involved in three or more halogen bonds, two-dimensional (2D) architectures can be formed. A frequently occurring pattern is a network consisting of honeycomb structures, which is formed when halide anions self-assemble with dihalocarbons (Figure 1.10).

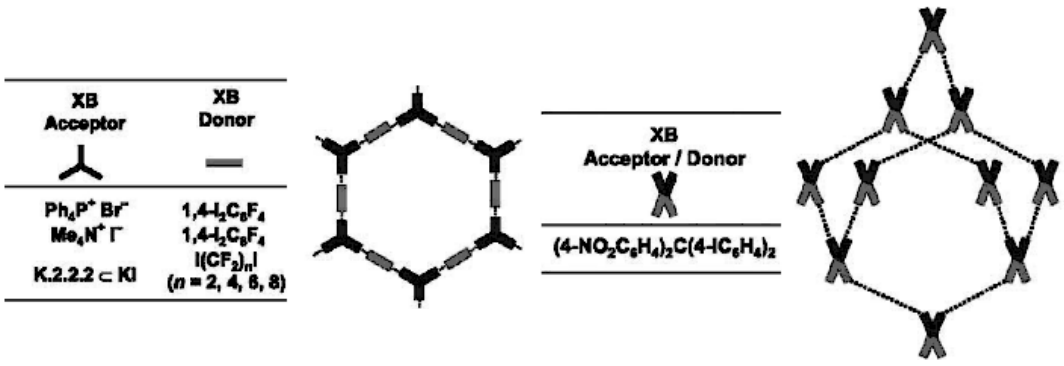

Figure 1.10 (Left) Honeycomb networks formed by the self-assembly of bidentate XB donors and tridentate acceptors; (Right) Self-assembly of three-dimensional networks by tridentate XB donors and tetradentate acceptors.

The halogen-bonded 2D and 3D networks described above frequently contain large cavities, as is the case for similarly sized networks assembled through hydrogen bonding or other interactions.[15] The empty space present in the overall crystal packing is filled by solvent molecules or through interpenetration.[16] Thus the formation of porous networks through halogen-bonding interactions is expected to become a field of great interest.

1.4 Halogen bonding application in material science

Halogen bonding interactions can also be applied in the design and development of new compounds and materials. The great potential of developing high-value functional materials based on the formation of halogen bond is well-established.[17] The halogen bonded supramolecular architectures have thus been applied in materials such as liquid crystals, organic semiconductors, and paramagnetic materials.

In material science, some non-covalent interactions, such as hydrogen bond and charge transfer interactions, were used in the development of new families of supramolecular mesogens by the process of self-assembly. At the same time, another efficient strategy to exert control over the supramolecular organization and improve the physical properties of liquid crystals is through the incorporation of fluorinated groups into mesogens.[18] In these non-covalent interactions, halogen bond interaction is particularly unique due to the presence of the related halogen atom. For example, haloperfluorocarbons are particularly effective tectons for self-assembly through the formation of halogen bonds, and more specifically, these self-assembly processes are driven by the formation of N···I interactions in all of the cases reported to date. Thermotropic liquid crystals with both low molar mass and high molar mass (polymeric) have been obtained, which form smectic A (SmA) and/or nematic phases.[19]

A related example of thermotropic liquid crystals obtained from a self-assembly driven by the formation of halogen bond in nonmesomorphic starting materials is shown in Figure 1.11.[19a] The adduct **1^{n}** was obtained from the evaporation of equimolar solutions of iodopentafluorobenzene and 4-alkoxystilbazoles ((*E*)-4-(4-alkoxystyryl) pyridines) and halogen-bonded dimers (n= 4 to 12, Figure 1.11, Top) were formed. In a similar manner, using a different linker in which the halogen bond donor has two active site at the *para* position, adducts **2$^{X\text{-}n}$** (X= I, n= 4 to 12) were the only adducts formed when 1,4-diiodotetrafluorobenzene and alkoxystilbazoles were mixed in 1:2 ratio or when other ratios were used.[19b]

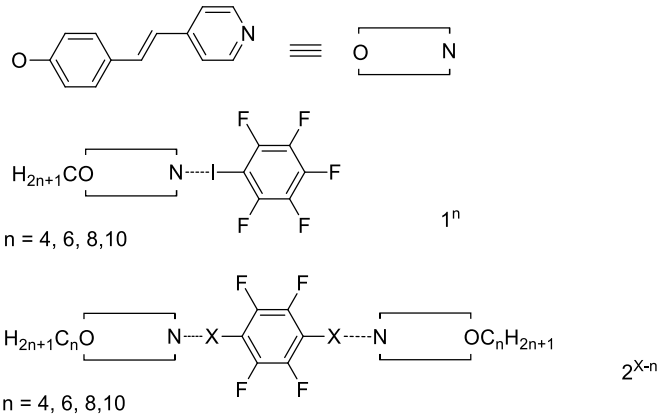

Figure 1.11 Supramolecular mesogens formed by self-assembly through halogen bond.

Generally, the magnetic and conductive properties of molecular materials can be improved through the modification of its structure by changing the formation of halogen bond. The partially filled conduction bands of molecular conductors typically depend on the 1D, 2D and 3D architectures resulting from the intermolecular interactions between the molecules. This is similar to electronic bands magnetic interactions, which are extremely sensitive to minute structural modifications. Nitroxide free radicals are usually known as halogen bond acceptors with oxygen atoms at the functional sites, and they have been used extensively as building blocks in molecular magnetic materials. Lucarini and co-workers studied the reaction of TEMPO (2,2,6,6-tetramethyl-1-piperidinyloxy) radicals in a

halocarbon solution by ESR spectroscopy. When the halogen bonded complex was formed, the amplification of the hyperfine splitting of the nitrogen atom on addition of halocarbons was detected.[20] During the formation of the halogen bond, the unpaired spin density was transferred from the nitroxide moiety to the iodine atom partially in a classic non-covalent bond formation, and at the same time the delocalization of electrons on the nitrogen atom was increased. The single-crystal 1:1 adduct formed between 4-amino-TEMPO and 1,4-diiodotetrafluorobenzene was isolated and analyzed by X-ray, providing important evidence for the formation of halogen bond, which involves the nitroxide radicals in the solid phase (Figure 1.12).[21] The crystal packing was characterized as an one-dimensional chain in which the two components are linked through N···I and O···I halogen bonds involving the amino nitrogen and nitroxyl oxygen atoms respectively. At the same time, the strong halogen acceptor characteristics of nitroxyl radicals was confirmed by the short O···I distance (2.827 Å) as 4-(4-Iodobenzylideneamino)-TEMPO crystallizes as two polymorphs, with one of them exhibiting O···I contacts. Interestingly, the halogen-bonded polymorph was antiferromagnetic, and the polymorph which does not contain halogen bonds shows a ferromagnetic transition.[22]

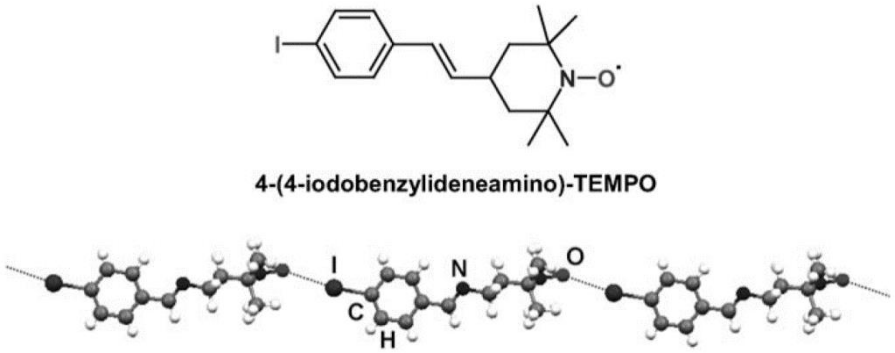

Figure 1.12 1D chain fragment of 4-(4-iodobenzylideneamino)-TEMPO.

1.5 Halogen bonding in biological systems

Due to the limitation of high-resolution X-ray in probing the interactions between complex biomolecular structures and halogenated molecules, the possible role of halogen

bonds in the binding of biological molecules has been generally neglected.[23a] Nevertheless, understanding how halogenated molecules bind to biological substrates can undoubtedly provide new and more effective approaches to drug development, as well as rationalize the adverse health effects of chemical exposure to substances such as polyhalogenated molecules. At the same time, halogenated proteins and nucleic acids are also associated with a number of diseases. The most notable example is the correlation of chlorotyrosines levels with chronic respiratory diseases in infants. Bromotyrosines have also been associated with allergen-induced asthma and these effects might be related to the formation of halogen bonding interactions.[23b] Similar to the simple halogen bond pair, most of halogen-bonded biomolecular complexes were constructed with involvement of donors and acceptors.[24] The halogen bond donor is represented by a small halogenated molecule, while the corresponding acceptor is one or more specific sites of a biomacromolecule (typically a protein). The distance between the donor and acceptor is typically shorter than the sum of their respective van der Waals radii, hence is a non-covalent bond interaction. In addition, the minimum angle of acceptor-to-donor approach of 120°, which is another unique property of halogen bond. Generally, the interaction between the small molecule (donor) and the biomacromolecule (acceptor) can be fine-tuned by modifying the structure of the related donor and acceptor, in which changing the halogen bond donor is easier than the acceptor, such as changing the active site to Cl, Br and I atoms.

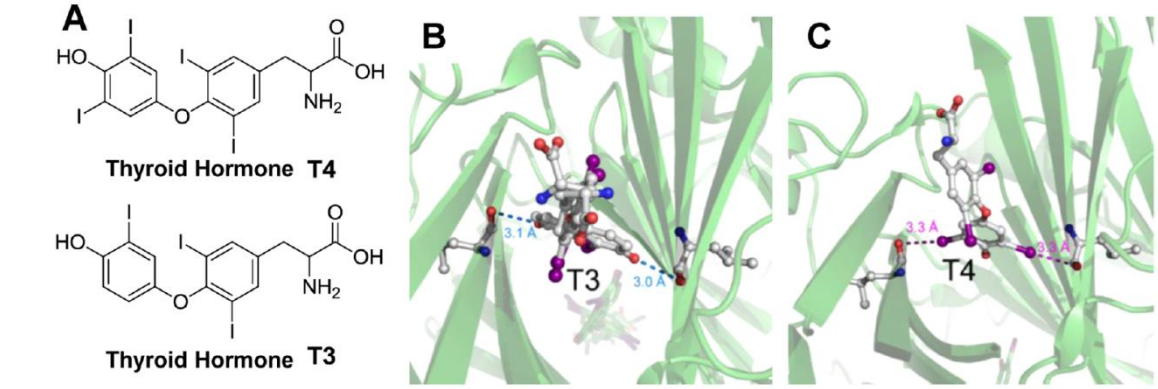

Figure 1.12 (A) Chemical formulae of the thyroid hormones **T4** and **T3**. (B) HBs formed by **T3** and (C) halogen bond formed by **T4** with TTR.

The iodinated thyroid hormones **T4** (thyroxine, 3,5,3′,5′-tetraiodothyronine) and **T3** (3,5,3′-triiodothyronine) are halogenated compounds which contain four and three iodine atoms respectively, and act as halogen bond donors in biomolecular systems (Figure 1.12).[25] In vertebrates, proper development of the brain, skeleton and organs is assisted by thyroid hormones through mediation by thyroid hormone receptors (THRs). The I···O interaction is important in the process of thyroid hormone recognition, and it was proposed that the higher T3 selectivity toward THRα in comparison to THRβ arises from the interaction involving iodine. [26] In the blood, only a very small fraction (0.03−0.3%) of thyroid hormones is present in the biologically active free form, with the rest bound to transporter proteins, such as transthyretin (TTR),[25] which has a higher selectivity for T4 than T3. It was shown that the iodine atoms in the phenolic ring of T4 engage in two XBs with the TTR backbone, while this is not the case for the single iodine present on the phenol ring of T3.

At the same time, halogen introduction is a traditional tool in drug optimization, for instance, in increasing the membrane permeability and half-life *in vivo*, hence the growing interest in halogenated drugs is quite fast in recent years.[27]

1.6 Halogen bonding in catalysis

Hydrogen bond donors, such as thiourea and guanidine derivatives, are widely used in catalytic processes, especially in organocatalysis and asymmetric synthesis. Yet, despite the large structural variety of the currently known non-covalent organocatalysts, virtually all are based on the same fundamental principles: positively polarized hydrogen and the high directionality of hydrogen bond.[28] Theoretically, XBs can be used in organocatalysis, such as hydrogen bonding, but its application in this area has been neglected. Due to the unique nature of halogen bonding, the catalytic system possesses peculiar advantages compared with the

analogous catalytic system based on hydrogen bonding. Such advantages include: 1) halogen bonding can be used in the design of multi-dentate catalyst (usually as a halogen bond donor) because of its higher directionality, and the catalyst potentially has higher selectivity toward different substrates.[29] 2) As halogen atoms are involved, especially for the strong halogen bond donors which are based on the fluorinated backbones, halogen bonding can be considered as a hydrophobic alternative to hydrogen bonding. Accordingly, halogen bond donors are more soluble in non-polar solvents than the associated hydrogen bond donor, which on the other hand, often suffers from the competition involving more polar hydrogen bond donor/ acceptor in solvents.[30] 3) Since I, Br, Cl, and in some cases F atoms, can all be involved in halogen bond, the strength of the halogen bond interaction can be easily tuned by changing the halogen atom.[31] 4) Halogens are more polarizable and bigger in size than hydrogen, and halogen bond donors can be classified as "softer" Lewis acids than those based on hydrogen bonding, with important consequences for substrate preference of the final halogen bond-based organocatalysts.

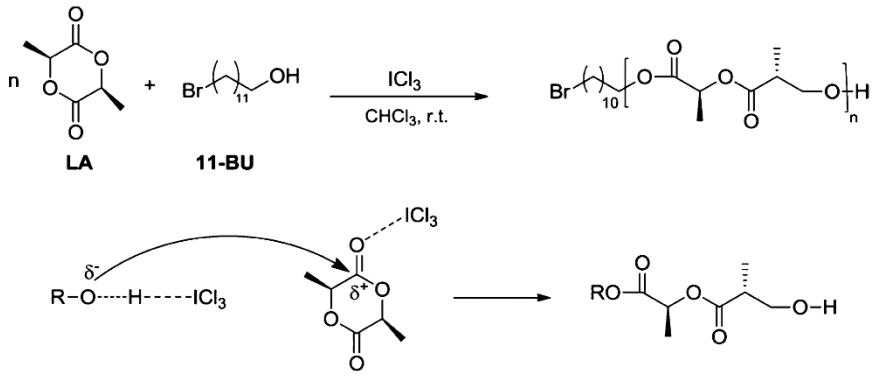

Figure 1.13 (Top) Polymerization of L-lactide to poly(L-lactide) with ICl_3. (Bottom) Proposed mechanism for the 2-fold activation.

With the increasing number of studies on halogen bond interaction in solution-phase,[32] fundamental studies[33] and reports on anion receptors,[34] the applications of halogen bond in organocatalysis has generated significant research interest.

Elemental iodine was known to accelerate some organic reactions, and its use in organic synthesis is well known.[35] In several cases, it was hypothesized that the catalytic activity of I_2 is related to its Lewis acidity, similar to reactions with carbonyl groups such as Strecker-type reactions,[36] acetal formation and cleavage,[37] imine formation and Michael additions.[35a, c] However, no detailed mechanistic studies have been reported in this respect, and modes of action of I_2 as a Lewis acid are not completely understood. Similarly in 2010, iodine trichloride (ICl_3) was reported as the catalyst in the ring-opening reaction of L-lactide in the presence of 11-bromo-1-undecanol (11-BU) as an initiator (Figure 1.13, top).[38] Through precise FTIR and NMR studies, the authors proposed a plausible mechanism of the polymerization, which occurs through multiple activation of both the monomer L-lactide and 11-BU by the XB donor ICl_3. The electrophilic activation of the carbonyl group of L-lactide by ICl_3 was demonstrated by a blue shift of the C=O vibrational band in FTIR and the downfield shift split of the ^{13}C NMR signals of L-lactide, which implies that the electron density was transferred from the oxygen to the iodine atom. On the other hand, a large downfield shift of the OH resonance of 11-BU suggested the formation of OH···Cl hydrogen bond. In the suggested polymerization pathway, halogen bonding and hydrogen bonding act in a concerted manner to accelerate the reaction (Figure 1.13, bottom). However, trace amounts of HCl and HIO_3 generated from the ICl_3 hydrolysis could be present in the reaction mixture, and it is a challenge to ascertain if they have important effect in the activation mechanism.

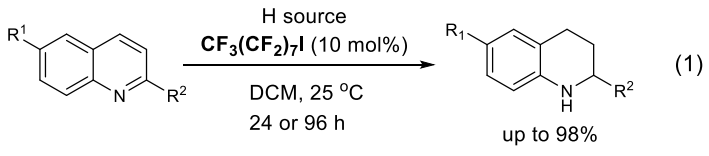

Figure 1.14 Hydrogenation of quinolone with Hantzsch ester in the presence of iodoperfluorooctane.

Bolm[32a] and Huber[32b-g] are the first to recognize that halogen bonding can be exploited for organocatalysis. *N*-heterocycles are well-known as efficient halogen bond acceptors in the

study of halogen bonding.[33] In 2008, Bolm and co-workers reported that haloperfluoroalkanes, which are classical XB donors, can be used as catalysts for the reduction of 2-phenylquinoline using Hantzsch ester (Figure 1.14).[32a] This transfer hydrogenation required a long duration (generally from 24 to 96 hours) in the presence of 10 mol% catalyst for a high conversion. In addition, ^{13}C and ^{19}F NMR studies conducted with the 1:1 mixture of 1-iodoperfluorooctane and quinolone in the CD_2Cl_2 resulted in the chemical-shift variation (1.1 ppm for CF_2I and 0.15-0.44 ppm for CF_3 and CF_2) to be observed. However, due to limitations of the analysis method, the NMR evidence provided was insufficient to prove that it is a real halogen bond donor induced reaction.

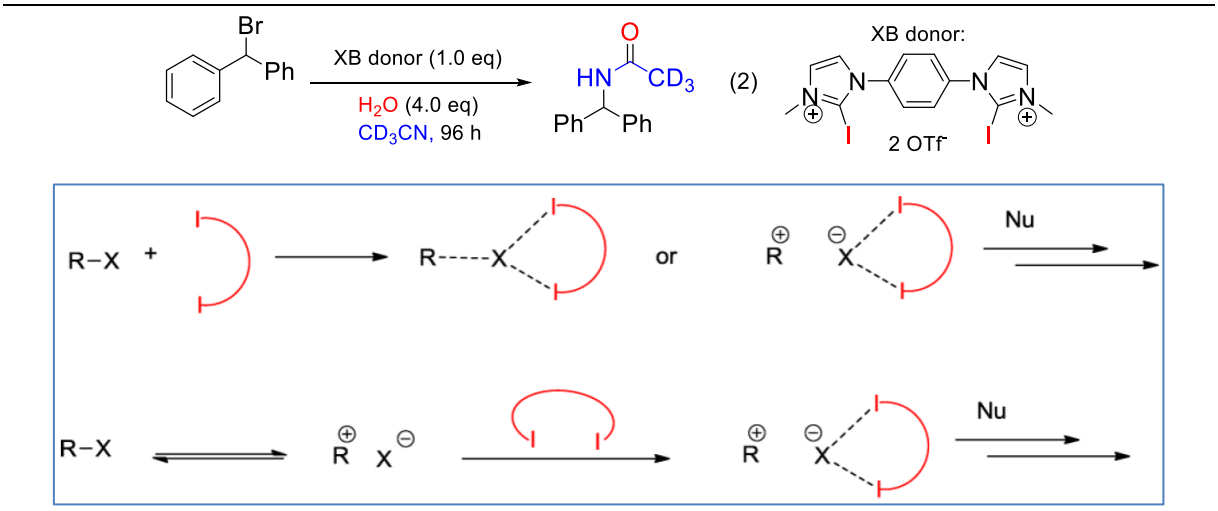

Figure 1.15 (Top) Bisimidazolium-based halogen bond donor as activator in the Ritter-type reaction; (Bottom) Possible modes of activation of a halogenated substrate by the bidentate halogen bond donor catalyst (shown in red).

In 2011, evidence for a halogen bonding induced reaction was reported by Huber, who developed charge-assisted imidazolium halogen bond donors as activators of benzhydryl bromide for Ritter-type reaction with acetonitrile (Figure 1.15).[32b] A series of charge assistant bidentate halogen bond donors were synthesized and these halogen bond donors have strong interactions with halide anions, which act as halogen bond acceptors (for instance Br^-, with binding constant in the order of 10^6). The reaction which uses the corresponding non-halogenated imidazolium as activator was investigated, and the yield of product was

discovered to be lower than that of the halogen bonding donor. At the same time, X-ray and NMR studies prove that halogen bonding plays an important role in the activation of substrate. However, since the reaction was not catalytic in nature, stoichiometric amount of halogen bond donors is required to promote the reaction. This limitation derives mainly from the strong interactions between halogen bond donors with halide anions, which will form a stable complex and deactivate the corresponding halogen bond donor. The solubility of the charge assistant imidazole derivative is not high and only dissolves in acetonitrile. This is a limit for its application in organocatalysis.

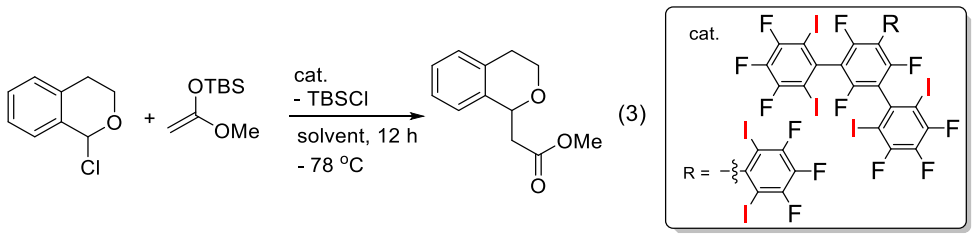

Figure 1.16 Reaction using neutral poly-fluorinated arenes as activator.

In 2013, Huber further developed another kind of halogen bond donor, neutral poly-fluorinated arenes, as catalysts for the addition of ketene silyl acetal to 1-chloroisochroman.[32g] This is unlike the previous example, in which the leaving halide binds to the halogen bond donor strongly and deactivates the catalyst; in this reaction, the leaving group Cl^- can be trapped by the silyl group after the C-Cl bond breaks, hence the halogen bond donors can be regenerated in the reaction (Figure 1.16).

More recently, Huber *et al.* demonstrated that dicationic halogen bond donors with noncoordinating counteranions can also activate neutral carbonyl substrates toward Diels−Alder reactions (Figure 1.17). [32e] The substrate α,β-unsaturated ketone can be activated by the catalyst through halogen bonding interaction, and then react with 1,3-cyclopentadiene. Although the Diels-Alder reaction is a well-known reaction catalyzed by Lewis acids, and halogen bonding can be seen as a unique type of interaction between a Lewis acid and Lewis

base, the precise difference of halogen bonding from a classical Lewis acid was in doubt. Hence, the authors conducted control experiments and mechanistic studies on this reaction.

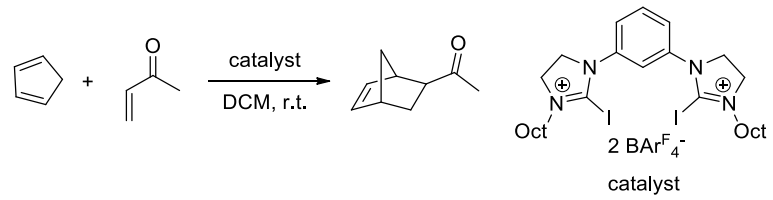

Figure 1.17 (Left) Diels−Alder benchmark reaction. (Right) Dicationic halogen bond donor activating agent $BAr^F = B[3,5\text{-}(CF_3)_2C_6H_3]_4^-$.

Through DFT calculations, the pivotal role of halogen bonding in the activation of the carbonyl group toward the Diels−Alder reaction was demonstrated. Through a series of experiments the involvement of traces of acid was ruled out and the role of the different structural features of the halogen bond donor was further confirmed. In a closely related work, Takeda *et al.* reported that 2-haloimidazolium salts could efficiently catalyze the aza-Diels-Alder reaction of aldimines with the Danishefsky diene (Figure 1.18).[39] In contrast to the classical Diels−Alder reaction reported by Huber, the halogen bonding interaction occurs between the substrate imine and the halide atom of the donor was confirmed. Further control experiments demonstrated that no reaction occurs in the absence of catalysts, and that the classical halogen bond donors, such as perfluoroalkyl iodides and iodoperfluorobenzenes, were inactive. On the other hand, a 57% conversion was obtained in the presence of catalyst A, and the yield was increased to 80% by the introduction of CF_3 substituents on the molecular scaffold (catalyst C). No reaction occurred in the absence of iodine (catalyst D) or with the neutral halogen bond donor E. All these experiments clearly demonstrated that the stronger the halogen bond donor, the higher the yield and once again suggested the important role of halogen bond in the activation mechanism.

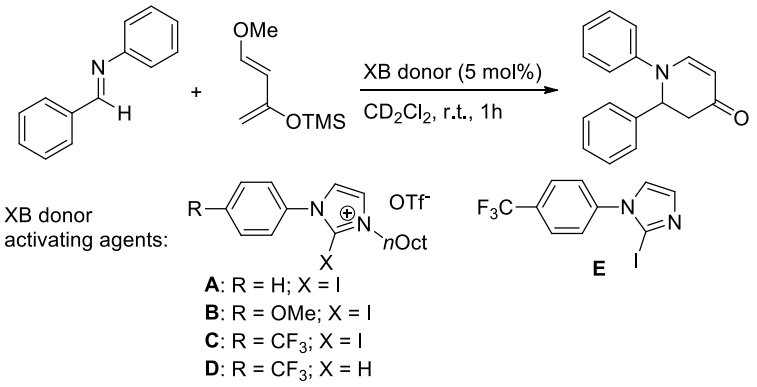

Figure 1.18 (Top) Aza-Diels−Alder reaction of an aldimine with the Danishefsky diene; (Bottom) structure of the used XB donor activating agents.

Based on these studies and the preceding work of our group on organocatalysis, [40] we envision that halogen-based organocatalysts and hydrogen-bond donors would be able to complement each other.

At present, our studies have primarily focused on the proof-of-principle character to demonstrate the feasibility of halogen-bond based organocatalysis. In the long term, halogen-bond donors might be especially suitable for Lewis basic substrates featuring heavier elements (such as sulfur, phosphorous, or the halogens) or for certain reaction conditions. Finally, the high directionality of halogen bonds might prove advantageous in future halogen-bond-catalyzed enantioselective transformations.

1.7 Summary

As a non-covalent bond interaction, halogen bonding has several unique properties. Due to the high directionality and strong interaction, halogen bonding has been widely used in crystal engineering, material science and even in the biological system. In the previous study of halogen bond application in these area, the focus was on the halogen bond donors and acceptors, and on how to control and construct the structure of the supra-molecular structures through the association of different donors and acceptors. However, the application of halogen bond in catalysis is rare, despite its properties being very similar with hydrogen bond,

which has been widely used in catalysis. Therefore, a systemic study of halogen bond in catalysis is needed for the development of halogen bond-based applications.

The aim for this project is the study of the nature of halogen bonding and the halogen bonding induced reaction. Specifically, my research includes the following points: 1) in-depth study of the nature of halogen bonding, where the key point is how to control this interaction; 2) devise a useful strategy for the design of unique halogen bond donors and synthesis of the donor guide by this strategy; 3) explore new reactions which can be induced or promoted by halogen bonding. This work is an important contribution to this field.

References

[1] *Halogen Bonding: Fundamental and Application;* Metrangolo, P., Resnati, G., Eds.; Springer: Berlin, 2008.

[2] Hassel, O. *Science* **1970**, *170*, 497.

[3] (a) Saccone, M.; Cavallo, G.; Metrangolo, P.; Pace, A.; Pibiri, I.; Pilati, T.; Resnati, G.; Terraneo, G. *CrystEngComm* **2013**, *15*, 3102; (b) Bianchi, R.; Forni, A.; Pilati, T. *Acta Crystallogr., Sect. B: Struct. Sci.* **2004**, *60*, 559; (c) Lommerse, J. P. M.; Stone, A. J.; Taylor, R.; Allen, F. H. *J. Am. Chem. Soc.* **1996**, *118*, 3108; (d) Forni, A.; Metrangolo, P.; Pilati, T.; Resnati, G. *Cryst. Growth Des.* **2004**, *4*, 291; (e) Padgett, C. W.; Walsh, R. D.; Drake, G. W.; Hanks, T. W.; Pennington, W. T. *Cryst. Growth Des.* **2005**, *5*, 745.

[4] (a) Weiss, R.; Schwab, O.; Hampel, F. *Chem. Eur. J.* **1999**, *5*, 968; (b) Valerio, G.; Raos, G.; Meile, S. V.; Metrangolo, P.; Resnati, G.; *J. Phys. Chem. A* **2000**, *104*, 1617; (c) Clark, T.; Hennemann, M.; Murray, J.S.; Politzer, P. *J. Mol. Model.* **2007**, *13*, 291.

[5] (a). Zou, J-W.; Jiang, Y-J.; Guo, M.; Hu, G.-X.; Zhang, B.; Liu, H.-C.; Yu, Q.-S. *Chem. Eur. J.* **2005**, *11*, 740; (b) Gao, K.; Goroff, N. S.; *J. Am. Chem. Soc.* **2000**, *122*, 9320; (c) Borgen, B.; Hassel, O.; Romming, C. *Acta Chem. Scand.* **1962**, *16*, 2469; (d) Sun, A.; Lauher, J. W.; Goroff, N. S. *Science* **2006**, *312*,1030; (e) Cavallo, G.; Metrangolo, P.; Milani, R.; Pilati, T.; Priimagi, A.; Resnati, G.; Terraneo, G. *Chem. Rev.* **2016**, *116*, 2478; (f) Libri, S.; Jasim, N. A.; Perutz, R. N.; Brammer, L. *J. Am. Chem. Chem.* **2008**, *130*, 7842.

[6] (a) Kuhn, N.; Abu-Rayyan, A.; Eichele, K.; Schwarz, S.; Steimann, M.; *Inorg. Chim. Acta* **2004**, *357*, 1799; (b) Logothetis, T. A.; Meyer, F.; Metrangolo, P.; Pilati, T.; Resnati, G. *New J. Chem.* **2004**, *28*, 760; (c) Freytag, M.; Jones, P. G.; Ahrens, B.; Fischer, A. K. *New J. Chem.* **1999**, *23*, 1137.

[7] (a) Santis, A. De; Forni, A.; Liantonio, R.; Metrangolo, P.; Pilati, T.; Resnati, G.; *Chem. Eur. J.* **2003**, *9*, 3974; (b) Walsh, P. L.; Ma, S.; Obst, U.; Rebek, J.; Jr. *J. Am. Chem. Soc.* **1999**, *121*, 7973; (c) Messina, T.; Metrangolo, P.; Panzeri, W.; Ragg, E.; Resnati, G. *Tetrahedron Lett.* **1998**, *39*, 9069; (d) Metrangolo, P.; Panzeri, W.; Recupero, F.; Resnati, G. *J. Fluorine Chem.* **2002**, *114*, 27.

[8] Liantonio, R.; Metrangolo, P.; Pilati, T.; Resnati, G. *Cryst. Growth Des.* **2003**, *3*, 355.

[9] (a) Tebbe, K. F.; Grafe-Kavoosian, A.; *Z. Naturforsch. B* **1996**, *51*, 1007; (b) Bock, H.; Holl, S.; *Z. Naturforsch. B* **2002**, *57*, 843; (c) Rosokha, S. V.; Neretin, I. S.; Rosokha, T. Y.; Hecht, J.; Kochi, J. K. *Heteroat. Chem.* **2006**, *17*, 449; (d) Bailey, R. D.; Hook, L. L.; Watson, R.P.; Hanks, T.W.; Pennington, W. T. *Cry. Eng.***2000**,*3*,155.

[10] Simard, M.; Su, D.; Wuest, J. D. *J. Am. Chem. Soc*.**1991**, *113*, 4696

[11] (a) Gallant, M.; Wuest, J. D. *J. Org. Chem.* **1991**,*56*,2284; (b) Ducharme, Y.; Wuest, J. D. *J. Org. Chem.* **1988**, *53*, 5787.

[12] Selected reviews: (a) Metrangolo, P.; Neukich, H.; Pilati, T.; Resnati, G. *Acc. Chem. Res.* **2005**, *38*, 386. (b) Legon, A. C. *Phys. Chem. Chem. Phys*. **2010**, *12*, 7736. (c) Cavallo, G.;

Metrangolo, P.; Pilati, T.; Resnati, G.; Sansotera, M.; Terraneo, G. *Chem. Soc. Rev.* **2010**, *39*, 3772. (d) Metrangolo, P.; Meyer, F.; Pilati, T.; Resnati, G.; Terraneo, G. *Angew. Chem. Int. Ed.* **2008**, *47*, 6114. (e) Metrangolo, P.; Resnati, G. *Chem. Eur. J.* **2001**, *7*, 2511. (f) Metrangolo P.; Resnati, G. *Cryst. Growth Des*. **2012**, *12*, 5835.

[13] Recent publications: (a) Kilah, N. L.; Wise, M. D.; Serpell, C. J.; Thompson, A. L.; White, N. G.; Christensen, K. E.; Beer, P. D. *J. Am. Chem. Soc.* **2010**, *132*, 11893. (b) Hardegger, L. A.; Kuhn, B.; Spinnler, B.; Anselm, L.; Ecabert, R.; Stihle, M.; Gsell, B.; Thoma, R.; Diez, J.; Benz, J.; Plancher, J.-M.; Hartmann, G.; Banner, D.W.; Haap, W.; Diederich, F. *Angew. Chem. Int. Ed.* **2011**, *50*, 314. (c) Jentzsch, A. V.; Emery, D.; Mareda, J.; Metrangolo, P.; Resnati, G.; Matile, S. *Angew. Chem. Int. Ed.* **2011**, *50*, 11675. (d) Carlsson, A.-C. C.; Gräfenstein, J.; Budnjo, A.; Laurila, J. L.; Bergquist, J.; Karim, A.; Kleinmaier, R.; Brath, U.; Erdélyi, M. *J. Am. Chem. Soc.* **2012**, *134*, 5706. (e) Raatikainen, K.; Rissanen, K. *Chem. Sci*. **2012**, *3*, 1235. (f) Meazza, L.; Foster, J. A.; Fucke, K.; Metrangolo, P.; Resnati, G.; Steed, J.W. *Nat. Chem.* **2013**, *5*, 42. (g) Rissanen, K. *CrystEngComm* **2008**, *10*, 1107. (h) Brammer, L.; Espallargas, G. M.; Libri, S. *CrystEngComm* **2008**, *10*, 1712. (i) Fourmigué, M. *Curr. Opin. Solid State Mater. Sci.* **2009**, *13*, 36. (i) Bertani, R.; Sgarbossa, P.; Venzo, A.; Lelj, F.; Amati, M.; Resnati, G.; Pilati, T.; Metrangolo, P.; Terraneo, G. *Coord. Chem. Rev*. **2010**, *254*, 677.

[14] Santis, A. De; Forni, A.; Liantonio; R.; Metrangolo, P.; Pilati, T.; Resnati, G. *Chem. Eur. J.* **2003**, *9*, 3974.

[15] Batten, S. R.; Robson, R. *Angew. Chem. Int. Ed.* **1998**, *37*, 1460.

[16] (a) Grebe, J.; Geiseler, G.; Harms, K.; Dehnicke, K.; *Z. Naturforsch. B* **1999**, *54*, 77; (b) Liantonio, R.; Metrangolo, P.; Meyer, F.; Pilati, T.; Navarrini, W.; Resnati, G. *Chem. Commun.* **2006**, 1819; (c) Ghassemzadeh, M.; Harms, K.; Dehnicke, K. *Chem. Ber.* **1996**, *129*, 259; (d) Metrangolo, P.; Meyer, F.; Pilati, T.; Proserpio, D. M.; Resnati, G. *Chem. Eur. J.* **2007**, *13*, 5765.

[17] (a) Pollino, J. M.; Weck, M. *Chem. Soc. Rev.* **2005**, *34*, 193; (b) Kato, T.; Mizoshita, N.; Kishimoto, K. *Angew. Chem., Int. Ed.* **2005**, *45*, 38; (c) Hammond, M. R.; Mezzenga, R. *Soft Matter* **2008**, *4*, 952; (d) Ahn, S.; Kasi, R. M.; Kim, S.-C.; Sharma, N.; Zhou, Y. *Soft Matter* **2008**, *4*, 1151; (e) Noro, A.; Hayashi, M.; Matsushita, Y. *Soft Matter* **2012**, *8*, 6416; (f) Kato, T.; Hirai, Y.; Nakaso, S.; Moriyama, M. *Chem. Soc. Rev*. **2007**, *36*, 1857; (g) Castles, F.; Morris, S. M.; Hung, J. M. C.; Qasim, M. M.; Wright, A. D.; Nosheen, S.; Choi, S. S.; Outram, B. I.; Elston, S. J.; Burgess, C. *Nat. Mater.* **2014**, *13*, 817.

[18] Bruce, D. W. Halogen Bonding Fundamentals and Applications (Eds.: Metrangolo, P.; Resnati, G.), Springer, Berlin, 2008, pp. 161 – 180.

[19] (a) Nguyen, H. L.; Horton, P. N.; Hursthouse, M. B.; Legon, A. C.; Bruce, D.W. *J. Am. Chem. Soc.* **2004**, *126*, 16; (b) Bruce, W. D.; Metrangolo, P.; Meyer, F.; PrPsang, C.; Resnati, G.; Terraneo, G.; Whitwood, A. C. *New J. Chem*. **2008**, *32*, 477; (c) Metrangolo, P.; PrPsang, C.; Resnati, G.; Liantonio, R.; Whitwood, A. C.; Bruce, D. W. *Chem. Commun.* **2006**, 3290; (d) Xu, J.; Liu, X.; Lin, T.; Huang, J.; He, C. *Macromolecules* **2005**, *38*, 3554; (e) Xu, J.; Liu, X.; Ng, J. K.-P.; Lin, T.; He, C. *J. Mater. Chem.* **2006**, *16*, 3540.

[20] Mugnaini, V.; Punta, C.; Liantonio, R.; Metrangolo, P.; Recupero, F.; Resnati, G.; Pedulli, G. F.; Lucarini, M. *Tetrahedron Lett*. **2006**, *47*, 3265.

[21] Boubekeur, K.; Syssa-MagalR, J. L.; Palvadeau, P.; SchTllhorn, B. *Tetrahedron* Lett. 2006, 47, 1249.

[22] Iwasaki, F.; Yoshikawa, J. H.; Iwasaki, F.; Yoshikawa, J. H.; Yamamoto, H.; Kan-nari, E.; Takada, K.; Yasui, M.; Ispida, T.; Nogami, T. *Acta Crystallogr. Sect. B* **1999**, *55*, 231.

[23] (a) Relibase 2.2.1 search of the RCSB Protein Data Bank containing 45865 structures as of 18 September 2007. Relibase is X of the Cambridge Crystallographic Data Centre; (b) Howard, E.; Sanishvili, R.; Cachau, R.E.; Mitschler, B.; Bart, P.; Lamour, V.; Zandt, M. V.;

Sibley, E.; Bon, C.; Moras, D.; Schneider, T. R.; Joachimiak, A.; Podjarny, A. *Proteins Struct. Funct. Genet.* **2004**, *55*, 792.

[24] Parisini, E.; Metrangolo, P.; Pilati, T.; Resnati, G.; Terraneo, G. *Chem. Soc. Rev.* **2011**, *40*, 2267.

[25] (a) Auffinger, P.; Hays, F. A.; Westhof, E.; Ho, P. S. *Proc. Natl. Acad. Sci. U. S. A.* **2004**, *101*, 16789; (b) Griffin, J. E. The Thyroid. In Textbook of Endocrine Physiology, 2nd ed.; Griffin, J. E., Ojeda, S. R., Eds.; Oxford University Press: New York, 1992; pp 224−246. (c) Bartelena, L.; Robbins, J. *Clin. Lab. Med.* **1993**, *13*, 583.

[26] (a) Wojtczak, A.; Cody, V.; Luft, J. R.; Pangborn, W. *Acta Crystallogr., Sect. D: Biol. Crystallogr.* **2001**, *57*, 1061; (b) Valadares, N. F.; Salum, L. B.; Polikarpov, I.; Andricopulo, A. D.; Garratt, R. C. *J. Chem. Inf. Model*. **2009**, *49*, 2606.

[27] Xu, Z.; Yang, Z.; Liu, Y.; Lu, Y.; Chen, K.; Zhu, W. *J. Chem. Inf. Model.* **2014**, *54*, 69.

[28] Taylor, M. S.; Jacobsen, E. N. *Angew. Chem. Int. Ed.* **2006**, *45*, 1520.

[29] Kniep, F.; Jungbauer, S. H.; Zhang, Q.; Walter, S. M.; Schindler, S.; Schnapperelle, I.; Herdtweck, E.; Huber, S. M. *Angew. Chem., Int. Ed.* **2013**, *52*, 7028.

[30] Lu, Y.; Li, H.; Zhu, X.; Zhu, W.; Liu, H. *J. Phys. Chem. A* **2011**, *115*, 4467.

[31] Riley, K. E.; Murray, J. S.; Fanfrlík, J.; Řezáč, J.; Solá, R. J.; Concha, M. C.; Ramos, F. M.; Politzer, P. *J. Mol. Model.* **2011**, *17*, 3309.

[32] (a) Bruckmann, A.; Pena, M. A.; Bolm, C. *Synlett* **2008**, 900; (b) Walter, S. M.; Kniep, F.; Herdtweck, E.; Huber, S. M. *Angew. Chem. Int. Ed.* **2011**, *50*, 7187; (c) Huber, S. M.; Jimenez-Izal, E.; Ugalde, J. M.; Infante, I. *Chem. Commun.* **2012**, *48*, 7708; (d) Kniep, F.; Rout, L.; Walter, S. M.; Bensch, H. K. V.; Jungbauer, S. H.; Herdtweck, E.; Huber, S. M. *Chem. Commun.* **2012**, *48*, 9299. (e) Walter, S. M.; Kniep, F.; Rout, L.; Schmidtchen, F. P.; Herdtweck, E.; Huber, S. M. *J. Am. Chem. Soc.* **2012**, *134*, 8507; (f) Kniep, F.; Walter, S. M.; Herdtweck, E.; Huber, S. M. *Chem. Eur. J.* **2012**, *18*, 1306; (g) Kniep, F.; Jungbauer, S. H.;

Zhang, Q.; Walter, S. M.; Schindler, S.; Schnapperelle, I.; Herdtweck, E.; Huber S. M. *Angew. Chem. Int. Ed.* **2013**, *52*, 7028.

[33] (a) Amino, V.; Meille, S. V.; Corradi, E.; Messina, M. T.; Resnati, G. *J. Am. Chem. Soc.* **1998**, *120,* 8261. (b) Corradi, E.; Meille, S. V.; Messina, M. T.; Metrangolo, P.; Resnati, G. *Angew. Chem. Int. Ed.* **2000**, *39*, 1782.

[34] Murai, K.; Morishita, M.; Nakatani, R.; Fujioka, H.; Kita, Y. *Chem. Commun.* **2008**, 4498.

[35] (a) Banerjee, A. K.; Vera, W.; Mora, H.; Laya, M. S.; Bedoya, L.; Cabrera, E. V. *J. Sci. Ind. Res*. **2006**, *65*, 299; (b) Togo, H.; Iida, S. *Synlett* **2006**, 2159; (c) Jereb, M.; Vražič, D.; Zupan, M. *Tetrahedron* **2011**, *67*, 1355.

[36] Alcaide, B.; Almendros, P.; Cabrero, G.; Ruiz, M. P. *Synthesis* **2008**, 2835.

[37] Das, S.; Borah, R.; Devi, R. R.; Thakur, A. J. *Synlett.* **2008**, 2741.

[38] Coulembier, O.; Meyer, F.; Dubois, P. *Polym. Chem.* **2010**, *1*, 434.

[39] Takeda, Y.; Hisakuni, D.; Lin C.-H.; Minakata, S. *Org. Lett.* **2015**, *17*, 318.

[40] (a) Yang, Y.; Moinodeen, F.; Chin, W.; Ma, T.; Jiang, Z.; Tan, C. H. *Org. Lett.* **2012**, *14*, 4762; (b) Wang, C.; Zong, L.; Tan, C. H. *J. Am. Chem. Soc.* **2015**, *137*, 10677.

Chapter 2

Design and synthesis of novel halogen bond donors

2.1 Introduction

The study of halogen bonding commenced in 1863, and is related to another non-covalent bond, which is hydrogen bonding. Hydrogen bonding plays an important role in the field of non-covalent bond organocatalysis,[1] and several hydrogen bond donor catalysts have been widely used in organocatalysis.[2] Due to the similar features of hydrogen bond and halogen bond, particularly their effectiveness in anion recognition,[3] many researchers have investigated the use of halogen bond donor species as catalysts in organic synthesis. The potential of the halogen bond in this field may arise mainly from the unique properties of halogen-bonded systems as compared to the analogous hydrogen-bonded systems.[4] Such distinct advantages are: 1) the higher directionality of halogen bond [5] can achieve higher selectivity when using multi-dentate halogen bond donors as catalyst or additive towards different substrates;[6] 2) halogen bond can be used as a hydrophobic alternative to hydrogen bond, as most of the halogen bond donors generally contains halogen atoms, and may be associated with multi-fluorinated backbones. Accordingly, XB donors are more soluble in non-polar solvents than their HB counterparts;[7] 3) the strength of interactions can be fine-tuned with ease by changing the associated I, Br, Cl, and in some cases F atoms in the active site of the halogen bond;[8] 4) Furthermore, halogen atoms are more polarizable and bigger than hydrogen atom, hence halogen bond donors are softer Lewis acids than donors in the related hydrogen bond, and are more preferred for the substrates involved in organocatalysts reactions. Our strategy of designing new halogen bond donors as catalysts leverages on maximizing the unique properties, in the hope of exploring new catalysis.

2.2 Strategy of the catalyst design

Increasing the activity of the catalyst is usually the key issue in the development of new catalysts. In terms of halogen bond donors, increasing the electron withdrawing ability will

lead to an enhancement in activity, hence there are several strategies that can be used to design a new XBs donor.

1) As a well-known structure, pincer-type catalyst/ligand has stronger interaction with the acceptor than the monodentate catalyst/ligand, due to the presence of two or more coordination sites. Huber has developed a series of bidentate halogen bond donors,[9] and this class of catalysts have been used in debromination and Diels-Alder reaction.[9a,b] Inspired by these works, we chose a bidentate backbone as the scaffold for the synthesis of our new halogen bond donor.
2) Theoretically, electron poor species has stronger electron withdrawing ability, which corresponds to a higher activity in halogen bond donors. Through previous studies on halogen bond, our strategy is to use a positively charged heterocyclic backbone to enhance the electron withdrawing ability of the halogen bond donor. Generally, the charged heterocyclic compound is a salt, which has low solubility in organic solvents, limiting the applications of such catalysts.[9a] However, by adding an alkyl group on the heterocyclic backbone, the solubility can be improved, and a new halogen bond donor can be designed.
3) Finally, our ultimate objective is to use halogen bonding interaction to realize asymmetric transformations. Therefore, the backbone of the XBs donor should include several chiral centers, which can be used to control enantioselectivity.

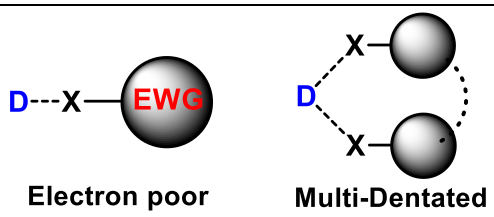

Figure 2.1 Design of halogen-bond donor.

2.3 Halogen bond donor based on the charge assistant imidazoline

2.3.1 Design and synthesis

Guided by the strategy as summarized above, our investigation of halogen bond donors commenced with the simplest structure plan**.** The synthesis of a mono-dentate halogen bond donor based on a heterocyclic compound was first attempted and the activity was tested.

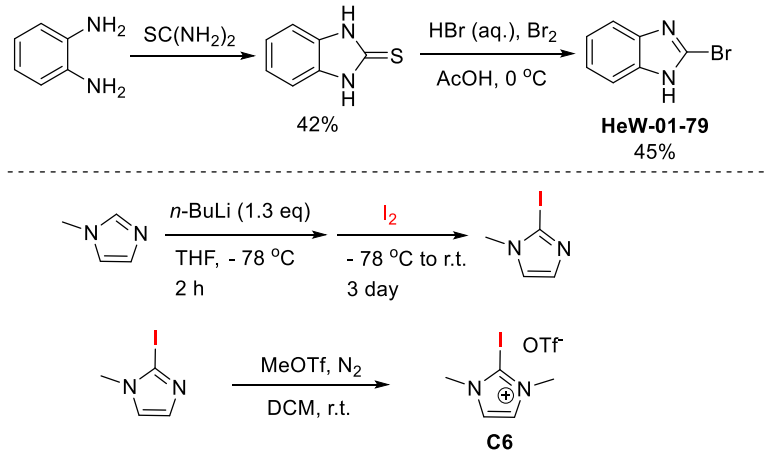

Figure 2.2 Synthesis of mono-dentate XBs donors **HeW-01-79** and **C6**.

Diamine was used as the starting material in the first step, and mono-dentate neutral halogen bond donor, compound **HeW-01-79**, was obtained, with the active site at the bromine atom (Figure 2.2). By changing the starting material to 2-methyl imidazole, iodination and methylation at nitrogen atom with methyl triflate were carried out, and the charge assistant mono-dentate halogen bond donor, compound **C6**, was obtained in moderate yield. (Figure 2.2, bottom) These two compounds can be seen as a neutral and charged assistant halogen bond donors, as they contain bromine and iodine atoms as active sites, respectively. They were designed as models to study the properties of halogen bond donor systematically, and investigate the various influences on the related halogen bond induced reaction.

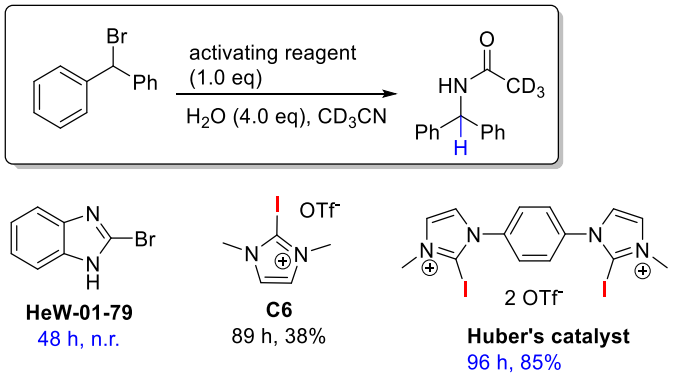

Figure 2.3 Comparing the activity of different XBs donors in the Ritter-type reaction.

In the initial stage, the Ritter-type reaction, reported by Huber in 2011, was used as a comparison of activity of the different halogen bond donors. As anticipated, this reaction can be activated by **C6**, but the conversion was low, at 38% after 89 h (Figure 2.3). However, using the neutral halogen bond donor, **HeW-01-79**, no reaction occurred even after 48 h. Hence, it is evident that the activity of the neutral donor is lower than the charged donor, and the mono-dentate donor is much weaker than the bidentate one for this reaction, confirming the hypothesis that was made earlier.

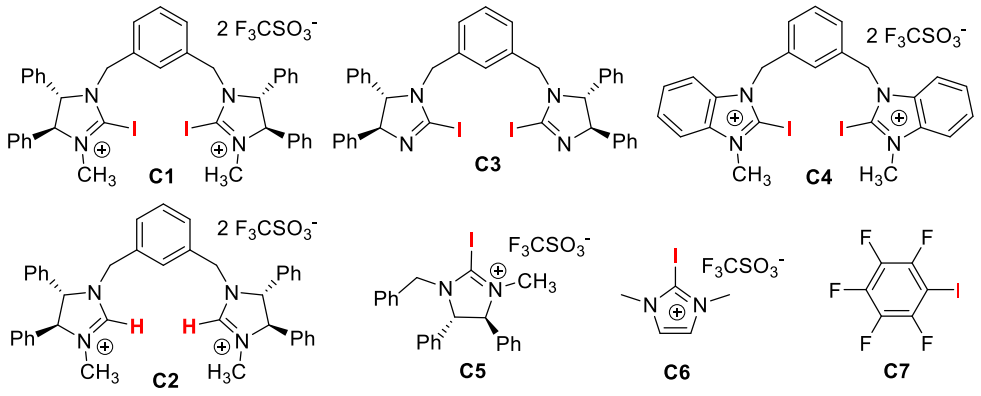

Figure 2.4 Halogen bond donors **C1** – **C7**.

Based on the above results, a new halogen bond donor **C1** was designed (Figure 2.4). Such donors are based on a pincer type structure, and contains two charged iodinated imidazoline as active sites, hence should ideally be a stronger halogen bond donor. On the other hand, due to the phenyl substitution on the imidazoline, **C1** possesses a higher solubility in organic solvents

than Huber's catalyst, which is highly advantageous. **C1** was then used in the Ritter-type reaction. [9a] Interestingly, a high conversion was achieved within 39 h, which is a much shorter duration than Huber's catalyst.

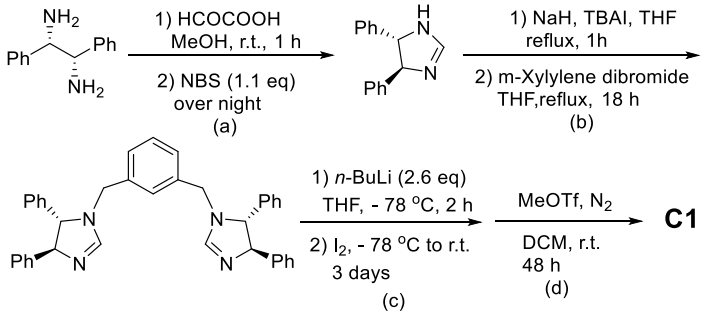

Figure 2.5 Synthesis of halogen bond donor **C1**.

The synthesis of **C1** is shown in Figure 2.5, which is inspired by findings in the reported literature. [10, 9d] Starting from commercially available chiral diamine, the imidazolidine product was obtained in high yield through condensation with glyoxylic acid, followed by oxidative decarboxylation with NBS. [10a] The di-imidazolidine framework was assembled using *m*-xylylene dibromide. Neutral iodo-imidazoline was obtained and subsequent methylation resulted in the formation of cationic imidazolium **C1**. By using a similar synthetic route, other halogen bond donors **C2**, **C3**, **C4** and **C5** were also obtained in good yields. These donors were purified by flash chromatography followed by recrystallization, and represent several different kinds of catalyst. For example, **C2** is the corresponding non-iodinated catalyst; **C3** is neutral; **C4** consists of an imidazole and has poorer solubility in organic solvent than **C1**; **C5** and **C6** are mono-dentate donors based on imidazolium and imidazole scaffolds respectively; while **C7** is the most common halogen bond donor, which can be used as a standard for comparison with our donors. These donors can be used in a model reaction separately, and a trend can be derived through the investigation of their activity in the reaction. Guided by this trend, further design and modifications can be made to obtain more efficient catalysis.

2.3.2 X-ray study of the halogen bond donor

The activity of these donors in the model reaction is only indicative of the donor strength; in order to understand the halogen bond donor further, we need to gain insight into the structure of the donor. X-ray structure is a powerful method in this context as it has been widely used in the study of halogen bonding.[11] Hence, compound **C1** was chosen as the structure for single crystal formation and investigation. The structure of **C1** was confirmed using X-ray crystallography (Figure 2.6).

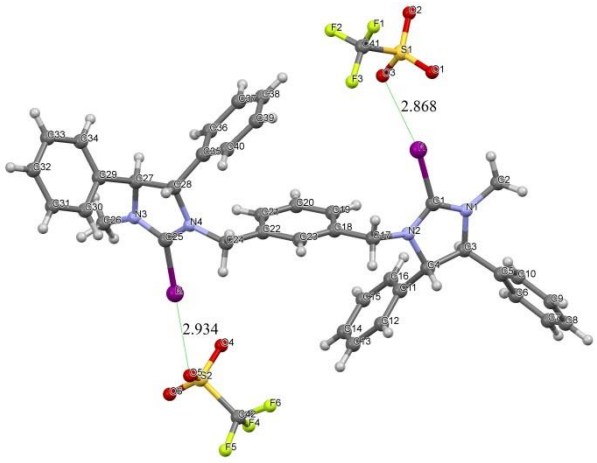

Figure 2.6 X-ray structure analysis of the halogen bond donor **C1** (elipsol at 50% probability); selected bond lengths [Å] and angles [o]: C1-I1 2.088(10), C1-N1 1.309(9), C1-N2 1.322(10), C3-N1 1.499(8); N1-C1-N2 114.0(8).

The distance between the iodine and oxygen atoms of the triflate counter anions is 2.868 Å, which is shorter than the sum of the van der Waals radii.[12] This indicates that there is a non-covalent interaction between these two atoms, which is a type of halogen bonding. The pincer-type compound, which contains electron poor iodinated imidazolium acts as the donor. The triflate counter anion is the acceptor and the electron rich oxygen atom on the sulfonate group is the active site. At the same time, the bond angle of C-I bond with I-O bond is around 180^{o} which is highly directional in nature and is a unique characteristic of halogen bonding. In the solid phase, the two iodine atoms were distributed at the two sides of the phenyl ring due to the steric hindrance of the bulky substituents on the imidazolium. However, the

1,3-xylylene constitutes a flexible linker, hence in solution, the linker can rotate such that the two iodine atoms in **C1** can coordinate to a single halogen acceptor (or substrate) concurrently. A similar phenomenon was demonstrated in a previous study, and further proved by DFT calculation. [9a] Hence, it is reasonable to hypothesize that the two iodine atoms, which act as the active site of halogen bond donor, can coordinate to one substrate in the model reaction, explaining why the multi-dentate donor has higher activity than the corresponding mono one.

2.3.3 ITC study of the halogen bond donor

Until now, the applications of halogen bonds are mainly in crystal engineering, and most of investigations regarding halogen bond have been performed in the solid state, [13] such as X-ray crystallography. In these cases, the strength of the bond is usually inferred by the extent of the distance which in the interaction falls below the sum of the van der Waals radii of the involved atoms. With the development of studies involving halogen bonds, such interactions in solution [14a, b] and in the gas phase [14c, d] are also well established, but applications based on halogen bond in solution have rarely been developed so far. [15] Recently, the application of halogen bond in catalysis generated significant research interest, and further development would require more information on the thermodynamics of halogen bond complex formation involving cationic halogen bond donor in solution. Therefore, developing an efficient method to measure the halogen bond interaction in solution is of utmost importance.

Isothermal titration calorimetry (ITC) is a physical technique that can be used to detect the thermodynamic parameters of interaction in solution. [16] It is most often used to study the binding of small molecules, such as medicinal compounds, to larger macromolecules. [17] In 2012, the ITC technique was first used to determine the bond strength of halogen bond donors. [9d] The binding constant and ΔH, which are important data to measure the strength of the XBs donor, can be measured by ITC. Hence, **C1** and **C4** were chosen as donors and

dissolved in acetonitrile, which act as the hosts of ITC. Solution of Bu_4NBr in acetonitrile was used as the guest. The corresponding binding constants (K) and other thermodynamic data of guest with host can then be measured. (Table 2.1).

Table 2.1 Isothermal calorimetric titrations of halogen-bond donors with halide

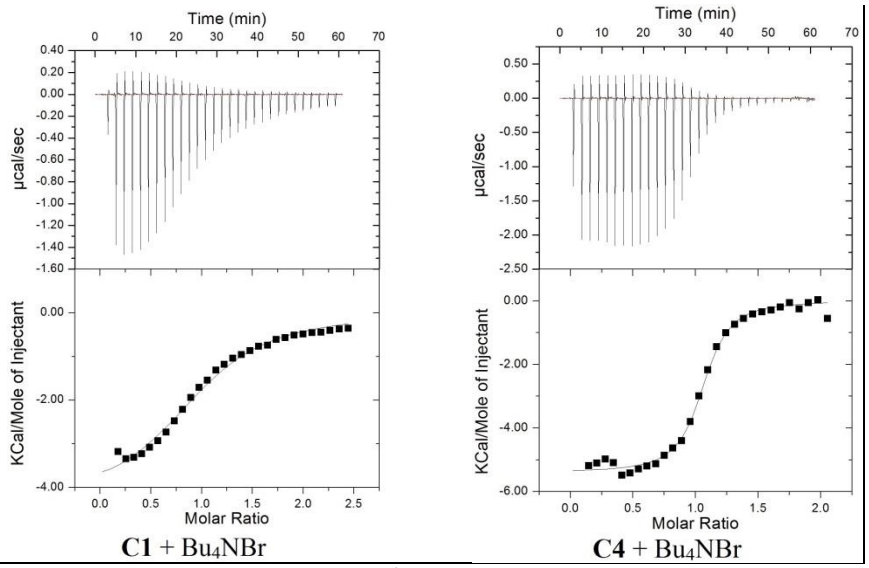

Entry	Guest	Host	K [mol^{-1}]	ΔH [kJ/mol]	$T\Delta S$ [kJ/mol]
1	**1a**	**C1**	-	-	-
2	Bu_4NBr	**C1**	3.29E4	-18.0	7.8
3	Bu_4NBr	**C4**	4.57E5	-22.6	9.7

Conditions: Halogen bond donors (0.2 mM), halide (2 mM)

The binding constant of **C4** is larger than **C1**, which means that **C4** is a stronger halogen bond donor than **C1**. Interestingly, experimental data showed that **C4** is an inferior catalyst compared to **C1** (Table 3.2, entries 1 and 4). This phenomenon can be explained such that with stronger interaction with the acceptor, **C4** is much easier to be deactivated during the reaction by strong Lewis bases, such as the by-product pyridine and quinoline, than **C1**. Hence, although a complex can be formed, it cannot be regenerated in the catalytic cycle. When we used quinoline **1a** as guest to test its interaction with **C1**, no obvious peak was found in the spectra. This implies that the interaction between quinoline with **C1** is not strong

enough, hence **C1** is regenerated in this reaction. Hence, the effectiveness of a XB donor as a catalyst probably follows the "goldilocks" principle.

2.4 Halogen bond donor based on bipyridinium back bone

2.4.1 Halogen bond donor design and synthesis

Since its discovery at the end of nineteenth century, [18] the bipyridine ligand has been used extensively in the complexation of metal ions. The structural variations of bipyridine ligands can be classified as symmetrical isomers (2,2', 3,3', and 4,4') and asymmetrical ones (2,3', 2,4', and 3,4') (Figure 2.7), and of these, only the 2,3'- and the 3,3'-bipyridines are found to be naturally abundant in certain varieties of tobacco.[19] Depending on the different ability of coordination, these isomers can coordinate to different metals as catalysts. Due to the strongest coordination, 2,2'-bipyridine is the most frequently used ligand, and many useful derivatives has been explored based on the 2,2'-bipyridine backbone.

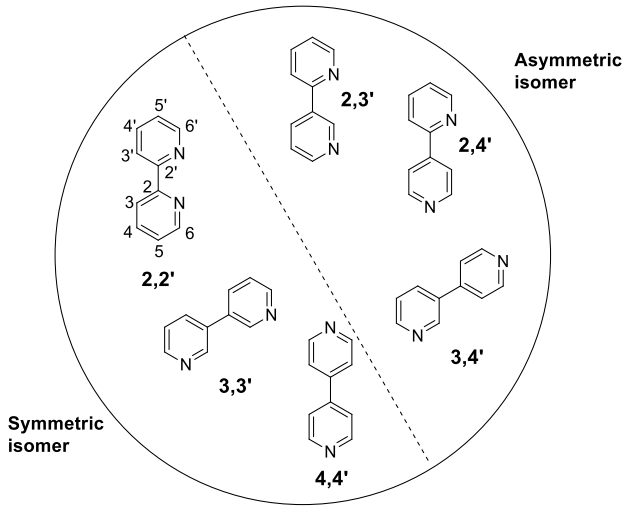

Figure 2.7 Symmetric and asymmetric isomers of bipyridine.

Bipyridines substituted with chiral functional groups have also been explored as chiral ligands in asymmetric reactions. Despite the chiral substituted group, there is a C2 symmetric axis in 2,2'-bipyridine structure, hence it exists as a *meso* compound with both *R* and *S* configurations. Generally, if there is no substituent on the pyridine ring, the two pyridine rings

can rotate freely around this C2 axis due to the low energy barrier, and the *R* or *S* enantiomer cannot be separated. However, if a bulky substituent is present at the 1- and 3- position of the two pyridine ring, free rotation is hindered, and due to the higher energy barrier of the rotation, the enantiomers can potentially be separated.

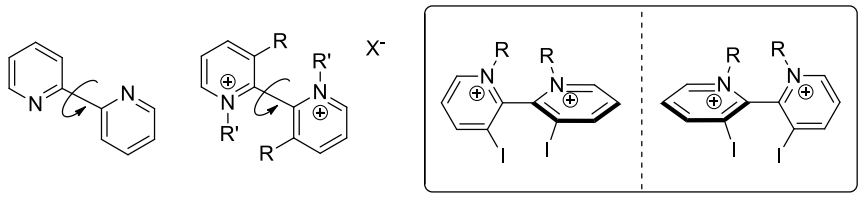

Figure 2.8 (Left) Structure of 2,2'-bipyridine. (Right) Enantiomer of 2,2'-bipyridine.

Initially, we plan to use the 2,2'-bipyridine as the backbone. With iodination on the 3,3'-position of the pyridine and ionization at the nitrogen atom, a bidentate charge assistant halogen bond donor can be obtained. Such bipyridine halogen bond donors contain a C2 symmetric axis, and the iodine atom and R group are sterically bulky enough to prevent the free rotation of the pyridine (Figure 2.8). With a suitable chiral resolution method, a chiral halogen bond donor can be obtained. In addition, as this is a pyridine salt and the pyridinium is an electron poor group, the strength of the halogen bonding should be stronger than that in a neutral compound. The rigidity of the bipyridine backbone may also result in a shorter distance between the two iodine atoms, which can further improve the strength of the halogen bonding.

2.4.2 Synthesis of halogen bond donor

The synthesis of the 2,2'-bipyridine type halogen bond donor was commenced from 2-chloro-3-nitro-pyridine. After a homo-coupling in the presence of copper, 3,3'-dinitro-2,2'-bipyridine was obtained in 63% yield. The nitro group was then reduced to amine by $SnCl_2$, and iodination was subsequently carried out to afford the desired 3,3'-diiodo-2,2'-bipyridine.

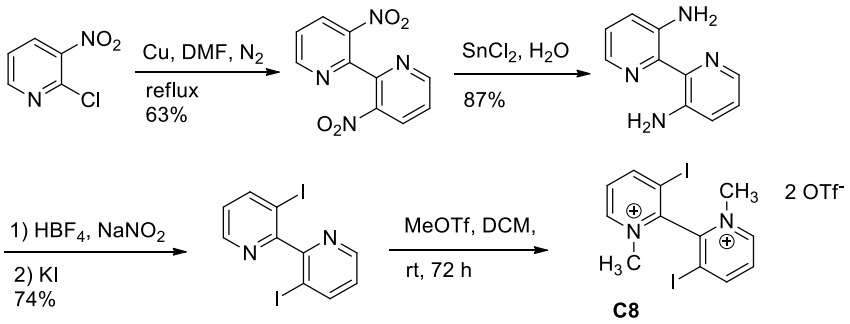

Figure 2.9 Synthesis of 2,2'-(*N*, *N*'-methyl-3,3'-iodio)-bipyridinium triflate salt.

Due to the steric hindrance, substitution on the nitrogen atom is more challenging than in other heterocyclic compounds. After screening many reagents, it was found that only methyl group is suitable for the substitution, and the methylated product was obtained by adding methyl triflate in the DCM solution of 3,3'-diiodo-2,2'-bipyridine. After stirring for 3 days at room temperature, (*N*, *N*'-methyl-3,3'-iodo)- 2,2'-bipyridinium triflate salt **C8** precipitated from the solution. At the same time, the (*N*-methyl-3,3'-iodio)- 2,2'-bipyridinium triflate salt, which is the corresponding mono-methylated halogen bond donor, can be obtained by changing the amount of methyl triflate.

2.4.3 X-ray study of the halogen bond donor

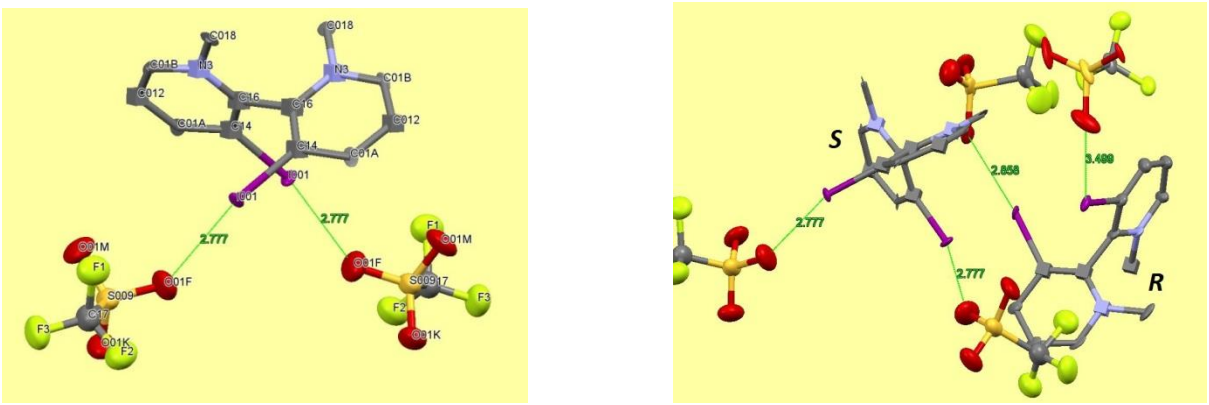

Figure 2.10 (Left) X-ray structure of 2,2'-(*N*, *N*'-methyl-3,3'-iodio)-bipyridinium triflate **C8**. (Right) A pair of enantiomers of halogen bond donor in the same pack.

To further understand the halogen bond donor and provide evidence for our hypothesized structure, the single crystal of the (*N*,*N*'-methyl-3,3'-iodio)-2,2'-bipyridinium triflate was

isolated and subjected to X-ray crystallographic analysis (Figure 2.10). As hypothesized, the two iodine atoms are the active sites of the donor, and the oxygen atom of the sulfonate group is the active site of the related acceptor. The distance between the iodine and oxygen atoms is around 2.777 Å, and this value is shorter than the sum of van der Waals radii of these two atoms; additionally, it is shorter than the previous imidazolium-type halogen bond donor, which is 2.955 Å (Figure 2.6). Hence, the interaction between the iodine and oxygen atoms is non-covalent, and is a halogen bond. As anticipated, the iodine atom and the methyl group are sterically bulky enough to prevent the free rotation of these two pyridine rings. As shown in the X-ray structure, there is a pair of enantiomers in the same unit cell: for the *R* configuration, the distance between the iodine atom with the nearest oxygen is 2.858 Å and another is 3.499 Å which is equal to the van der Waals radii. This value longer than that in the *S* configuration, which could be due to the different steric hindrance in the same unit cell. Based on the X-ray study of this halogen bond donor, this enantiomer appeared separable by chiral resolution technique.

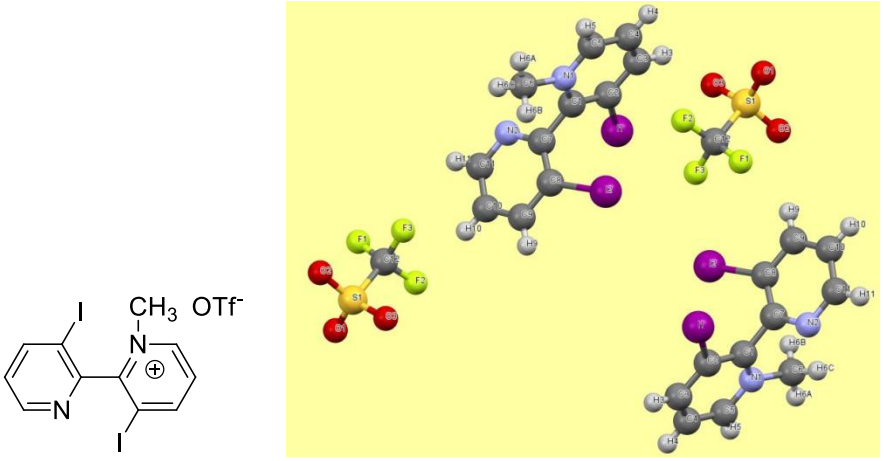

Figure 2.11 X-ray structure of 2,2'-(*N*-methyl-3,3'-iodio)-bipyridinium triflate **C14**.

Under the similar condition, the single crystal of mono-methylated donor, compound **C14**, was isolated and analyzed by X-ray (Figure 2.11). This compound remains an enantiomer,

even though there is only one substituted group on pyridine ring. The steric hindrance of the one methyl group is sufficient to block the free rotation of these two pyridines.

2.4.4 Modification of halogen bond donor

With these halogen bond donors in hand, separation of the enantiomers by chiral resolution was attempted. The most common method of chiral resolution is using a chiral source mixed with the target compound together in a solution, with the optically pure compound obtained through recrystallization. Theoretically, the *R* or *S* configuration of this compound should have different interactions with the chiral source and can be separated by recrystallization. Therefore, chiral amino acid was mixed with the bipyridine halogen bond donor **C8**, the recrystallization was conducted several times. The solid was analyzed by the polarimeter to confirm the optical rotations. Several conditions, such as solvents and chiral amino acid were examined to achieve optical resolution. Nevertheless, in all the attempts the optical rotation of the recrystallized sample was closed to zero. These results may indicate that the enantiomer cannot be separated efficiently by this method.

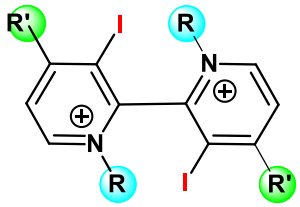

Figure 2.12 Strategy of modification of halogen bond donor with chiral functional group.

Following the unsuccessful chiral resolution, another approach to chiral bipyridine based halogen bond donor was conceived. As shown in Figure 2.12, if R or R′ is a chiral substituent, this compound should exist as a mixture of diastereomers, which can be separated more easily by method such as column chromatography. In general, the modification of the pyridine is usually at the 1- or 4- position of the ring.

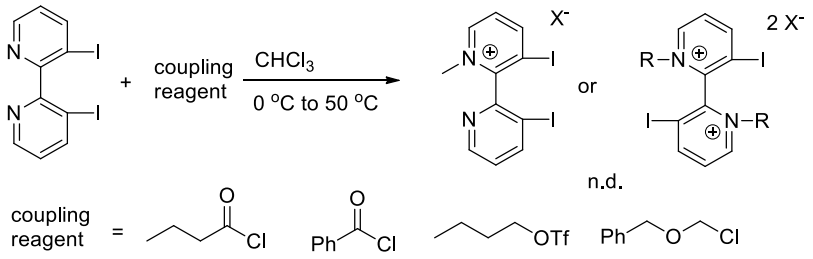

Figure 2.13 Modification of (*N*,*N*'-methyl-3,3'-iodio)-2,2'-bipyridinium triflate salt.

A chiral -R group was first substituted on the nitrogen atom to get the corresponding pyridinium salt. Several different coupling reagents were used to react with 3,3'-iodo-2,2'-bipyridine (Figure 2.13). Generally, acid chloride reacts with pyridine very easily, and a pyridinium salt is formed. Hence, butyryl chloride and benzoyl chloride were utilized as coupling reagents to react with 3,3'-iodo-2,2'-bipyridine. However, unlike in the simple pyridine, no desired product was detected, even when the reaction mixture was heated to 50 °C and the reaction time was prolonged. The poor yield may be due to the high steric hindrance at the 1- and 3-position of pyridine ring. Other electrophiles such as *n*-butyl triflate and [(chloromethoxy)methyl] benzene also failed to react with 3,3'-iodo-2,2'-bipyridine. That means only the methyl group can be added at the nitrogen atom of pyridine; other groups are too bulky for the 3,3'-iodo-2,2'-bipyridine backbone.

The halogen donor was also subjected to modifications at the 4- position of pyridine ring. Starting from 4-methyl-2-chloro-3-nitro-pyridine, through self-coupling and oxidation, the acid compound was obtained in moderate yield (Figure 2.14).

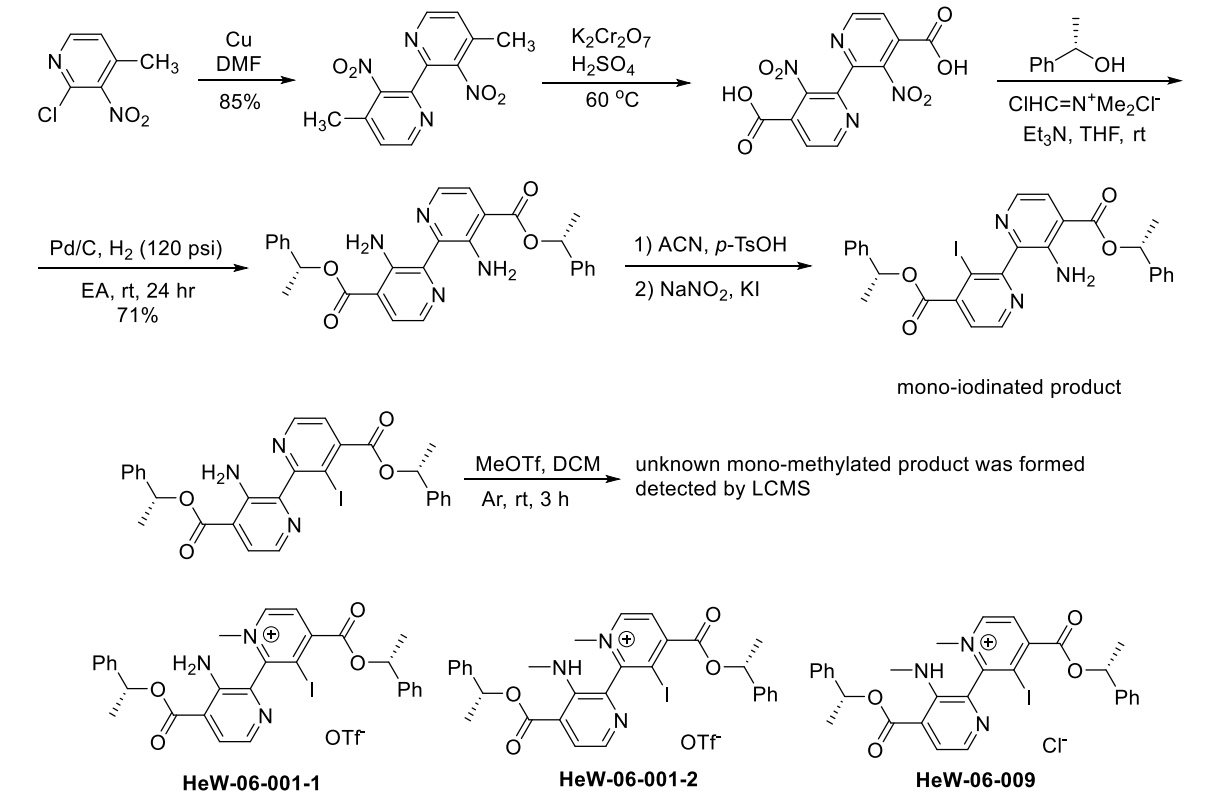

Figure 2.14 Synthesis of 4-substituted 2,2'-(*N*, *N*'-methyl-3,3'-iodio)-bipyridinium triflate salt.

After the reaction of this acid with a chiral alcohol, the corresponding chiral ester was formed and the nitro group was reduced to amine in the presence of H_2 gas and Pd/C. However, unlike the previous compound, only the mono-iodinated compound can be formed by using the same method. In addition, due to the high steric hindrance, only mono-methylated pyridium salt was obtained after reacting with excess amount of methyl triflate, even when high temperature was used. Although a pure compound was obtained following column chromatography, the exact identity of the final compound cannot be determined, despite further NMR and MS analyses. The probable structures of the compound are thus presented in Figure 2.14 as **HeW-06-001-1**, **HeW-06-001-2** and **HeW-06-009**.

2.4.5 Synthesis of the halogen bond donor with different counter anions

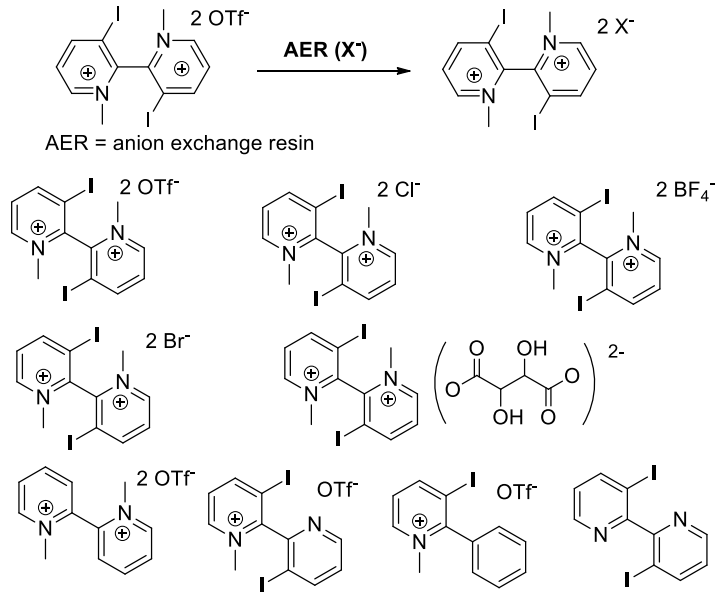

Figure 2.15 Halogen bond donor with different counter anions through anion exchange.

The halogen bond donor based on the bipyridinium exists in the form of a salt, and the counter anion can potentially affect the activity or the strength of the halogen bonding donor in the reaction. Therefore, a series of halogen bond donor with different counteranions were synthesized by using anion exchange resin (AER). The initial anion exchange resin is basic, AER (OH^-), hence an aqueous acid, for example HX, was used to flush the AER column until the pH value of the eluent is equivalent to that of the acid solution. Thereafter, the counteranion in the resin column would be the same as the acid used, generating AER (X^-). After the AER (X^-) column was prepared, the (*N*,*N*'-methyl-3,3'-iodo)- 2,2'-bipyridinium triflate solution was introduced into the column and flushed by methanol until elution of all of the compound was complete. The counter anion of the halogen bond donor was thus exchanged to become X^-. The structure of these donors can be confirmed by NMR, and the polarity of these donors is different due to the different anions. By using these donors in the model reaction, the role of the anion can be further elucidated.

2.5 Halogen bond donor based on the chiral backbone

Similar to hydrogen bonding, the halogen bond is a highly directional non-covalent bonding interaction between a donor and acceptor. Therefore, halogen bonding can potentially be involved in organo-catalysis of asymmetric reactions. Based on the results in the preceding section, it is apparent that iodinated imidazolium is a strong halogen bond donor. If a chiral linker is used to connect the two electron poor moieties (Figure 2.16), such bidentate halogen bond donors based on a chiral backbone can potentially be used to control the enantioselectivity.

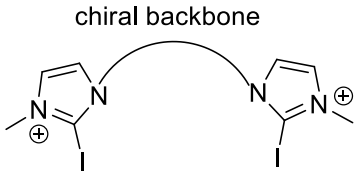

Figure 2.16 Halogen bond donor with chiral backbone.

The first chiral backbone chosen is the classic chiral tartaric acid, and the synthetic route is depicted in Figure 2.17. After the esterification reaction of chiral tartaric acid with methanol, the chiral diol was protected by adding 2,2-dimethoxypropane. Next, the ester was reduced by $LiAlH_4$, and reacted with imidazole to form the compound **VI**, which contains two imidazole moieties that are connected by a chiral linker. During iodination on the imidazole ring, a neutral halogen bond donor, compound **VII** was obtained. As in my previous work, it was intended that the reaction between methyl triflate and compound **VII** would ideally yield the corresponding imidazolium salt. However, the desired product was not obtained, as ring-opening of the protecting group (five-membered ring) occurred, presumably due to the strong acidity of methyl triflate. The ring-opening could not be suppressed even when the reaction was performed at a lower temperature for a shorter time.

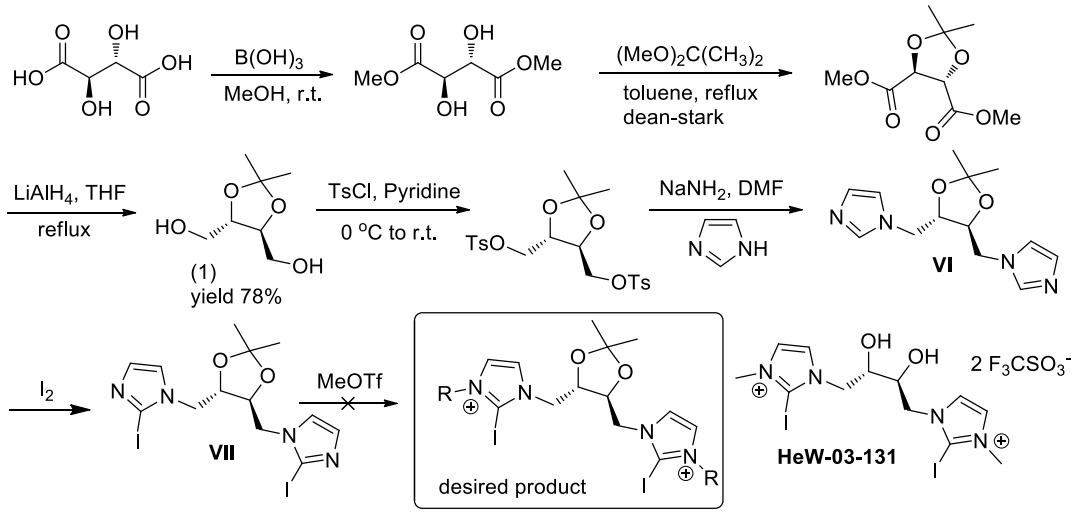

Figure 2.17 Synthesis of the XB donor with chiral backbone.

In order to obtain the more stable halogen bond donor with an intact ring, another synthetic route was used. A similar starting material was used to obtain the iodinated compound, however, the chiral diol was protected by cyclohexanone in the form of a spirocyclic acetal (Figure 2.18, compound **I**), which has higher stability in acidic conditions. At the same time, OMe_3BF_4, which is less acidic than methyl triflate, was used as the methylation reagent. As a result, the desired product was successfully obtained in moderate total yield. Using the same synthetic route, two other XB donors containing different imidazolium groups were obtained. This kind of XB donor has a chiral backbone, and the chirality of enantiopure tartaric acid was retained during the synthesis.

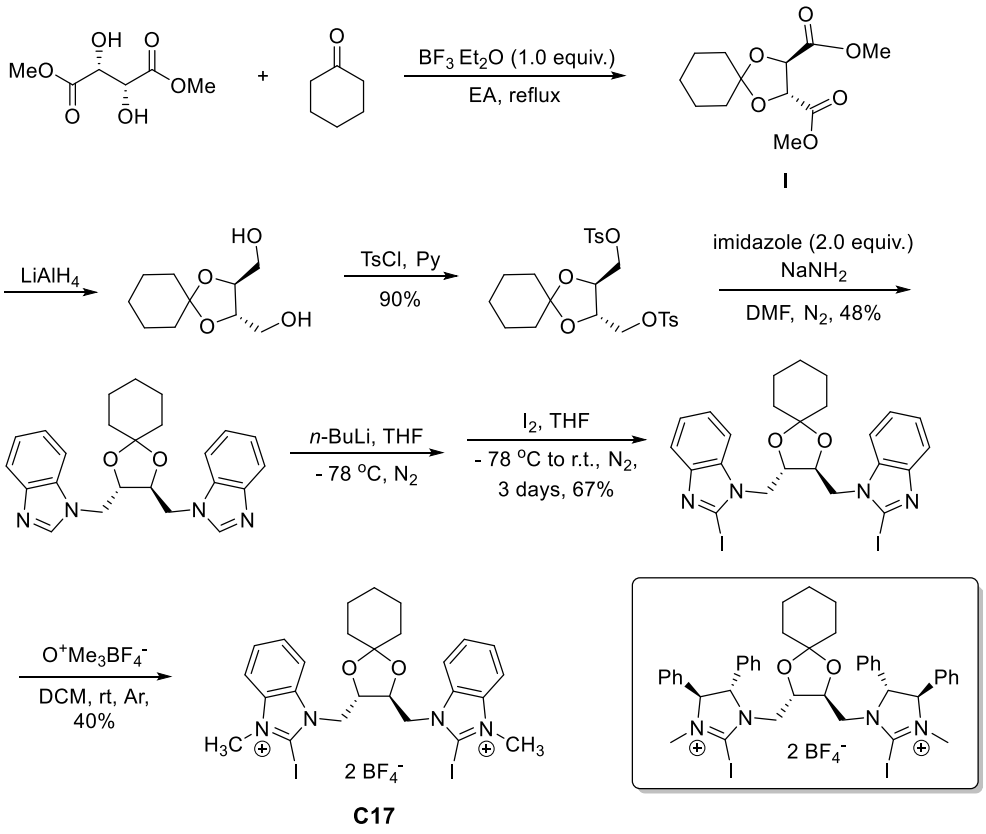

Figure 2.18 Synthesis of the halogen bond donor **C17**.

The preceding halogen bond donors consist of a chiral backbone, hence for further exploration in asymmetric reactions, mono-dentate donors comprising of chiral functionalities tethered on a scaffold were synthesized (Figure 2.18). Such donors are based on a charged imidazolinium, with a chiral proline on the nitrogen and a bulky *n*-butyl group substituted on another nitrogen atom. The design of the donor allows it to act like a bifunctional organocatalyst, which can ideally interact with the substrate through halogen bonding, with the enantioselectivity controlled by the chiral proline moiety.

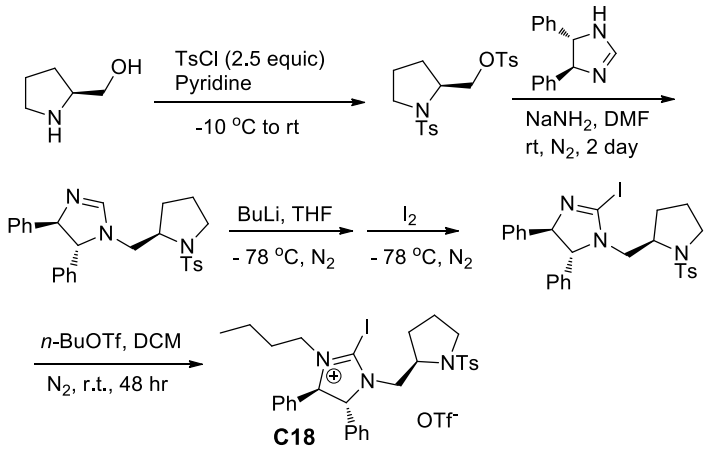

Figure 2.19 Synthesis of halogen bond **C18**.

2.6 Conclusion

Inspired by the previous related work, we have developed a systematic strategy for the design of halogen bond donors. 1) using the bidentated backbone to improve the strength and the selectivity of the halogen bond donor; 2) using the charge assistant halogen bond donor to increase the strength of the interaction; 3) using a chiral backbone in the halogen bond donor to realize the asymmetric induction. Guide by these strategies, several types of novel halogen bond donors were synthesized based on bidentate dihydroimidazoline, bipyridinium and chiral backbone respectively. Additionally, several analytical techniques such as NMR, X-ray and ITC have been used to analyze these donors. Key parameters concerning binding constant, bond length and bond strength, which can be used to measure the interaction between substrate and catalyst have been obtained. To some extent, the strength of the interaction is indicative of the activity of the catalyst in the related reactions, hence these data will help us to further understand the mechanism of halogen bonding interaction, particularly in the applications in catalytic reactions. Through the systematic studies on halogen bond donors and the bonding interactions, our strategy of catalyst design has proved to be valuable for the new halogen bond donor synthesis. This work is an important contribution to the study of halogen bonding in catalysis.

REFERENCES

[1] (a) Jeffrey, G. A. An Introduction to Hydrogen Bonding; Oxford University Press: Oxford, U.K., 1997; (b) Steed, J. W.; Atwood, J. L. Supramolecular Chemistry, 2nd ed.; Wiley: Weinheim, Germany, 2009.

[2] (a) Hine, J.; Linden, S.-M.; Kanagasabapathy, V. M. *J. Am. Chem. Soc*. **1985**, *107*, 1082; (b) Etter, M. C. *Acc. Chem. Res.* **1990**, *23*, 120; (c) Curran, D. P. *Tetrahedron Lett.* **1995**, *36*, 6647; (d) Gholami, M. R.; Talebi, B. A. *J. Phys. Org. Chem.* **2003**, *16*, 79; (e) Schreiner, P. R. *Chem. Soc. Rev*. **2003**, *32*, 289; (f) Zhang, Z.; Schreiner, P. R. *Chem. Soc. Rev*. **2009**, *38*, 1187.

[3] (a) Schreiner, P. R. *Chem. Soc. Rev*. **2003**, *32*, 289; (b) Metrangolo, P.; Pilati, T.; Terraneo, G.; Biella, S.; Resnati, G. *CrystEngComm* **2009**, *11*, 1187; (c) Zhang, Z.; Schreiner, P. R. *Chem. Soc. Rev.* **2009**, *38*, 1187; (d) Biella, S.; Gattuso, G.; Notti, A.; Metrangolo, P.; Pappalardo, S.; Parisi, M. F.; Pilati, T.; Resnati, G.; Terraneo, G. *Supramol. Chem.* **2009**, *21*, 149; (e) Cavallo, G.; Metrangolo, P.; Pilati, T.; Resnati, G.; Sansotera, M.; Terraneo, G. *Chem. Soc. Rev.* **2010**, *39*, 3772.

[4] Schindler, S.; Huber, S. M. Halogen Bonds in Organic Synthesis and Organocatalysis. In Halogen Bonding II: Impact on Material Chemistry and Life Science; Metrangolo, P., Resnati, G., Eds.; Springer International Publishing: Cham, Switzerland, **2015**; pp 167−203.

[5] Politzer, P.; Murray, J. S.; Clark, T. *Phys. Chem. Chem. Phys.* **2010**, *12*, 7748.

[6] Kniep, F.; Jungbauer, S. H.; Zhang, Q.; Walter, S. M.; Schindler, S.; Schnapperelle, I.; Herdtweck, E.; Huber, S. M. *Angew. Chem., Int. Ed.* **2013**, *52*, 7028.

[7] Lu, Y.; Li, H.; Zhu, X.; Zhu, W.; Liu, H. *J. Phys. Chem. A* **2011**, *115*, 4467.

[8] Riley, K. E.; Murray, J. S.; Fanfrlík, J.; Řezáč, J.; Solá, R. J.; Concha, M. C.; Ramos, F. M.; Politzer, P. *J. Mol. Model.* **2011**, *17*, 3309.

[9] (a) Walter, S. M.; Kniep, F.; Herdtweck, E.; Huber, S. M. *Angew. Chem. Int. Ed.* **2011**, *50*, 7187; (b) Huber, S. M.; Jimenez-Izal, E.; Ugalde, J. M.; Infante, I. *Chem. Commun.* **2012**, *48*, 7708; (c) Kniep, F.; Rout, L.; Walter, S. M.; Bensch, H. K. V.; Jungbauer, S. H.; Herdtweck, E.; Huber, S. M. *Chem. Commun.* **2012**, *48*, 9299; (d) Walter, S. M.; Kniep, F.; Rout, L.; Schmidtchen, F. P.; Herdtweck, E.; Huber, S. M. *J. Am. Chem. Soc.* **2012**, *134*, 8507; (e) Kniep, F.; Walter, S. M.; Herdtweck, E.; Huber, S. M. *Chem. Eur. J.* **2012**, *18*, 1306; (f) Kniep, F.; Jungbauer, S. H.; Zhang, Q.; Walter, S. M.; Schindler, S.; Schnapperelle, I.; Herdtweck, E.; Huber S. M. *Angew. Chem. Int. Ed.* **2013**, *52*, 7028.

[10] (a) Murai K.; Morishita M.; Nakatani R.; Fujioka H.; Kita Y. *Chem. Commun*, **2008**, 4498; (b) Zhang Y.; Zhao L.; Patra P. K.; Hu D.; Ying J. Y. *Nano Today* **2009**, *4*, 13.

[11] Riley, K. E.; Hobza, P. *Cryst. Growth Des.* **2011**, *11*, 4272.

[12] van der Waals radii or iodine and oxygen atom are: 1.93 Å and 1.52 Å.

[13] Selected reviews: (a) Metrangolo, P.; Resnati, G. *Chem.-Eur. J.* **2001**, *7*, 2511; (b) Rissanen, K. *CrystEngComm* **2008**, *10*, 1107; (c) Brammer, L.; Espallargas, G. M.; Libri, S. *CrystEngComm* **2008**, *10*, 1712; (d) Bertani, R.; Sgarbossa, P.; Venzo, A.; Lelj, F.; Amati, M.; Resnati, G.; Pilati, T.; Metrangolo, P.; Terraneo, G. Coord. *Chem. Rev.* **2010**, *254*, 677.

[14] See, for example: (a) Di Paolo, T.; Sandorfy, C. *Can. J. Chem.* **1974**, *52*, 3612; (b) Metrangolo, P.; Panzeri, W.; Recupero, F.; Resnati, G. *J. Fluorine Chem*. **2002**, *114*, 27; (c) Legon, A. C. *Angew. Chem., Int. Ed.* **1999**, *38*, 2686; (d) Legon, A. C. in Halogen Bonding: Fundamentals and Applications; Metrangolo, P., Resnati, G., Eds.; Springer: Berlin, 2008, pp 17.

[15] Selected recent publications: (a) Mele, A.; Metrangolo, P.; Neukirch, H.; Pilati, T.; Resnati, G. *J. Am. Chem. Soc*. **2005**, *127*, 14972; (b) Sarwar, M. G.; Dragisic, B.; Sagoo, S.; Taylor, M. S. *Angew. Chem., Int. Ed.* **2010**, *49*, 1674; (c) Dimitrijevic, E.; Kvak, P.; Taylor, M. S. *Chem. Commun*. **2010**, *46*, 9025; (d) Serpell, C. J.; Kilah, N. L.; Costa, P. J.; Félix, V.; Beer,

P. D. *Angew. Chem., Int. Ed.* **2010**, *49*, 5322; (e) Caballero, A.; White, N. G.; Beer, P. D. *Angew. Chem., Int. Ed*. **2011**, *50*, 1845; (f) Walter, S. M.; Kniep, F.; Herdtweck, E.; Huber, S. M. *Angew. Chem., Int. Ed*. **2011**, *50*, 7181; (g) Jentzsch, A. V.; Emery, D.; Mareda, J.; Metrangolo, P.; Resnati, G.; Matile, S. *Angew. Chem., Int. Ed*. **2011**, *50*, 11675; (h) Kniep, F.; Walter, S. M.; Herdtweck, E.; Huber, S. M. *Chem.-Eur. J.* **2012**, *18*, 1306.

[16] (a) Schmidtchen, F. P. Isothermal Titration Calorimetry in Supramolecular Chemistry. In Supramolecular Chemistry: from Molecules to Nanomaterials; Steed, J. W., Gale, P. A., Eds.; Wiley: Chichester, 2012; pp 275 − 296; (b) Ball, V.; Maechling, C. *Int. J. Mol. Sci.* **2009**, *10*, 3283.

[17] ITC measurements have frequently been employed for the determination of interaction strengths of supra-molecular complexes and protein−ligand complexes, see e.g.: Koch, C.; Heine, A.; Klebe, G. *J. Mol. Biol.* **2011**, *406*, 700. For the important role of entropy in supramolecular interactions, see: (a) Schmidtchen, F. P. *Coord. Chem. Rev.* **2006**, *250*, 2918; (b) Schmidtchen, F. P. *Chem. Soc. Rev.* **2010**, *39*, 3916. (c) Ursu, A.; Schmidtchen, F. P. *Angew. Chem., Int. Ed.* **2012**, *51*, 242.

[18] Blau, F. *Monatsh. Chem.* **1889**, *10*, 375-388.

[19] (a) Schumacher, J. N.; Green, C. R.; Best, F. W.; Newell, M. P. *J. Agric. Food Chem.* **1977**, *25*, 310-320; (b) Foder, G. B.; Colasanti, B. In *Alkaloids*: *Chemical and Biological Perspectives*; Pelletier, S. W. Ed.; Wiley: New York, 1985; Vol. 3, Chapter 1; (c) Jacob, P.; Benowitz, N.; Yu, L.; Duan, M. J.; Liang, G. *Addiction* **1997**, *92*, 626.

Chapter 3

Halogen bonding induced transfer hydrogenation of C=N bond with Hantzsch ester

3.1 Introduction

Among various asymmetric reactions, asymmetric hydrogenation is by far the most extensively studied in academia and applied in the industry, as exemplified by the Nobel Prize in Chemistry awarded to two prominent researchers in this field, Knowles and Noyori, in 2001.[1] In traditional hydrogenation reaction, the hydrogen gas supplied under high pressure is usually used as a reductant in the presence of transition metals. However, limitations of this method are numerous, which include limited substrate scope, difficulty in catalyst separation and recycling, and safety considerations in handling high pressure of hydrogen gas.

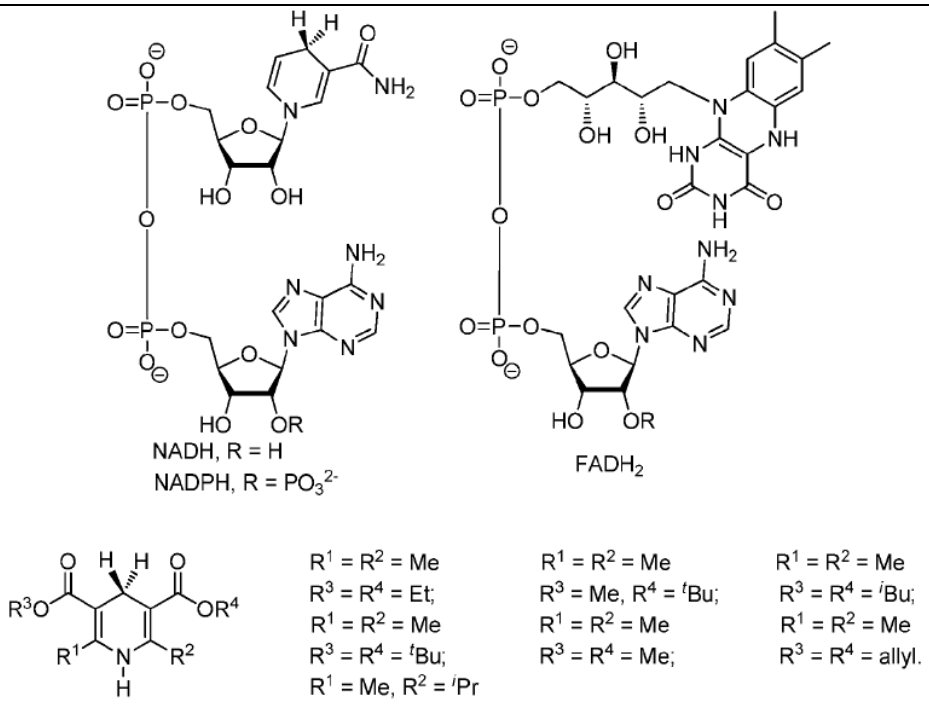

Figure 3.1 Structures of naturally occurring hydride-reduction cofactors and Hantzsch esters.

Biomimetic transfer hydrogenation is inspired by the manner reduction is conducted in nature, [2] and uses Hantzsch ester and compounds such as NADH mimic in the presence of catalytic amount of organo-catalyst (Figure 3.1). Hantzsch esters (HEH) were first discovered in 1882 by Arthur Hantzsch, and the derivatives exhibit important pharmacological properties,

such as antihypertensive, antibiotic, anti-inflammatory and antifungal activity. [3] In the past few decades, Hantzsch esters have been widely used as a reductant in transfer hydrogenation reactions,[4] which include both racemic[5] and asymmetric reactions. Substrates which contain double bonds, such as C=C, C=N and C=O, can particularly be reduced efficiently under mild condition. Using Hantzsch ester as a hydrogen source, a mild method to reduce nitrogen containing compounds is achieved, with the first report on the catalytic transfer hydrogenation reaction of C=N double bond with HEH published in 1989 by Singh and Batra.[6] In the reaction, chiral amino acids, camphor sulfonic acid and tartaric acid, were used as catalyst.

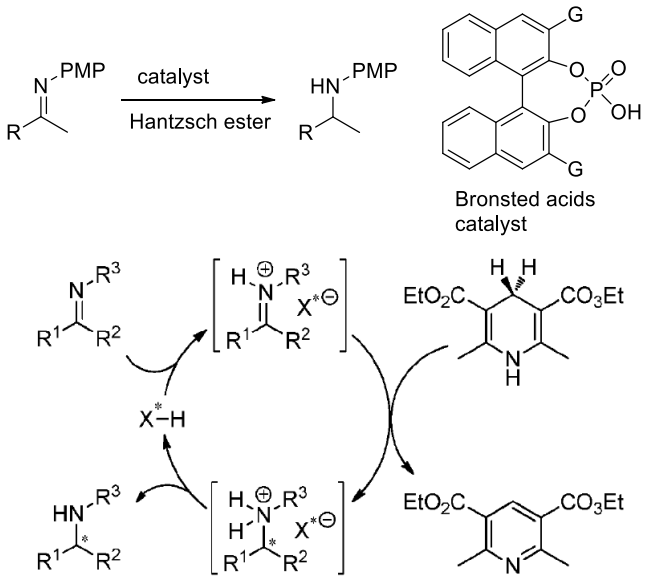

Figure 3.2 (Top) Catalytic transfer hydrogenation reaction of ketimines. (Bottom) Mechanism of the transfer hydrogenation.

HEH has been used in the transfer hydrogenation of imine, and the most prominent example is a catalytic system involving Brønsted acids, since the latter are particularly good catalysts to promote such reactions.[7] The generally accepted mechanism involves the protonation of the ketimine substrate by the Brønsted acid in the initiation step. The iminium intermediate then reacts with Hantzsch ester to generate the amine product and pyridine by-product, and the Brønsted acid catalyst can be regenerated in the last step of the cycle

(Figure 3.2).[8] Most of the transfer hydrogenation reactions catalyzed by Brønsted acids follow a similar mechanism. Besides imine, many nitrogen-containing heterocyclic compounds, such as pyridine and quinoline derivatives, can also be reduced by HEH in presence of a catalyst.

Unlike the case of Brønsted acid, the organic Lewis acid catalyzed C=N bond transfer hydrogenation with Hantzsch ester is rarely reported. The main reason is because Lewis acids are more easily deactivated by the pyridine and other *N*-heterocyclic by-product, which are strong Lewis bases. To date, only some Lewis acidic organometallic compounds have been used as catalysts in the transfer hydrogenation. When combined with chiral ligands, asymmetric induction can be achieved. For example, Zhou and co-workers used Hantzsch esters instead of hydrogen gas in the Ir-catalyzed asymmetric hydrogenation of 2-substituted quinolones with a chiral phosphine ligand.[9] Corresponding tetrahydroquinolines can be obtained in up to 98% yield and 88% *ee* (Figure 3.3). Therefore, developing an organic Lewis acid as the catalyst remains a challenge for transfer hydrogenation reactions with HEH.

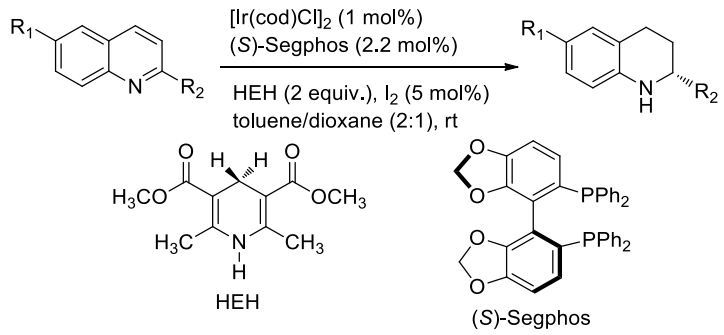

Figure 3.3 Ir-catalyzed asymmetric hydrogenation of quinolones.

Because of the stabilized aromatic structure is an impediment to the reduction, direct transfer hydrogenation of simple pyridine compound with HEH is also a challenge. At the same time, the pyridine substrate will deactivate the hydrogenation catalyst. Hence, few examples on the hydrogenation of pyridine have been published to date.

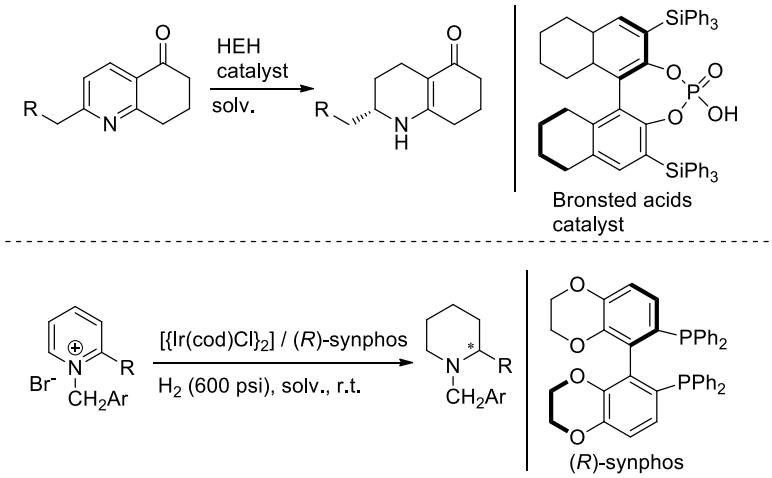

Figure 3.4 (Top) Brønsted acid catalyzed hydrogenation of inactivated pyridine. (Bottom) Hydrogenation of activated pyridine.

In 2007, Rueping and co-workers explored a method using Brønsted acid as catalyst,[10] and Hanstzch ester as the hydrogen source. The pyridine was reduced in high yield with high *ee* of up to 90%. The mechanism involves the protonation of the pyridine by the acid, and hydrogen transfer occurred in presence of HEH (Figure 3.4, top). Another example of hydrogenation of pyridine was published by Zhou and co-workers in 2012.[11] The pyridine substrate was first activated by benzyl bromide, and the generated pyridinium salt was reduced in the presence of high pressure hydrogen gas and Ir catalyst (Figure 3.4, bottom).

3.2 Experiment of transfer hydrogenation of C=N double bond

Inspired by the preceding work, and taking into consideration the dearth of research publications involving Lewis acids in the transfer hydrogenation with Hantzsch esters, we hypothesize that halogen bond donors can act as Lewis acids in the presence of pyridines and *N*-heterocycles, which is a unique property of halogen bond donors. The effectiveness of a halogen bond donor as a catalyst can be explained by the "goldilocks" principle, in which a weak halogen bond donor might not be sufficiently Lewis acidic to decrease the HOMO of C=N. In contrast, a strong halogen bond donor may bind too tightly to the product/reagent of the reaction and inhibit the catalytic cycle. A suitable halogen bond catalyst is thus a dynamic

halogen bond donor with moderate Lewis acid strength. Bolm has reported using pentafluoroiodobenzene, a classic halogen bond donor, as the catalyst in a transfer hydrogenation of quinolone and Hantzsch ester, [5m] in the first example of using halogen bond interaction to activate the substrate. However, the limitation of the method is the long reaction time (nearly 4 days, as shown in Figure 1.14).

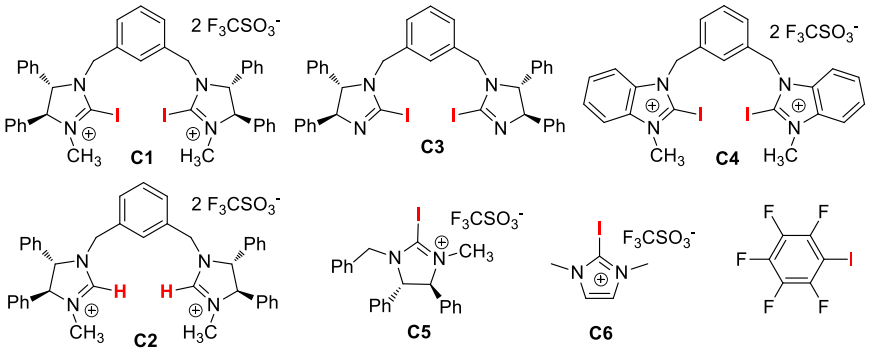

Figure 3.1 Halogen bond donors **C1** – **C7**.

With a series of halogen bond donors in hand (Figure 3.1), we explored the use of these donors as catalyst for transfer hydrogenation of C=N bond as well as the nature of the halogen bonding involved therein. The transfer hydrogenation of quinoline **1a** with HEH was first selected as a model reaction for our initial investigation (Table 3.1). With 10 mol% of imidazolium **C1** as the catalyst, complete reaction was achieved within 1 hour, affording the desired amine in an isolated yield of 92% (Table 3.1, entry 1). The yield remained very high even when the reaction time was reduced to 30 min, indicating the high activity of donor **C1** in this reaction. For non-halogen bond donor imidazolium salt **C2**, the non-iodine containing analogue of **C1**, the reaction did not complete even after 24 h (Table 3.1, entry 2). Additionally, only around 10% of the reduced adduct was detected using GC after 1 h. This phenomenon proves that halogen bonding interaction plays an important role in this reaction. Using the neutral imidazoline **C3**, which is the non-methylated variant of **C1**, the reaction was again incomplete after 24 h (Table 3.1, entry 3). Hence, both the presence of the iodo group and the electron-withdrawing tendency of the imidazolium cationic core are essential for catalytic

activity. The benzoimidazolinium salt **C4** has poor solubility in DCM, but possesses stronger interaction with halogen bond acceptors than **C1**. This interaction can be measured by ITC (chapter 2). The reaction using **C4** afforded the product in only 78% yield after 19 hours (Table 3.1, entry 4). This result shows that this catalytic process probably follows the "goldilocks" principle.

Table 3.1 Transfer hydrogenation of quinolone **1a** with Hantzsch ester in the presence of different catalysts.

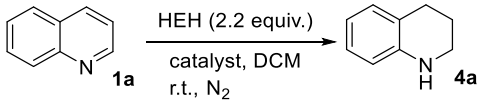

Entry	catalyst (mol%)	t (h)	Yield (%)[a]
1	**C1** (10)	1	99 (92)[b]
2	**C2** (10)	24	68
3	**C3** (10)	24	45
4	**C4** (10)	19	78
5	**C5** (10)	3	91
6	**C6** (10)	21	trace
7	**C7** (10)	67	30
8[c]	**C1** (10)	2.5	99
9	-	19	trace

HEH: Hantzsch ester; [a] Determined using GC-MS. [b] Isolated yield in parentheses. [c] 20 mol% K_2CO_3 added.

The poor solubility of charged imidazole type catalysts is also a limitation, which is similar to Huber's catalyst. Halogen bond donor **C5**, the mono-dentate version of **C1**, was able to catalyze the reaction with high efficiency (Table 3.1, entry 5) period. However, the activity is significantly lower than the bidentate catalyst. No product formation was detected when imidazolium **C6** was used (Table 3.1, entry 6) presumably due to the poor solubility and weak interaction with the substrate. Pentafluoroiodobenzene **C7**, a well-known halogen bond donor, exihibited rather sluggish catalytic activity (Table 3.1, entry 7). The triflate salt is moisture sensitive and is able to generate triflate acid, hence the involvement of Brønsted acid in this reaction cannot be ruled out.[12] In order to preclude the possible role of the residual acid as a

catalyst, 20 mol% K_2CO_3 was added in a separate experiment, which proceeded smoothly (Table 3.1, entry 8). In the absence of catalyst, only trace amount of product was detected after 19 h (Table 3.1, entry 9). Through the reaction optimization, it was concluded that: 1) a strong halogen bond donor is necessary for this reaction; 2) bidentate halogen bond donor is more efficient than the corresponding mono-dentate donor; 3) charged halogen bond donor is preferred to neutral halogen bond donor; 4) the strongest halogen bond donor **C4** did not give the best result, which is congruent with the "goldilocks" principle.

With further optimization, we found that transfer hydrogenation of quinoline **1a** can be catalyzed with 2 mol% of **C1** (Table 3.2, entry 1). Under the optimized reaction conditions, a variety of mono-and di-substituted quinolines were reduced in high yields (entries 2-9). For the substrate that contains a methyl group on the 2-position of quinoline, the reaction time was prolonged to 24 h to achieve a high yield (Table 3.2, entry 2). The 4- substituted quinoline derivative also required longer reaction time to obtain high conversion than the 2- substituted quinoline analogue (Table 3.2, entry 3). This phenomenon implies that the hydrogen transfer process takes place in a 1,4-addition manner. Installing an electron-withdrawing substituent at 2-position of quinoline, such as phenyl (Table 3.2, entry 4), accelerates the reduction, even with a *p*-methoxy-phenyl substituted group (Table 3.2, entry 5), the yield is very high. These results could be because the electron-withdrawing group can decrease the LUMO of substrate. It was further discovered that halogens are tolerated under this condition (Table 3.2, entry 6), and the nature of the substituent on the 6-position has little effect on yield (Table 3.2, entries 7 and 8). It is worth noting that for the substrate containing a hydroxy group on the 8-position of quinoline, although the hydroxyl group can act as a hydrogen bond donor, high yield can also be achieved (Table 3.2, entry 9). The investigation of the quinoline substrate scope revealed that the halogen bond donor can be widely used in such transfer hydrogenation reactions, and a variety of substituents is tolerated.

Table 3.2 Transfer hydrogenation of quinoline derivatives in the presence of **C1**

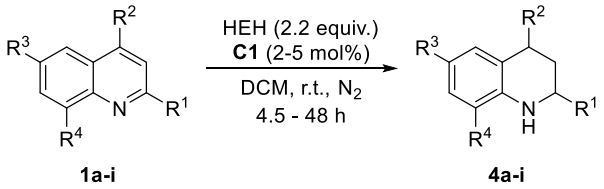

1a-i **4a-i**

Entry	1	**C1** (mol%)	t (h)	Yield (%)[a]
1	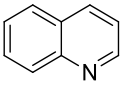	2	4.5	95
2	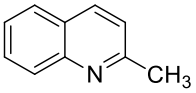	2	24	95
3	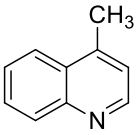	5	48	95
4	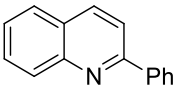	2	5	95
5	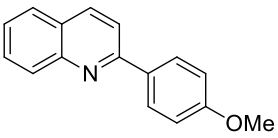	2	5	93
6	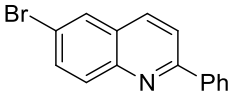	2	15	95
7	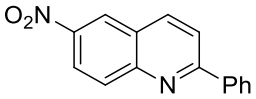	2	3	90
8	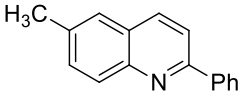	2	24	90
9	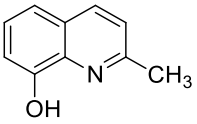	5	7	90

Condition: N_2 atmosphere, HEH (2.2 equiv.), in DCM, room temperature, [a] Isolated yield.

Thereafter, another type of C=N double bond compounds in the form of imine derivatives, was tested by transfer hydrogenation reaction with HEH in the presence of **C1** (Table 3.3). The most common imine, compound **2a** was tested first (Table 3.3, entry 1) and this compound was quickly reduced to the corresponding product in high yield. Substituents

on the benzyl ring were investigated (Table 3.3, entry 2 and 3), and the yield obtained are similar with compound 2a. An imine containing a naphthalene group also reacted smoothly to produce the desired compound in high yield (Table 3.3, entry 4). Electron-rich substituents on the phenyl ring can accelerate the reaction, resulting in a faster reaction (Table 3.3, entry 5). However, the imine containing highly electron-withdrawing substituent was unreactive (Table 3.3, entry 6). Steric hindrance on the double bond also affects the reaction significantly, and a longer reaction duration is required for the high yield of compound **5g** to be obtained (Table 3.3, entry 7).

Table 3.3 Transfer hydrogenation of imine derivatives in the presence of **C1**.

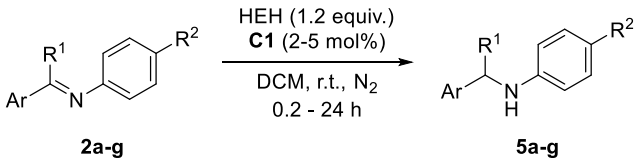

Entry	Structures of **2a-g**	**C1** (mol%)	5	t (h)	Yield (%)[a]
1	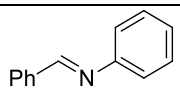	2	**5a**	1	90
2	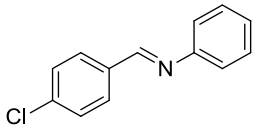	5	**5b**	1	92
3	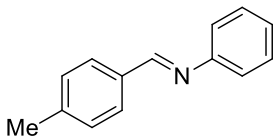	2	**5c**	1	90
4	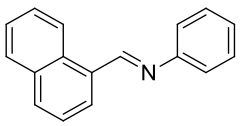	2	**5d**	2	86
5	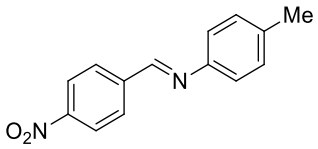	2	**5e**	0.2	90

6	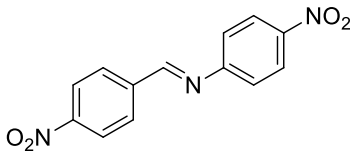	2	**5f**	24	n.r.[b]
7	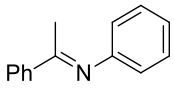	5	**5g**	24	93

Condition: N_2 atmosphere, HEH (1.2 equiv.), in DCM, room temperature, [a] Isolated yield. [b] No reaction. HEH: Hantzsch ester;

Having obtained positive results in the transfer hydrogenation reaction with quinoline and imime derivatives, challenges which were previously unresolved were attempted. Generally, the reduction of unactivated pyridine is non-trivial and there are only a limited number of reports.[13] The transfer hydrogenation reaction of pyridine is usually incompatible with Lewis acidic catalyst because of the strong Lewis basic nitrogen atom, which deactivates the Lewis acid. Using the aforementioned "goldilocks" principle of halogen bond, we envisioned that the donor we synthesized could be used as catalyst in the transfer hydrogenation reaction of pyridine with HEH. Under a similar reaction condition, 3-acetyl pyridine derivatives **3k-l** can be reduced in high yield to tetrahydropyridines **4k-l**, albeit with long reaction time (Scheme 3.1, equation 2). In addition, 1,10-phenanthroline **1j**, which cannot be reduced by other strategies, can be reduced to the corresponding 1,2,3,4-tetrahydro-1,10-phenanthroline **4j** in the presence of 5 mol% of **C1**.

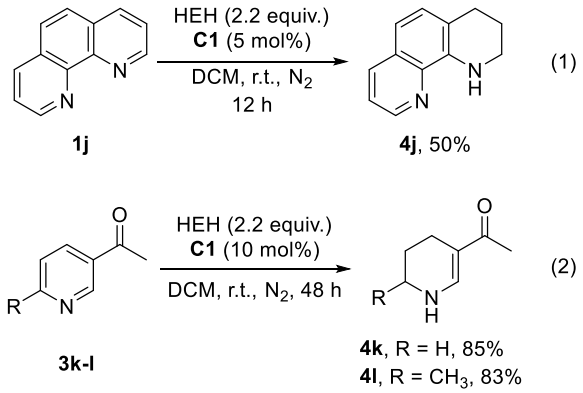

Scheme 3.1 Transfer hydrogenation of pyridine derivatives in the presence of **C1**.

3.3 NMR experiments

Although the transfer hydrogenation of C=N double bond compound with Hantzsch ester can be catalyzed by the halogen bond donor smoothly, the exact mechanism remained to be elucidated. Hence, mechanistic studies were conducted through control experiments and various characterization techniques with the goal of obtaining direct evidence to prove that the reaction is indeed induced by halogen bonding.

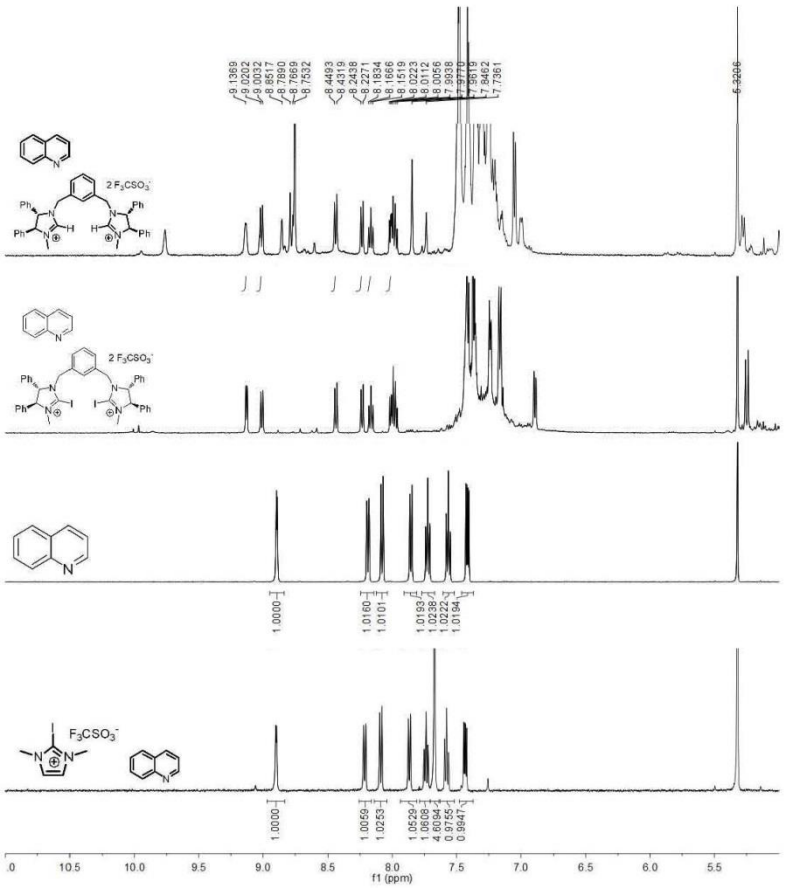

Figure 3.2 ^{1}H NMR of quinoline with different halogen bond donors in CD_2Cl_2.

In order to verify the presence of the proposed *N*-halogen interaction, we conducted several NMR experiments (Figure 3.2 and 3.3). ^{1}H NMR was used to investigate the interaction between quinoline with the halogen bond donors. Figure 3.2 shows the ^{1}H spectra of the quinoline substrate (spectrum 3). When the quinoline was mixed with 1 equivalent of halogen bond donor **C1**, the peak which belongs to the 2-position of the quinoline at 8.85 ppm was

shifted downfield significantly (Figure 3.2, spectrum 2). At the same time, when the corresponding de-iodinated complex **C2** was mixed with quinoline, since no halogen bonding interaction is possible between the starting material and the catalyst, no peak shift was observed (Figure 3.2, spectrum 1). This result can be used to explain why the reaction time required for catalyst **C2** is much longer than that for **C1** (Table 3.1, entry 2), and that halogen bonding plays a vital role in the reaction. In addition, when the NMR study was conducted with the mono-dentate halogen bonding donor **C6**, which is weaker donor than **C1,** no significant shift was observed, correlating well with our experimental results. In addition, the quinoline proton peak has no significant shift when deuterated acetonitrile (ACN) was used as the solvent. This phenomenon can be explained by the difference in polarity of the solvents, which can affect the halogen bonding interaction. Another reason is that ACN has a lone pair and it is a weak Lewis base, hence competition between ACN and quinoline weakens the NMR signal intensity of quinoline.

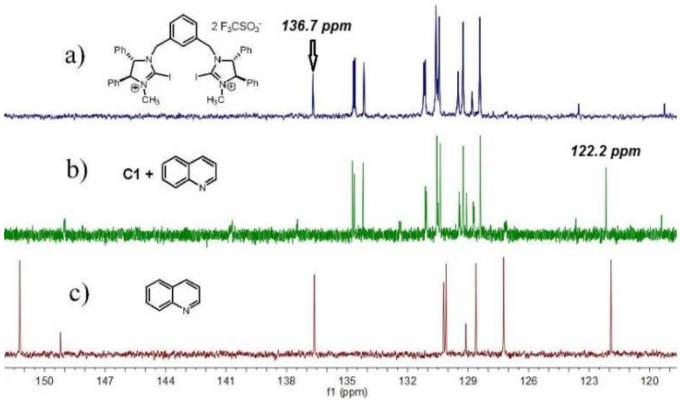

Figure 3.3 ^{13}C NMR spectra of **C1** and **1a** in CD_2Cl_2, a) **C1**; b) **C1** + **1a** (1:1); c) **1a**.

As ^{13}C NMR may be able to provide more information about the mechanism, further experiments were conducted with ^{13}C NMR to measure the shift of iodine-substituted carbon of **C1.** Through DEPT and 2D NMR (HMQC and HMDC), we concluded that the iodine-substituted carbon of **C1** has a δ = 136.7 ppm in ^{13}C NMR (Figure 3.3, spectrum a). When 1 equivalent of **1a** is added to **C1**, the peaks of **1a** were much reduced (spectrum b). On

closer inspection, it is apparent that the peaks of **1a** broadened, indicating the presence of a number of non-equivalent conformations. At the same time, the iodine-substituted carbon of **C1** shifts upfield by 14.5 ppm. Such observation was not present when triflic acid (TfOH) was added to **1a**. These NMR experiments provide indication that there is a clear interaction between the nitrogen atom of **1a** and iodine atom of **C1**. Resnati and co-workers reported the ^{19}F NMR study of the halogen bonding between halo-perfluorocarbons (halogen bond donor) and heteroatom (halogen bond acceptor).[14] Due to the halogen bonding interaction, it was observed that ^{19}F peak of the halogen bond donor shifted upfield significantly. Huber and co-workers also made similar observations in the ^{13}C NMR spectra of imidazolium halogen bond donor with its acceptor. [14]

Isothermal titration calorimetry (ITC) is a physical technique used to determine the thermodynamic parameters of interactions in solution. It is often used to study the binding of small molecules (such as medicinal compounds) and larger macromolecules. In 2012, ITC was first used to determine the halogen bond strength of XB donors by Huber.[14] The binding constant and ΔH, which are important data to measure the strength of the XB donors, can be measured by using ITC. As a brief explanation of ITC, the sample cell in the ITC instrument is involved in keeping the cell at constant temperature. The sample in the cell is termed host, while guest is the sample of interest, with which interaction with the host can be tested by introducing into the cell by a syringe at a constant rate. When each drop is injected into the cell, thermal effects are detected by the instrument, and this corresponds to a peak in the spectra. Through calculations conducted with a software, the molarity, ΔH, ΔS and the binding constant of this interaction between host and guest can be obtained. The strength of the interaction between these two compounds is then inferred from the binding constant. Hence, we envision that ITC can be used in our study of the halogen bond donor to gain further insights into the reaction mechanism.

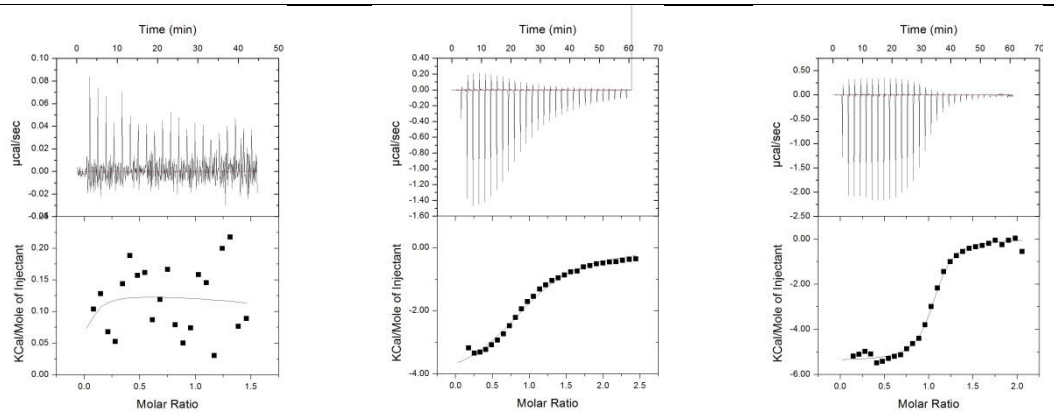

a) **C1** + quinoline b) **C1** + *n*Bu$_4$NBr **c) C4** + *n*Bu$_4$NBr

Figure 3.4 ITC spectra of halogen bond donor with acceptor.

The halogen bond donor **C1** and quinoline substrate were first used as the titration host and guest, respectively, and the resultant titration curve was obtained (Figure 3.4, a). As seen from the figure, no significant thermal effect between catalyst and substrate was observable. However, when anionic bromide, a classic halogen bond acceptor, was used as the titration guest, a standard titration curve was obtained with a significant thermal effect observed between **C1** and bromide (Figure 3.4, b), in a classic halogen bonding interaction. Donor **C4** was then used as host and Br^- was titrated into this solution, which resulted in the bonding constant larger than **C1**. Interestingly, in the previous experiments, **C4** was a less effective catalyst as compared to **C1** (Table 3.2, entries 1 and 4). The apparent disparity could be due to the fact that as compared to **C1**, the interaction of **C4** with the acceptor can be more easily disrupted by strong Lewis bases, such as the pyridine by-product and quinoline. A complex may be formed, and the catalyst cannot be regenerated in the catalytic cycle. At the same time, the binding constant of **C1** with quinoline is so weak that no obvious peak was found in the spectrum. This implies that the interaction between quinoline with **C1** is not strong enough for irreversible complex formation, hence **C1** can be regenerated in this reaction. Thus, the effectiveness of a halogen bond donor as a catalyst as observed in our experimental studies

conforms to the “goldilocks” principle, which is a unique property of halogen bond donor as a catalyst.

Table 3.4 ITC data of halogen bond donor with acceptor.

Entry	Guest	Host	K [mol^{-1}]	ΔH [kJ/mol]	$T\Delta S$ [kJ/mol]
1	**1a**	**C1**	-	-	-
2	Bu_4NBr	**C1**	3.29E4	-18.0	7.8
3	Bu_4NBr	**C4**	4.57E5	-22.6	9.7

Conditions: Halogen bond donors (0.2 mM), halide (2 mM)

3.4 Chiral version of transfer hydrogenation reaction of quinoline with HEH

After investigation of the achiral hydrogenation reaction of quinoline with HEH, and considering the unique properties of halogen binding, we envisioned that a chiral halogen bond donor could be used to control the enantioselectivity of this reaction. Several chiral halogen bond donors were synthesized, which are shown in Figure 3.5. The effectiveness of these chiral halogen bond donor as catalysts in the transfer hydrogenation reaction of 2-phenyl quinoline with HEH as model reaction were then investigated.

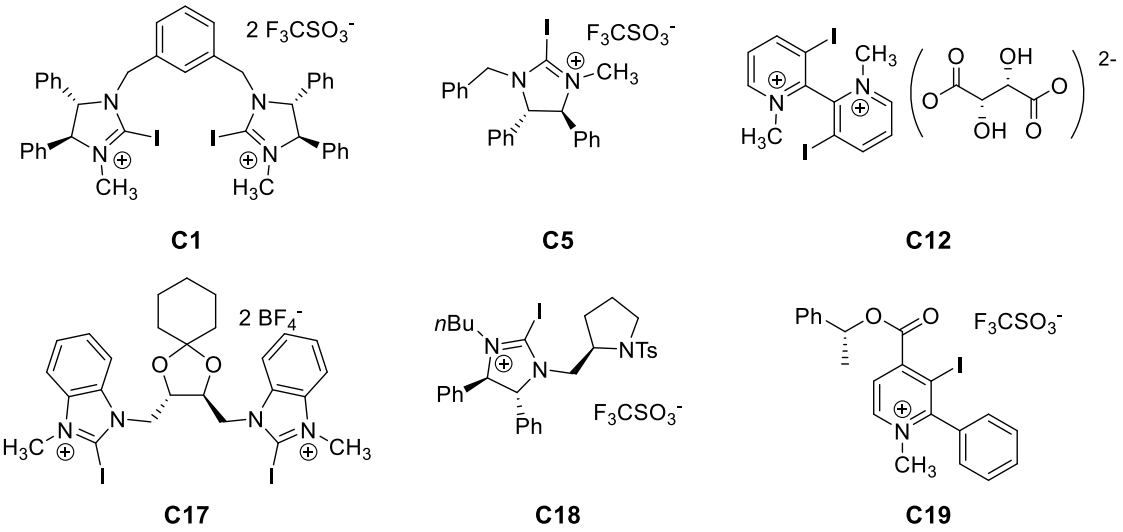

Figure 3.5 Chiral halogen bond donors.

Table 3.5 Screening of conditions for the chiral transfer hydrogenation.

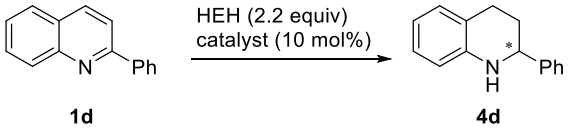

1d 4d

Entry	Catalyst	Solvent	T (°C)	t (hour)	Yield[a] (%)	*ee*[b]
1	**C1**	DCM	r.t.	2	> 95	0
2	**C1**	THF	r.t.	2	90	< 2
3	**C1**	ACN	r.t.	2	90	< 2
4	**C1**	Toluene	r.t.	2	85	< 2
5	**C1**	Hexane	r.t.	2	70	< 2
6	**C1**	Et_2O	r.t.	2	85	< 2
7	**C1**	DCM	0	24	84	< 2
8	**C1**	DCM	-10	24	83	< 2
9	**C1**	DCM	-30	48	85	< 2
10	**C5**	DCM	r.t.	5	90	< 2
11	**C12**	DCM	r.t.	5	89	< 2
12	**C17**	DCM	r.t.	3	92	< 2
13	**C18**	DCM	r.t.	5	93	< 2
14	**C19**	DCM	r.t.	5	83	< 2

Condition: N_2 atmosphere, HEH (2.2 equiv.), in DCM, room temperature, [a]Isolated yield. HEH: Hantzsch ester.

Several commonly used solvents were tested in the model reaction in presence of **C1** as catalyst (Table 3.5, entries 1-6). We found no significant change in the enantioselectivity when different solvents were used, and almost all of *ee* values of the product obtained were close to 0. However, the yield of these reactions is high. Due to the apparent lack of influence of solvent choice on the enantioselectivity, different chiral halogen bond donors were subjected to the reaction conditions in the model reaction. Donors **C5** and **C18** (Table 3.5, entries 10 and 13), which are the mono-dentate catalysts with a chiral functional group, showed no enantioselectivity for this reaction. Donor **C12** is based on the bipyridine backbone and contains a chiral counter anion. However, when tested, no *ee* of significance was obtained (Table 3.5, entry 11). No enantioselectivity was obtained in presence of 10 mol% of donor **C17**,

which has a chiral backbone (Table 3.5, entry 12). Similar results were obtained when donor **C19** was used as the catalyst (Table 3.5, entry 14). All of these halogen bond donors can catalyze this reaction smoothly, but without any enantioselectivity. The model reaction was conducted at low temperature, 0 °C, -10 °C and -30 °C, with **C1** as catalyst to investigate the effect of temperature on the reaction selectivity (Table 3.5, entries 7-9). As anticipated, the reaction rate decreased significantly so that a longer reaction time was required to achieve a good yield. However, no enantioselectivity was observed as was the case for the reaction at room temperature.

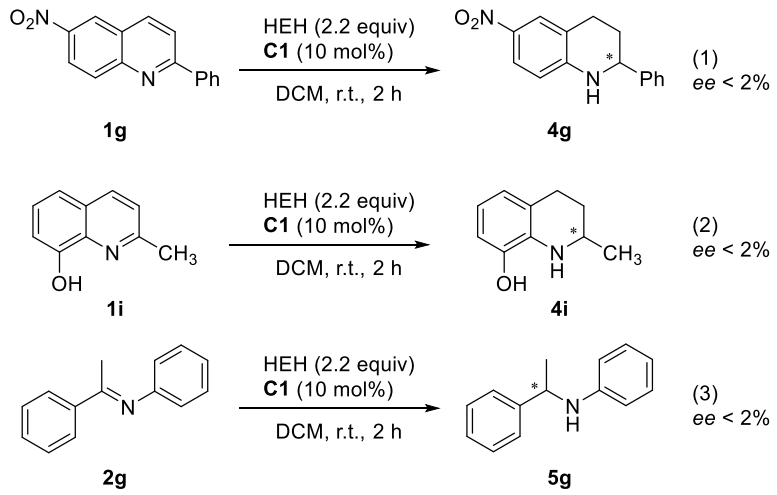

Scheme 3.2 Chiral version of transfer hydrogenation of C=N compounds.

Different substrates were tried in the chiral version of transfer hydrogenation reaction with **C1** as the catalyst (Scheme 3.2). As the nitro group is a classic halogen bond acceptor, the quinoline substrate with a nitro group on the 6-position was first tested, but no enantioselectivity was obtained (Scheme 3.2, eq. 1). Reduction of **1i** took place smoothly but with no enantioselectivity. Finally, when imine-type starting material **2g** was tested, similar results as the quinoline substrates were obtained, and no selectivity was observed (Scheme 3.2, eq. 2).

Through the investigation of the chiral version of the transfer hydrogenation reaction of C=N compounds with HEH, no enantioselectivity was obtained despite the range of halogen

bond donors tested, although it has been demonstrated that this reaction was indeed activated by halogen bonding interaction. Such results are in-line with the literature, in which no example of halogen bond induced asymmetric reaction has been reported to date. Considering the results which have been published and our experimental results, we propose that due to the long bond length of the C-X bond (for example the bond length of C-I is 2.08 Å), the active site on the substrate is far away from the chiral group of the catalyst in the halogen bonding induced reaction. Therefore, the chiral control is difficult to achieve when a simple chiral halogen bond donor is used. Further optimization of the halogen bonding interaction induced asymmetric reaction would likely include the design and synthesis of a new type of donor to overcome this key limitation.

3.5 Conclusion

In conclusion, we have prepared a series of novel halogen-bonding donors based on a bidentate dihydroimidazoline core. One of these donors, imidazolium **C1**, was found to be an efficient catalyst for the transfer hydrogenation of C=N bond with Hantzsch ester. Highly efficient reactions were observed for quinolines and imines with low catalyst loading of 2 mol%. The presence of halogen bonding was confirmed using NMR studies and isothermal calorimetric titrations. Binding constants of the halogen bond donors were also measured using isothermal titration calorimetry (ITC). Imidazolium **C1** was found to have a lower binding constant than an analogue **C4**, indicating that the effectiveness of a XB donor as a catalyst can be predicted by the "goldilocks" principle. The asymmetric transfer hydrogenation of the C=N bond with HEH was further investigated by using different types of chiral halogen bond donors. However, poor enantioselectivity was observed, presumably due to the long distance between the active site and the chiral functional group of the halogen bond donor, which constitutes the greatest difficulty that has to be overcome in future studies.

References

[1] For selected reviews, see: (a) Knowles, W. S. *Angew. Chem., Int. Ed.* **2002**, *41*, 1998; (b) Noyori, R. *Angew. Chem., Int. Ed.* **2002**, *41*, 2008; (c) Tang, W.; Zhang, X. *Chem. Rev.* **2003**, *103*, 3029; (d) Blaser, H.-U.; Malan, C.; Pugin, B.; Spindler, F.; Steiner, H.; Studer, M. *Adv. Synth. Catal.*, **2003**, *345*, 103; (e) Cui, X.; Burgess, K. *Chem. Rev.* **2005**, *105*, 3272; (f) Jäkel, C.; Paciello, R. *Chem. Rev.,* **2006**, *106*, 2912; (g) Gladiali, S.; Alberico, E. *Chem. Soc. Rev.* **2006**, *35*, 226.

[2] (a) Alberts, B.; Bray, D.; Lewis, J.; Raff, M.; Roberts, K.; Watson, J. D.; Molecular Biology of the Cell, Garland, New York & London, 3rd edn, **2002**; (b) Berg, J. M.; Tymoczko, J. L.; Stryer, J. L. L.; Biochemistry, W. H. Freeman & Company, New York, 5th edn, 2002.

[3] (a) Hantzsch, A. *Ber. Dtsch. Chem. Ges.*, **1881**, *14*, 1637; (b) Hantzsch, A. *Justus Liebigs Ann. Chem.*, **1882**, *215*, 1–82.

[4] For reviews on transfer hydrogenation reactions with Hantzsch esters, see: (a) Adolfsson, H. *Angew. Chem., Int. Ed.* **2005**, *44*, 3340; (b) Rosen, J. *Chemtracts*, **2005**, *18*, 65; (c) You, S.-L. *Chem.–Asian J.* **2007**, *2*, 820; (d) Ouellet, S. G.; Walji, A. M.; MacMillan, D. W. C. *Acc. Chem. Res.* **2007**, *40*, 1327; (e) Connon, S. J. *Org. Biomol. Chem.* **2007**, *5*, 3407; (f) Wang, C.; Wu, X.; Xiao, J. *Chem.–Asian J.* **2008**, *3*, 1750; (g) Rueping, M.; Sugiono, E.; Schoepke, F. R. *Synlett* **2010**, 852; (h) Rueping, M.; Dufour, J.; Schoepke, F. R. *Green Chem.* **2011**, *13*, 1084; (i) Zheng, C.; You, S.-L. *Chem. Soc. Rev.* **2012**, *41*, 2498.

[5] For selected examples of racemic transfer hydrogenation with Hantzsch esters, see: (a) Steevens, J. B.; Pandit, U. K.; *Tetrahedron*, **1983**, *39*, 1395; (b) Fujii, M.; Aida, T.; Yoshihara, M.; Ohno, A. *Bull. Chem. Soc. Jpn.* **1989**, *62*, 3845; (c) Itoh, T.; Nagata, K.; Kurihara, A.; Miyazaki, M.; Ohsawa, A. *Tetrahedron Lett.* **2002**, *43*, 3105; (d) Zhang, Z.; Gao, J.; Xia, J.-J.; Wang, G.-W. *Org. Biomol. Chem.* **2005**, *3*, 1617; (e) Menche, D.; Hassfeld, J.; Li, J.; Menche,

G.; Ritter, A.; Rudolph, S. *Org. Lett.* **2006**, *8*, 741; (f) Liu, Z.; Liu, Q.; Zhang, W.; Mu, R.; Yang, L.; Liu, Z.-L.; Yu, W. *Synthesis* **2006**, 771; (g) Menche, D.; Arikan, F. *Synlett* **2006**, 841; (h) Rueping, M.; Theissmann, T.; Antonchick, A. P.; *Synlett* **2006**, 1071; (i) Menche, D.; Böhm, S.; Li, J.; Rudolph, S.; Zander, W. *Tetrahedron Lett.* **2007**, *48*, 365; (j) Zhang, Z.; Schreiner, P. R. *Synthesis* **2007**, 2559; (k) Zhang, Z.; Schreiner, P. R. *Synlett* **2007**, 1455; (l) Zhou, J.; List, B. *Synlett* **2007**, 2037; (m) Bruckmann, A.; Pena, M. A.; Bolm, C. *Synlett* **2008**, 900; (n) Che, J.; Lam, Y. *Synlett* **2010**, 2415; (o) Zhang, M.; Yang, H.; Zhang, Y.; Zhu, C.; Li, W.; Cheng, Y.; Hu, H. *Chem. Commun.* **2011**, *47*, 6605.

[6] Singh, S.; Batra, U. K. *Indian J. Chem.* **1989**, *28B*, 1.

[7] For selected reviews, see: (a) Akiyama, T.; *Chem. Rev.* **2007**, *107*, 5744; (b) Terada, M. *Chem. Commun.* **2008**, 4097; (c) Terada, M. *Synthesis* **2010**, 1929; (d) Terada, M. *Bull. Chem. Soc. Jpn.* **2010**, 101; (e) Zamfir, A.; Schenker, S.; Freund, M.; Tsogoeva, S. B. *Org. Biomol. Chem.* **2010**, *8*, 5262; (f) Rueping, M.; Kuenkel, A.; Atodiresei, I. *Chem. Soc. Rev.* **2011**, *40*, 4539; (g) Rueping, M.; Nachtsheim, B. J.; Ieawsuwan, W.; Atodiresei, I. *Angew. Chem., Int. Ed.* **2011**, *50*, 6706.

[8] Rueping, M.; Sugiono, E.; Azap, C.; Theissmann, T.; Bolte, M. *Org. Lett.* **2005**, *7*, 3781.

[9] (a) Lu, S.-M.; Wang, Y.-Q.; Han, X.-W.; Zhou, Y.-G. *Chin. J. Catal.* **2005**, *26*, 287; (b) Wang, D.-W.; Zeng W.; Zhou, Y.-G. *Tetrahedron: Asymmetry* **2007**, *18*, 1103.

[10] Rueping, M.; Antonchick, A. P. *Angew. Chem., Int. Ed.* **2007**, *46*, 4562.

[11] Ye, Z.-S.; Chen, M.-W.; Chen, Q.-A.; Shi, L.; Duan, Y.; Zhou, Y.-G. *Angew. Chem. Int. Ed.* **2012**, *51*, 10181.

[12] Dang, T. T.; Boeck, F.; Hintermann, L. *J. Org. Chem*. **2011**, *76*, 9353.

[13] Mentrangolo, P.; Panzeri, W.; Recupero, F.; Resnati, G. *J. Fluorine. Chem.* **2002**, *114*, 27.

[14] Walter, S. M.; Kniep, F.; Herdtweck, E.; Huber, S. M. *Angew. Chem. Int. Ed.* **2011**, *50*, 7187.

Chapter 4

Halogen bonding interaction induced [3+2] cycloaddition

4.1 Introduction

1,3-Dipolar cycloaddition reactions are among the most useful methods for the synthesis of five-membered heterocycles.[1] In fact, the five-membered heterocyclic rings found in the structures of some natural products can be constructed directly through such reactions.[1c, 2] The structure and stereochemistry of the cycloadducts depend largely on electronic nature of dipole and dipolarophile as 1,3-dipolar cycloaddition typically proceeds via a concerted mechanism.[1] Like nitrile oxides, nitrones are among the most useful 1,3-dipoles for dipolar cycloaddition.[3] Thus, cycloadditions involving nitrones, followed by functional group transformations, which include reductive cleavage of the nitrogen-oxygen bond of cycloadducts, have found wide synthetic applications in the construction of complex structures in natural products. [4]

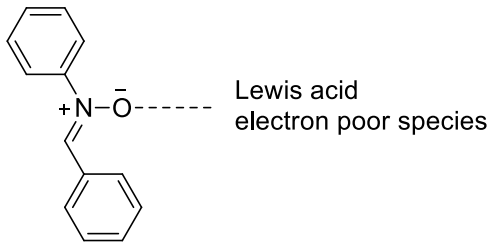

Figure 4.1 Deactivation of normal Lewis acid in presence of nitrone.

Based on numerous reports on successful Lewis acid-catalyzed Diels-Alder reactions with high stereo-control, [5] similar Lewis acid catalysis is expected to be applicable in dipolar cycloadditions. However, only several metal-based Lewis acid catalyzed reactions have been reported to date[6] and examples of organic Lewis acid catalysis are very rare. A possible impediment in these reactions is that 1,3-dipoles act as much stronger bases than dienes and show zwitterionic character. Most of the 1,3-dipoles are known to react with Lewis acids to give stable ionic salts, which are reluctant to undergo cycloaddition. Only a few 1,3-dipoles have been known to react with Lewis acids to give unstable ionic salts that exhibit 1,3-dipolar nature and undergo highly selective cycloaddition reaction with dipolarophiles.[7] On the other hand, halogen bonding donors have been demonstrated to activate carbonyl compound in a

similar manner as Lewis acids, and halogen bonding donors are stable in the presence of Lewis bases. Considering these advantages, the efficiency of halogen bonding donors synthesized were investigated in the [3+2] cycloaddition of nitrones with the alkenes.

4.2 Experiment

A series of halogen bond donors synthesized in the previous study were used in the [3+2] cycloaddition of nitrones with alkene. The alkene chosen was an α, β-unsaturated carbonyl compound. First, bipyridinium type halogen bond donor **C8** was used as the catalyst, with *N*-phenyl-*N*-[(*Z*)-phenylmethylene] amine oxide and ethyl methacrylate as the starting materials (Figure 4.2). The major product, compound **8**, was obtained in moderate yield with high *d.r.* value. When a classic strong Lewis acid, $MgBr_2$, was used instead, a low yield of only 15% was achieved. In the absence of catalyst, the reaction can occur under heating conditions, but the major product is compound **9**, and the *d.r.* is only 5:1. With these initial results, more detailed condition screening was conducted to probe the mechanism.

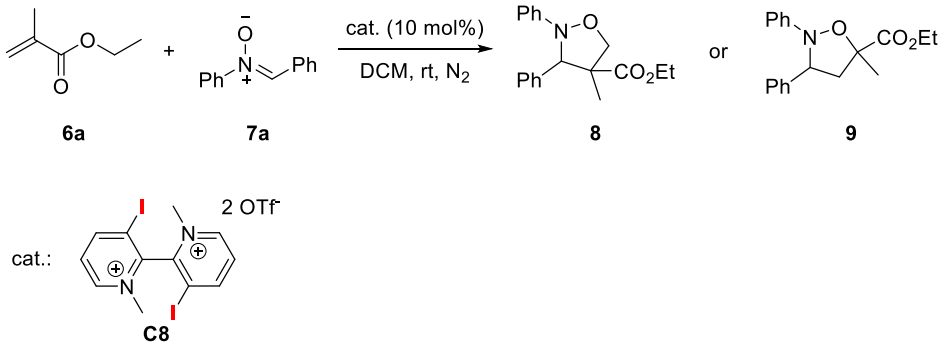

Figure 4.2 Initial results of using XBs donor as catalyst in [3+2] cycloaddition.

The temperature, reaction time and solvent were first varied to find optimal reaction conditions. The reaction in DCM resulted in a lower yield than that in ACN, which could be due to the poor solubility of the catalyst in DCM (Table 4.1, entry 1). Similar results were obtained by using THF, hexane and toluene as the solvent (Table 4.1, entries 3-5). The reaction became sluggish at a lower temperature of – 20 ^{o}C (Table 4.1, entry 6). In the absence of

halogen bond donor catalyst, only trace amount of **7a** was consumed even after a prolonged reaction time to 48 h (Table 4.1, entry 7).

Table 4.1 Reaction condition screening of [3+2] cycloaddition.

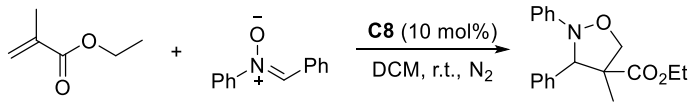

6a **7a** **8a**

Entry	Temp. (°C)	Solvent	t (hour)	Yield (%)[a]
1	r.t.	DCM	24	42
2	r.t.	ACN	24	79
3	r.t.	THF	24	35
4	r.t.	Hexane	24	22
5	r.t.	Toluene	24	32
6	- 20	ACN	24	10
7[b]	r.t.	ACN	48	10
8	r.t.	ACN	10	60

Condition: **6a** (0.4 mmol), **7a** (0.2 mmol), in 1 mL solvent; [a] Isolated yield. ACN = acetonitrile; [b] no catalyst.

Upon determination of the optimal solvent and temperature, several halogen bond donors were evaluated (Figure 4.3). The desired product was obtained in 79% yield in the presence of charged bipyridinium donor **C8**. The reaction using the singly-charged donor **C14** gave a much lower yield of 40%. A further decrease was observed in the reaction with mono-dentate donor **C15** as the catalyst. It is thus apparent that stronger halogen bond donors have higher activity. Additionally, when neutral donor **C16** was tested, the yield decreased dramatically, with only trace amount of product detected. When compound **C13**, which is the non-iodine containing analogue of **C8** and does not act as a halogen bond donor, was used, the reaction did not complete even after 24 h. The halogen bonding interaction is thus necessary for this reaction. During the catalyst synthesis, a halogen bond donor with a chiral counter anion was obtained, and this donor **C12** was used in the [3+2] cycloaddition. While the activity of **C12** is similar to

that of a non-chiral donor, no enantioselectivity was obtained. It is hence concluded that the charge assistant halogen bond donor is better than the corresponding neutral donor, and bidentate donors have higher activity than the mono-dentate analogues. More importantly, the halogen bond donor is significantly better than corresponding non-halogen containing compounds, which provides direct evidence to prove the key role of halogen bonding interaction in this reaction.

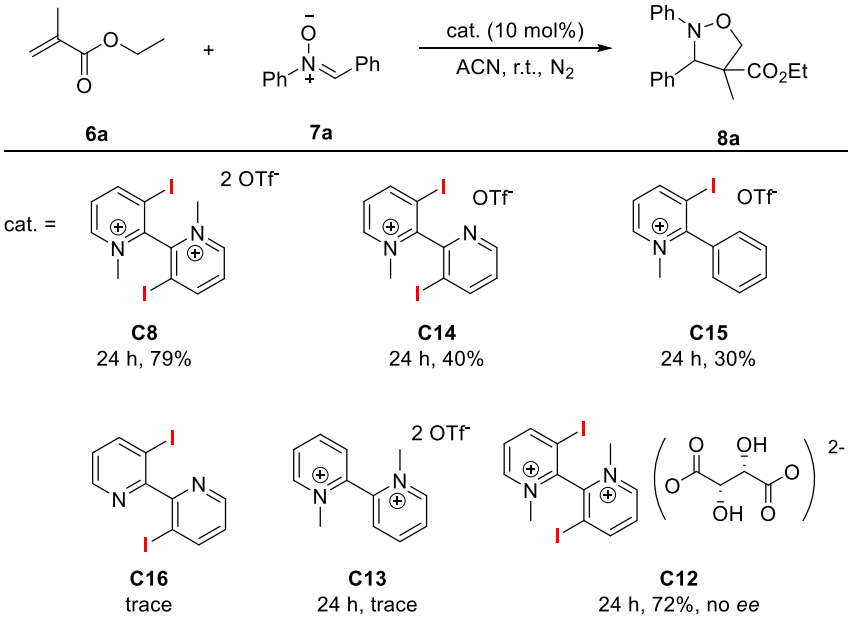

Figure 4.3 Halogen bond donor screening.

With the optimal conditions in hand, the substrate scope was further explored to investigate the functional group compatibility of the reaction (Table 4.2). For α, β-unsaturated carbonyl compounds, substrates with substituted methyl, ethyl and even sterically bulky *tert*-butyl were tolerated in the reaction, and the desired products were isolated in high yield (Table 4.2, entries 2-4). When the ester functionality was substituted with a phenyl ring, the yield of the product remained high (Table 4.2, entry 5). However, if compounds **6g** and **6h**, which consist of further modifications on the alkene functionality, were used as starting materials, only trace product was obtained (Table 4.2, entries 7-8). Hence, only terminal alkene is suitable in this catalyst system.

Table 4.2 Substrate scope of the [3+2] cycloaddition.

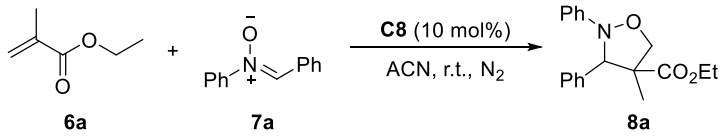

Entry	7	6	8	Yield (%)[a]
1	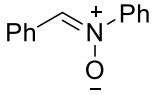 **7a**	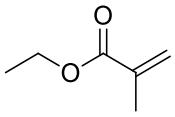 **6a**	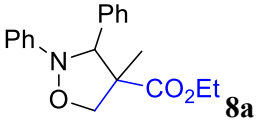 **8a**	65
2	**7a**	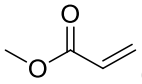 **6b**	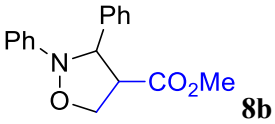 **8b**	82
3	**7a**	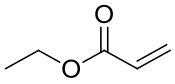 **6c**	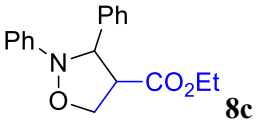 **8c**	79
4	**7a**	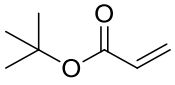 **6d**	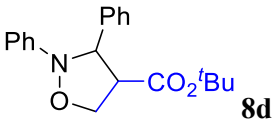 **8d**	77
5	**7a**	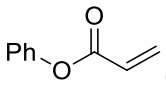 **6e**	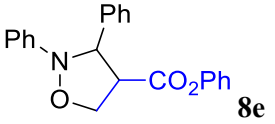 **8e**	81
6	**7a**	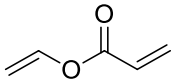 **6f**	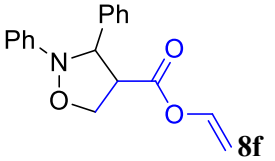 **8f**	76
7	**7a**	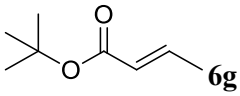 **6g**	**8g**	trace
8	**7a**	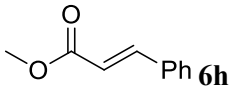 **6h**	**8h**	trace
9	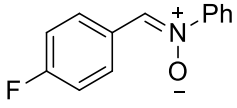 **7b**	**6a**	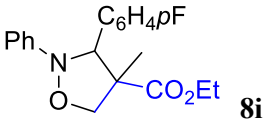 **8i**	68
10	**7b**	**6b**	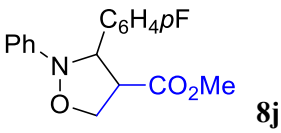 **8j**	83

11	**7b**	**6c**	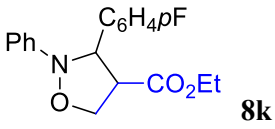 **8k**	81
12	**7b**	**6d**	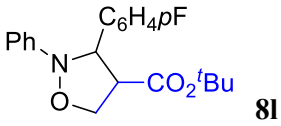 **8l**	75
13	**7b**	**6f**	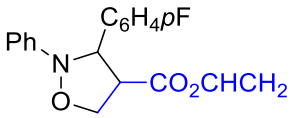 **8m**	75

Condition: **6** (0.4 mmol), **7** (0.2 mmol), in 1 mL ACN; 24 h[a] Isolated yield.

ACN = acetonitrile

In the substrate scope analysis, most of α, β-unsaturated carbonyl compounds tested are suitable for this halogen bond interaction induced reaction. However, the lack of direct evidence to prove the involvement of halogen bond interaction in the reaction remains a key issue. Hence, further mechanistic studies were conducted to investigate the interaction between catalyst and starting material.

4.3 NMR study

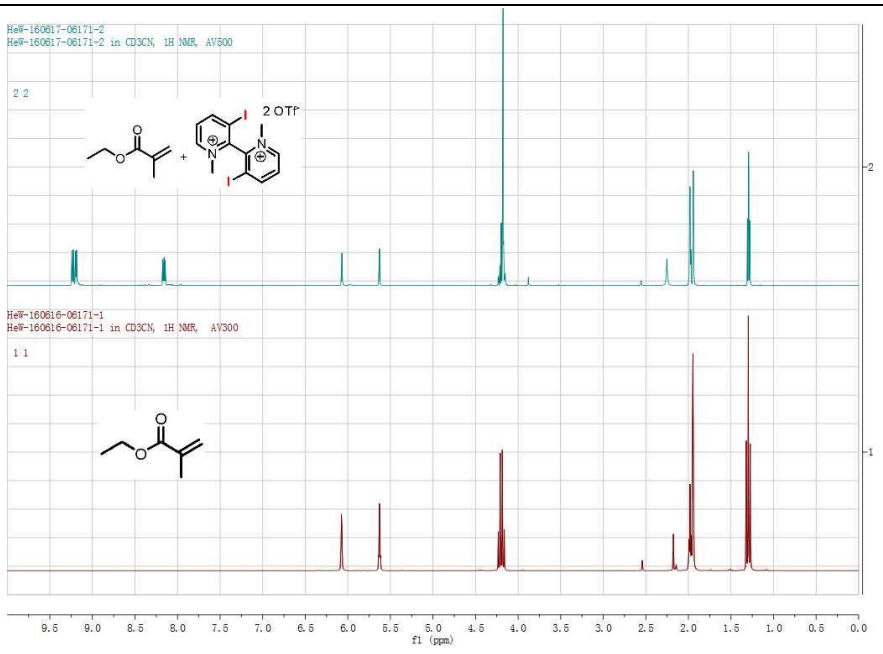

Figure 4.4 ^{1}H NMR spectra of **6a** mixed with halogen bond donor **C8** in 1:1 ratio.

The interaction of catalyst with starting material was first investigated with NMR. The ^{1}H NMR of starting material **6a** in deuterium acetonitrile was obtained (Figure 4.4, bottom), and 1.0 equivalent of halogen bond donor **C8** was added into the **6a** sample for comparison of these two NMR spectra. From the spectra, there is no shifting or weakness of the peak of **6a** observed (Figure 4.4, top), indicating that no polymerization occurred when the catalyst was added into the alkene starting material. From the outcome of the 1H NMR study, it can be assumed that there is no significant interaction between the starting material with the catalyst. Inspired by the previous work about halogen bonding study, it was decided that further studies would be carried out with ^{13}C NMR.

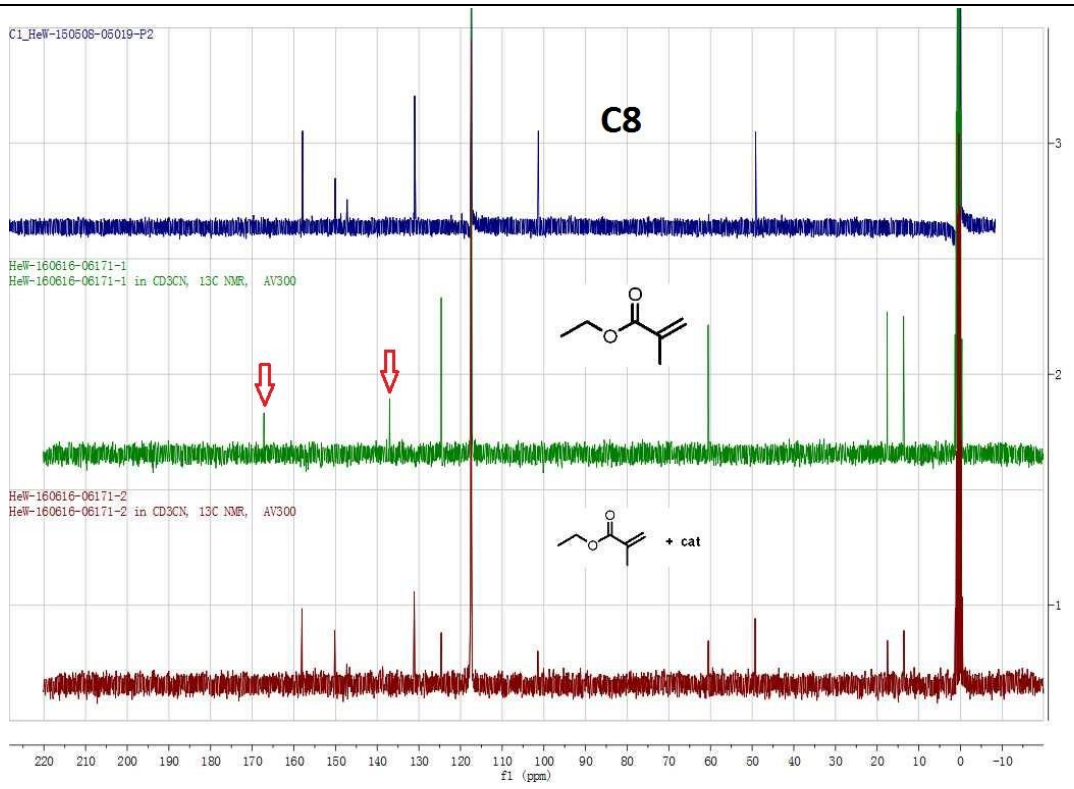

Figure 4.5 ^{13}C NMR spectra of **6a** mixed with halogen bond donor **C8** in CD_3CN.

The ^{13}C NMR test was repeated under the same reaction conditions to prove that the absence of a non-covalent interaction between starting material and the XB donor. From the spectra (Figure 4.5, bottom), it can be observed that when 1 equivalent of XB donor was added into the **6a** sample, the peak at 167.19 ppm corresponding to the carbon of the carbonyl, and the

peak at 137.02 pm corresponding to the carbon of the double bond, were significant weakened, although the rest of the peaks remain identical with that of the pure **6a** compound. It is known that the carbonyl can act as a Lewis base, and it is a halogen bonding acceptor also.[8] Hence, it is proposed that the double bond can be activated during the halogen bonding interaction between the carbonyl group and catalyst **C8**.

Similar NMR experiments were conducted by using nitrone **7a** mixed with catalyst **C8**. No significant change was observed in both ^{1}H and ^{13}C NMR spectra, which proves that the nitrone compound cannot deactivate the catalyst, even though it is a strong Lewis base. This finding thus presents the advantage of using halogen bond donor as catalyst in such reactions.

4.4 IR study

FTIR is commonly used to investigate the existence of the halogen bonding and when combined with other analytical techniques, the strength of halogen bonding can be measured. In the scenario that there is interaction between the acceptor and donor, the vibration of the bond will be inhibited, affecting the intensity of the peak. Conversely, the peak which is activated by halogen bonding usually exhibit a shift from high (blue shift) to low (red shift) wave numbers. In the FTIR spectrum of sample **6a**, the peak corresponding to the vibrational stretching of C=O is at 1720.50 cm^{-1}, and C=C is at 1635.64 cm^{-1} (Table 4.3). In the presence of 1.0 equivalent of catalyst **C8**, which is a halogen bonding donor, the spectrum of **6a** shows a significant weakening of the C=O peak, and the C=C peak was shifted to lower wave numbers of 1597.06 cm^{-1}.

Combined with the experimental results obtained earlier, a reasonable mechanism can be proposed in which the catalytic effect is on the carbonyl group of the substrate and is through halogen bonding interaction. This subsequently leads to the activation of the conjugated C=C double bond.

Table 4.3 IR shift of starting material **6a** mixed with catalyst.

Bond	**6a**	**6a + C8**	**Result**
C=O	1720.50 cm^{-1}	1720.50 cm^{-1}	weakened
C=C	1635.64 cm^{-1}	1597.06 cm^{-1}	red shift 38.58 cm^{-1}

IR spectra (a): pure compound **6a**

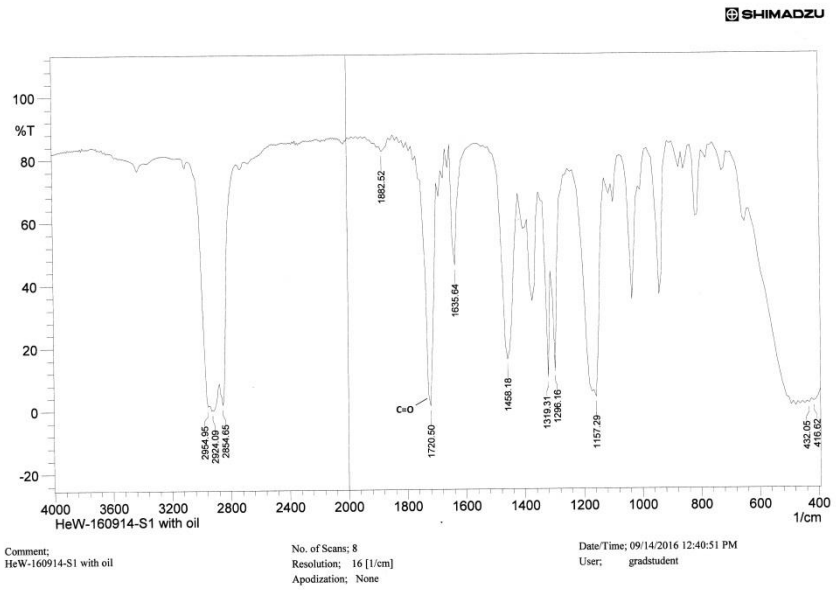

IR spectra (b): pure compound **6a** + catalyst **C8** (1:1)

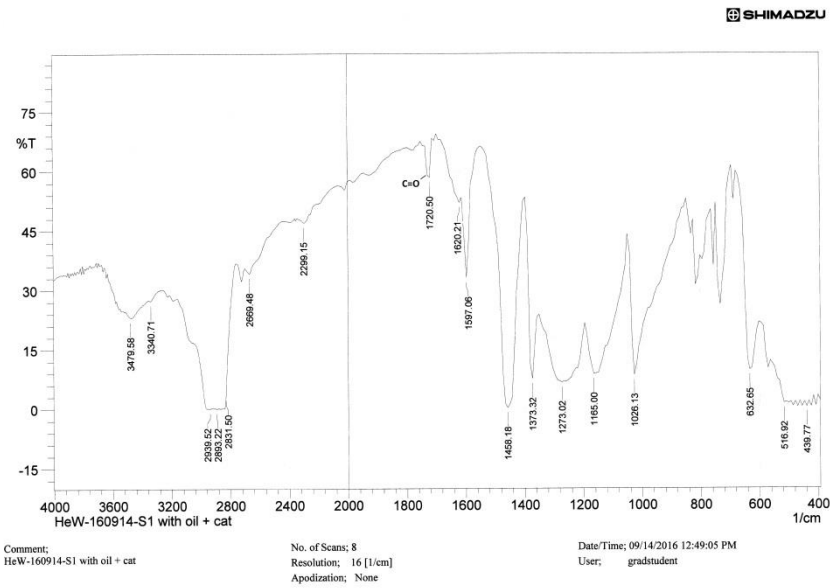

4.4 Conclusion

In conclusion, we have prepared a series of novel halogen-bonding donors based on a bipyridine core. Out of these donors, bidentate **C8** was found to be an efficient catalyst for the [3+2] cycloaddition of nitrones with alkene, which is difficult to be catalyzed by normal organic Lewis acid. Highly efficient reactions were observed for α, β-unsaturated ester when a catalyst loading of 10 mol% was used. The presence of halogen bonding was further confirmed using NMR, FTIR, and X-ray.

References

[1] (a) Padwa, A. (ed.), "1,3-Dipolar Cycloaddition Chemistry," Interscience, New York, 1984; (b) Bianchi G.; Micheli C. D.; Gandolfi R.; "The Chemistry of Doublebonded Functional Groups," Vol. 1, ed. by Patai S., Interscience, New York, 1977, pp. 369-532; (c) Carruthers W. "Cycloaddition Reaction in Organic Synthesis," Pergamon Press, New York, 1990, pp. 269-331.

[2] Confalone, P. N.; Huie, E. M. *Org. React.* **1988**, *36*, 1-173.

[3] (a) TufaIiellO, J. J. "Nitrones," as Chapter 9 of Vo1 2 of "1,3-Dipolar Cycloaddition Chemistry," ed by Padwa, A.; John Wiley & Sons, New York (1984), pp 83-168; (b) Breuer, E.; Aurich, H. G.; Nielsen, A. "Nitrones. nitronates and nitroxides." ed by Patai, S.; Rappoport, Z., John Wiley & Sons, New York (1989), pp 139-312.

[4] (a) Desimoni, G.; Tacconi, G.; Barco, A.; Pollini. G. P. "Natural Product Synthesis through Pericyclic Reactions," American Chemical Society, Washington (1983), pp. 89-117; (b) Padwa, A.; Schoffstall, A. M. "Jntramolecular 1,3-Dipolar Cycloaddition Chemistry," in "Advances in Cycloaddition," ed by Curran, D. P., Vol 2, JAI Press, Greenwich (1990), pp. l-89.

[5] (a) Taschner, M. J. "Asymmetric Diels-Alder Reactions," in "Organic Synthesis - Theory and Applications," ed by Hudlicky, T., Vol 1. JAI Press, Greenwich (1989). pp. l-101; (b)

Carmthers, W. “Cycloaddition Reactions in Organic Synthesis,” Pergamon Press, Oxford (1990), pp. l-208.

[6] Metal-assisted dipolar cycloadditions: (a) Barr, D. A.; Grigg, R.; Gunaratune, H. Q. N.; Kemp, J.; McMeekin, P.; Stidhamn. V. *Tetrahedron* **1988**, *44*, 557; (b) Tsuge, O.; Kanemasa, S.; Yoshioka, M. *J. Org. Chem.* **1988**, *53*,1384; (c) Allway, P.; Grigg. R. *Tenahedron Lett.* **1991**, *32*, 5817.

[7] (a) Tamura, O.; Yamaguchi, T.; Okabe, T.; Sakamoto, M. *Synlett* **1994**, 620; (b) Glibertson, S. R.; Dawson, D. P.; Lopez, O. D.; Marshall, K. L.; *J. Am. Chem. Soc.* **1995**, *117*, 4431; (c) Kanemasa, S.; Tsuruoka, T.; Yamamoto, H. *Tetrahedron Lett.* **1995**, *36*, 5019; (d) Kanemasa, S; Tsuruoka, T.; *Chem. Lett.* **1995**, 49; (e) Gothelf, K. V.; Thomsen, I.; Jørgensen, K. A.; *J. Am. Chem. Soc.* **1996**, *118*, 59; (f) Gothelf, K. V.; Jørgensen, K. A.; *Acta Chem. Scand.* **1996**, *50*, 652; (g) Gothelf, K. V.; Jørgensen, K. A.; *Chem. Rev.* **1998**, *98*, 863; (h) Gothelf, K. V.; Jørgensen, K. A. J. *Chem. Soc. Chem. Commun.* **2000**, 1449.

[8] Kniep, F.; Walter, S. M.; Herdtweck, E.; Huber, S. M. *Chem. Eur. J.* **2012**, *18*, 1306.

Chapter 5

Experimental

5.1 General information

A. Chemicals

Chemicals were obtained from ABCR, Acros Organics, Alfa Aesar, Merck, Sigma-Aldrich or VWR. Unless otherwise stated, commercially available reagents and starting materials were used without further purification. Solvents which were to be used in moisture-sensitive experiments were taken from a solvent drying system by M. Braun (MB SPS-800) and stored under an argon atmosphere. Other solvents were used after single distillation.

For reactions including oxygen- or moisture-sensitive reagents, glassware was baked out in high vacuum conditions and reaction procedures were carried out under an argon atmosphere. Reagents were injected via a septum or added under argon counter-flow.

B. Instrumentations and materials

Isothermal titration calorimetry (ITC) experiments were performed on a MicroCal iTC200 system.

Thin layer chromatography (TLC) was performed on plates from Merck (silica gel 60, F_{254}). Detection was carried out by fluorescence detection under UV light (wavelength, λ = 254 nm). The corresponding R_f values and eluent solvents are listed in the experimental section. Column chromatography was performed with silica gel (grain size 0.04-0.063 cm, *Merck, Si60*) at approximately 1.5 atm (hand pump). The eluent ratio used are listed with the respective experiments。

Nuclear magnetic resonance (NMR) spectra were obtained on Bruker AV300 and AV500 MHz NMR instruments. Chemical shifts (δ) are given as parts per million (ppm) and deuterated solvents were used ($CDCl_3$, CD_3CN and CD_2Cl_2). The following abbreviations were used for the assignment of the signals and their multiplicities: s (singlet), d (doublet), t (triplet), q (quartet), m (multiplet). The given coupling constants *J* are listed as an average.

UV-spectra (UV/Vis-spectra) were measured on a Lambda 35 spectrometer from Perkin Elmer Instruments.

Low resolution mass spectra (LRMS) were obtained on the ThermoFinnigan PolarisQ MS and ThermoFinnigan LCQ Fleet MS. High resolution mass spectra (HRMS) were obtained on the Q-Tof Premier mass spectrometer (Waters Corporation). LRMS and HRMS were reported in units of mass of charge ratio (m/z).

X-ray crystallography analysis was performed on Bruker X8 APEX X-ray diffractionmeter.

5.2 Experimental procedures related to the halogen bond donor synthesis

5.2.1 Synthesis of halogen bond donors C1-C7 based on imidazolinium scaffold

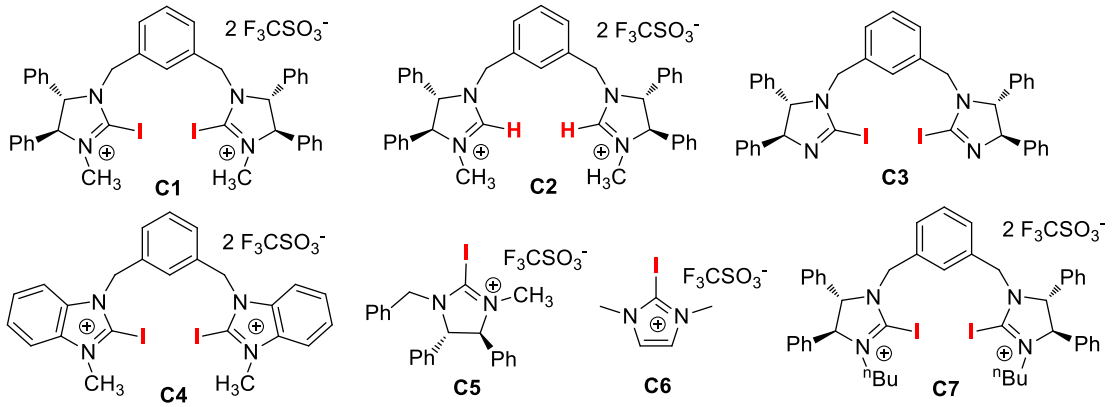

Figure 5.1 Halogen bond donors **C1** – **C7**.

The synthetic scheme of **C1**, **C2**, **C3**, **C5** and **C7** is presented in Scheme 5.1.

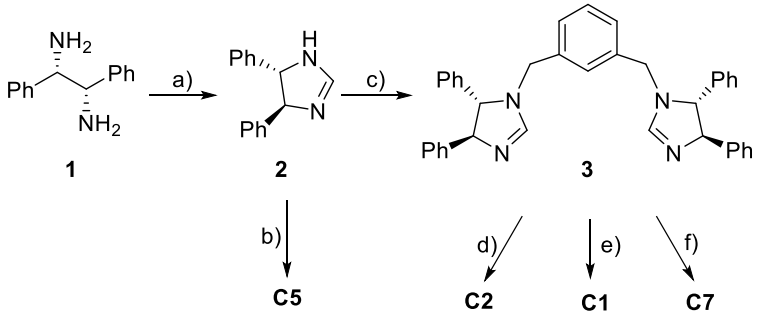

Scheme 5.1 Synthesis of the XB donors **C1**, **C2**, **C3**, **C5** and **C7**.

a) glyoxylic acid monohydrate (1.1 equiv.), MeOH, r.t.; NBS (1.1 equiv.); b) 1. NaH, TBAI, Benzyl bromide (1.1 equiv.), THF, reflux; 2. *n*BuLi (1.2 equiv.), THF, -78 °C, I_2 (1.2 equiv.), THF; 3. MeOTf (2.0 equiv.), DCM, r.t.; c) NaH, TBAI, *m*-xylylene dibromide (0.5 equiv.), THF, reflux; d) MeOTf (4.0 equiv.), DCM, r.t.; e) 1. *n*-BuLi (2.2 equiv.), THF, -78 °C; I_2 (2.2 equiv.), THF, -78 °C; 2. MeOTf (4.0 equiv.), DCM ; f) 1. *n*-BuLi (2.2 equiv.), THF, -78 °C; I_2 (2.2 equiv.), THF, -78 °C; 2. *n*-BuOTf (4.0 equiv.), DCM.

a) Synthesis of 1-*H*-4,5-*trans*-diphenyl-4,5-dihydro-1*H*-imidazole **2**.

A mixture of diamine (1 mmol) and glyoxylic acid monohydrate (1.1 mmol) in dry MeOH (10 mL) were stirred at r.t. for 1 h under N_2. NBS (1.1 mmol) was added to the mixture and the resulting solution was stirred at r.t. overnight. The reaction was quenched by the addition of aqueous sat. $Na_2S_2O_5$, and MeOH was evaporated *in vacuo*. 5% aq. NaOH was added to the residue, and the solution was extracted with EtOAc. The combined organic layer was dried over Na_2SO_4, and evaporated *in vacuo*. The residue was purified by SiO_2 column chromatography to give the title product. Yield: 98%.

b) Synthesis of 1-benzyl-[(4*S*,5*S*)-4,5-dihydro-4,5-diphenyl]-2-iodo-3-methyl-1*H*-imidazolium-(trifluoromethane sulfonate), **C5**

1. A solution of (*S, S*)-4,5-diphenyl-imidazoline **2** (0.48 mmol) in dry THF (5 mL) was added to a suspension of NaH (0.6 mmol, suspended in paraffin) in dry THF (10 mL), and the mixture was heated to reflux for 10 min. After the addition of benzyl bromide (0.48 mmol) in dry THF (2 mL), the solution was heated for another 18 h. It was then cooled to room temperature, and water (20 mL) was added. The aqueous phase was extracted twice with DCM (10 mL). The combined organic layers were dried over Na_2SO_4. After solvent evaporation, the crude product was purified by column chromatography on silica gel using DCM/methanol (8:1) to yield the product 1-benzyl-[(4*S*,5*S*)-4,5-dihydro-4,5-diphenyl]-1*H*-imidazole (81%).

2. Under an argon atmosphere, 1-benzyl-[(4*S*,5*S*)-4,5-dihydro-4,5-diphenyl-]-1*H*-imidazole (0.48 mmol) was dissolved in 150 mL of THF and cooled to -78 °C. Over the course of 1 h, 0.23 mL of 2.5 M *n*-BuLi (0.58 mmol, 1.2 equiv.) was added dropwise and the mixture was

stirred for 2 h at -78 °C. Subsequently, iodine (147 mg, 0.58 mmol, 1.2 equiv.) in 50 mL THF was added slowly, and the mixture was warmed to room temperature over several hours. After stirring for 64 h at room temperature, the solvent was removed. The resulting residue was re-dissolved in 300 mL of CH_2Cl_2 and was washed sequentially with H_2O (200 mL), a saturated solution of $Na_2S_2O_3$ (200 mL), and brine (200 mL). The organic phase was dried over Na_2SO_4 and the solvent was evaporated, yielding 1-benzyl-[(4*S*,5*S*)-4,5-dihydro-4,5-diphenyl]-2-iodo-1*H*-imidazole (4.33 mmol, 91%) as a yellow solid.

3. Under a nitrogen atmosphere, 1-benzyl-[(4*S*,5*S*)-4,5-dihydro-4,5-diphenyl]-2-iodo-1*H*-imidazole (0.48 mmol, 1.0 equiv.) was dissolved in 25 mL of DCM. Thereafter, methyl trifluoromethane sulfonate (0.20 mL, 0.96 mmol, 1.9 equiv.) was added dropwise and the resulting yellow suspension was stirred at room temperature for 48 h. The suspension was filtered and the residue was rinsed with Et_2O (2 × 15 mL). 1-benzyl-[(4*S*,5*S*)-4,5-dihydro-4,5-diphenyl]-2-iodo-3-methyl-1*H*-imidazolium-(trifluoromethane sulfonate) **C5** was obtained as a white solid (0.36 mmol, 76%).

c) Synthesis of 1,1'-[1,3-phenylenebis(methylene)]-bis[(4*S*,4'*S*,5*S*,5'*S*)-4,5-dihydro-4,5-diphenyl]-1*H*-imidazole **3**

A solution of (*S*, *S*)-4,5-diphenyl-imidazoline (0.48 mmol) in dry THF (5 mL) was added to a suspension of NaH (0.6 mmol, suspended in paraffin) in dry THF (10 mL), and the mixture was heated to reflux for 10 min. After the addition of *m*-xylylene dibromide (0.24 mmol) in dry THF (2 mL), the solution was heated for another 18 h. It was then cooled to room temperature, and water (20 mL) was added. The aqueous phase was extracted twice with DCM (10 mL). The combined organic layers were dried over Na_2SO_4. After solvent evaporation, the crude product was purified by column chromatography on silica gel using DCM/methanol (8:1) to yield the product 1,1'-[1,3-phenylenebis(methylene)]-bis[(4*S*,4'*S*,5*S*,5'*S*)-4,5-dihydro-4,5-diphenyl]-1*H*-imidazole (0.40 mmol, 83%).

d) Synthesis of 1,1'-[1,3-phenylenebis(methylene)]-bis[(4*S*,4'*S*,5*S*,5'*S*)-4,5-dihydro-4,5-diphenyl]- 3,3'-methyl-1*H*-imidazolium-bis(trifluoromethane sulfonate), **C2**

Under a nitrogen atmosphere, 1,1'-[1,3-phenylenebis(methylene)]-bis[(4*S*,4'*S*,5*S*,5'*S*)-4,5-dihydro-4,5-diphenyl]-1*H*-imidazole (0.10 g, 0.48 mmol, 1.0 equiv.) was dissolved in 25 mL of DCM. Thereafter, methyl trifluoromethane sulfonate (0.20 mL, 1.82 mmol, 3.8 equiv.) was added dropwise and the resulting yellow suspension was stirred at room temperature for 48 h. The suspension was filtered and the residue was rinsed with Et_2O (2 x 15 mL). The product **C2** was obtained as the residue (0.195 g, 0.38 mmol, 79%) in the form of a white solid.

e) Synthesis of 1,1'-[1,3-phenylenebis(methylene)]-bis[(4*S*,4'*S*,5*S*,5'*S*)-4,5-dihydro-4,5-diphenyl]- 2,2'-iodo-3,3'-methyl-1*H*-imidazolium-bis(trifluoromethane sulfonate), **C1**

1. Under an argon atmosphere, 1,1'-[1,3-phenylenebis(methylene)]-bis[(4*S*,4'*S*,5*S*,5'*S*)-4,5-dihydro-4,5-diphenyl]-*1H*-imidazole (0.48 mmol) was dissolved in 150 mL of THF and cooled to -78 °C. Over the course of 1 h, 0.23 mL of 2.5 M *n*-BuLi (1.06 mmol, 2.2 equiv.) was added dropwise and the mixture was stirred for 2 h at -78 °C. Subsequently, iodine (1.06 mmol, 2.2 equiv.) in 50 mL THF was added slowly, and the mixture was warmed to room temperature over several hours. After stirring for 64 h at room temperature, the solvent was removed. The resulting residue was re-dissolved in 300 mL of CH_2Cl_2 and washed sequentially with H_2O (200 mL), a saturated solution of $Na_2S_2O_3$ (200 mL), and brine (200 mL). The organic phase was dried over Na_2SO_4 and the solvent was evaporated, yielding 1,1'-[1,3-phenylenebis(methylene)]-bis[(4*S*,4'*S*,5*S*,5'*S*)-4,5-dihydro-4,5-diphenyl]-2,2'-iodo-*1H*-imidazole, **C3** (0.44 mmol, 91%) as a yellow solid.

2. Under a nitrogen atmosphere, 1,1'-[1,3-phenylenebis(methylene)]-bis[(4*S*,4'*S*,5*S*,5'*S*)-4,5-dihydro-4,5-diphenyl]-2,2'-iodo-1*H*-imidazole (0.48 mmol, 1.0 equiv.) was dissolved in 25 mL of DCM. Therafter, 0.20 mL of methyl trifluoromethane sulfonate (1.82 mmol, 4.0 equiv.)

was added dropwise and the resulting yellow suspension was stirred at room temperature for 48 h. The suspension was filtered and the residue was rinsed with Et_2O (2 x 15 mL). The product **C1** was obtained as the residue (0.195 g, 0.36 mmol, 76%) in the form of a white solid.

f) Synthesis of 1,1'-[1,3-phenylenebis(methylene)]-bis[(4*S*,4'*S*,5*S*,5'*S*)-4,5-dihydro-4,5-diphenyl]- 2,2'-iodo-3,3'-butyl-1*H*-imidazolium-bis(trifluoromethane sulfonate), **C7**

1. Under an argon atmosphere, 1,1'-[1,3-phenylenebis(methylene)]-bis[(4*S*,4'*S*,5*S*,5'*S*)-4,5-dihydro-4,5-diphenyl]-1*H*-imidazole (0.48 mmol) was dissolved in 150 mL of THF and cooled to -78 °C. Over the course of 1 h, 0.23 mL of 2.5 M *n*-BuLi (1.06 mmol, 2.2 equiv.) was added dropwise and the mixture was stirred for 2 h at -78 °C. Subsequently, iodine (1.06 mmol, 2.2 equiv.) in 50 mL THF was added slowly, and the mixture was warmed to room temperature over several hours. After stirring for 64 h at room temperature, the solvent was removed. The resulting residue was re-dissolved in 300 mL of CH_2Cl_2 and was washed sequentially with H_2O (200 mL), a saturated solution of $Na_2S_2O_3$ (200 mL), and brine (200 mL). The organic phase was dried over Na_2SO_4 and the solvent was evaporated, yielding 1,1'-[1,3-phenylenebis(methylene)]-bis[(4*S*,4'*S*,5*S*,5'*S*)-4,5-dihydro-4,5-diphenyl]-2,2'-iodo-*1H*-imidazole, **C3** (0.44 mmol, 91%) as a yellow solid.

2. Under a nitrogen atmosphere, 1,1'-[1,3-phenylenebis(methylene)]-bis[(4*S*,4'*S*,5*S*,5'*S*)-4,5-dihydro-4,5-diphenyl]-2,2'-iodo-1*H*-imidazole (0.48 mmol, 1.0 equiv.) was dissolved in 25 mL of DCM. Thereafter, 0.20 mL of *n*-butyl trifluoromethane sulfonate (1.82 mmol, 4.0 equiv.) was added dropwise and the resulting yellow suspension was stirred at room temperature for 48 h. The suspension was filtrated and the residue was rinsed with Et_2O (2 x 15 mL). The product **C7** was obtained as the residue (0.36 mmol, 76%) in the form of a white solid.

The synthesis route of **C4** and **C6** is described in Scheme 5.2.

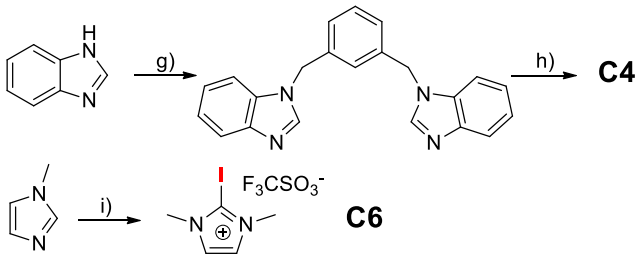

Scheme 5.2 Synthesis of the halogen bond donors **C4** and **C6**

g) NaH, THF, reflux, 10 min; then *m*-xylylene dibromide, THF, 18 h; h) 1) *n*-BuLi, -78 °C, 2 h; then I_2, -78 °C to r.t., 64 h. 2) methyl trifluoromethane sulfonate, DCM, r.t., 48 h; i) 1) *n*-BuLi, -78 °C, 2 h; then I_2, -78 °C to r.t., 64 h. 2) methyl trifluoromethane sulfonate, DCM, r.t., 48 h.

g) Synthesis of 1,1'-[1,3-phenylenebis(methylene)]-bis-1*H*- benzimidazole

A solution of (*S*,*S*)-4,5-diphenyl-imidazoline (0.48 mmol) in dry THF (5 mL) was added to a suspension of NaH (0.6 mmol, suspended in paraffin) in dry THF (10 mL), and the mixture was heated to reflux for 10 min. After the addition of *m*-xylylene dibromide (0.24 mmol) in dry THF (2 mL), the solution was heated for another 18 h. It was then cooled to room temperature, and water (20 mL) was added. The aqueous phase was extracted twice with DCM (10 mL). The combined organic layers were dried over Na_2SO_4. After solvent evaporation, the crude product was purified by column chromatography on silica gel using DCM/methanol (8:1) to yield the product 1,1'-[1,3-phenylenebis(methylene)]-bis-1*H*-benzimidazole (0.39 mmol, 81%).

h) Synthesis of 1,1'-[1,3-phenylenebis(methylene)]-bis-2,2’-iodo-3,3’-methyl-1*H*-benzimidazolium-bis(trifluoromethane sulfonate), **C4**

1. Under an argon atmosphere, 1,1'-[1,3-phenylenebis(methylene)]-bis[(4*S*,4'*S*,5*S*,5'*S*)-4,5-dihydro-4,5-diphenyl]-*1H*-imidazole (0.48 mmol) was dissolved in 150 mL of THF and cooled to -78 °C. Over the course of 1 h, 0.23 mL of 2.5 M *n*-BuLi (1.06 mmol, 2.2 equiv.) was added dropwise and the mixture was stirred for 2 h at -78 °C. Subsequently, 147 mg of iodine (1.06 mmol, 2.2 equiv.) in 50 mL THF was added slowly, and the mixture was warmed to room temperature over several hours. After stirring for 64 h at room temperature, the solvent was

removed. The resulting residue was re-dissolved in 300 mL of CH_2Cl_2 and was washed sequentially with H_2O (200 mL), a saturated solution of $Na_2S_2O_3$ (200 mL), and brine (200 mL). The organic phase was dried over Na_2SO_4 and the solvent was evaporated, yielding 1,1'-[1,3-phenylenebis(methylene)]-bis-2,2'-iodo-1*H*- benzimidazole (0.44 mmol, 91%) as a yellow solid.

2. Under a nitrogen atmosphere, 0.10 g of 1,1'-[1,3-phenylenebis(methylene)]-bis[(4*S*,4'*S*,5*S*, 5'*S*)-4,5-dihydro-4,5-diphenyl]-2,2'-iodo-*1H*-imidazole (0.48 mmol, 1.0 equiv.) was dissolved in 25 mL of DCM. Thereafter, 0.20 mL of methyl trifluoromethane sulfonate (1.82 mmol, 4.0 equiv.) was added dropwise and the resulting yellow suspension was stirred at room temperature for 48 h. The suspension was filtrated and the residue was rinsed with Et_2O (2 x 15 mL). The product **C4** was obtained as the residue (0.195 g, 0.36 mmol, 76%) in the form of a white solid.

i) Synthesis of 1-methyl-2-iodo-3-methyl-1*H*-imidazolium-trifluoromethane sulfonate, **C6**

1. Under an argon atmosphere, 1-methyl-1*H*-imidazole (0.48 mmol) was dissolved in 150 mL of THF and cooled to -78 °C. Over the course of 1 h, 0.23 mL of 2.5 M *n*-BuLi (0.58 mmol, 1.2 equiv.) was added dropwise and the mixture was stirred for 2 h at -78 °C. Subsequently, 147 mg of iodine (0.58 mmol, 1.2 equiv.) in 50 mL THF was added slowly, and the mixture was warmed to room temperature over several hours. After stirring for 64 h at room temperature, the solvent was removed. The resulting residue was re-dissolved in 300 mL of CH_2Cl_2 and was washed sequentially with H_2O (200 mL), a saturated solution of $Na_2S_2O_3$ (200 mL), and brine (200 mL). The organic phase was dried over Na_2SO_4 and the solvent was evaporated, yielding 1-methyl-2-iodo-1*H*-imidazole (0.44 mmol, 91%) as a yellow solid.

2. Under a nitrogen atmosphere, 1-methyl-2-iodo-1*H*-imidazole (0.48 mmol, 1.0 equiv.) was dissolved in 25 mL of DCM. Thereafter, 0.20 mL of methyl trifluoromethane sulfonate (0.96 mmol, 2.0 equiv.) was added dropwise and the resulting yellow suspension was stirred at room

temperature for 48 h. The suspension was filtrated and the residue was rinsed with Et_2O (2 x 15 mL). The product **C6** was obtained as the residue (0.195 g, 0.36 mmol, 76%) in the form of a white solid.

5.2.2 Synthesis of halogen bond donors based on bipyridine backbone

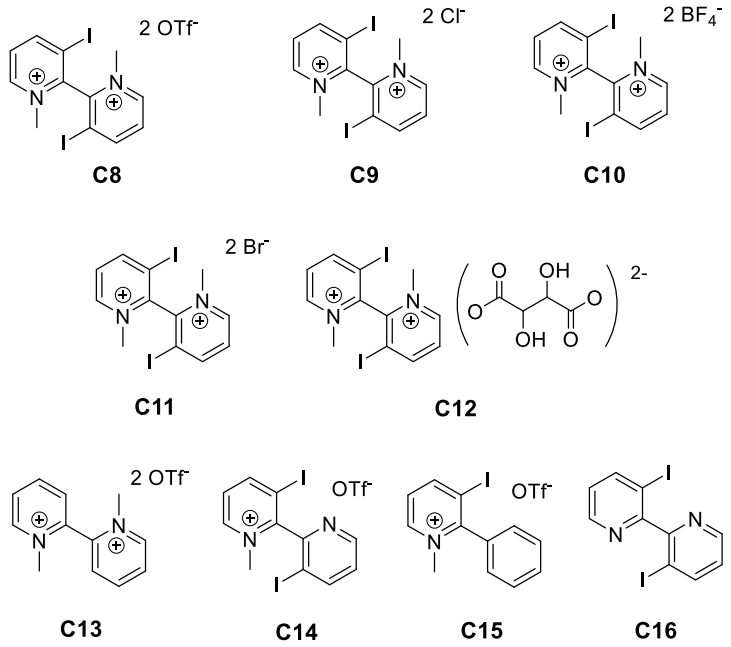

Scheme 5.3 Halogen bond donors based on bipyridine backbone **C8 – C16**.

5.2.2.1 Synthesis of halogen bond donors C8, C14 and C16

The synthesis route of **C8**, **C14** and **C16** is described in Scheme 5.4. [4,5]

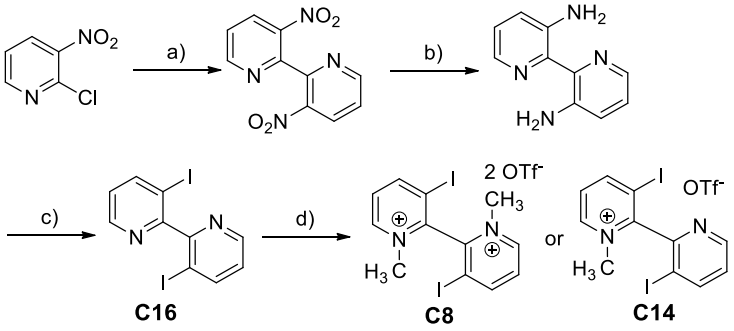

Scheme 5.4 Synthesis of 2,2'-(*N*,*N*'-methyl-3,3'-iodio)-bipyridinium triflate salt
a) N_2 atmosphere, Cu (2.5 equiv.), DMF 150 °C, 2.5 hr; b) $SnCl_2$ (9.0 equiv.), reflux in HCl (35%, aq); c) $NaNO_2$ (4.0 equiv.), HBF_4 (aq), - 10 °C, then KI (6.0 equiv.); d) N_2 atmosphere, MeOTf (2.0 or 4.0 equiv.) in DCM, 72 h.

a) 2-chloro-3-nitropyridine (2.00 g, 12.62 mmol) was reacted with freshly activated copper

bronze (2.00 g) in dry DMF (40 mL) at 150 °C under nitrogen for 2.5 h. After 2 h, TLC (SiO_2, DCM) analysis indicated complete consumption of the starting material. The resulting mixture was poured into water (40 mL), filtered immediately and then washed with concentrated ammonia (2 × 20 mL). The remaining solid was then extracted into boiling dioxane (2 × 150 mL), stirring for about 20 min each time. After evaporating the combined extracts to dryness, the solid was recrystallized from ethanol to give 3,3'-dinitro-2,2'-bipyridine as a yellow solid (yield 1.16 g, 73%). M.p. 205 - 206 °C.

b) The dinitro product (0.8 g, 3.25 mmol) was added to a solution of tin(II) chloride dihydrate (5.6 g, 29.5 mmol) in conc. HCl (32%, 14 mL). The solution was refluxed for 0.5 h, to give a yellow solution (**Important:** *do not let the solution cool, otherwise a green insoluble solid precipitates out of solution*). After adjustment of the pH to 12- 13 with a solution of NaOH, the solution was extracted with chloroform, and the solvents were evaporated to give 3,3'-diamine-2,2'-bipyridine as a yellow solid. (yield 0.5 g, 86%).

c) 3,3'-diamine-2,2'-bipyridine (0.9 g, 4.5 mmol) was suspended in 48% aqueous HBF_4 (25 mL) and cooled to -10 °C. To the resulting slurry was added portionwise over the course of about 1 hour, powdered sodium nitrite (1.3 g, 18.8 mmol), at such a rate that no nitric oxide evolution was detected. After a further 15 min stirring, the precipitate of diazonium salt was isolated by suction filtration, but not allowed to dry out. This was then added, portionwise over the course of about 30 min, to a cooled (-10 °C) solution of potassium iodide (5.1 g, 30.7 mmol) in an acetone–water (40: 60, 100 mL) solution. The reaction was then stirred for 30 min, and warmed to room temperature, giving a yellow–brown suspension. The mixture was neutralised by adding aqueous sodium carbonate, and then a little aqueous sodium thiosulfate solution was added to decolorise the solution phase. Extraction with dichloromethane (4 × 50 mL) gave a yellow solution, which was dried over magnesium sulfate and treated with activated carbon. Following filtration through an alumina pad (2 cm

diameter × 2 cm depth), the solvent was removed under vacuum to give the crude product. This was re-dissolved in hot ethanol, treated again with activated carbon, and filtered hot through celite. Upon cooling and storage at -10 °C the compound 3,3'-diiodine-2,2'-bipyridine, **C16**, was formed as a white crystalline solid, which was isolated by filtration and dried (0.66 g, 1.61 mmol, 33%).

d) Under a nitrogen atmosphere, 3,3'-diiodine-2,2'-bipyridine (0.48 mmol, 1.0 equiv.) was dissolved in 25 mL of DCM. Thereafter, 0.20 mL of methyl trifluoromethane sulfonate (1.82 mmol, 4.0 equiv.) was added dropwise and the resulting yellow suspension was stirred at room temperature for 48 h. The suspension was filtrated and the residue was rinsed with Et_2O (2 x 15 mL), and the crude product was purified by column chromatography. The product 3,3'-diiodine-*N*,*N*'-dimethyl-2,2'-bipyridinium triflate, **C8**, was obtained.

Another donor 3,3'-diiodine-*N*-methyl-2,2'-pyridinium triflate, **C14** was obtained by tuning the loading of MeOTf to 2.0 equiv.

5.2.2.2 Synthesis of halogen bond donor C15

The synthesis routeof **C15** is described in Scheme 5.5. [6]

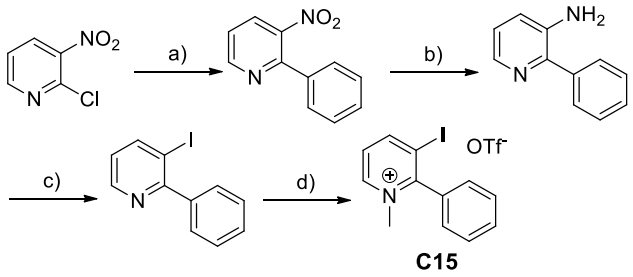

Scheme 5.5 Synthesis of *N*-methyl-2-phenyl- 3-iodio-pyridinium triflate salt **C15**
a) N_2 atmosphere, $Pd(PPh_3)_4$, $PhB(OH)_2$, Na_2CO_3, Solv., reflux 2 hr; b) $SnCl_2$ (9.0 equiv.), reflux in HCl (35%, aq); c) $NaNO_2$ (4.0 equiv.), HBF_4 (aq), - 10 °C, then KI (6.0 equiv.); d) N_2 atmosphere, MeOTf (2.0 equiv.) in DCM, 72 h.

a) To a solution of 2-chloro3-nitro-pyridine (2.0 mmol) in a co-solvent of toluene (7 mL), ethanol (1.5 mL), and H_2O (7 mL) was added Na_2CO_3 (1.57 g, 14.8 mmol) followed by $Pd(PPh_3)_4$ (0.06 mmol) and corresponding phenyl boronic acid (2.6 mmol) under argon in a

50 mL two-necked flask. The reaction mixture was refluxed for 12 h and cooled to room temperature. To the reaction mixture was added aqueous NH_4Cl (15 mL), and the mixture was extracted by EtOAc three times, dried over $MgSO_4$, and evaporated under reduced pressure to afford the crude product, which was further purified by flash chromatography on silica gel with *n*-hexane/EtOAc to give the corresponding 2-phenyl-3-nitro-pyridine.

b) 2-phenyl-3-nitro-pyridine (3.25 mmol) was added to a solution of tin(II) chloride dihydrate (5.6 g, 29.5 mmol) in conc. HCl (32%, 14 mL). The solution was refluxed for 0.5 h, to give a yellow solution (**Important:** *do not let the solution cool, otherwise a green insoluble solid precipitates out of solution*). After adjustment of the pH to 12- 13 with a solution of NaOH, the solution was extracted with chloroform, and the solvents were evaporated to give 2-phenyl-3-amine-pyridine as a yellow solid. (0.5 g, 86%).

c) 2-phenyl-3-amine-pyridine (4.5 mmol) was suspended in 48% aqueous HBF_4 (25 mL) and cooled to -10 °C. To the resulting slurry was added portionwise, over the course of about 1 hour, powdered sodium nitrite (9.5 mmol), at such a rate that no nitric oxide evolution was detected. After a further 15 min stirring, the precipitate of diazonium salt was isolated by suction filtration, but not allowed to dry out. This was then added, portionwise over the course of about 30 min, to a cooled (-10 °C) solution of potassium iodide (15.0 mmol) in an acetone–water (40: 60, 100 mL) solution. The reaction was then stirred for 30 min, and warmed to room temperature, giving a yellow–brown suspension. The mixture was neutralised by adding aqueous sodium carbonate, and then a little aqueous sodium thiosulfate solution was added to decolorise the solution phase. Extraction with dichloromethane (4 × 50 mL) gave a yellow solution, which was dried over magnesium sulfate and treated with activated carbon. Following filtration through an alumina pad (2 cm diameter × 2 cm depth), the solvent was removed under vacuum to give the crude product. This was re-dissolved in hot ethanol, treated again with activated carbon, and filtered hot through celite. Upon cooling

and storage at -10 °C the compound formed as a white crystalline solid, which was isolated by filtration and dried (1.61 mmol, 33%).

d) Under a nitrogen atmosphere, 2-phenyl-3-iodine-pyridine (0.48 mmol, 1.0 equiv.) was dissolved in 25 mL of DCM. Therafter, 0.20 mL of methyl trifluoromethane sulfonate (0.96 mmol, 2.0 equiv.) was added dropwise and the resulting yellow suspension was stirred at room temperature for 48 h. The suspension was filtrated and the residue was rinsed with Et_2O (2 x 15 mL), and the crude product was purified by column. The product 2-phenyl-3-iodine-N-methyl-pyridinium triflate, **C15**, was obtained as a brown solid.

5.2.2.3 Synthesis of halogen bond donor C13

The synthesis route of **C13** is described in Scheme 5.6.

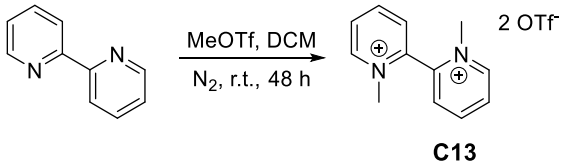

Scheme 5.6 Synthesis of *N*,*N*'-methyl- bipyridinium triflate salt **C13**.

Under a nitrogen atmosphere, 2,2'-bipyridine (0.48 mmol, 1.0 equiv.) was dissolved in 25 mL of DCM. Thereafter, 0.20 mL of methyl trifluoromethane sulfonate (0.96 mmol, 4.0 equiv.) was added dropwise and the resulting yellow suspension was stirred at room temperature for 48 h. The suspension was filtered and the residue was rinsed with Et_2O (2 x 15 mL). The crude was purified by column chromatography.

5.2.2.4 Synthesis of halogen bond donors C9, C10, C11 and C12

The halogen bond donors **C9**, **C10**, **C11** and **C12** have different counter anion as donor **C1**, and they were synthesized from **C1** through anion exchange through anion exchange resin. The procedure is described in Scheme 5.7. [7]

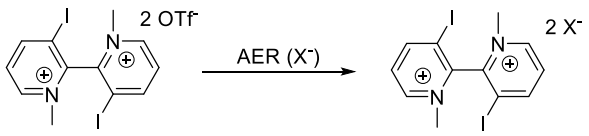

Scheme 5.7 The process of anion exchange.

1) Loading the AER (OH− Form) with acids or ammonium salts

A glass column (1 cm diameter) packed with 2.5 g (~3 mL) of commercial wet strongly basic anion exchange Amberlyst A-26 (OH− form) was washed with water, and the column bed was equilibrated progressively with water-solvent mixtures until reaching the selected solvent media intended for anion loading thereafter (~25 mL of each solvent mixture). A 1% acid or ammonium salt solution in the appropriate solvent was passed slowly through the resin until the eluates had the same pH value as the original selected acid solution, and then the resin was washed generously with solvent until the pH remains constant. The process was carried out at room temperature, using gravity as the driving force.

2) General procedure for anion exchange

A solution of the **C7** (0.5–0.6 mmol) in 10 mL of methanol was passed slowly through a column packed with ~3 mL of Amberlyst A-26 (X^- form), and then washed with 25 mL of solvent. The combined eluates were evaporated, and purified by a silica gel column again if necessary.

5.2.2.5 Modification of halogen bond donors based on bipyridine backbone

A chiral group was installed on the 4-position of pyridine, and the synthesis route is described in Scheme 5.8. [8,9]

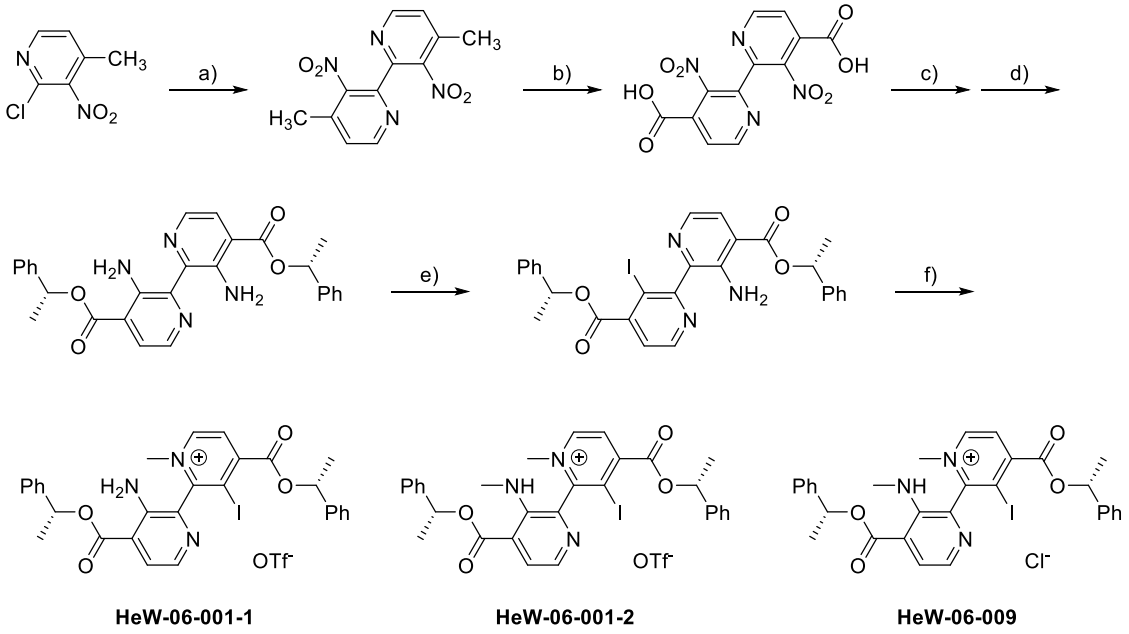

Scheme 5.8 Synthesis of chiral halogen bond donor based on bipyridine backbone
a) N_2 atmosphere, Cu (2.5 equiv.), DMF 150 °C, 2.5 h; b) $K_2Cr_2O_7$ (1.4 equiv.), 60 °C, H_2SO_4; c) (*R*)-1-phenylethyl alcohol (3.0 equiv.), oxacyl chloride (3.0 equiv.), DMF (3.3 equiv.), Et_3N (6.0 equiv.), THF, 16 h, r.t.; d) H_2 (120 psi), Pd/C (10 wt%), EtOAc, 24 h, r.t.; e) $NaNO_2$ (4.0 equiv.), HBF_4 (aq), -10 °C, then KI (6.0 equiv.); f) N_2 atmosphere, MeOTf (2.0 or 4.0 equiv.), DCM, 72 h.

a) 2-chloro-3-nitro-4-methyl-pyridine (12.62 mmol) was reacted with freshly activated copper bronze (2.00 g) in dry DMF (40 mL) at 150 °C under nitrogen for 2.5 h. After 2 h, TLC analysis (SiO_2, DCM) indicated the complete consumption of the starting material. The resulting mixture was poured into water (40 mL), the solid filtered immediately and then washed with concentrated ammonia (2 × 20 mL). The remaining solid was then extracted into boiling dioxane (2 × 150 mL), stirring for about 20 min each time. After evaporating the combined extracts to dryness, the solid was recrystallized from ethanol to give 3,3'-dinitro-4,4'-dimethyl -2,2'-bipyridine as a yellow solid (73%).

b) 3,3'-dinitro-4,4'-dimethyl-2,2'-bipyridine (2.3 mmol) was dissolved in concentrated H_2SO_4, and $K_2Cr_2O_7$ solid was added slowly. Then the mixture was heated to 60 °C for 8 hours. The mixture was cooled to room temperature, and added into ice water slowly; then the solution was extracted by EtOAc. The combined organic phase was dried with Na_2SO_4. The product, 3,3'-dinitro-(2,2'-bipyridine)-4,4'-dicarboxylic acid, was obtained after

evaporation as a white solid (92%).

c) To a stirred solution of DMF (1.37 mmol) and dry DCM (3.0 mL), oxalyl chloride (1,24 mmol) was added dropwise at 0 °C under an argon atmosphere. The mixture was stirred for 5 min at the same temperature, and solvent was evaporated. The white solid obtained was cooled to 0 °C and suspended in dry THF (3.0 mL). (*R*)-1-phenylethyl alcohol (1.24 mmol), Et_3N (2,49 mmol) and 3,3'-dinitro-(2,2'-bipyridine)-4,4'-dicarboxylic acid (0,43 mmol) were added sequentially. After the reaction mixture was stirred for 16 h at r.t., it was quenched with water. The mixture was extracted with EtOAc. The organic layer was washed with brine, dried over anhydrous Na_2SO_4, filtered, and concentrated. The crude product was purified by column to afford the desired product, bis[(*R*)-1-phenylethyl]-3,3'-nitro-(2,2'-bipyridine)-4,4'-dicarboxylate (61%).

d) Bis[(*R*)-1-phenylethyl]-3,3'-nitro-(2,2'-bipyridine)-4,4'-dicarboxylate (0.31 mmol) was dissolved in EtOAc and added into an autoclave in the presence of Pd/C (10 wt%). The autoclave was closed and H_2 (120 psi) gas was introduced. The mixture was stirred overnight at r.t. Thereafter, the solution was evaporated and the crude product was purified by silica gel column chromatography. The product bis[(*R*)-1-phenylethyl)]-3,3'-diamino-[2,2'-bipyridine]-4,4'-dicarboxylate was obtained as a yellow solid (80%).

e) Bis[(*R*)-1-phenylethyl)]-3,3'-diamino-[2,2'-bipyridine]-4,4'-dicarboxylate (4.5 mmol) was suspended in 48% aqueous HBF_4 (25 mL) and cooled to -10 °C. To the resulting slurry was added, portionwise over the course of about 1 hour, powdered sodium nitrite (18.0 mmol), at such a rate that no nitric oxide evolution was detected. After a further 15 min stirring, the precipitate of diazonium salt was isolated by suction filtration, but not allowed to dry out. This was then added, portionwise over the course of about 30 min, to a cooled (-10 °C) solution of potassium iodide (15.0 mmol) in an acetone–water (40: 60, 100 mL) solution. The

reaction was then stirred for 30 min, and warmed to room temperature, giving a yellow–brown suspension. This was neutralised by adding aqueous sodium carbonate, and then a little aqueous sodium thiosulfate solution was added to decolorise the solution phase. Extraction with dichloromethane (4 × 50 mL) gave a yellow solution, which was dried over magnesium sulfate and treated with activated carbon. Following filtration through an alumina pad (2 cm diameter × 2 cm depth), the solvent was removed under vacuum to give the crude product. The crude product was purified by silica gel column, and only mono-iodinated product was obtained, presumably due to the high steric hindrance of the ester group. The crude (0.48 mmol, 1.0 equiv.) was dissolved in 25 mL of DCM. Therafter, 0.20 mL of methyl trifluoromethane sulfonate (0.96 mmol, 2.0 equiv.) was added dropwise and the resulting yellow suspension was stirred at room temperature for 48 h. The suspension was filtrated and the residue was rinsed with Et_2O (2 x 15 mL), and the crude product was purified by column chromatography.

5.2.3 Synthesis of halogen bond donors based on chiral backbone

5.2.3.1 Synthesis of donor C17

The synthesis route of **C17** is described in Scheme 5.9. [10]

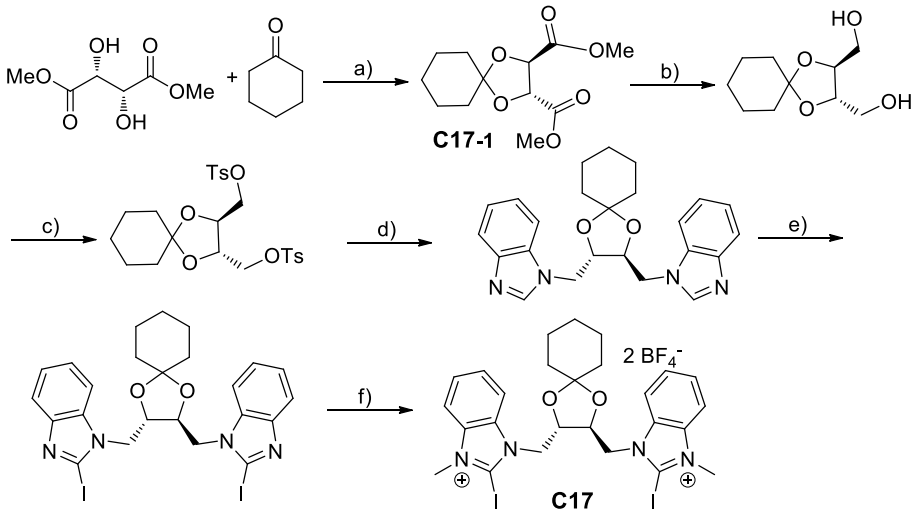

Scheme 5.9 Synthesis of chiral halogen bond donor based on a chiral backbone

a) BF_3Et_2O (1.0 equiv.), reflux, EtOAc; b) $LiAlH_4$ powder, THF; c) TsCl (2.5 equiv.), pyridine, 24 h, r.t.; d) N_2 atmosphere, 1*H*-benzo[*d*]imidazole (4.0 equiv.), $NaNH_2$ (4.0 equiv.), DMF, r.t., overnight; e) *n*-BuLi (2.2 equiv.), THF, -78 °C; I_2 (2.2 equiv.), THF, -78 °C, N_2 atmosphere; f) $O^+Me_3BF4^-$ (4.0 equiv.) in DCM, 72 h.

a) To a solution of L-dimethyltartrate (11.2 mmol, 1.0 equiv.) in EtOAc (10 mL) was added cyclohexanone (13.5 mmol, 1.2 equiv.) and $BF_3.Et_2O$ (28.0 mmol, 2.5 equiv.). The resulting mixture was refluxed for 7 hours. The reaction was then cooled to r.t. and carefully quenched with a solution of saturated aqueous $NaHCO_3$. The organic layer was washed sequentially with water and brine. After drying over $NaSO_4$, filtration and concentration *in vacuo*, the residue was purified by silica gel column chromatography to afford (2*S*,3*S*)-dioxaspiro-[4,5]-decane-2,3-dicarboxyldiethyl ester as an oil.

b) To a solution of (2*S*,3*S*)-dioxaspiro-[4,5]-decane-2,3-dicarboxyldiethyl ester in THF was added $LiAlH_4$ powder slowly. After 4 h of stirring, the mixture was quenched by adding NH_4Cl carefully, and then extracted with EtOAc. The combined organic layer was dried with Na_2SO_4 and evaporated *in vacuo*, and the residue was purified by silica gel column chromatography. The product, 2,3-*o*-cyclohexylidene-L-threitol, was obtained in 40% yield.

c) A solution of 2,3-*o*-Cyclohexylidene-L-threitol in pyridine was treated with *p*-toluenesulfonyl chloride and the resulting solution was stirred at r.t. for 5 hours. Then additional *p*-toluenesulfonyl chloride was added, and stirred for 19 hours. The mixture was diluted with EtOAc and brine, and extracted. The combined organic layer was dried by Na_2SO_4, and then evaporated under vacuum. The crude was purified by silica gel column chromatography, and the product, (2*S*,3*S*)-1,4-dioxaspiro[4.5]decane-2,3-diylbis(methylene)bis(4-methylbenzenesulfonate) was obtained as a yellow solid.

d) To a solution of 1*H*-benzo[*d*]imidazole (4.0 equiv.) and $NaNH_2$ (4.0 equiv.) in dry DMF (0.8 M), was added the corresponding ditosylate (1 equiv.). The mixture was stirred at room temperature for 24 hours, and the residue was purified by column chromatography using

mixtures of DCM: MeOH as eluent. The product, (2*S*,3*S*)-2,3-bis((1*H*-benzo[*d*]imidazol-1-yl)methyl)-1,4-dioxaspiro[4.5]decane was obtained as a white solid.

e) Under an nitrogen atmosphere, the solution of (2*S*,3*S*)-2,3-bis((1*H*-benzo[*d*]imidazol-1-yl)methyl)-1,4-dioxaspiro[4.5]decane (0.48 mmol) in THF (150 mL) and cooled to -78 °C. Over the course of 1 h, 0.23 mL of 2.5 M *n*-BuLi (1.06 mmol, 2.2 equiv.) was added dropwise and the mixture was stirred for 2 h at -78 °C. Subsequently, iodine (1.06 mmol, 2.2 equiv.) in 50 mL THF was added slowly, and the mixture was warmed to room temperature over several hours. After stirring for 64 h at room temperature, the solvent was removed. The resulting residue was re-dissolved in 300 mL of CH_2Cl_2 and was washed sequentially with H_2O (200 mL), a saturated solution of $Na_2S_2O_3$ (200 mL), and brine (200 mL). The organic phase was dried over Na_2SO_4 and the solvent was evaporated, yielding (2*S*,3*S*)-2,3-bis((2-iodo-1*H*-benzo[*d*]imidazol-1-yl)methyl)-1,4-dioxaspiro[4.5]decane, (0.44 mmol, 91%) as a yellow solid.

f) Under a nitrogen atmosphere (in the glove box), (2*S*,3*S*)-2,3-bis((2-iodo-1*H*-benzo[*d*]imidazol-1-yl)methyl)-1,4-dioxaspiro[4.5]decane (0.48 mmol, 1.0 equiv.) was dissolved in 25 mL of DCM. Thereafter, 0.20 mL of $O^+Me_3BF_4^-$ (1.82 mmol, 3.8 equiv.) was added dropwise and the resulting yellow suspension was stirred at room temperature for 48 h. The suspension was filtered and the residue was rinsed with Et_2O (2 x 15 mL). The residue was purified by silica gel column chromatography, with DCM/MeOH used as the eluent. 1,1'-((2*S*,3*S*)-1,4-dioxaspiro[4.5]decane-2,3-diylbis(methylene))bis(2-iodo-3-methyl-1*H*-benzo[*d*]imidazol-3-ium) tetrafluoroboric, **C17**, was obtained as a brown solid (0.38 mmol, 79%).

5.2.3.2 Synthesis of chiral halogen bond donor C18

The synthesis route of **C18** is described in Scheme 5.10. [11]

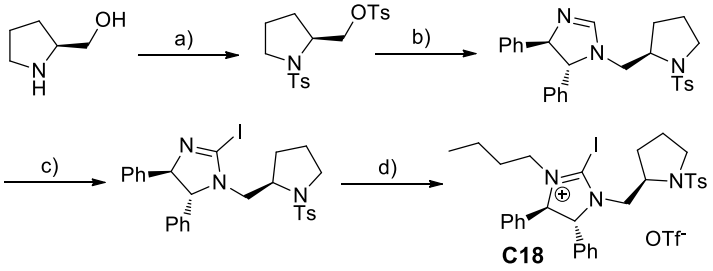

Scheme 5.10 Synthesis route of donor **C18**.

a) *p*-TsCl, r.t., 5 h; b) (4*R*,5*R*)-4,5-diphenyl-4,5-dihydro-1*H*-imidazole, $NaNH_2$, DMF, r.t., 24 h; c) *n*-BuLi, -78 °C, THF, 2 h; then I_2, THF, -78 °C to r.t., 64 h; d) methyl trifluoromethane sulfonate, r.t., 48 h.

a) A solution of (*S*)-pyrrolidin-2-ylmethanol in pyridine was treated with *p*-toluenesulfonyl chloride and the resulting solution was stirred at r.t. for 5 hours. Then additional *p*-toluenesulfonyl chloride was added, and stirred for 19 hours. The mixture was diluted with EtOAc and brine, then extracted with EtOAc. The combined organic layer was dried by Na_2SO_4, and then evaporated under vacuum. The crude was purified by silica gel column chromatography, and the product, (*S*)-(1-tosylpyrrolidin-2-yl)-methyl 4-methylbenzenesulfonate was obtained as a yellow solid.

b) To a solution of (4*R*,5*R*)-4,5-diphenyl-4,5-dihydro-1*H*-imidazole (2.0 equiv.) and $NaNH_2$ (4.0 equiv.) in dry DMF (0.8 M), was added the corresponding (*S*)-(1-tosylpyrrolidin-2-yl)-methyl 4-methylbenzenesulfonate (1.0 equiv.). The mixture was stirred at room temperature for 24 hours, and the residue was purified by column chromatography using mixtures of DCM: MeOH as eluent. (4*R*,5*R*)-4,5-diphenyl-1-[((*R*)-1-tosylpyrrolidin-2-yl)methyl]-4,5-dihydro-*1H*-imidazole was obtained as a white solid.

c) Under a nitrogen atmosphere, a solution of (4*R*,5*R*)-4,5-diphenyl-1-[((*R*)-1-tosylpyrrolidin-2-yl)methyl]-4,5-dihydro-1*H*-imidazole (0.48

mmol) in THF (150 mL) was cooled to -78 °C. Over the course of 1 h, 0.23 mL of 2.5 M *n*-BuLi (1.06 mmol, 2.2 equiv.) was added dropwise and the mixture was stirred for 2 h at -78 °C. Subsequently, iodine (1.06 mmol, 2.2 equiv.) in 50 mL THF was added slowly, and the mixture was warmed to room temperature over several hours. After stirring for 64 h at room temperature, the solvent was removed. The resulting residue was re-dissolved in 300 mL of CH_2Cl_2 and was washed sequentially with H_2O (200 mL), a saturated solution of $Na_2S_2O_3$ (200 mL), and brine (200 mL). The organic phase was dried over Na_2SO_4 and the solvent was evaporated, yielding (4*R*,5*R*)-2-iodo-4,5-diphenyl-1-[((*R*)-1-tosylpyrrolidin-2-yl)methyl]-4,5-dihydro-1*H*-imidazole as a yellow solid (0.44 mmol, 91%).

d) Under a nitrogen atmosphere (in glove box), (4*R*,5*R*)-2-iodo-4,5-diphenyl-1-[((*R*)-1-tosylpyrrolidin-2-yl)methyl]-4,5-dihydro-1*H*-imidazole (0.48 mmol, 1.0 equiv.) was dissolved in 25 mL of DCM. Thereafter, 0.20 mL of methyl trifluoromethane sulfonate (0.96 mmol, 2.0 equiv.) was added dropwise and the resulting yellow suspension was stirred at room temperature for 48 h. The suspension was filtrated and the residue was rinsed with Et_2O (2 x 15 mL). The residue was purified by silica gel column chromatography, and DCM/MeOH was used as the eluent. (4*R*,5*R*)-3-butyl-2-iodo-4,5-diphenyl-1-[((*R*)-1-tosylpyrrolidin-2-yl)methyl]-4,5-dihydro-1*H*-imidazol-3-ium triflate, **C18**, was obtained as a brown solid (0.38 mmol, 79%).

5.2.3.2 Synthesis of chiral halogen bond donor C19

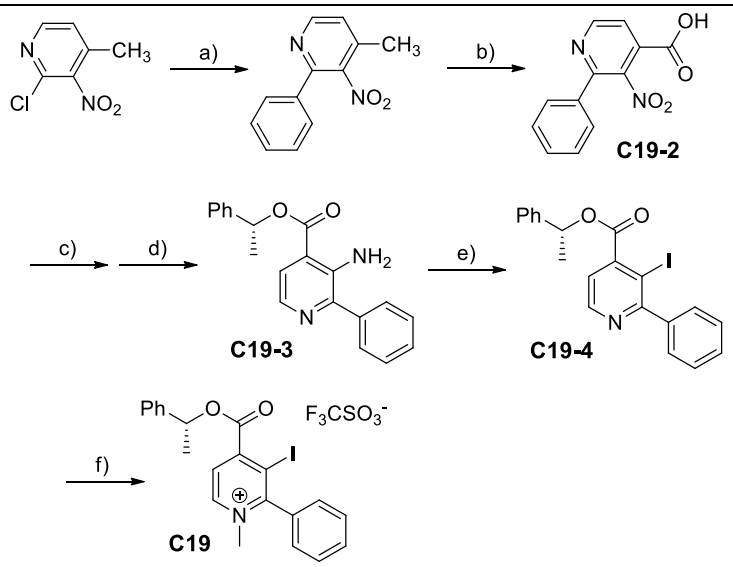

Scheme 5.8 Synthesis of chiral halogen bond donor **C19**

Conditions: a) N2 atmosphere, Pd(PPh3)4, PhB(OH)2, Na2CO3, Solv., reflux 2 hr; b) K2Cr2O7 (1.4 equiv.), 60 oC in H2SO4; c) (R)-1-phenylethyl alcohol (3.0 equiv.), oxacyl chloride (3.0 equiv.), DMF (3.3 equiv.), Et3N (6.0 equiv.) in THF stir 16 hr at r.t.; d) H2 (120 psi), Pd/C (10 wt%), in EA stir 24 hr at r.t.; e) NaNO2 (4.0 equiv.), HBF4 (aq), - 10 oC, then KI (6.0 equiv.); f) N2 atmosphere, MeOTf (2.0 or 4.0 equiv.) in DCM, 72 hrs.

a) To a solution of 2-chloro3-nitro-4-methyl-pyridine (2.0 mmol) in a co-solvent of toluene (7 mL), ethanol (1.5 mL), and H_2O (7 mL) was added Na_2CO_3 (1.57 g, 14.8 mmol) followed by $Pd(PPh_3)_4$ (0.06 mmol) and corresponding phenyl boronic acid (2.6 mmol) under argon in a 50 mL two-necked flask. The reaction mixture was refluxed for 12 h and cooled to room temperature. To the reaction mixture was added aqueous NH_4Cl (15 mL), extracted by EtOAc three times, dried over $MgSO_4$, and evaporated under reduced pressure to afford the crude product, which was further purified by flash chromatography on silica gel with n-hexane/EtOAc to give corresponding 2-phenyl-3-nitro-4-methyl-pyridine.

b) 2-phenyl-3-nitro-4-methyl-pyridine. (2.3 mmol) dissolve in concentrated H_2SO_4, and $K_2Cr_2O_7$ solid was added slowly. Then the mixture was heated to 60 ^oC for 8 hours. The mixture was cooled to room temperature, and added into ice water slowly; then the solution was extracted by EA, organic phase was combined and tried with Na_2So_4. The product, 2-phenyl-3-nitro-pyridine-4-carboxylic acid, **C19-2**, was obtained after evaporation as a

white solid. Yield is 92%

c) To a stirred solution of DMF (1.37 mmol) in dry DCM (3.0 mL), oxalyl chloride (1,24 mmol) was added dropwise at 0 ^{o}C under an argon atmosphere. The mixture was stirred for 5min at the same temperature, and solvent was evaporated. The obtained white solid was cooled down to 0 ^{o}C and suspended in dry THF (3.0 mL). (*R*)-1-phenylethyl alcohol (1.24 mmol), Et_3N (2,49 mmol) and 2-phenyl-3-nitro-pyridine-4-carboxylic acid (0,43 mmol) were added sequentially. After the reaction mixture was stirred for 16 hours at r.t., it was quenched with water. The mixture was extracted with EA. The organic layer was washed with brine, dried over anhydrous Na_2SO_4, filter, and concentrated. The crude was purified by column to afford the desired product, (*R*)-1-phenylethyl 3-nitro-2-phenylisonicotinate, yield is 61%.

d) (*R*)-1-phenylethyl-3-nitro-2-phenylisonicotinate (0.31 mmol) was dissolved in EA and added into autoclave in presence of Pd/C (10 wt%). Then close the autoclave and H_2 (120 psi) gas was introduce into. The mixture was stirred overnight at r.t.. After reaction, the solution was evaporated and the crude was purified by silica gel column. The product (*R*)-1-phenylethyl 3-amino-2-phenylisonicotinate, **C19-3**, was obtained as a yellow solid, yield is 80%.

e) (*R*)-1-phenylethyl-3-amino-2-phenylisonicotinate (4.5 mmol) was suspended in 48% aqueous HBF_4 (25 mL) and cooled to -10 ^{o}C. To the resulting slurry was added, portionwise over the course of about 1 hour, powdered sodium nitrite (18.0 mmol), at such a rate that no nitric oxide evolution was detected. After a further 15 min stirring, the precipitate of diazonium salt was isolated by suction filtration, but not allowed to dry out. This was then added, portionwise over the course of about 30 min, to a cooled (-10 ^{o}C) solution of potassium iodide (15.0 mmol) in an acetone–water (40 : 60, 100 mL) solution. The reaction was then stirred for 30 min, being allowed to warm to room temperature, giving a yellow–brown suspension. This was neutralised by adding aqueous sodium carbonate, and then a

little aqueous sodium thiosulfate solutionwas added to decolorise the solution phase. Extraction with dichloromethane (4 × 50 mL) gave a yellow solution, which was dried over magnesium sulfate and treated with activated carbon. Following filtration through an alumina pad (2 cm diameter × 2 cm depth), the solvent was removed under vacuum to give the crude product. The crude was purified by silica gel column, (*R*)-1-phenylethyl-3-iodine-2-phenylisonicotinate, **C19-4**, was obtained.

f) Under a nitrogen atmosphere, **C19-4** (0.48 mmol, 1.0 equiv.) were dissolved in 25 mL of DCM. Afterwards 0.20 mL of methyl trifluoromethane sulfonate (0.96 mmol, 2.0 equiv.) were added dropwise and the resulting yellow suspension was stirred at room temperature for 48 h. The suspension was filtrated and the residue was rinsed Et_2O (2 x 15 mL), and the crude was purified by column. (R)-3-iodo-1-methyl-2-phenyl-4-((1-phenylethoxy)carbonyl)-pyridin-1-ium trifluoromethanesulfonate, **C19**, was obtained on yield 90%.

5.3 Experimental procedures related to the hydrogen transfer reaction

5.3.1 Typical procedure of transfer hydrogenation of C=N bond with Hantzsch ester

Under a nitrogen atmosphere, a mixture of quinoline (0.5 mmol), Hantzsch ester (1.1 mmol) and catalyst **C1** (0.001 mmol, 2 mol %) was added to DCM (1 mL) and stirred at room temperature. The reaction progress was monitored by TLC and GC-MS. When the quinoline was consumed, the reaction was stopped and DCM was removed in vacuum. The residue was purified by SiO_2 column chromatography to give the title product in 98% yield.

5.3.2 Isothermal calorimetric titrations (ITC) measurement

All solvents used were purchased in the anhydrous form. Synthesized compounds used in the measurements were dried under high vacuum prior to use. The experiments were performed in an air-conditioned laboratory (room temperature: 20-22 °C).

Typical procedure of isothermal calorimetric titrations is shown as follows:

The solution of host and guest in CH_3CN was prepared first and the concentrations of the guest (X^-) and host (halogen bond donor) solutions in the experiments are shown in Table 5.1. The guest solution was titrated into the host solution in the cell, and the thermal data was collected automatically.

Table 5.1 Isothermal calorimetric titrations of halogen-bond donors with halides at 25 °C in ACN.

Entry	Guest	Host	K [mol^{-1}]	ΔH [kJ/mol]	$T\Delta S$ [kJ/mol]
1	**1a**	**C1**	-	-	-
2	Bu_4NBr	**C1**	3.29E4	-18.0	7.8
3	Bu_4NBr	**C4**	4.57E5	-22.6	9.7

Conditions: Halogen bond donors (0.2 mM), halide (2 mM). Guest into Host.

The plots on the following pages show data gathered in the ITC experiments. The legend shows the following thermodynamic properties:

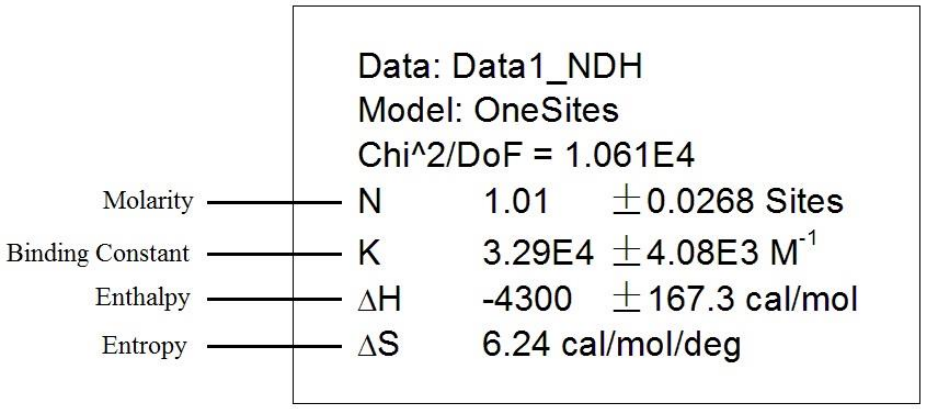

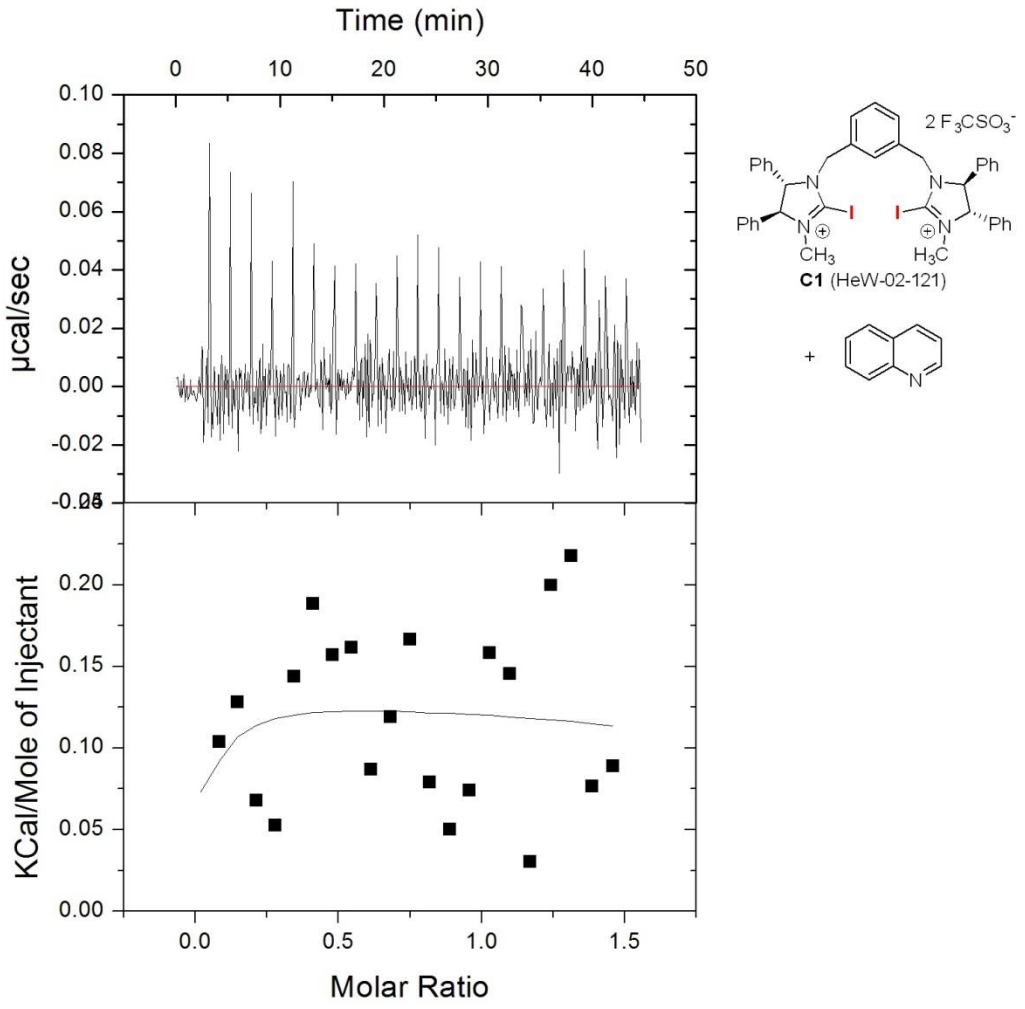

Quinoline **1a** to **C1** in CH_3CN, 25 °C

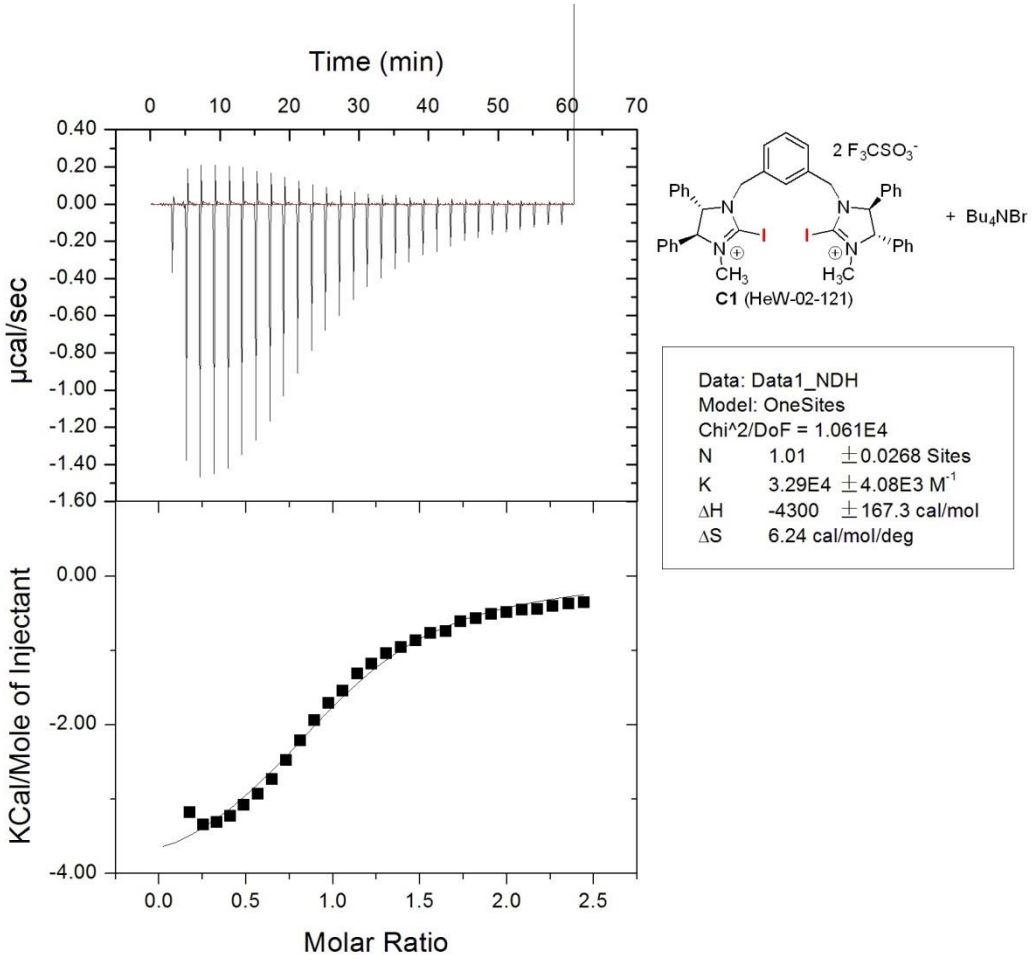

n-Bu_4NBr to **C1** in CH_3CN, 25 °C

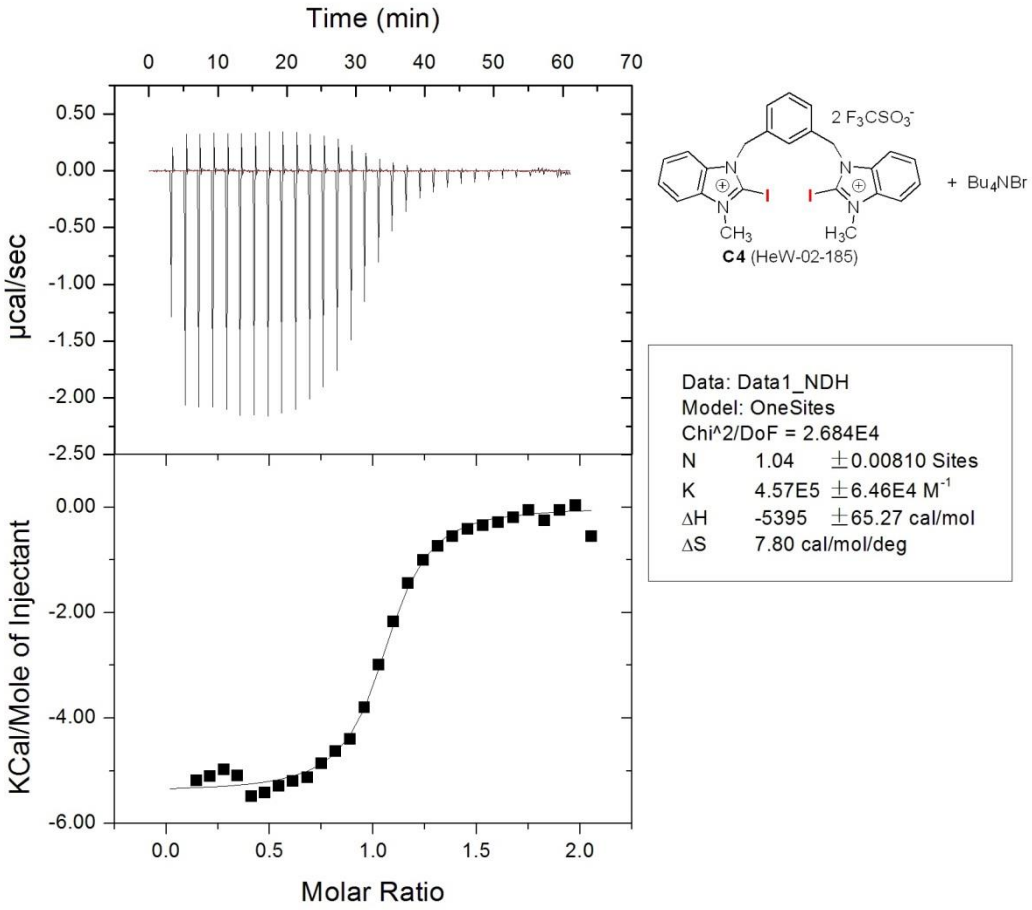

n-Bu_4NBr to **C4** in CH_3CN, 25 °C

5.4 Experimental procedures related to [3+2] cycloaddition reaction

5.4.1 Typical procedure of synthesis of nitrone compound 6

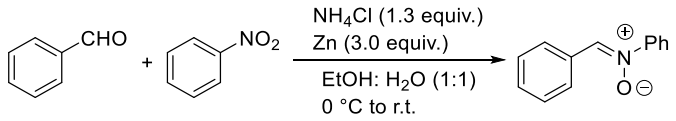

Nitrobenzene (11.6 g, 94.2 mmol), benzaldehyde (10 g, 94.2 mmol), NH_4Cl (6.6 g, 122.5 mmol), EtOH (100 mL) and water (100 mL) were added into a 500 mL RBF. The reaction mixture was cooled to 0 °C and zinc (12.3 g, 188.5 mmol) was added slowly over 3-4 hour. The suspension was then warmed to r.t. and stirred for 12 hours. The reaction mixture was filtered through celite and washed with DCM and then dried by $MgSO_4$. The resulting crude mixture was then concentrated and purified by column chromatography to afford the desired nitrone **7a** as a yellow solid. (82%).

5.4.2 Typical procedure of [3+2] cycloaddition reaction

Under a nitrogen atmosphere, a mixture of nitro compound **7** (0.5 mmol), α, β-unsaturated carbonyl compound **8** (1.1 mmol) and catalyst **C8** (0.05 mmol, 10 mol %) was added in solvent (1 mL) and stirred at room temperature. The reaction was monitored by TLC analysis. When the reaction was completed, the solvent was removed in vacuum. The residue was purified by SiO_2 gel column chromatography to give the desired product.

5.4.3 NMR study of substrate 6a with C8

Starting material **6a** was dissolved in CD_3CN and ^1H and ^{13}C NMR experiments were conducted (100 scan numbers). To the same **6a** NMR sample was added, 1.0 equivalent of halogen bond donor **C8**, and the ^1H and ^{13}C NMR experiments were repeated (100 scan numbers) again.

5.5 Analytical data

The spectral data of novel compounds were shown as follows:

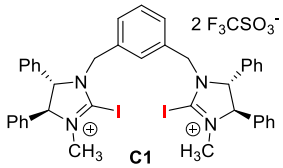

C1

1,1'-[1,3-phenylenebis(methylene)]-bis[(4*S*,4'*S*,5*S*,5'*S*)-4,5-dihydro-4,5-diphenyl]-2,2'-iodo-3,3'-methyl-1*H*-imidazolium-bis(trifluoromethane sulfonate), **C1:**

1H NMR (500 MHz, CD2Cl2) δ 7.47 – 7.29 (m, 12H), 7.29 – 7.21 (m, 5H), 7.17 (dd, J = 7.4, 4.5 Hz, 5H), 6.92 (d, J = 7.7 Hz, 2H), 5.26 (d, J = 10.9 Hz, 2H), 4.89 (dd, J = 19.8, 13.3 Hz, 4H), 4.56 (d, J = 15.8 Hz, 2H), 3.25 (s, 6H).

13C NMR (126 MHz, CD2Cl2) δ 136.61 (s), 134.61 (d, J = 10.6 Hz), 134.12 (s), 131.12 (d, J = 8.1 Hz), 130.64 – 130.30 (m), 129.44 (s), 129.24 (s), 128.72 (s), 128.40 (s), 122.65 (s), 120.10 (s), 76.37 (s), 75.14 (s), 38.91 (s).

HRMS (Q-Tof): calcd. for $C_{41}H_{38}F_3I_2N_4O_3S$ [M-OTf$^-$]+: 977.0701, found 977.0721.

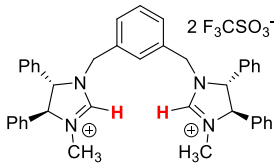

C2

1,1'-[1,3-phenylenebis(methylene)]-bis[(4*S*,4'*S*,5*S*,5'*S*)-4,5-dihydro-4,5-diphenyl]-3,3'-methyl-1*H*-imidazolium-bis(trifluoromethane sulfonate), **C2**:

^{1}H NMR (500 MHz, CD_2Cl_2) δ 8.74 (s, 2H), 7.87 (s, 1H), 7.62 – 7.35 (m, 16H), 7.28 (dd, *J* = 10.9, 8.8 Hz, 5H), 7.08 (d, *J* = 7.5 Hz, 2H), 4.99 (d, *J* = 10.4 Hz, 2H), 4.83 (d, *J* = 10.3 Hz, 2H), 4.66 (d, *J* = 14.1 Hz, 2H), 4.32 (d, *J* = 14.1 Hz, 2H), 3.12 (d, *J* = 9.1 Hz, 6H).

^{13}C NMR (126 MHz, $CDCl_3$) δ 159.72 (s), 134.31 (d, *J* = 7.3 Hz), 133.51 (s), 131.06 (s), 130.78 (s), 130.57 – 130.14 (m), 130.04 (d, *J* = 10.4 Hz), 128.55 (s), 127.90 (d, *J* = 18.3 Hz), 126.56 (s), 122.32 (s), 119.78 (s), 75.98 (s), 74.84 (s), 50.40 (s), 33.88 (s).

HRMS (Q-Tof): calcd. for $C_{41}H_{40}F_3N_4O_3S$ [M-OTf$^-$]+: 725.2768, found 725.2776.

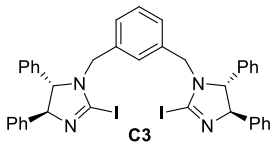

C3

1,1'-[1,3-phenylenebis(methylene)]-bis[(4*S*,4'*S*,5*S*,5'*S*)-4,5-dihydro-4,5-diphenyl]-2,2'-iodo-*1H*-imidazole, **C3**:

^{1}H NMR (500 MHz, $CDCl_3$) δ 7.30 – 7.20 (m, 6H), 7.18 – 7.09 (m, 7H), 7.06 (dd, *J* = 7.7, 1.5 Hz, 4H), 7.01 (dd, *J* = 7.6, 1.6 Hz, 4H), 6.92 (d, *J* = 6.5 Hz, 3H), 4.93 (d, *J* = 9.2 Hz, 2H), 4.59 (d, *J* = 15.9 Hz, 2H), 4.13 (d, *J* = 9.2 Hz, 2H), 3.84 (d, *J* = 15.9 Hz, 2H).

^{13}C NMR (126 MHz, $CDCl_3$) δ 142.54 (s), 140.02 (s), 138.88 – 138.72 (m), 136.76 (s), 129.36 (s), 128.79 (d, *J* = 17.5 Hz), 127.77 (d, *J* = 7.5 Hz), 126.90 (s), 81.05 (s), 51.69 (s).

HRMS (Q-Tof): calcd. for C38H32I2N4 [M]+: 799.0716, found 799.0788

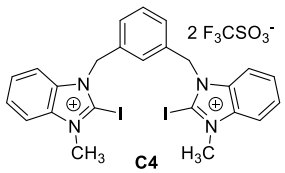

C4

1,1'-[1,3-phenylenebis(methyle

ne)]-bis-2,2'-iodo-3,3'-methyl-1*H*-benzimidazolium-bis(trifluoromethane sulfonate), **C4**:

^{1}H NMR (500 MHz, CD_3CN) δ 7.91 (d, *J* = 8.3 Hz, 2H), 7.75 – 7.61 (m, 4H), 7.55 (t, *J* = 7.8 Hz, 2H), 7.43 (t, *J* = 7.7 Hz, 1H), 7.33 (d, *J* = 7.6 Hz, 2H), 7.23 (s, 1H), 5.71 (s, 4H), 4.10 (s, 6H).

^{13}C NMR (126 MHz, CD_3CN) δ 135.19 (s), 134.23 (s), 130.85 (s), 128.71 (s), 128.00 (d, *J* = 1.5 Hz), 127.38 (s), 114.37 (s), 113.98 (s), 53.48 (s), 37.69 (s).

HRMS (Q-Tof): calcd. for C25H22F3I2N4O3S [M-OTf^-]+: 768.9449, found 768.9435.

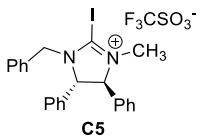

C5

1-benzyl-[(4*S*,5*S*)-4,5-dihydro-4,5-diphenyl]-2-iodo-3-methyl-1*H*-

imidazolium-(trifluoromethane sulfonate), **C5**:

^{1}H NMR (500 MHz, CD_3CN) δ 7.43 (dd, *J* = 15.8, 7.1 Hz, 7H), 7.37 (s, 4H), 7.27 (dd, *J* = 18.2, 6.5 Hz, 5H), 7.18 (s, 2H), 7.10 (d, *J* = 21.5 Hz, 1H), 5.23 (d, *J* = 10.4 Hz, 1H), 4.95 (dd, *J* = 19.6, 13.3 Hz, 2H), 4.44 (d, *J* = 16.0 Hz, 1H), 3.18 (s, 3H).

HRMS (Q-Tof): calcd. for C23H22IN2 [M-OTf$^-$]+: 453.0822, found 453.0847.

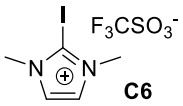

C6

1-methyl-2-iodo-3-methyl-1*H*-imidazolium-trifluoromethane sulfonate, **C6**:

^{1}H NMR (400 MHz, CD_3CN) δ 7.60 (s, 2H), 3.87 – 3.72 (m, 6H).

^{13}C NMR (101 MHz, CD_3CN) δ 127.23 (s), 40.32 (s).

HRMS (Q-Tof): calcd. for C5H8IN2 [M-OTf$^-$]+: 222.9727, found 222.9726.

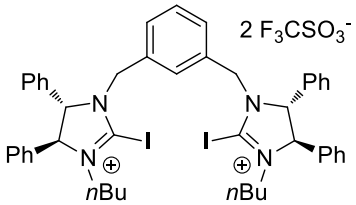

C7

1,1'-[1,3-phenylenebis(methylene)]-bis[(4*S*,4'*S*,5*S*,5'*S*)-4,5-dihydro-4,5-diphenyl]-2,2'-iodo-3,3'-butyl-1*H*-imidazolium-bis(trifluoromethane sulfonate), **C7**:

1H NMR (500 MHz, CDCl3) δ 7.35 – 7.09 (m, 22H), 6.88 (d, J = 8.0 Hz, 2H), 5.12 (d, J = 10.5 Hz, 2H), 4.94 (d, J = 10.5 Hz, 2H), 4.88 (d, J = 7.0 Hz, 2H), 4.52 (d, J = 16.0 Hz, 2H), 3.69 – 3.65 (m, 2H), 3.34 – 3.31 (m, 2H), 1.52 (m, 2H), 1.42 – 1.39 (m, 2H), 1.23 – 1.16 (m, 4H), 0.79 (t, J = 7.2 Hz, 6H)

13C NMR (126 MHz, CDCl3) δ 135.24 (s), 133.95 (s), 133.85 (s), 133.76 (s), 130.64 (s), 130.52 (s), 130.01 (s), 129.90 (s), 129.74 (s), 129.65 (s), 129.36 (s), 129.16 (s), 128.76 (s), 128.43 (s), 128.21 (s), 128.02 (s), 127.93 (s), 127.93 (s), 127.75 (s), 126.49 (s), 121.84 (s), 119.29 (s), 116.75 (s), 74.33 (s), 54.07 (s), 51.03 (s), 29.45 (s), 19.81 (s), 13.51 (s).

HRMS (Q-Tof): calcd. for C47H50F3I2N4O3S [M-OTf$^-$]+: 1061.1640, found 1061.1645.

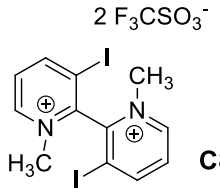

C8

3,3'-diiodine-N,N'-dimethyl-2,2'-bipyridinium triflate, **C8**:

^{1}H NMR (500 MHz, CD_3CN) δ 9.22 (d, *J* = 7.9 Hz, 2H), 9.18 (d, *J* = 6.1 Hz, 2H), 8.15 (dd, *J* = 7.9, 6.1 Hz, 2H), 4.16 (s, 6H).

^{13}C NMR (126 MHz, CD_3CN) δ 157.92 (s), 150.10 (s), 147.21 (s), 131.02 (s), 101.34 (s), 49.18 (s).

HRMS (Q-Tof): calcd. for C13H12F3I2N2O3S [M-OTf$^-$]+: 586.8605, found 586.8607.

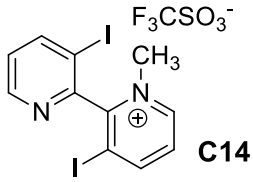

C14

3,3'-diiodine-N-methyl-2,2'-pyridinium triflate, **C14**:

^{1}H NMR (500 MHz, CD_3CN) δ 9.16 (d, *J* = 8.4 Hz, 1H), 9.06 (dd, *J* = 5.2, 1.2 Hz, 1H), 9.01 (d, *J* = 6.0 Hz, 1H), 8.94 (d, *J* = 8.3 Hz, 1H), 8.00 (dd, *J* = 8.4, 6.2 Hz, 1H), 7.84 (dd, *J* = 7.0, 5.2 Hz, 1H), 4.09 (s, 3H)

^{13}C NMR (126 MHz, CD_3CN) δ 156.81 (s), 153.61 (s), 147.99 (s), 147.90 (s), 129.69 (s), 129.19 (s), 100.06 (s), 97.24 (s), 49.18 (s).

HRMS (Q-Tof): calcd. for C11H9I2N2 [M-OTf$^-$]+: 422.8850, found 422.8846.

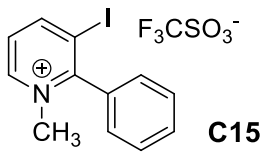

C15

2-phenyl-3-iodine-N-methyl-pyridinium triflate, **C15**:

^{1}H NMR (500 MHz, CD_3CN) δ 9.00 (d, *J* = 1.5 Hz, 1H), 8.83 (d, *J* = 10.5 Hz, 1H), 7.78-7.70

(m, 3H), 7.48-7.43 (m, 2H), 4.01 (s, 3H).

^{13}C NMR (126 MHz, CD_3CN) δ 155.64 (s), 146.38 (s), 134.87 (s), 131.54 (s), 129.82 (s), 127.91 (s), 127.57 (s), 100.45 (s), 49.79 (s).

HRMS (Q-Tof): calcd. for C12H11IN [M-OTf$^-$]+: 295.9931, found 295.9928.

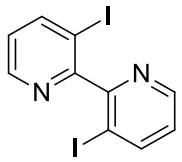

C16

3,3'-diiodine-2,2'-bipyridine, **C16**:

^{1}H NMR (500 MHz, $CDCl_3$) δ 8.69 (dd, *J* = 4.7, 1.4 Hz, 2H), 8.26 (dd, *J* = 7.1, 0.4 Hz, 2H), 7.10 (dd, *J* = 8.0, 4.7 Hz, 2H).

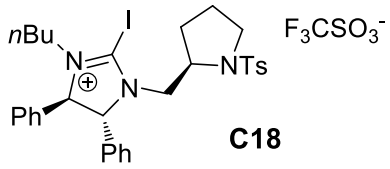

C18

(4R,5R)-3-butyl-2-iodo-4,5-diphenyl-1-(((R)-1-tosylpyrrolidin-2-yl)methyl)-4,5-dihydro-1H-imidazol-3-ium triflate, **C18**:

^{1}H NMR (500 MHz, $CDCl_3$) δ 7.50-7.17 (m, 14H), 5.07 (d, *J* = 9.0 Hz, 1H), 4.55 (d, *J* = 9.0 Hz, 1H), 3.60-3.56 (m, 1H), 3.43-3.37 (m, 2H), 3.17 (m, 1H), 2.87 (m, 1H), 2.41 (s, 3H), 1.84 (m, 2H), 1.51 (m, 2H), 1.31-1.29 (m, 5H), 1.20 (m, 2H), 0.92-0.91 (m, 2H)

^{13}C NMR (126 MHz, CD_3CN) δ 143.59 (s), 141.74 (s), 141.19 (s), 133.46 (s), 129.70 (s), 129.38 (s), 128.83 (s), 128.62 (s), 128.02 (s), 127.87 (s), 127.63 (s), 126.65 (s), 81.46 (s), 75.59 (s), 58.40 (s), 55.02 (s), 49.45 (s), 29.88 (s), 28.26 (s), 23.74 (s), 21.70 (s).

HRMS (Q-Tof): calcd. for C31H37IN3O2S [M-OTf$^-$]+: 642.1646, found 642.1649.

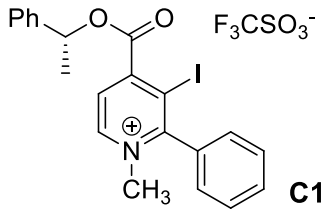

C19

(R)-3-iodo-1-methyl-2-phenyl-4-((1-phenylethoxy)carbonyl)pyridin-1-ium trifluoromethanesulfonate, **C19**:

^{1}H NMR (500 MHz, $CDCl_3$) δ 9.20 (d, *J* = 6.0 Hz, 1H), 7.90 (d, *J* = 6.0 Hz, 1H), 7.55 (m, 3H), 7.36-7.19 (m, 7H), 6.10 (t, *J* = 6.5 Hz, 1H), 4.12 (s, 3H), 1.64 (d, *J* = 8.5 Hz, 3H)

^{13}C NMR (126 MHz, $CDCl_3$) δ 163.45 (s), 160.15 (s), 153.82 (s), 148.45 (s), 139.63 (s), 135.16 (s), 131.94 (s), 130.26 (s), 128.95 (s), 128.06 (s), 128.01 (s), 126.77 (s), 125.74 (s), 51.05 (s), 21.96 (s).

HRMS (Q-Tof): calcd. for C21H19INO2 [M-OTf^-]+: 444.0455, found 444.0452.

References

[1] Murai, K.; Morishita, M.; Nakatani, R.; Fujioka, H.; Kita, Y. *Chem. Commun.* **2008**, 4498.

[2] Zhang, Y.G.; Zhao, L.; Patra, P. K.; Hu, D. Y.; Ying, J. Y. *Nano Today* **2009**, *4*, 13

[3] Walter, S. M.; Kniep, F.; Rout, L.; Schmidtchen, F. P.; Herdtweck, E.; Huber, S. M. *J. Am. Chem. Soc.* **2012**, *134*, 8507.

[4] Rice, C. R.; Onions, S.; Vidal, N.; Wallis, J. D.; Senna, M.-C.; Pilkington, M.; Stoeckli-Evans, H. *Eur. J. Inorg. Chem.* **2002**, 1985.

[5] Adams, C. J.; Bowen, L. E.; Humphrey, M. G.; Morrall, J. P. L.; Samoc, M.; Yellowlees, L. J. *Dalton Trans.***2004**, 4130.

[6] Kim, J.; Park, S.-W.; Baik, M.-H.; Chang, S. *J. Am. Chem. Soc.*, **2015**, *137*, 13448

[7] Alcalde, E.; Dinarès, I.; Ibáñez, A.; Mesquida, N. *Molecules* **2012**, *17*, 4007.

[8] Tagawa, Y.; Yamashita, K.; Higuchi, Y.; Goto, Y. *Heterocycles*, **2003**, 60, 953

[9] Nagao, H.; Michida, M.; Mukaiyama, T. *Synthetic Communications*, **2008**, 38, 18, 3208

[10] Soler-Padrós, J.; Pérez-Mayoral, E.; Domínguez, L.; López-Larrubia, P.; Soriano, E.; Marco-Contelles, L. J.; Cerdán, S.; Ballesteros, P. *J. Med. Chem.* **2007**, *50*, 4539

Appendix

(4*S*,5*S*)-4,5-diphenyl-4,5-dihydro-1*H*-imidazole, **C1-1**

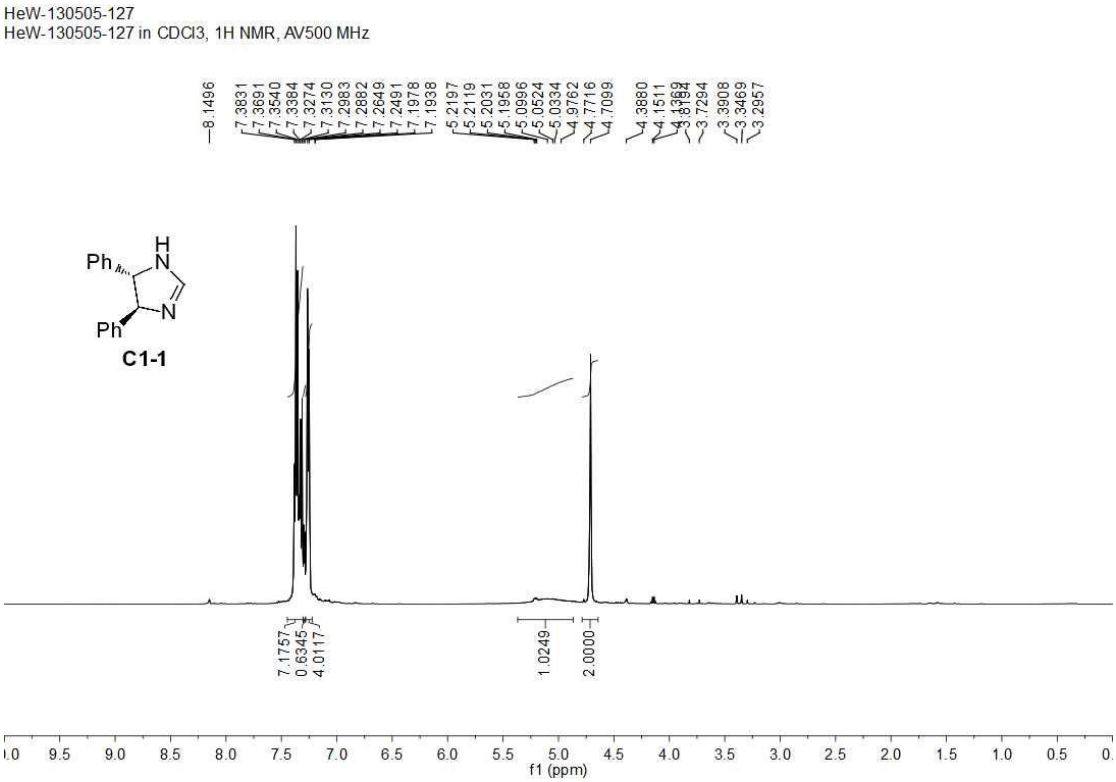

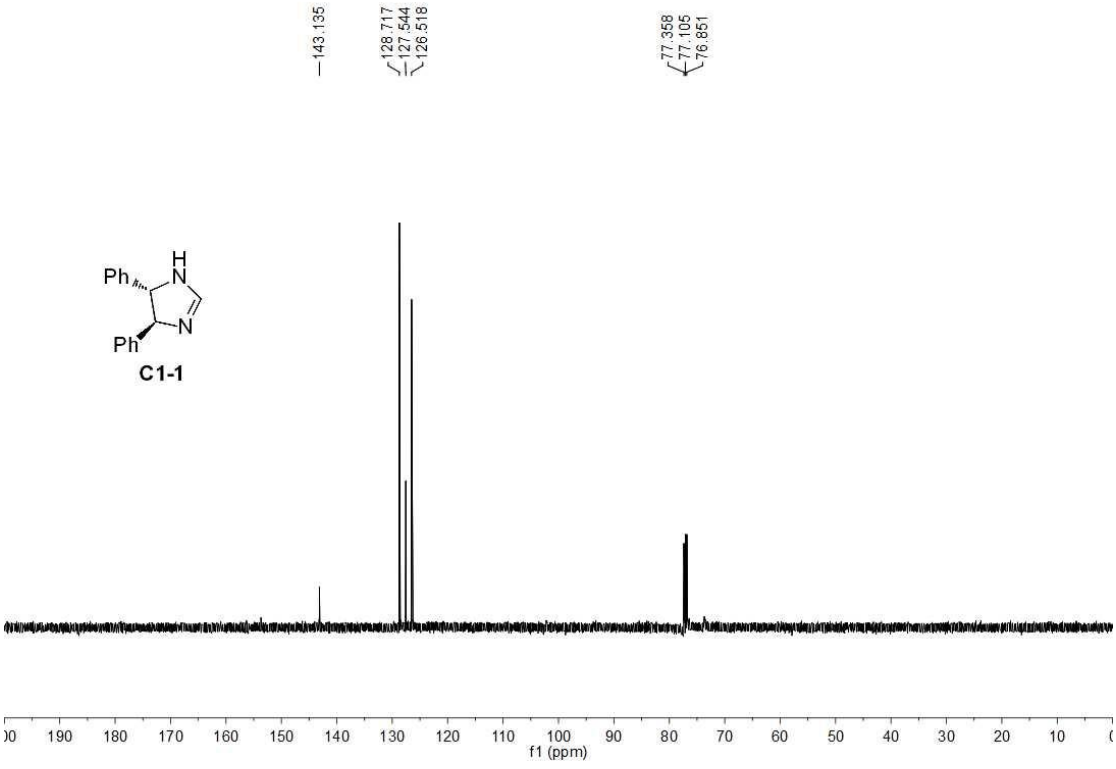

1-[((4*R*,5*R*)-4,5-diphenyl-4,5-dihydro-1*H*-imidazol-1-yl)methyl]-3-[((4*S*,5*S*)-4,5-diphenyl-4,5-dihydro-1*H*-imidazol-1-yl)methyl]benzene, **C1-2**

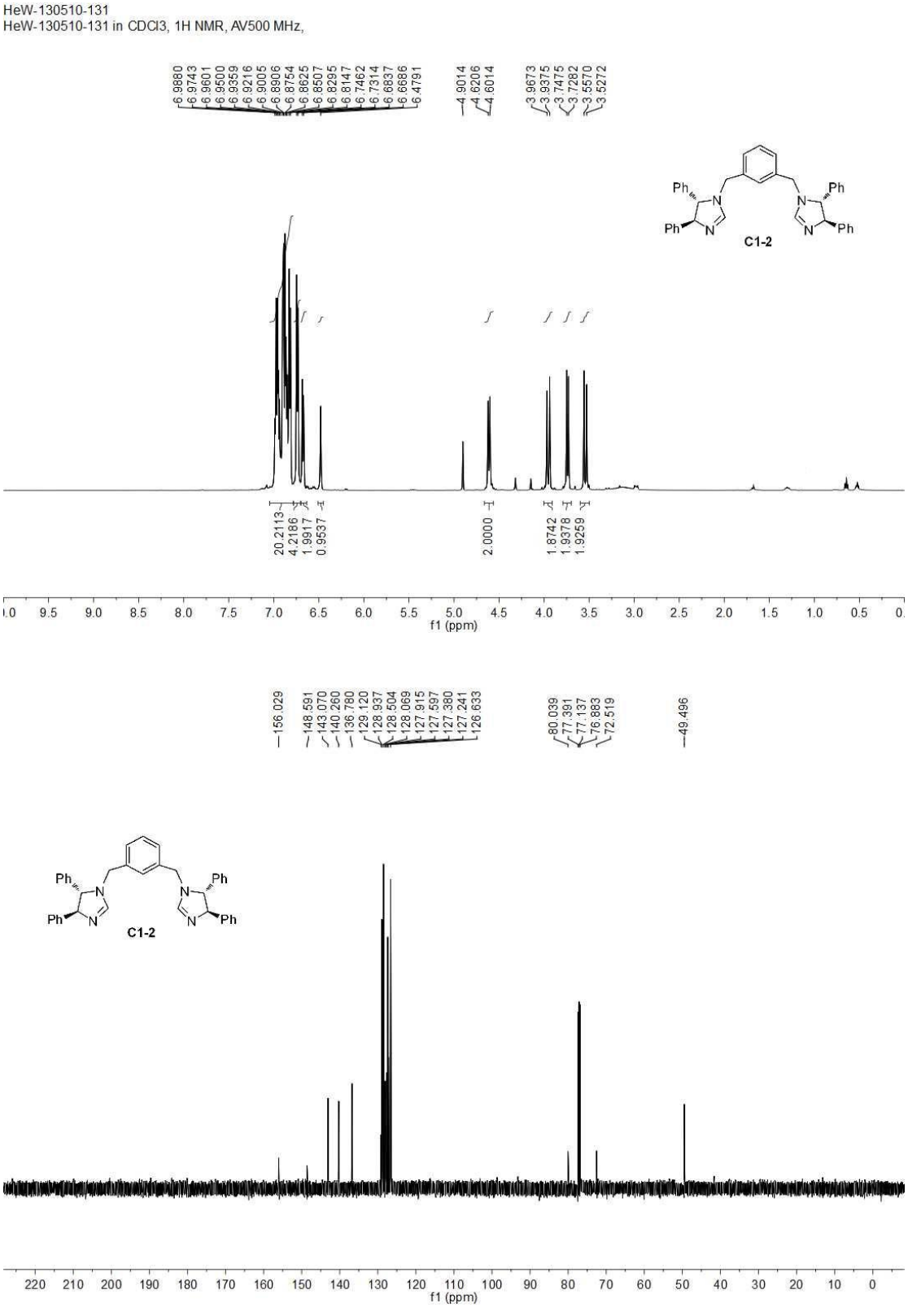

1,1'-[1,3-phenylenebis(methylene)]-bis[(4*S*,4'*S*,5*S*,5'*S*)-4,5-dihydro-4,5-diphenyl]-2,2'-iodo-3,3'-methyl-1*H*-imidazolium-bis(trifluoromethane sulfonate), **C1**

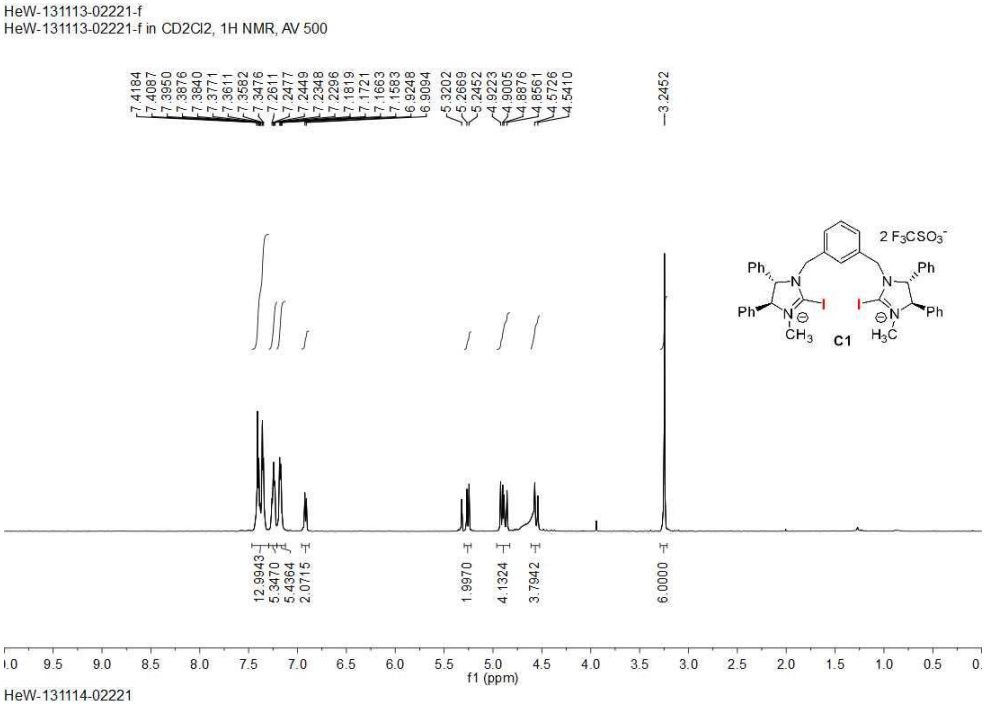

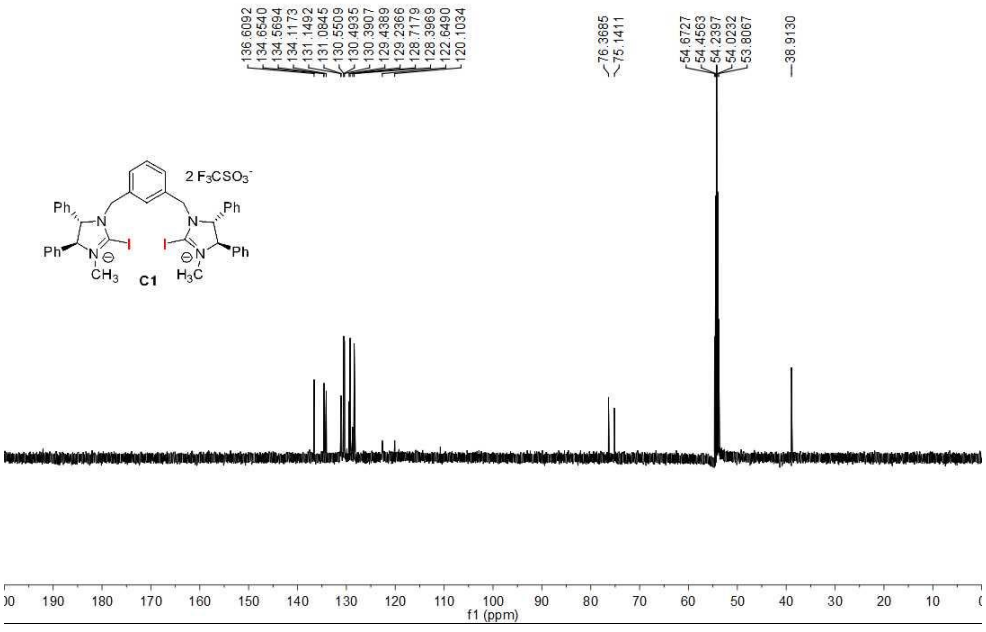

1,1'-[1,3-phenylenebis(methylene)]-bis[(4*S*,4'*S*,5*S*,5'*S*)-4,5-dihydro-4,5-diphenyl]-3,3'-methyl-1*H*-imidazolium-bis(trifluoromethane sulfonate), **C2**

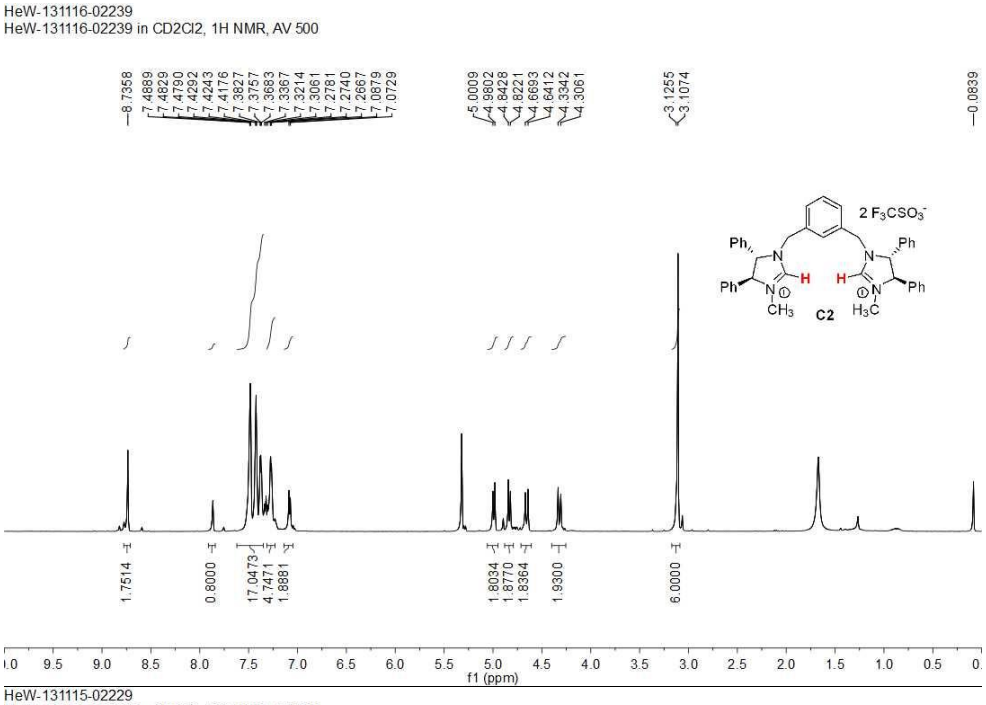

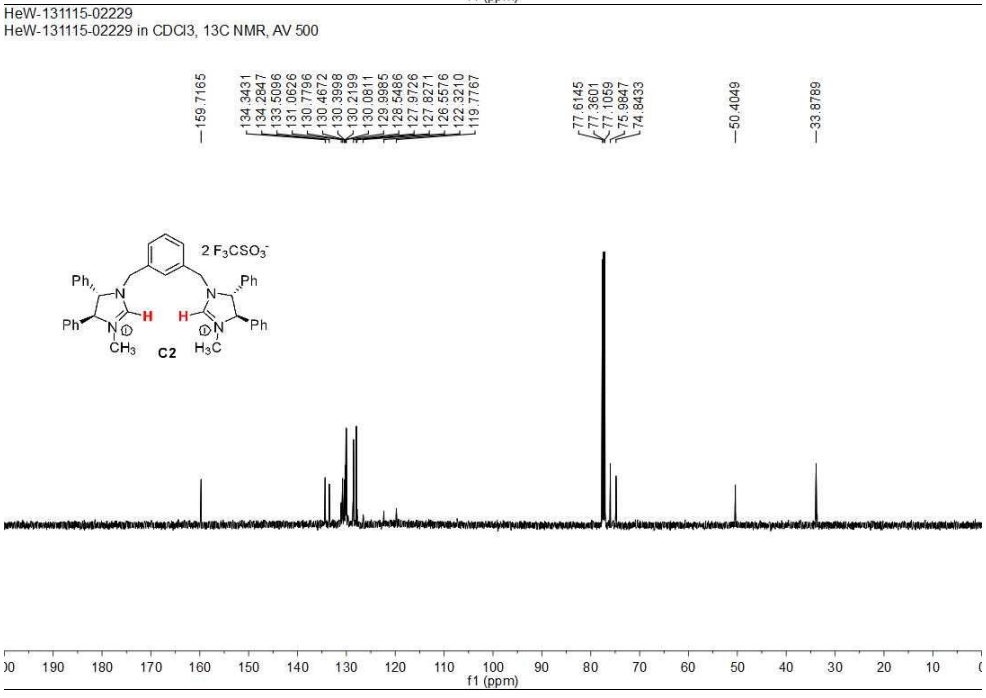

1,1'-[1,3-phenylenebis(methylene)]-bis[(4*S*,4'*S*,5*S*,5'*S*)-4,5-dihydro-4,5-diphenyl]-2,2'-iodo-1*H*-imidazole, **C3**

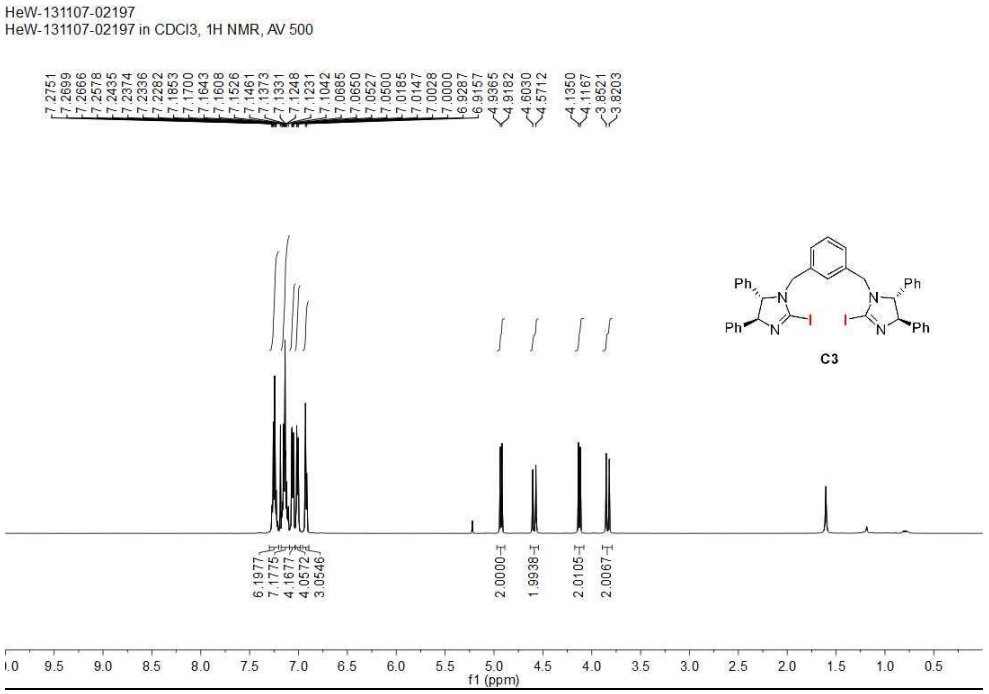

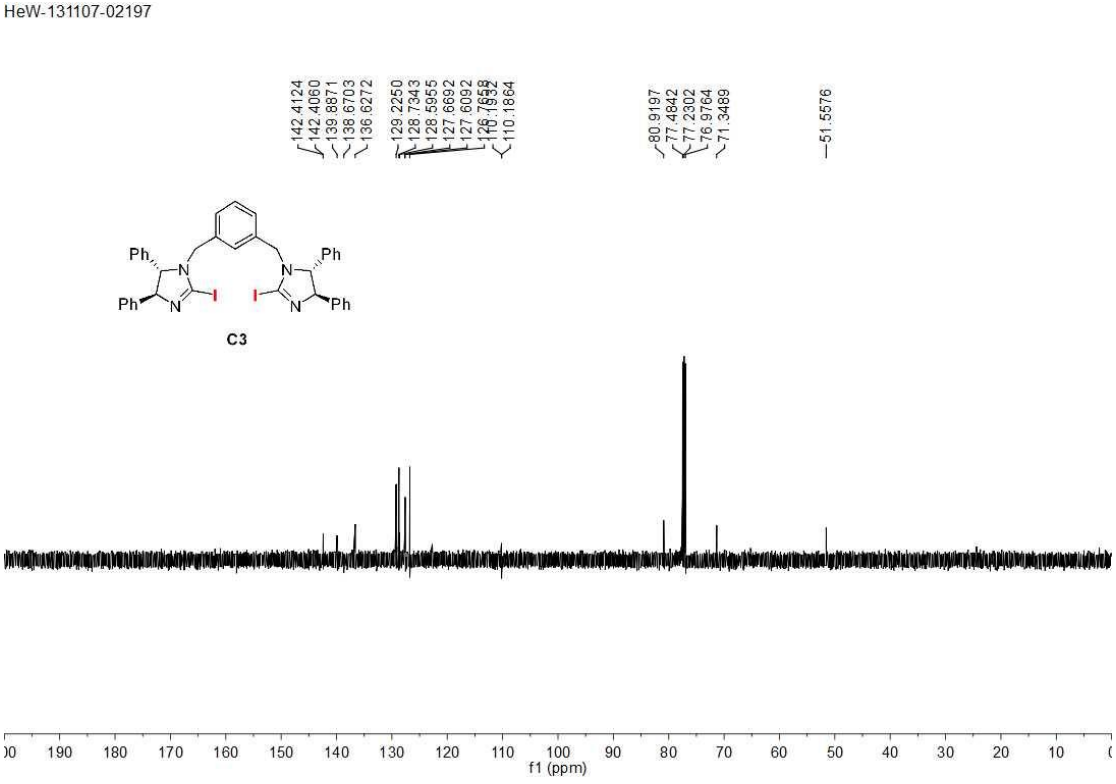

1,3-bis((1*H*-benzo[*d*]imidazol-1-yl)methyl)benzene, **C4-2**

HeW-130627-233-1

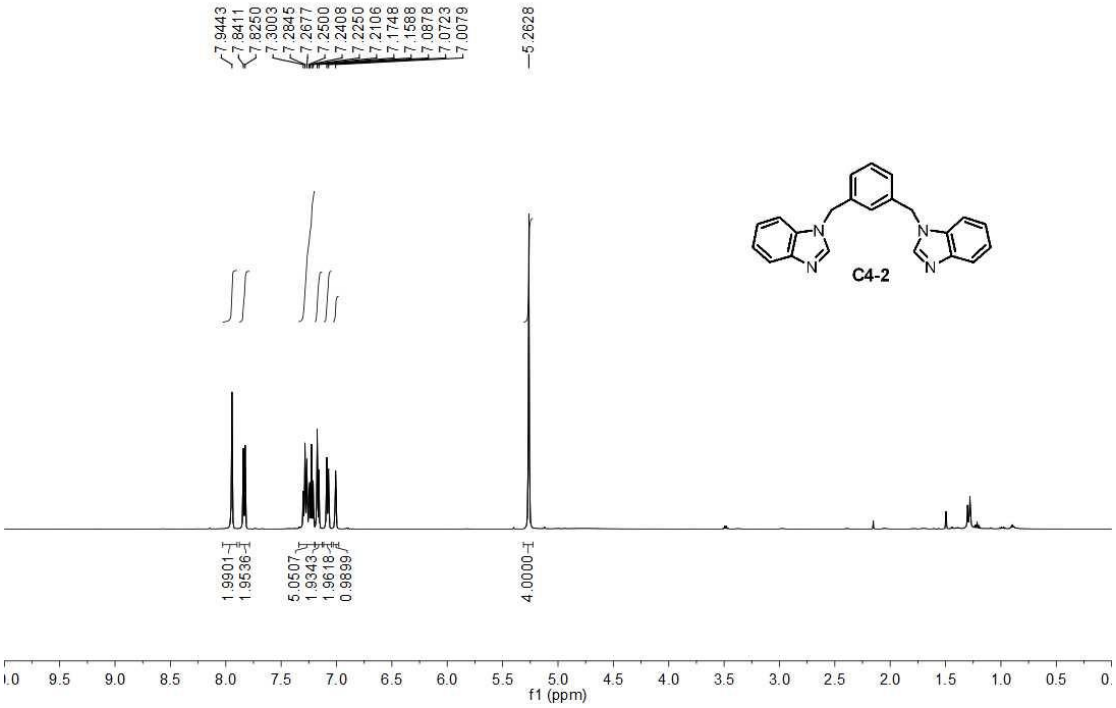

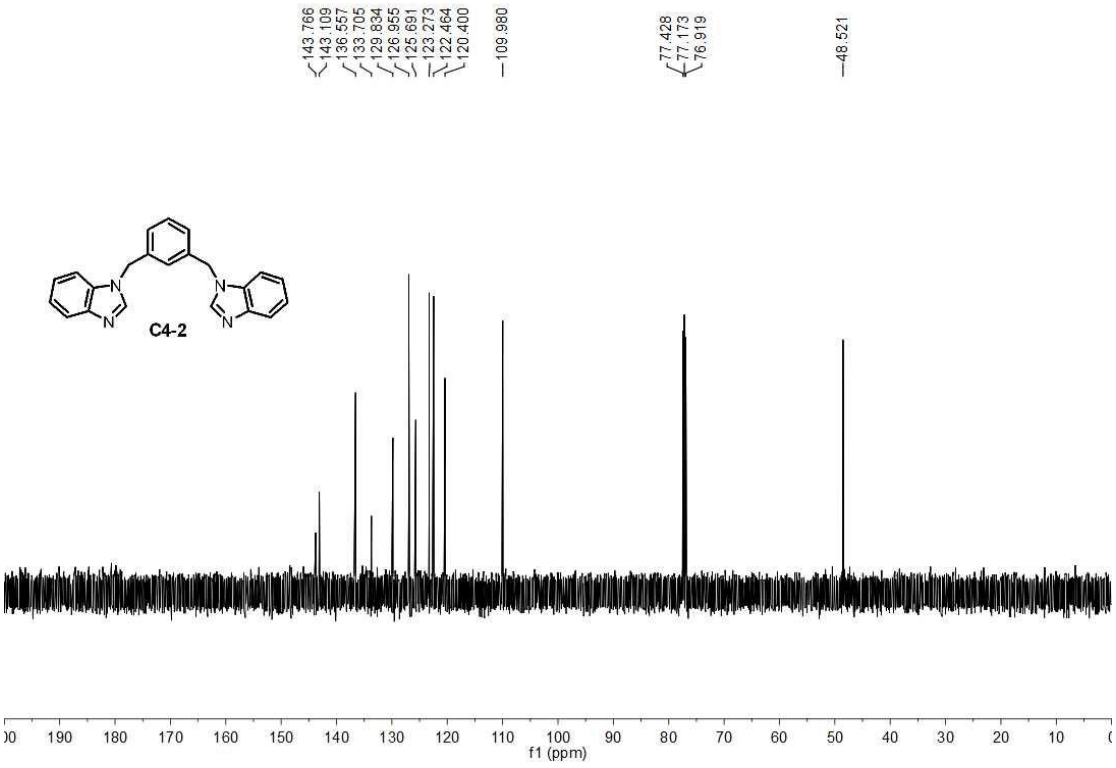

1,1'-[1,3-phenylenebis(methylene)]-bis-2,2'-iodo-1*H*- benzimidazole, **C4-3**

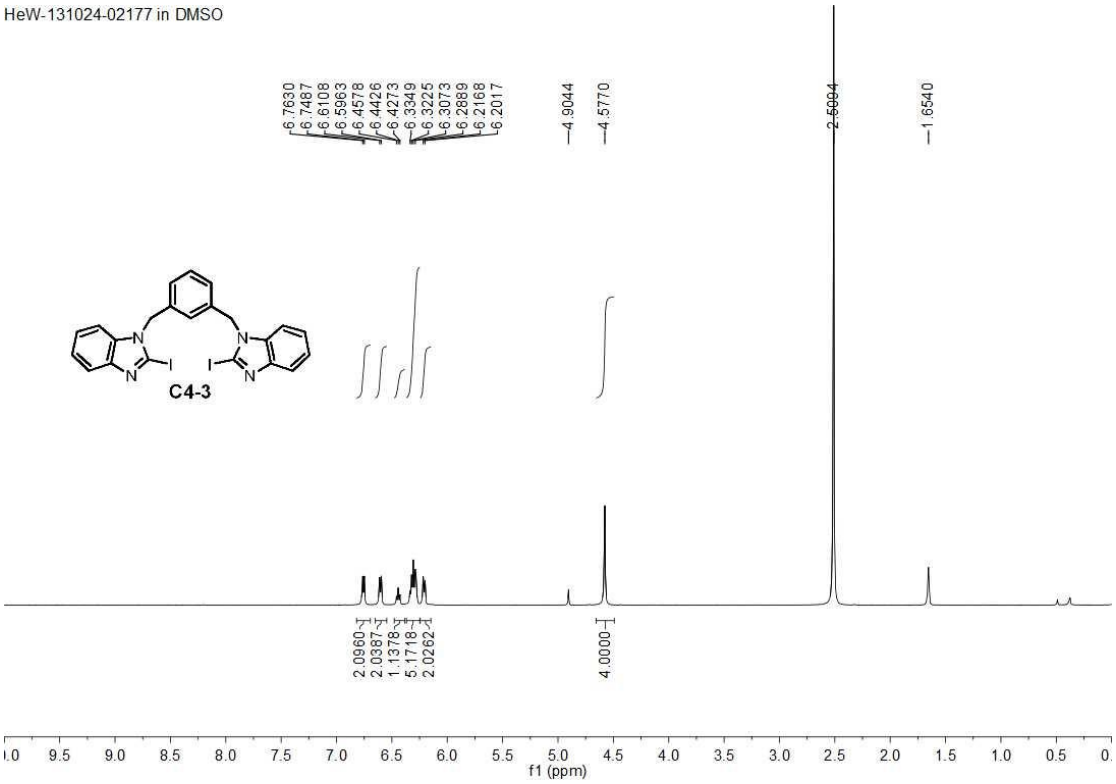

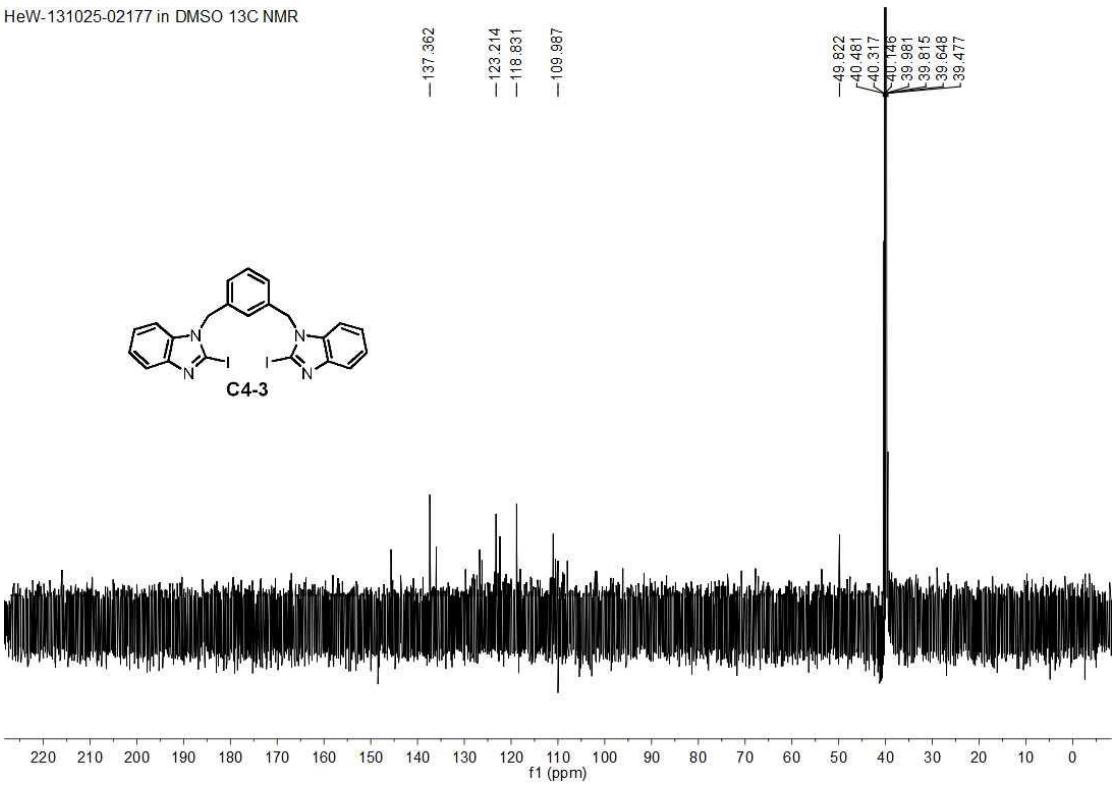

1,1'-[1,3-phenylenebis(methylene)]-bis-2,2’-iodo-3,3’-methyl-1*H*-benzimidazolium-bis(triflu oromethane sulfonate), **C4**

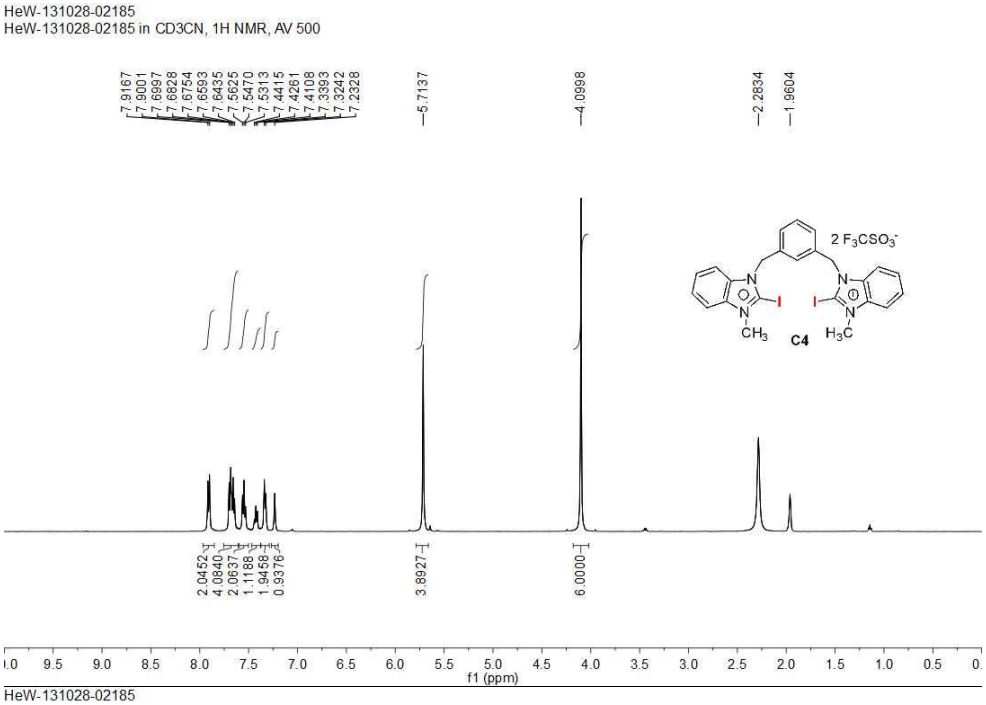

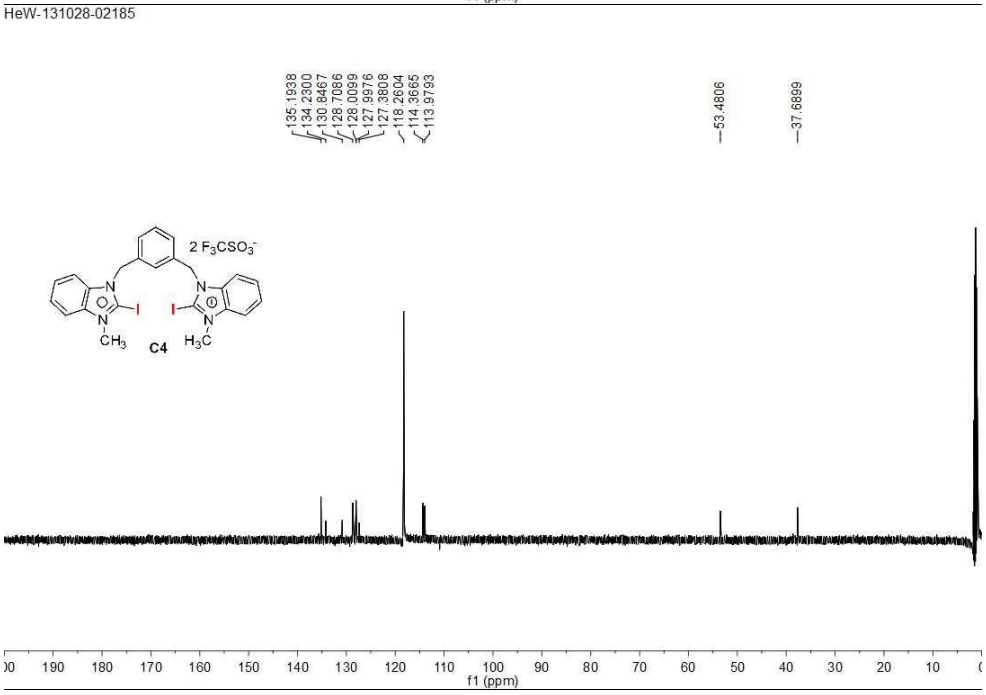

1-benzyl-[(4*S*,5*S*)-4,5-dihydro-4,5-

diphenyl]-2-iodo-3-methyl-1*H*-imidazolium-(trifluoromethane sulfonate), **C5**

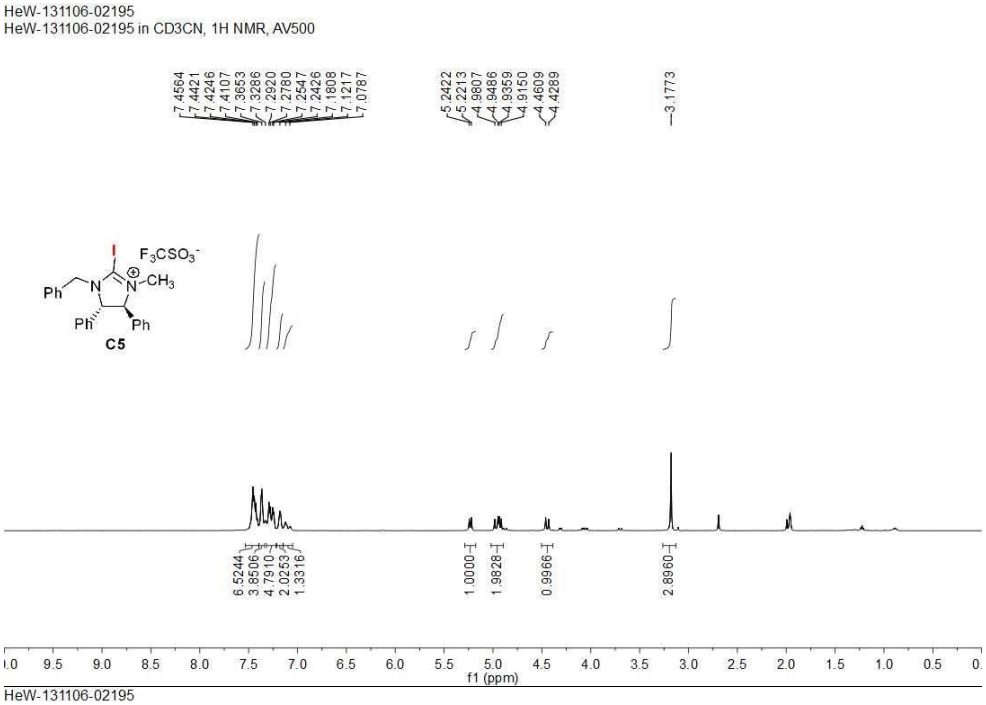

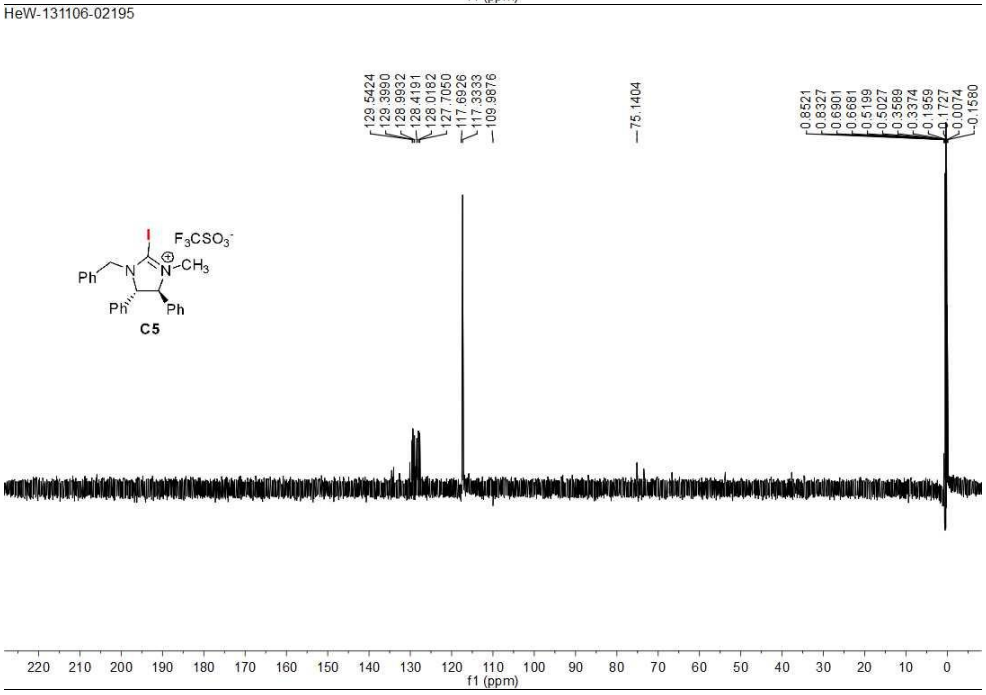

1-methyl-2-iodo-3-methyl-1*H*-imidazolium-trifluoromethane sulfonate, **C6**

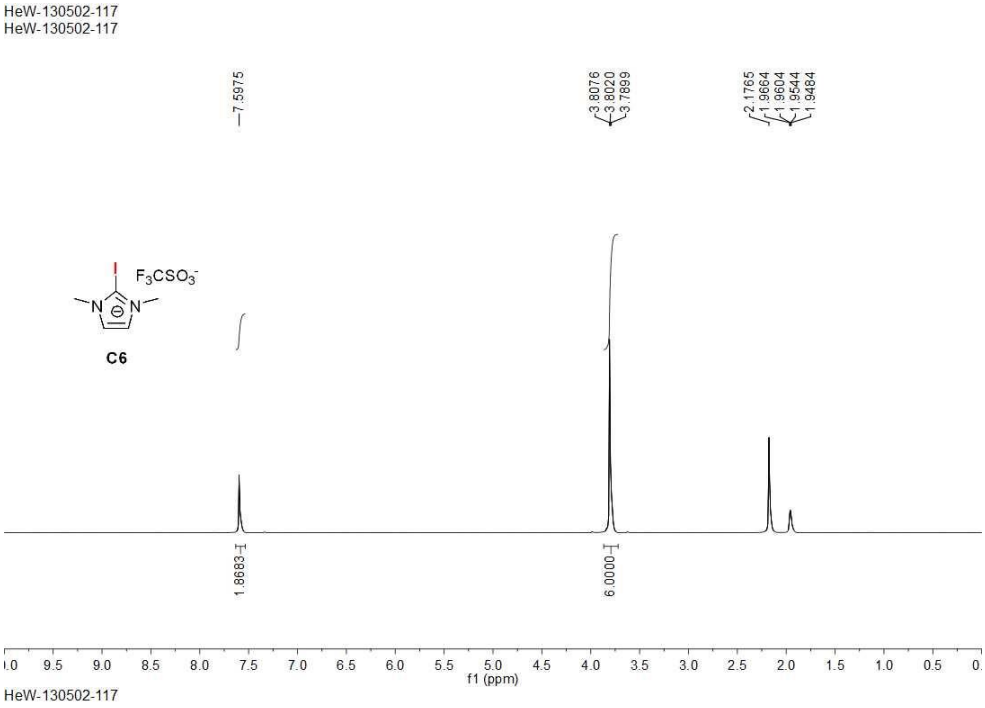

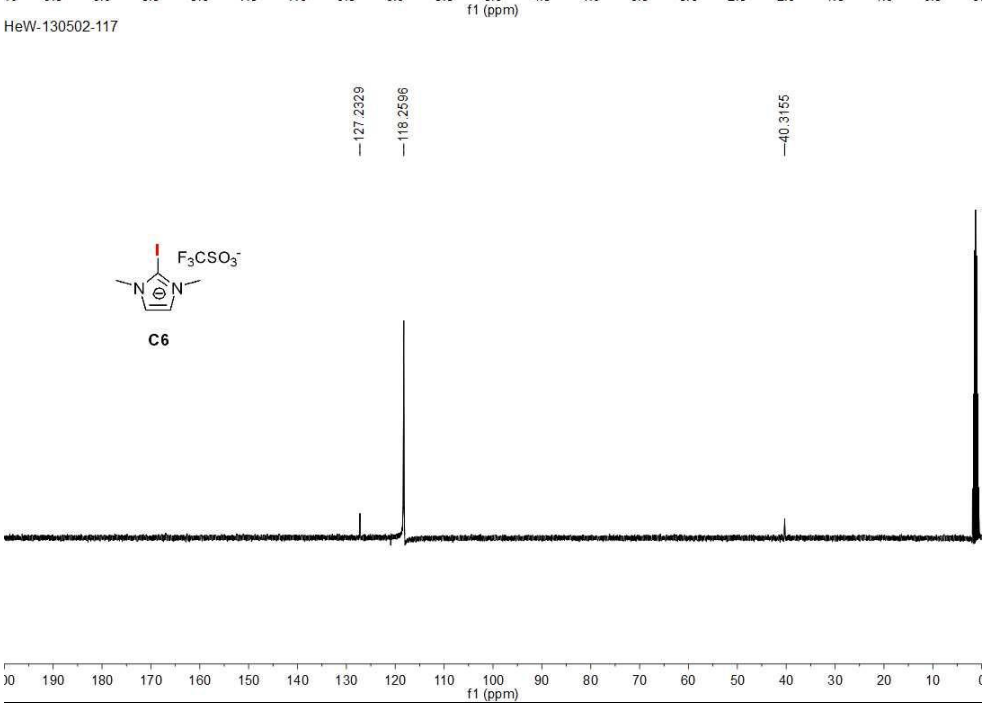

1,1'-[1,3-phenylenebis(methylene)]-bis[(4*S*,4'*S*,5*S*,5'*S*)-4,5-dihydro-4,5-diphenyl]-2,2'-iodo-3,3'-*n*-butyl-1*H*-imidazolium-bis(trifluoromethane sulfonate), **C7**

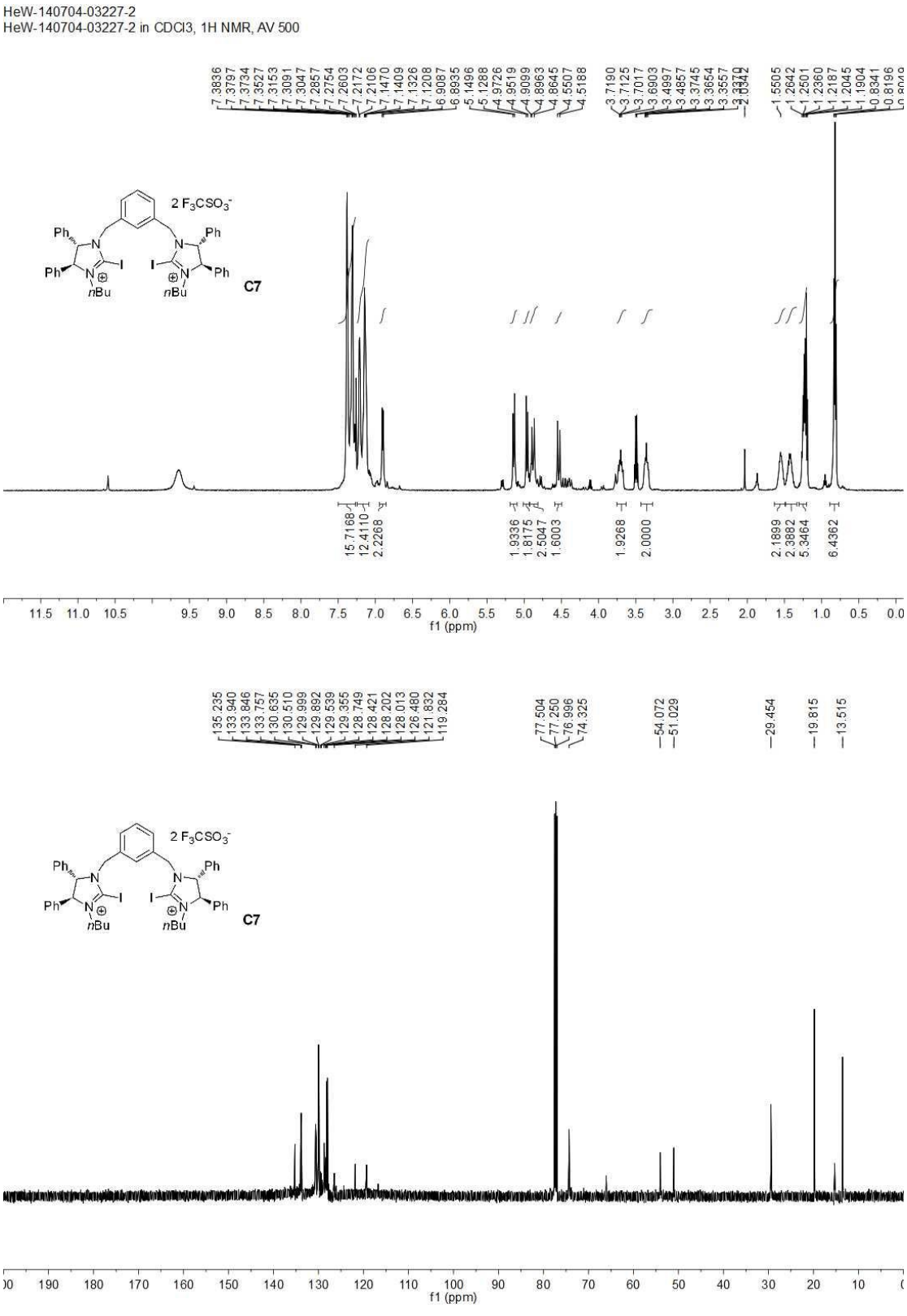

3,3'-diiodine-*N*,*N*'-dimethyl-2,2'-bipyridinium triflate, **C8**

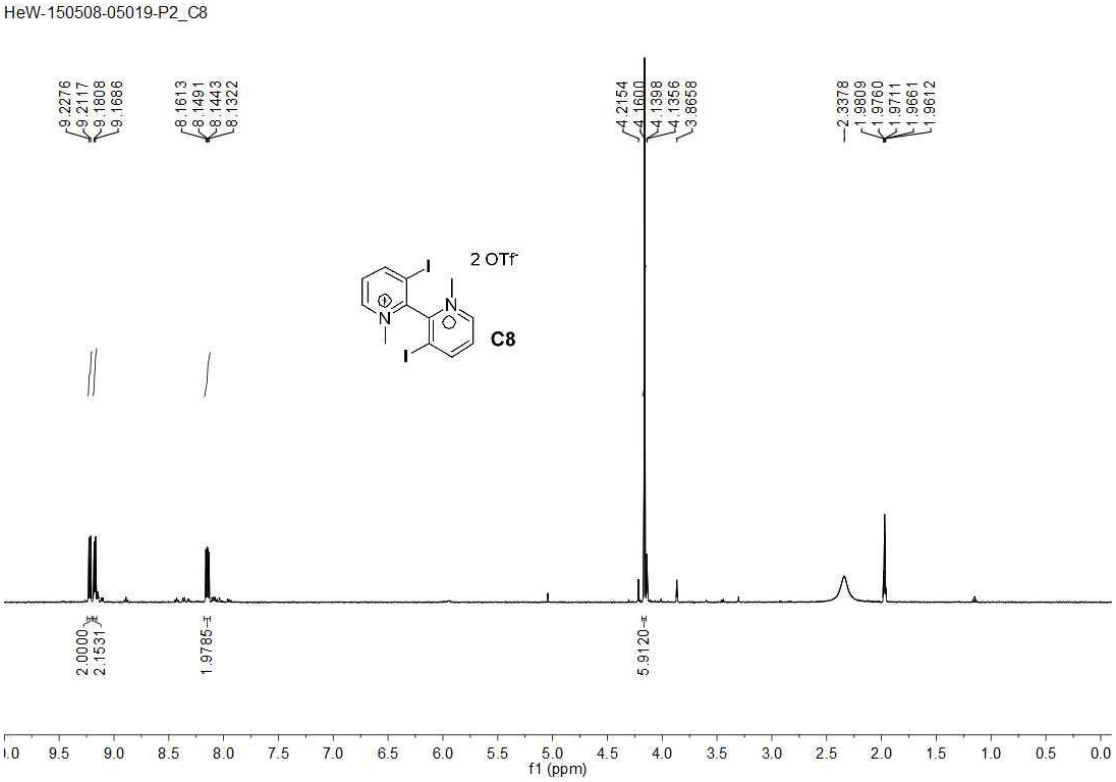

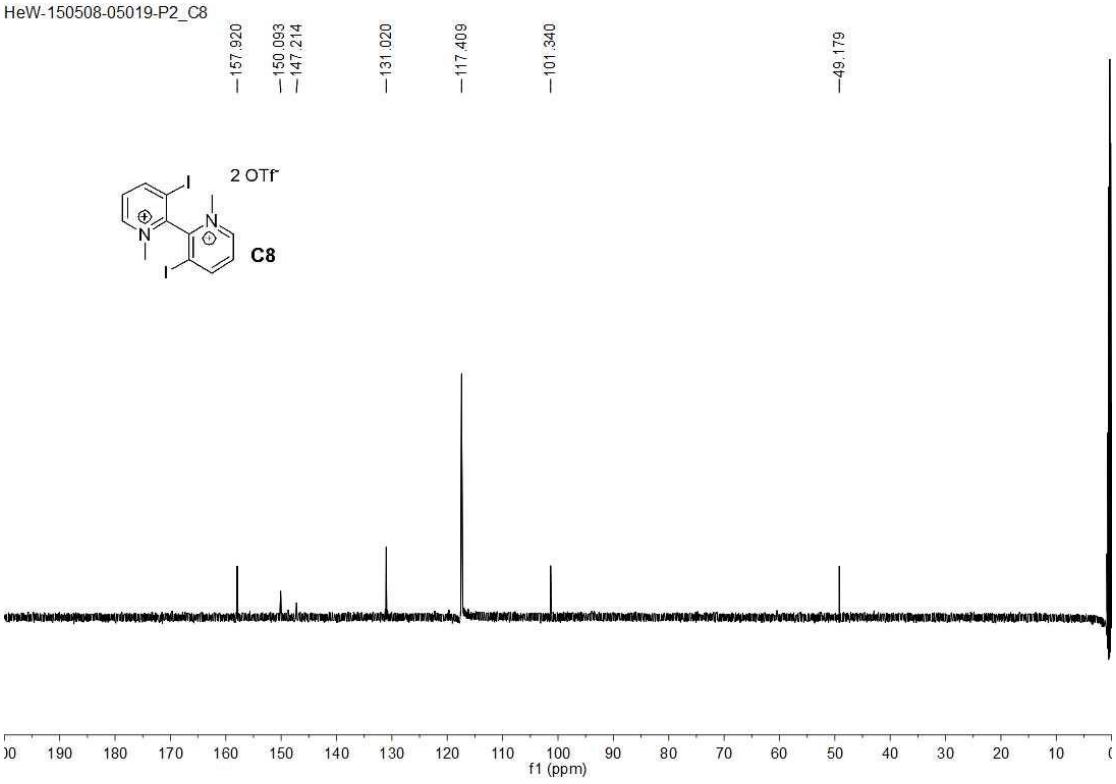

mono(3,3'-diiodo-1,1'-dimethyl-[2,2'-bipyridine]-1,1'-diium)mono(((1*R*,4*R*)-7,7-dimethylbicyclo[2.2.1]heptan-1-yl)methanesulfonate), **C11**

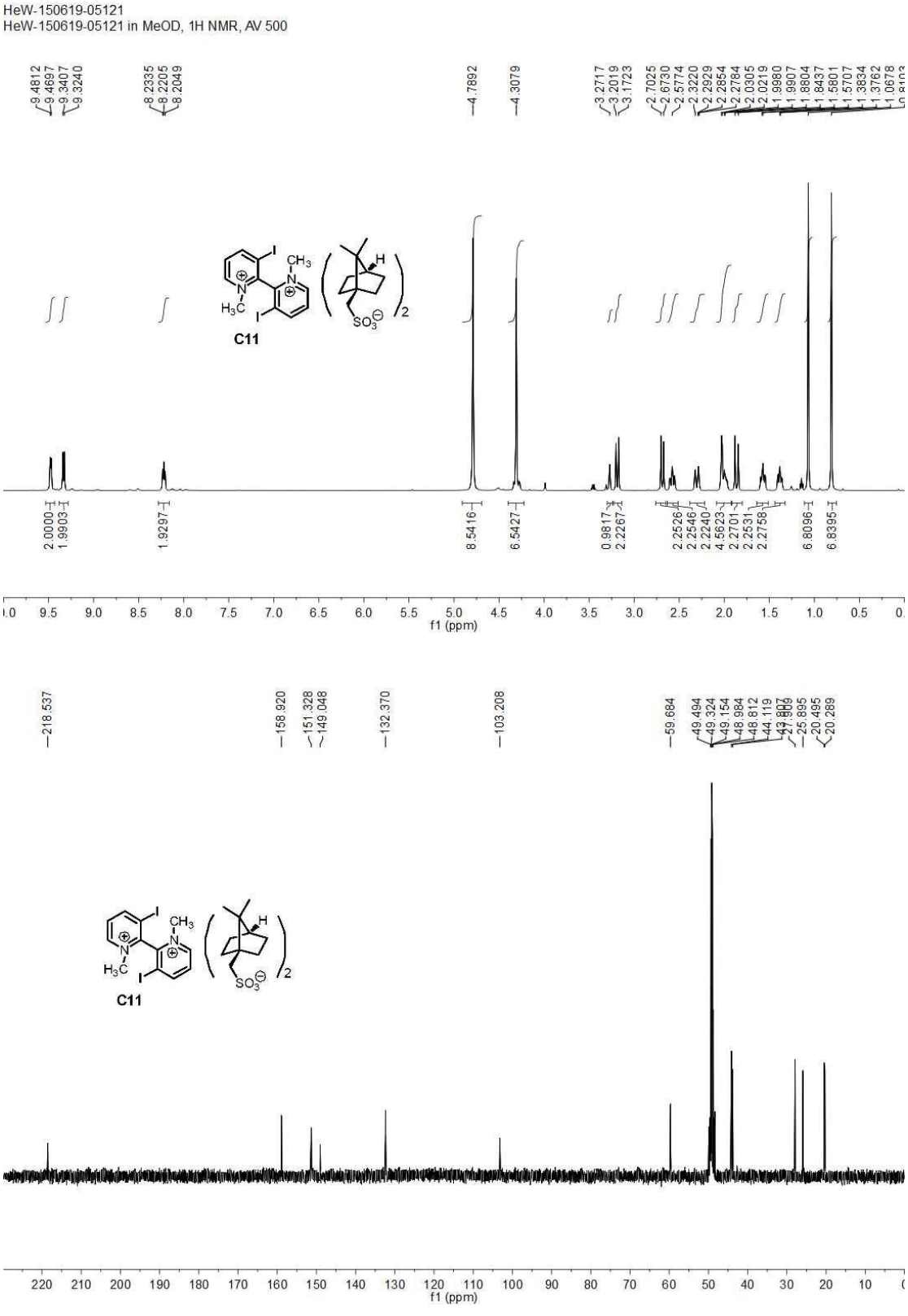

3,3'-diiodo-1,1'-dimethyl-[2,2'-bipyridine]-1,1'-diium 2,3-dihydroxysuccinate, **C12**

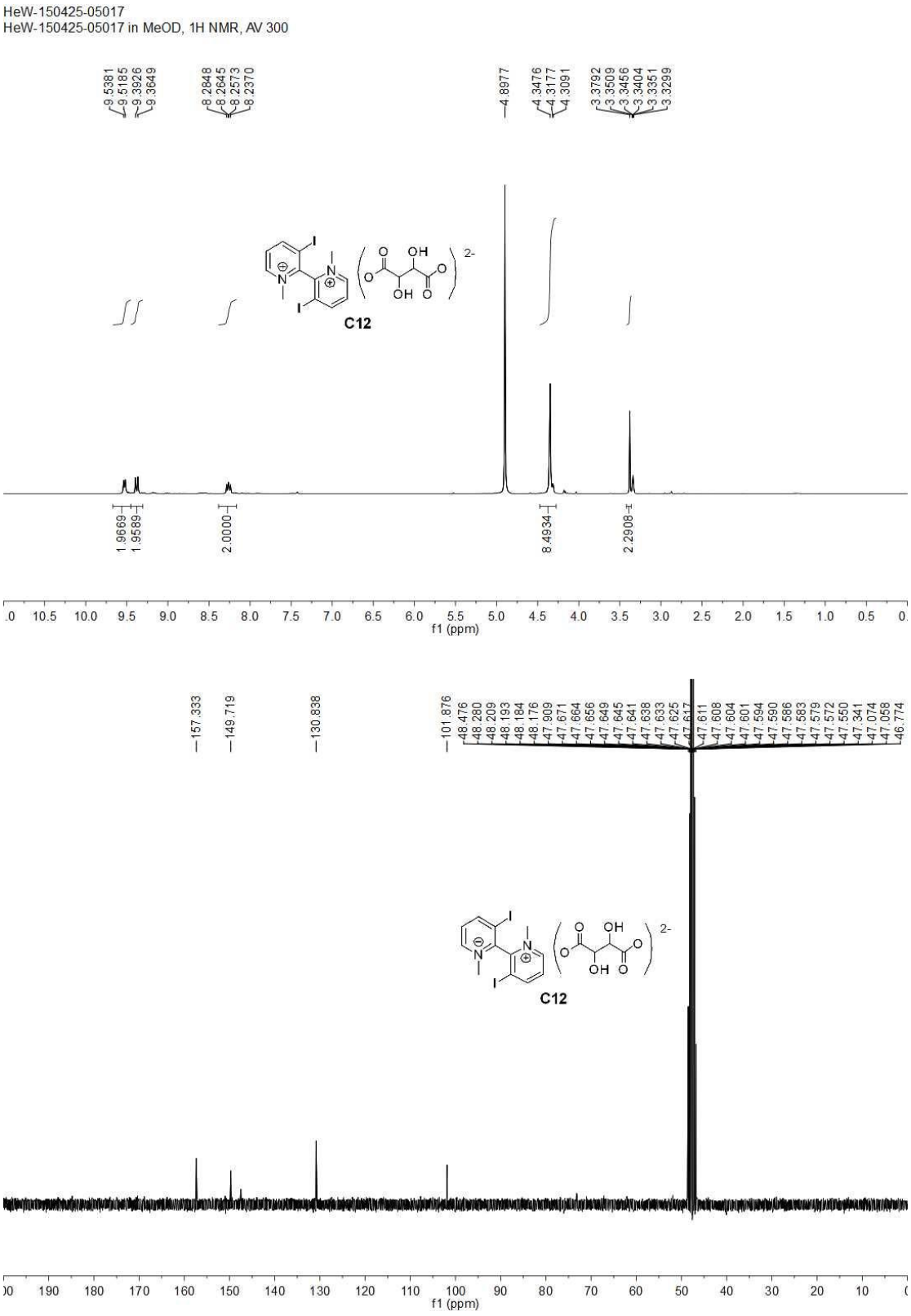

3,3'-diiodine-*N*-methyl-2,2'-pyridinium triflate, **C14**

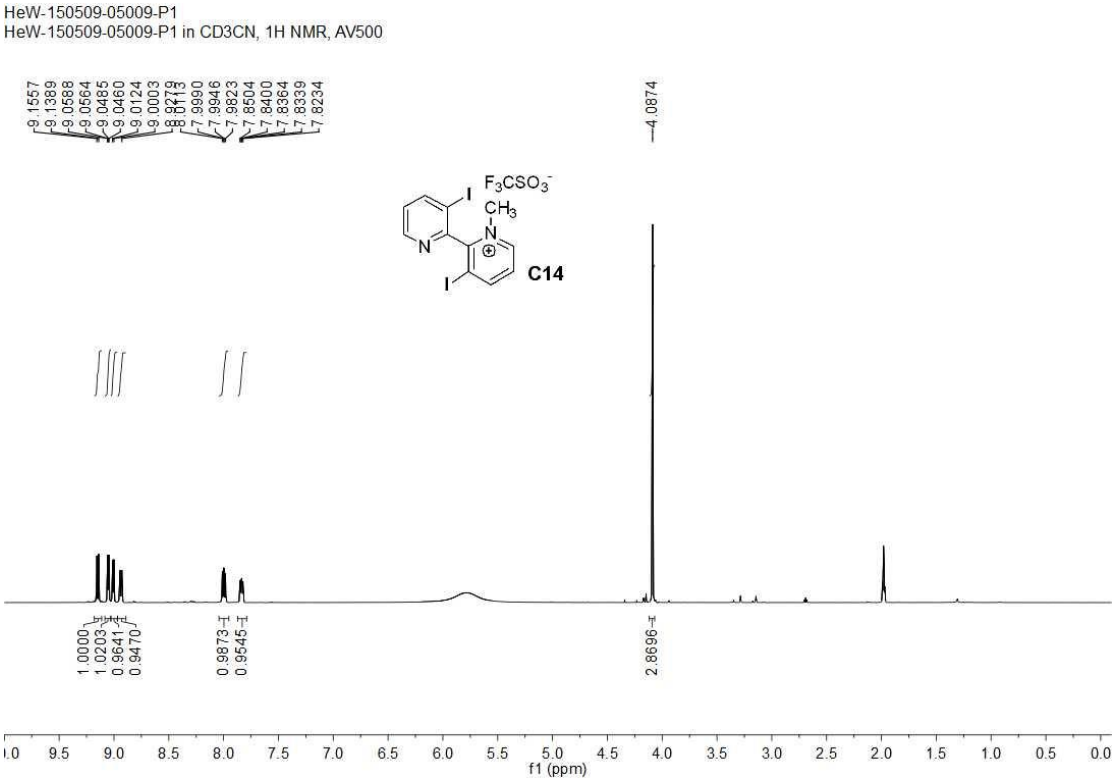

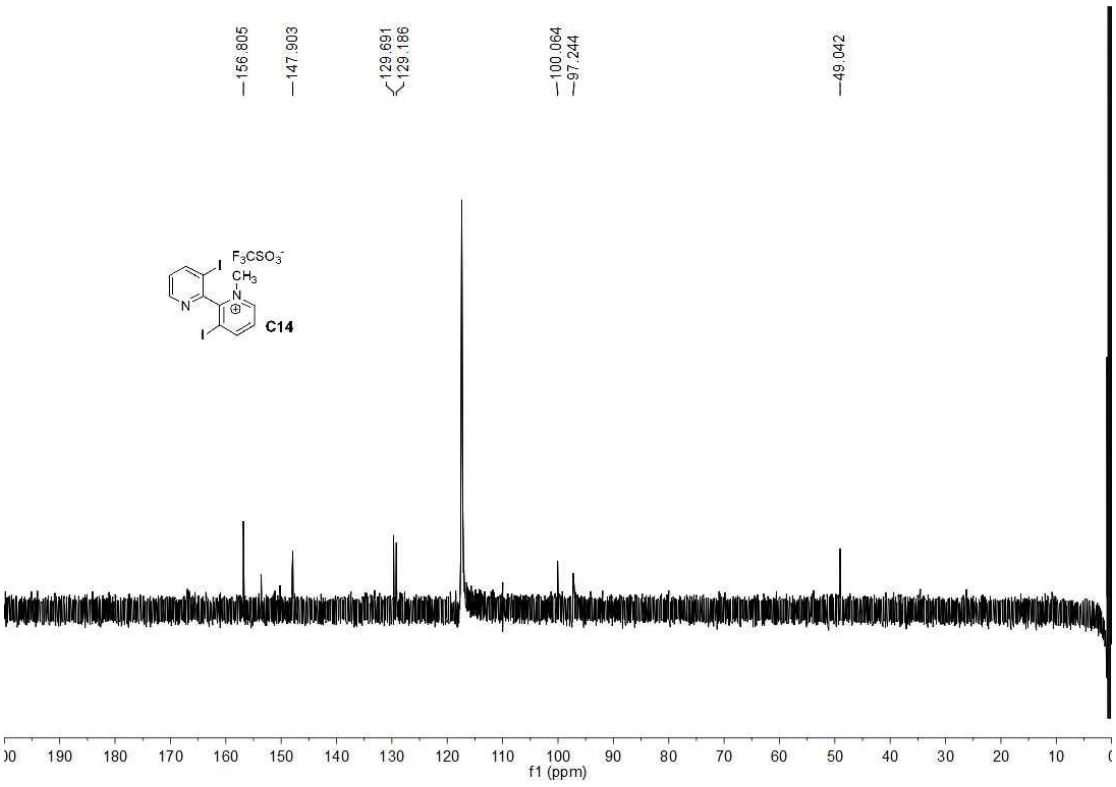

2-phenyl-3-iodine-*N*-methyl-pyridinium triflate, **C15**

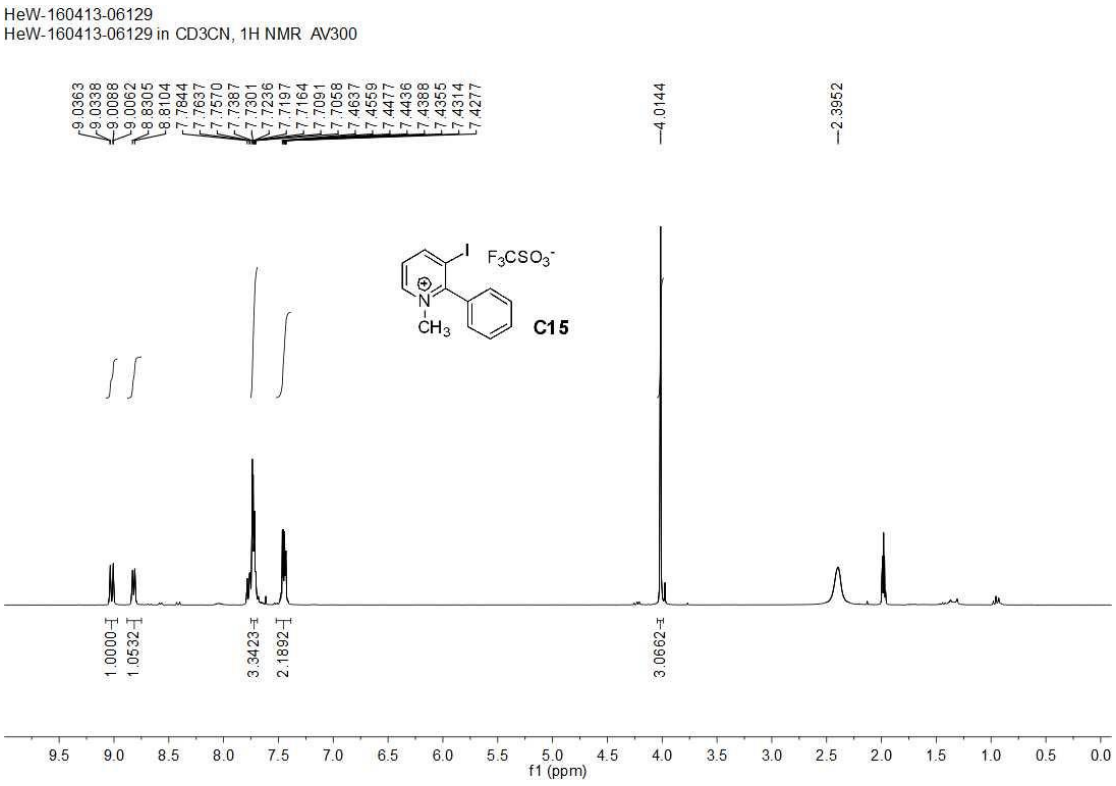

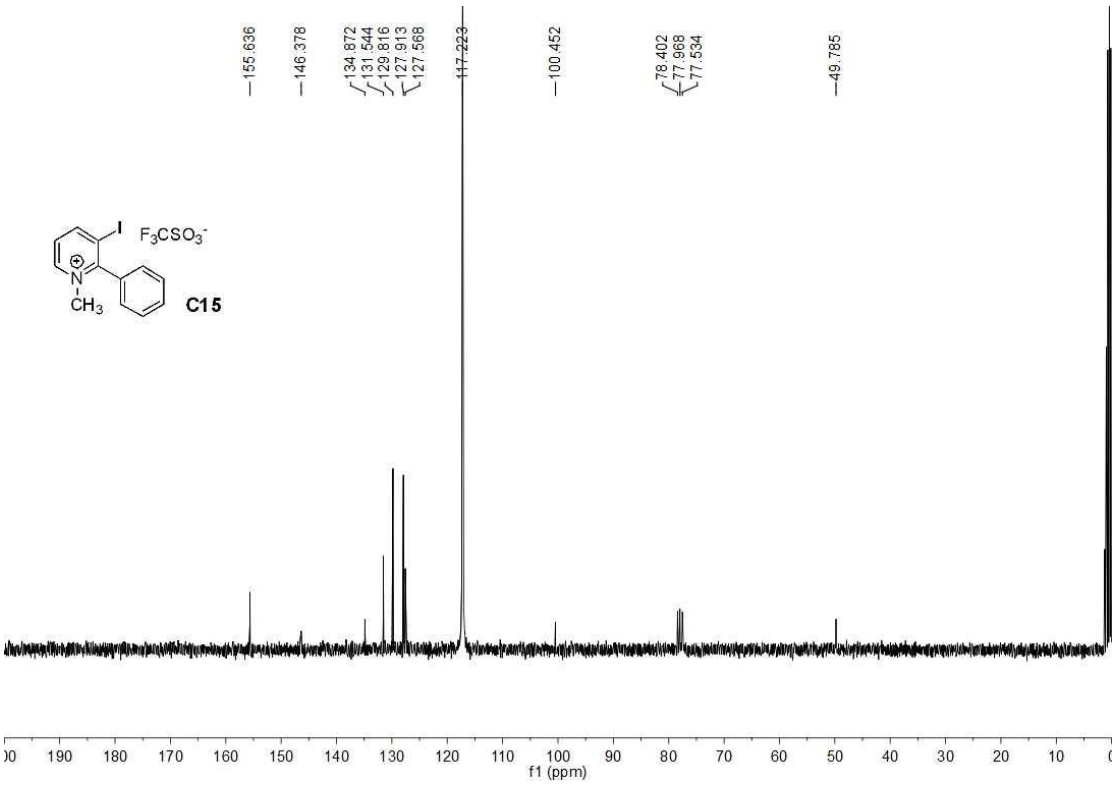

3,3'-diiodine-2,2'-bipyridine, **C16** ^{1}H NMR

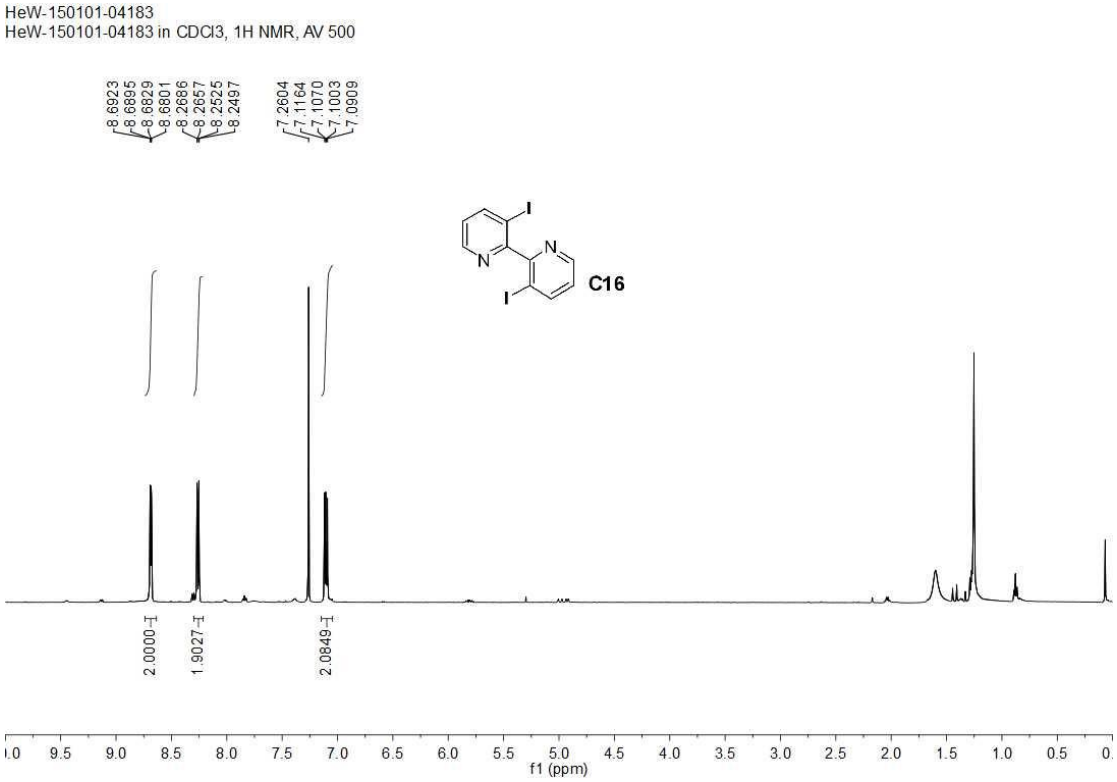

(2*S*,3*S*)-2,3-bis((1*H*-benzo[*d*]imidazol-1-yl)methyl)-1,4-dioxaspiro[4.5]decane, **C17-4**

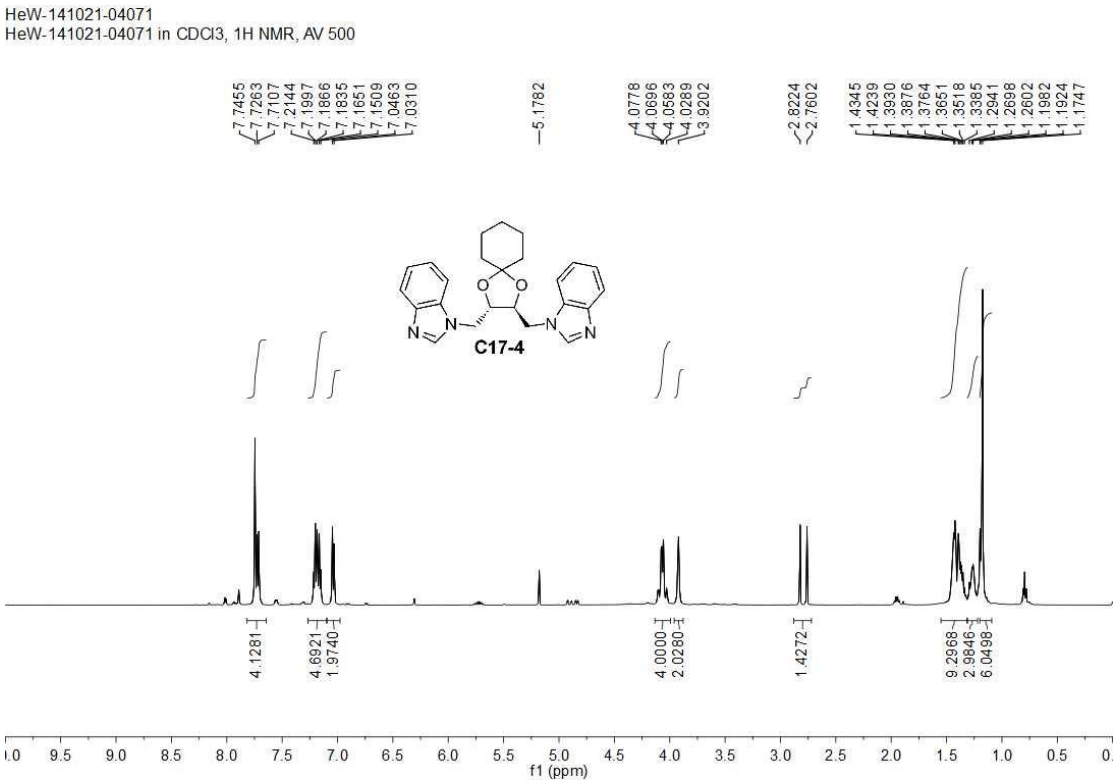

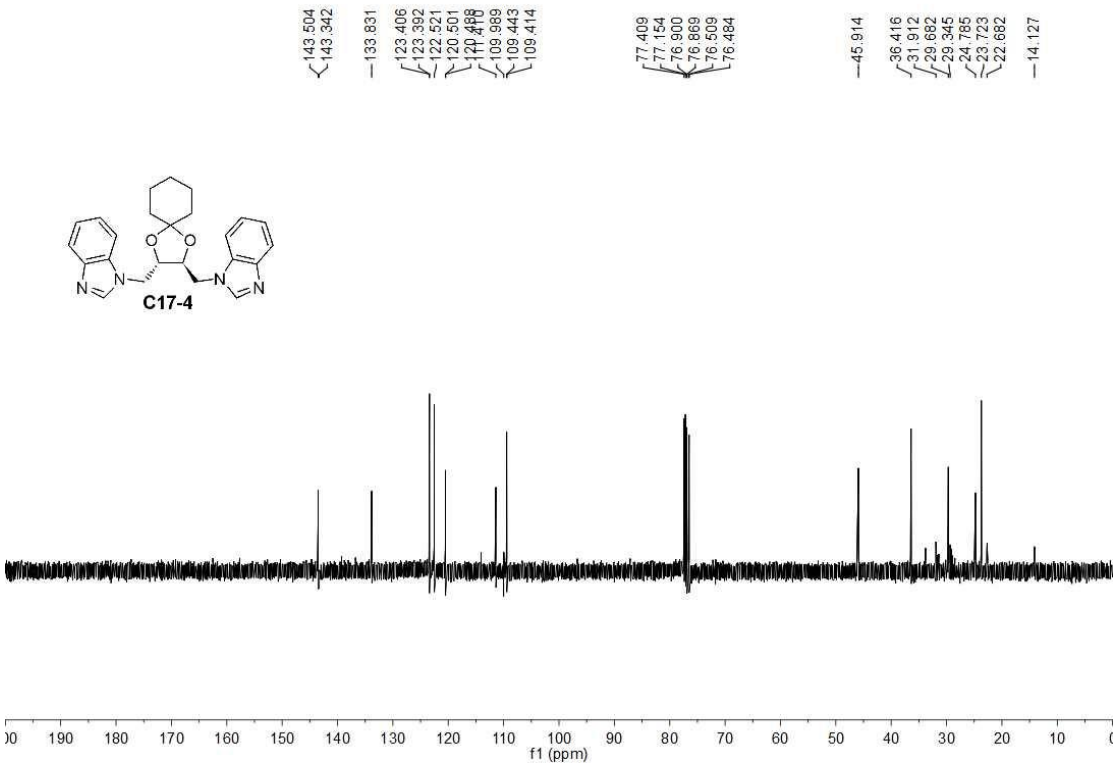

(2*S*,3*S*)-2,3-bis((2-iodo-1*H*-benzo[*d*]imidazol-1-yl)methyl)-1,4-dioxaspiro[4.5]decane, **C17-5**

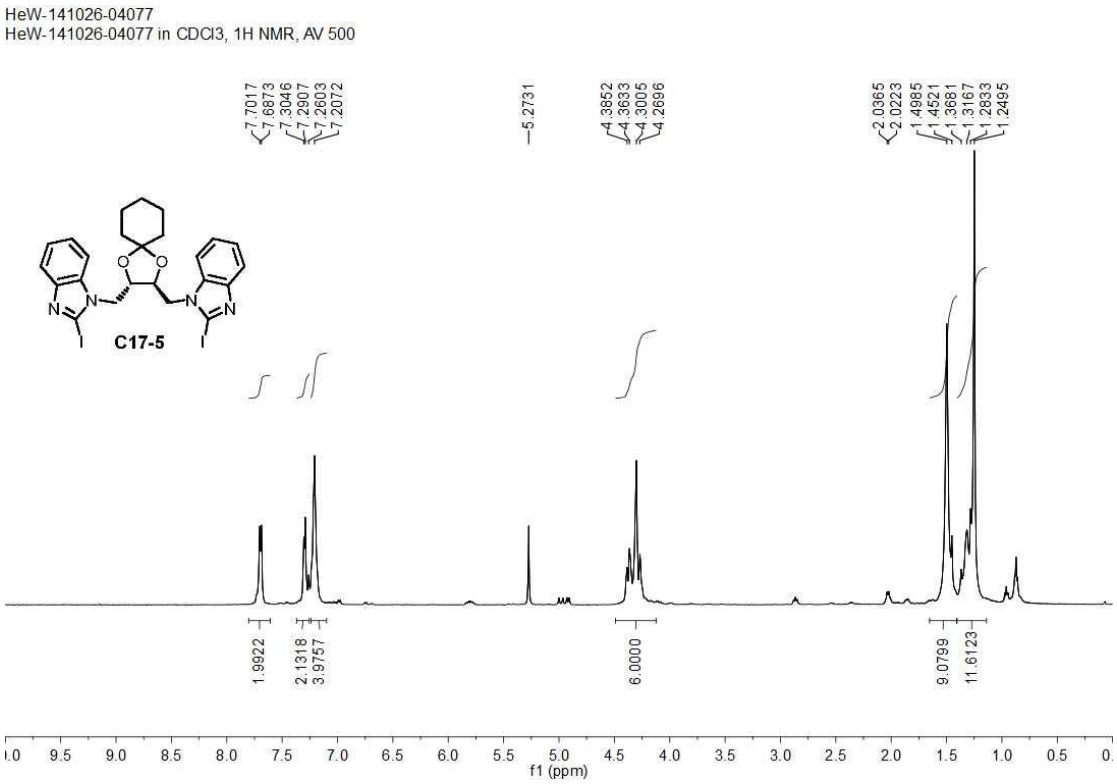

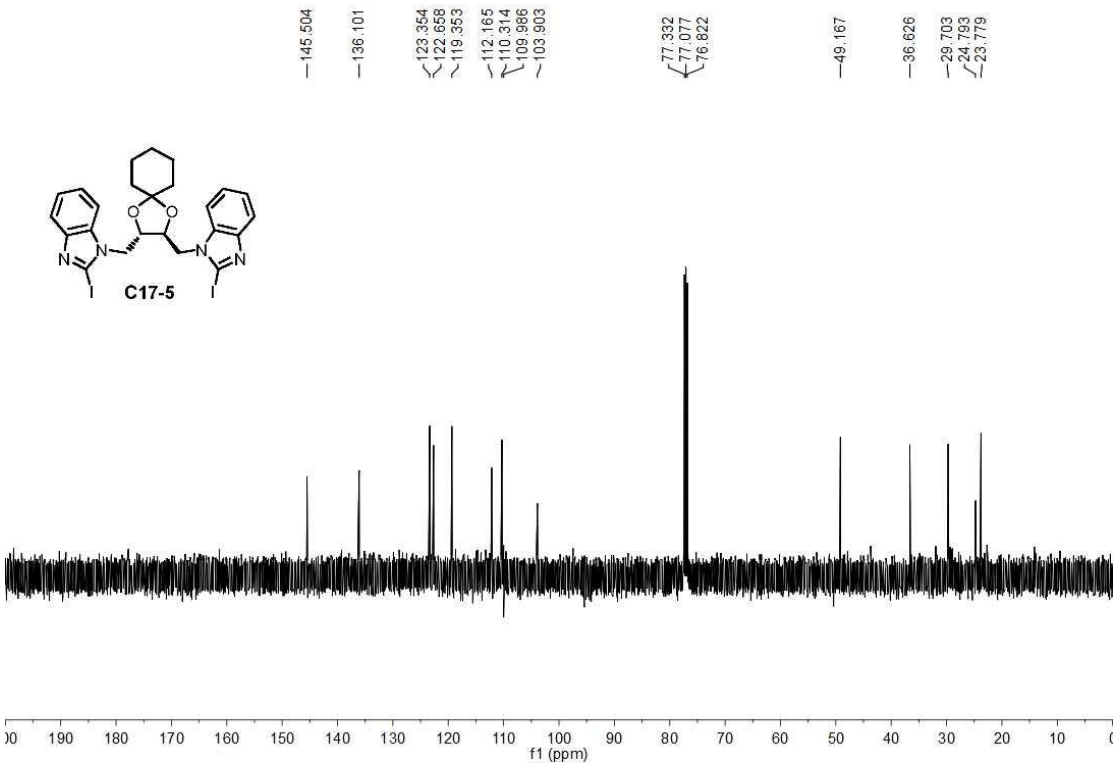

1,1'-((2*S*,3*S*)-1,4-dioxaspiro[4.5]decane-2,3-diylbis(methylene))bis(2-iodo-3-methyl-1*H*-benzo[*d*]imidazol-3-ium) tetrafluoroboric, **C17**

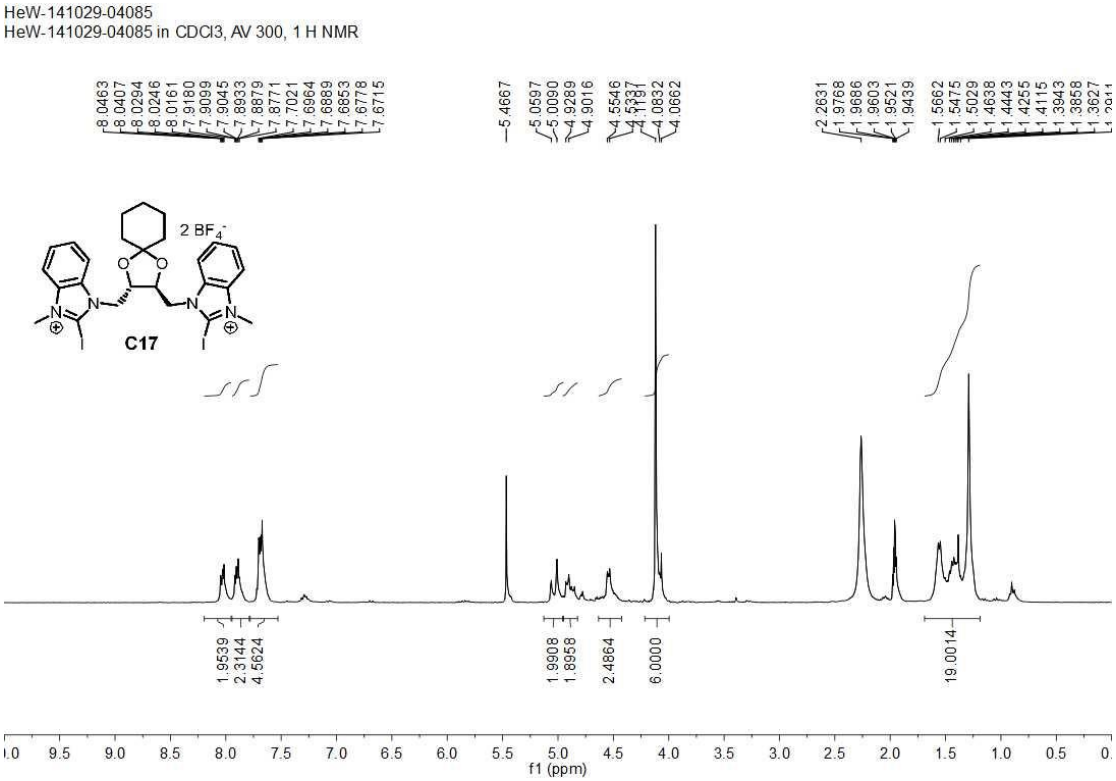

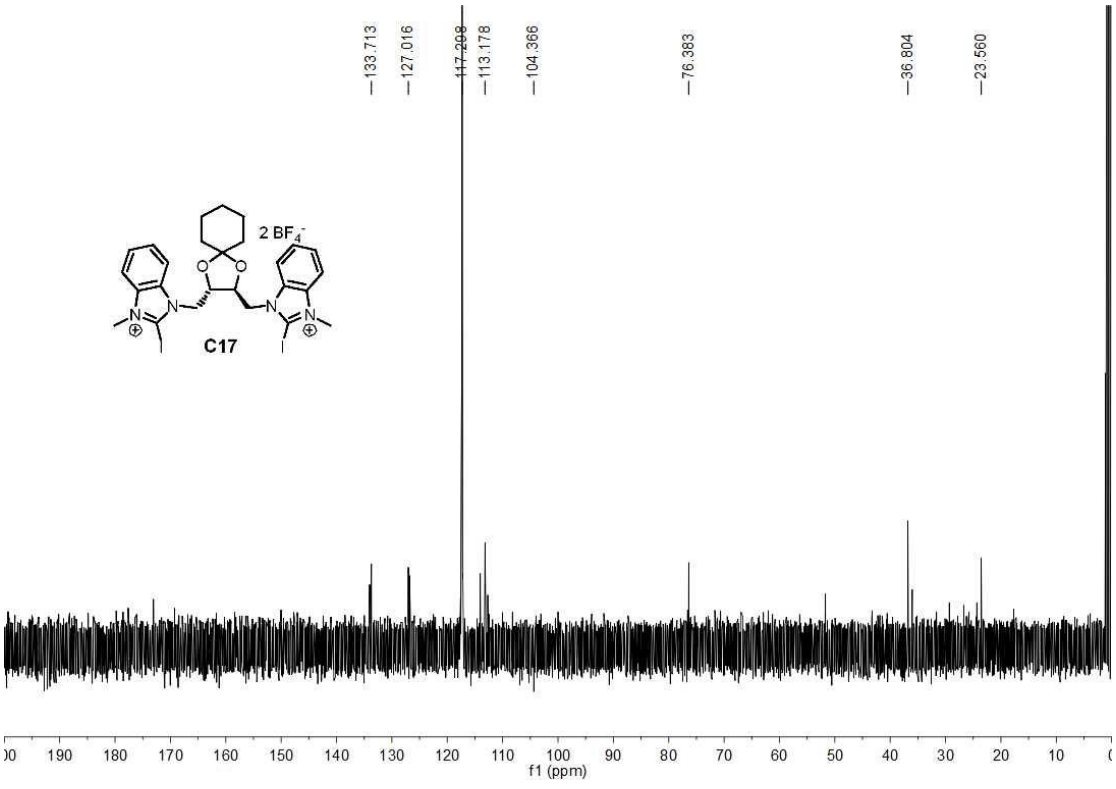

(4*R*,5*R*)-3-butyl-2-iodo-4,5-diphenyl-1-[((*R*)-1-tosylpyrrolidin-2-yl)methyl]-4,5-dihydro-1*H*-imidazol-3-ium triflate, **C18**

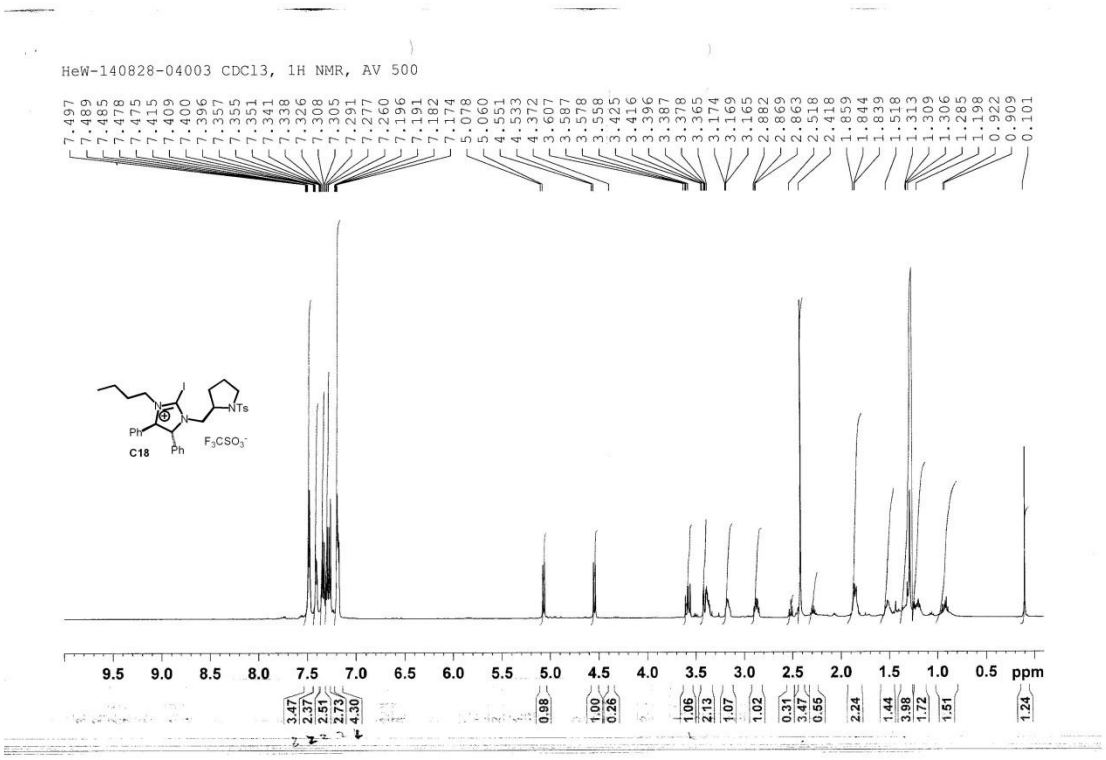

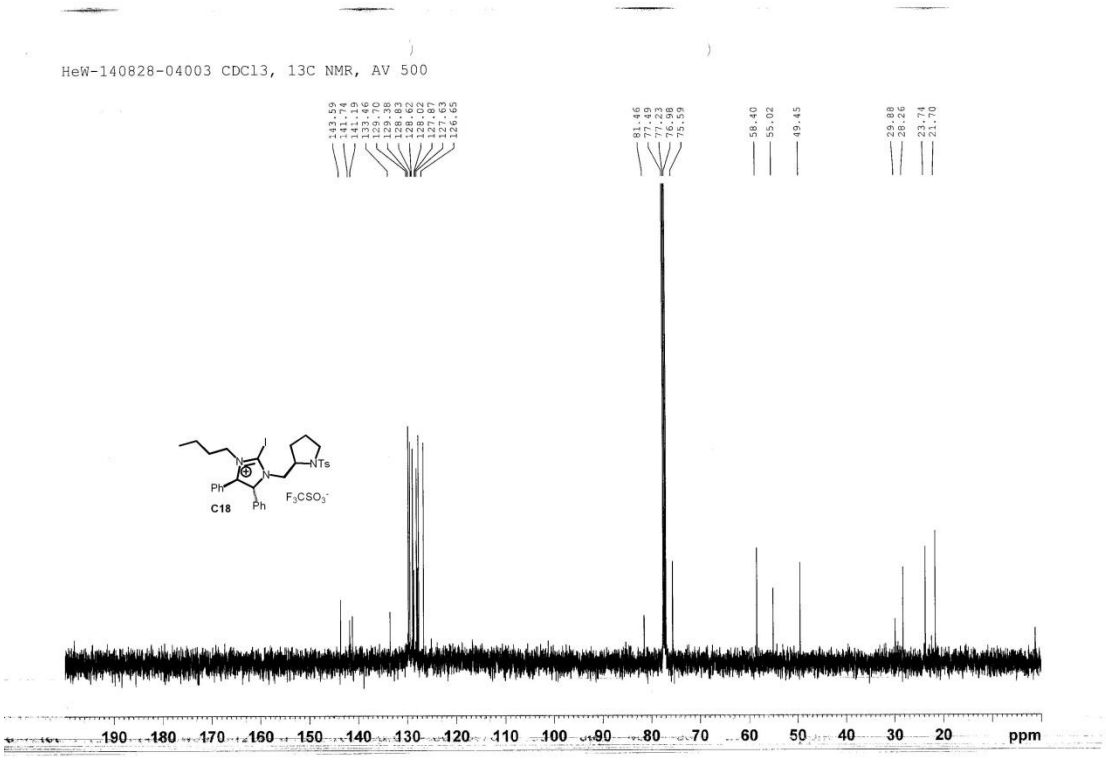

(*R*)-1-phenylethyl-3-amino-2-phenylisonicotinate, **C19-3**

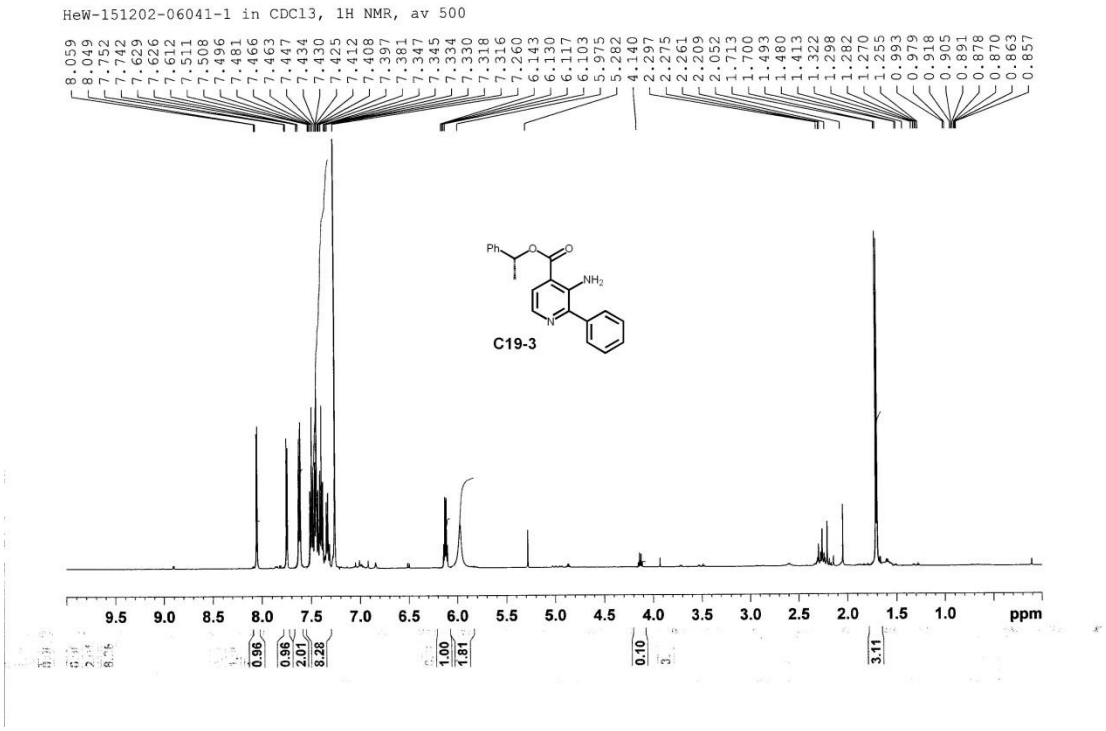

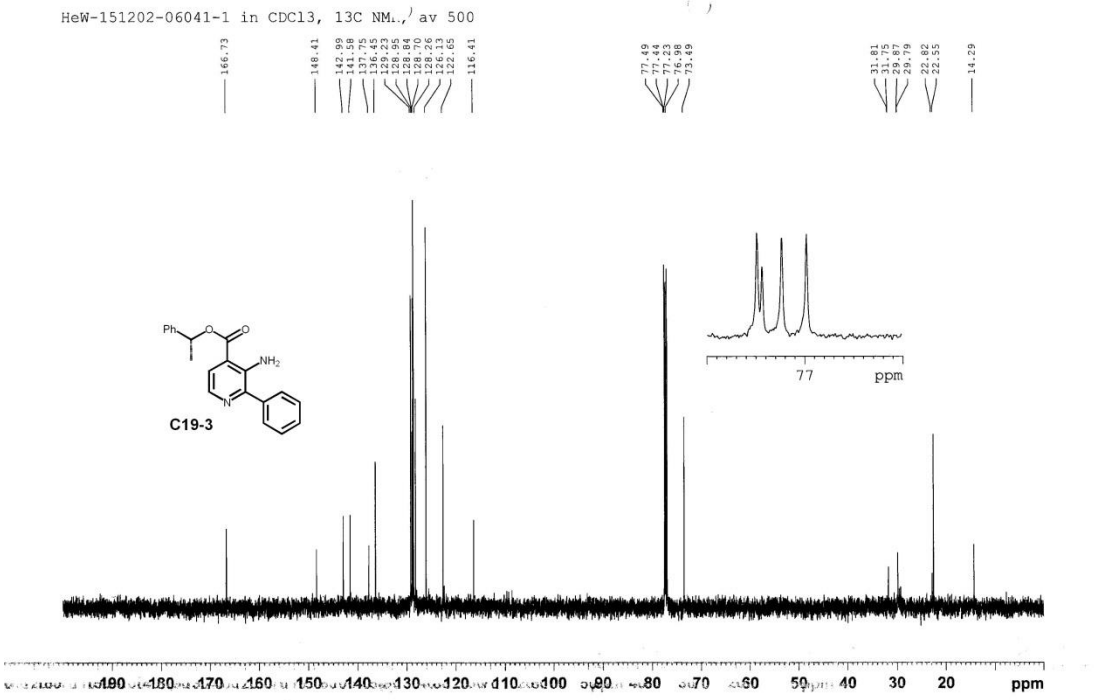

(*R*)-1-phenylethyl-3-iodine-2-phenylisonicotinate, **C19-4**

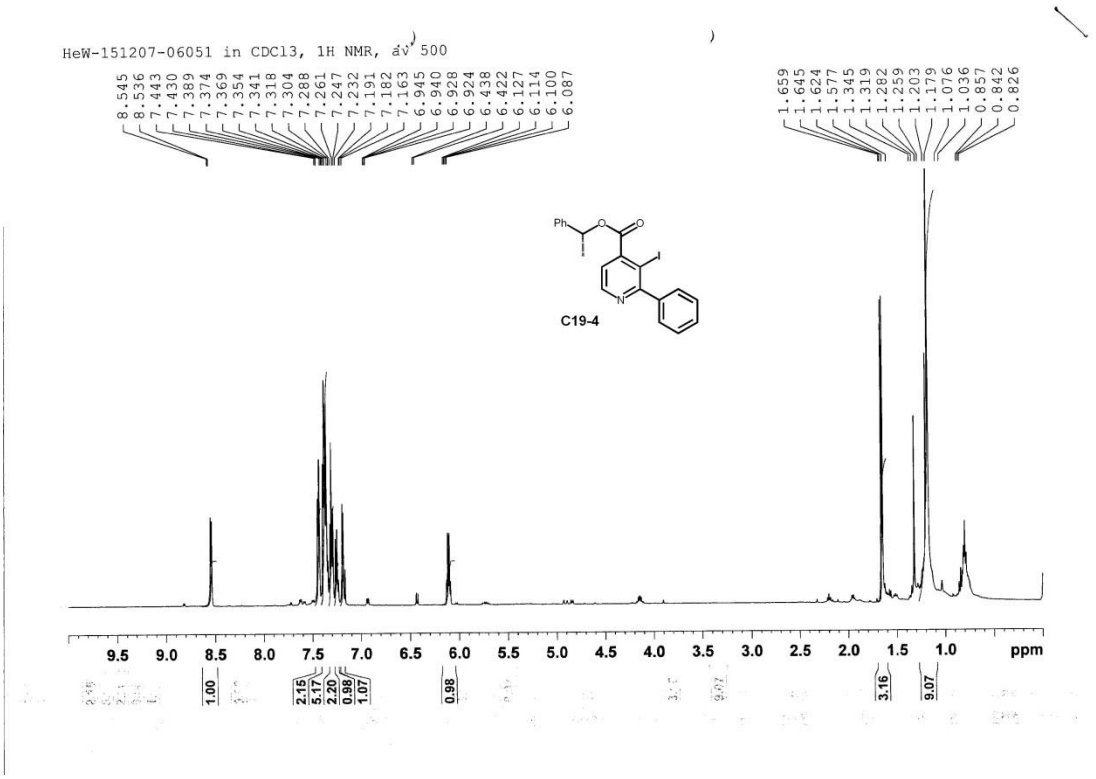

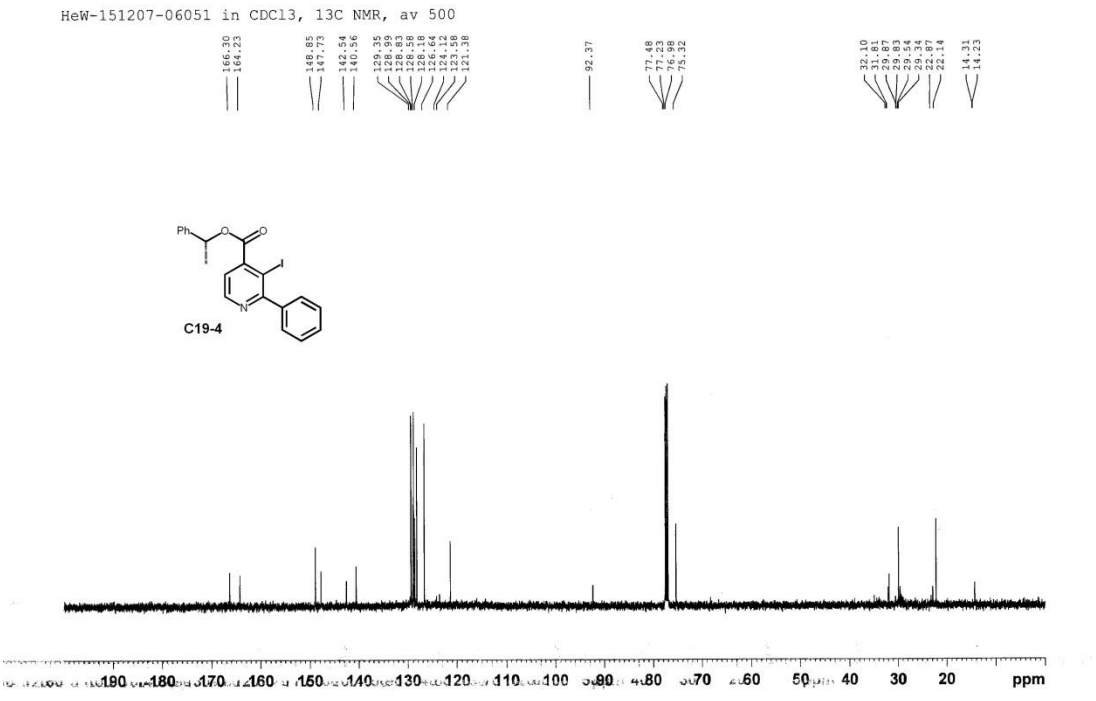

(*R*)-3-iodo-1-methyl-2-phenyl-4-[(1-phenylethoxy)carbonyl]pyridin-1-ium trifluoromethanesulfonate, **C19**

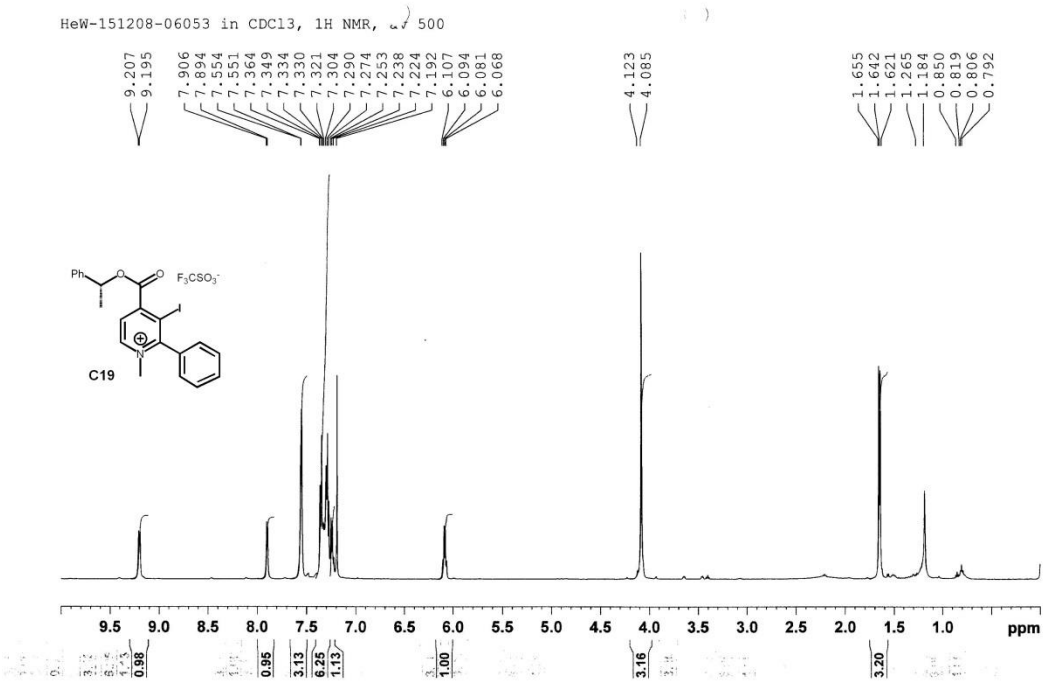

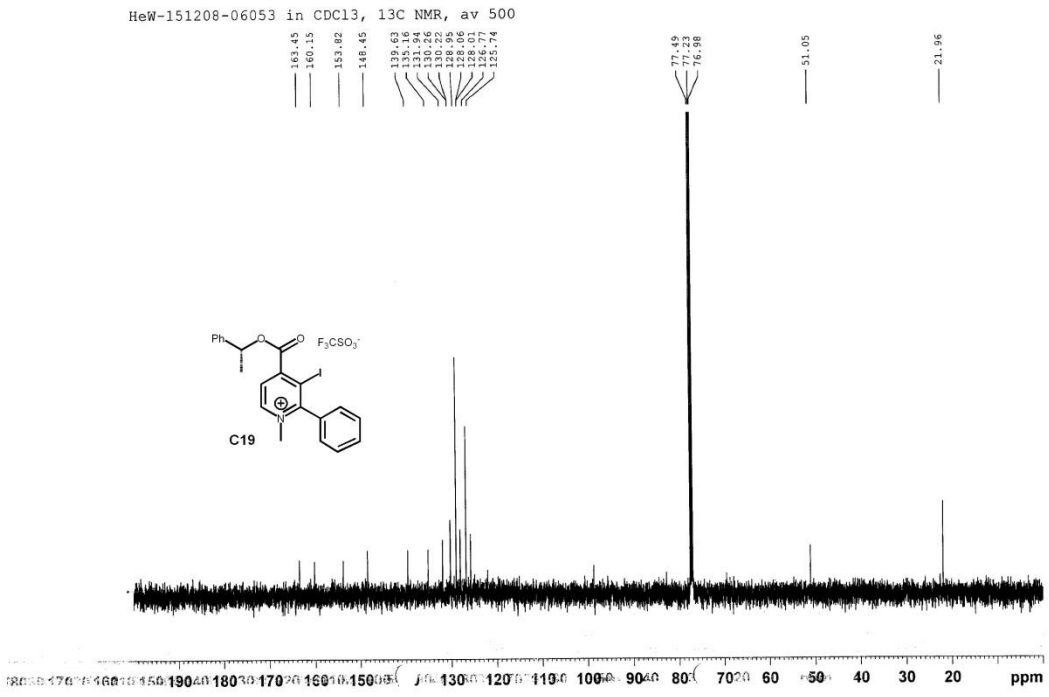

bis((R)-1-phenylethyl) 3-amino-3'-iodo-[2,2'-bipyridine]-4,4'-dicarboxylate

HeW-151014-05273
HeW-151014-05273 in CDCl3, 1H NMR, AV 500

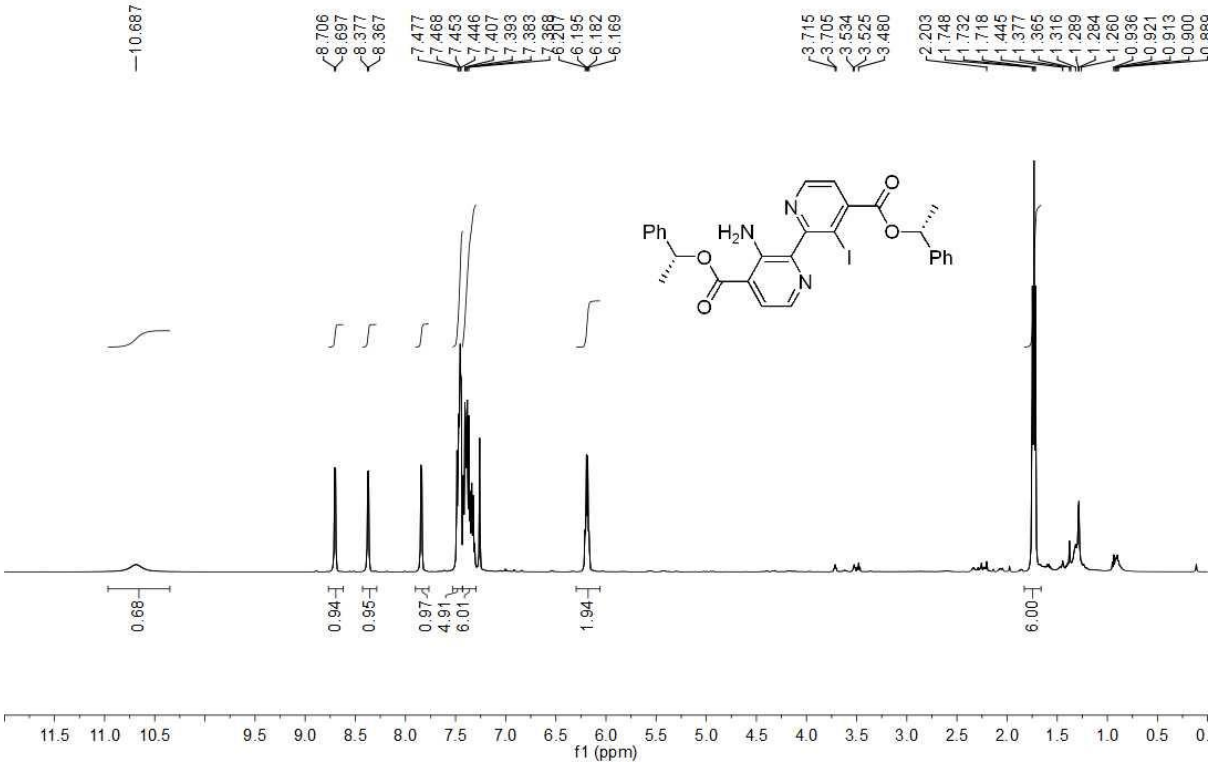

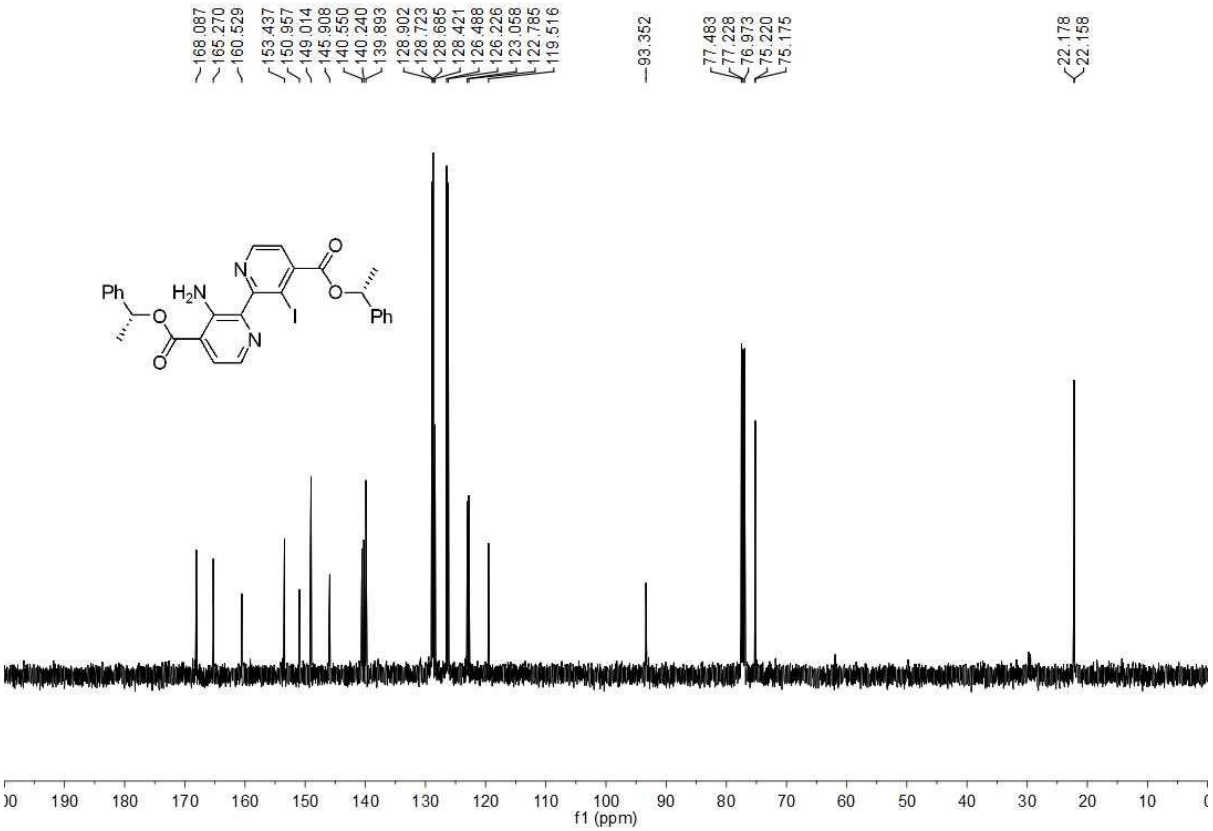

1,2,3,4-tetrahydroquinoline, **4a**

HeW-130609-195
HeW-130609-195 in CDCl3, 1H NMR, AV 500

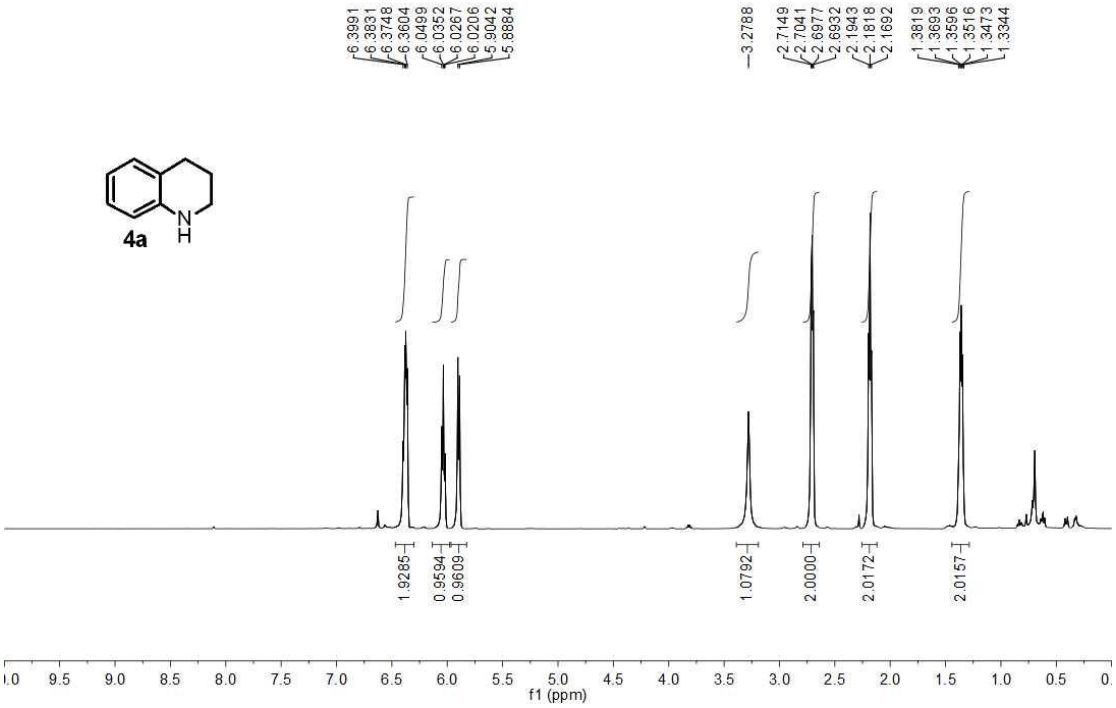

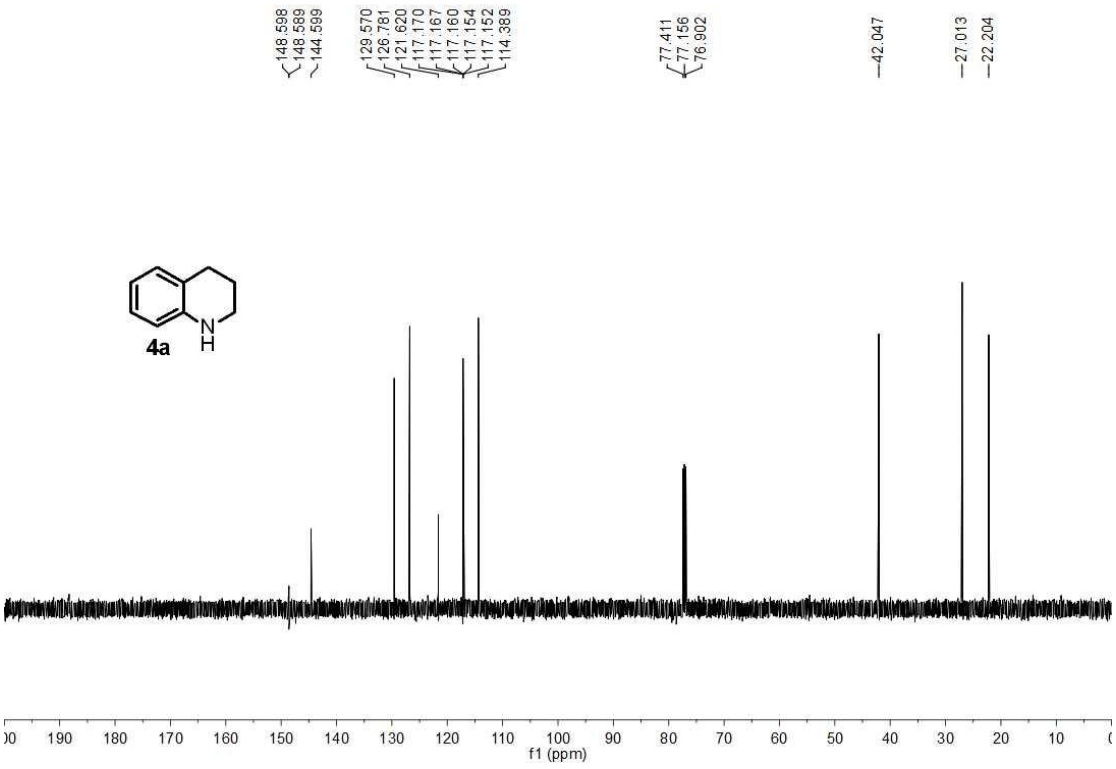

1,3,4-tetrahydro-2-methyl-quinoline, **4b**

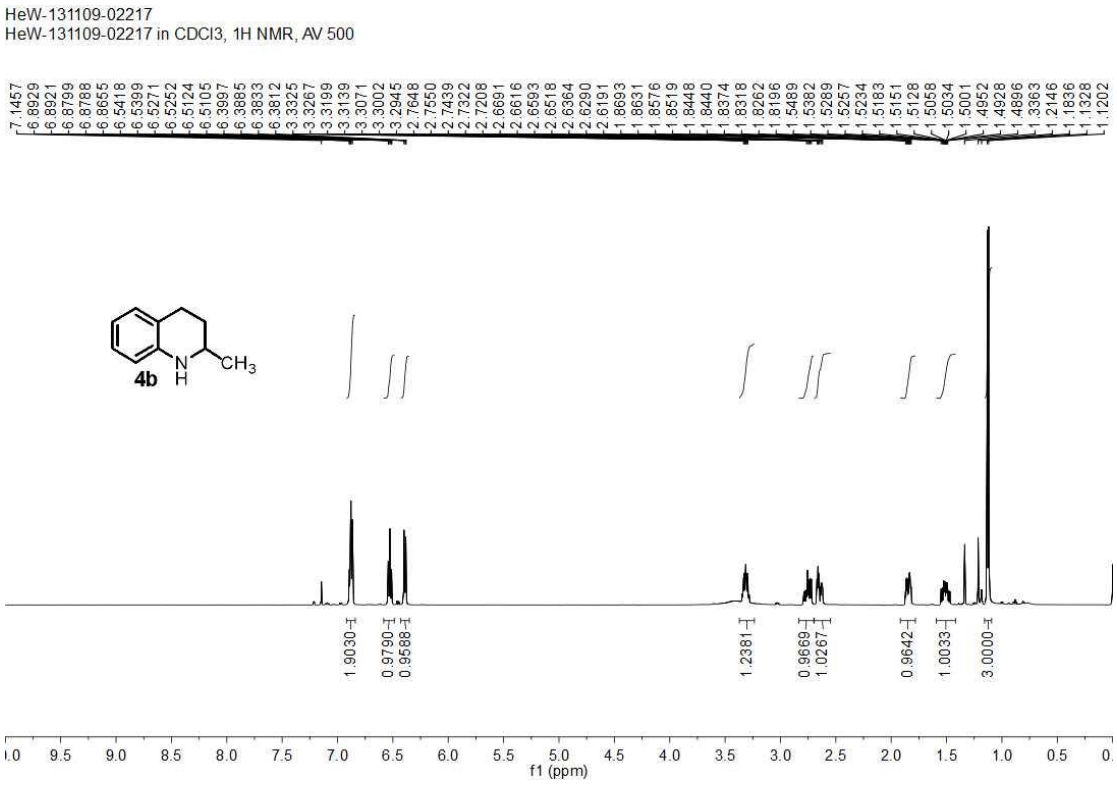

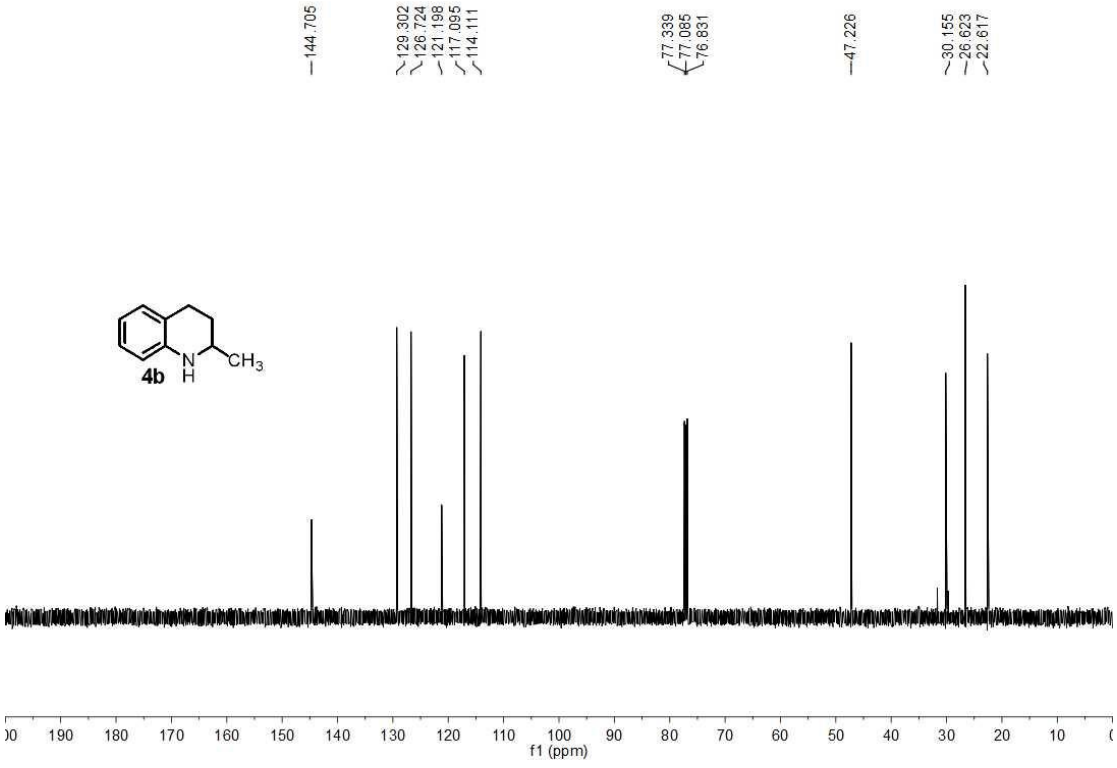

1,2,3-tetrahydro-4-methyl-quinoline, **4c** ^{1}H NMR

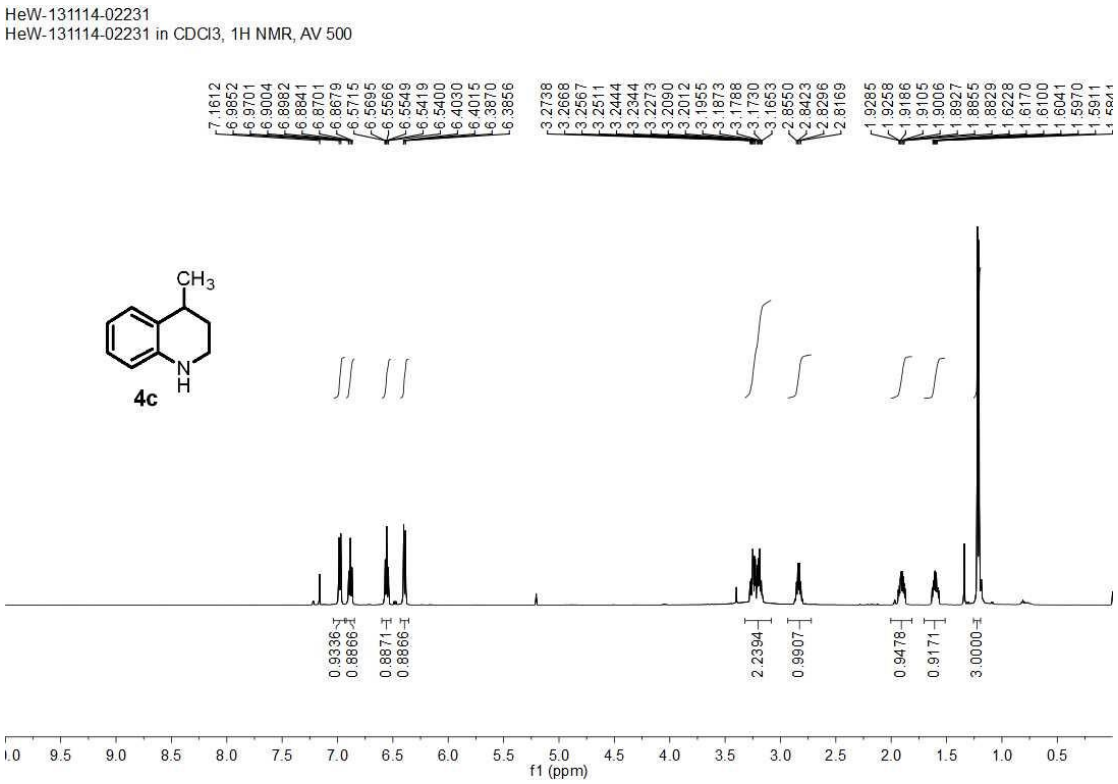

1,3,4-tetrahydro-2-phenyl-quinoline, **4d** ^{1}H NMR

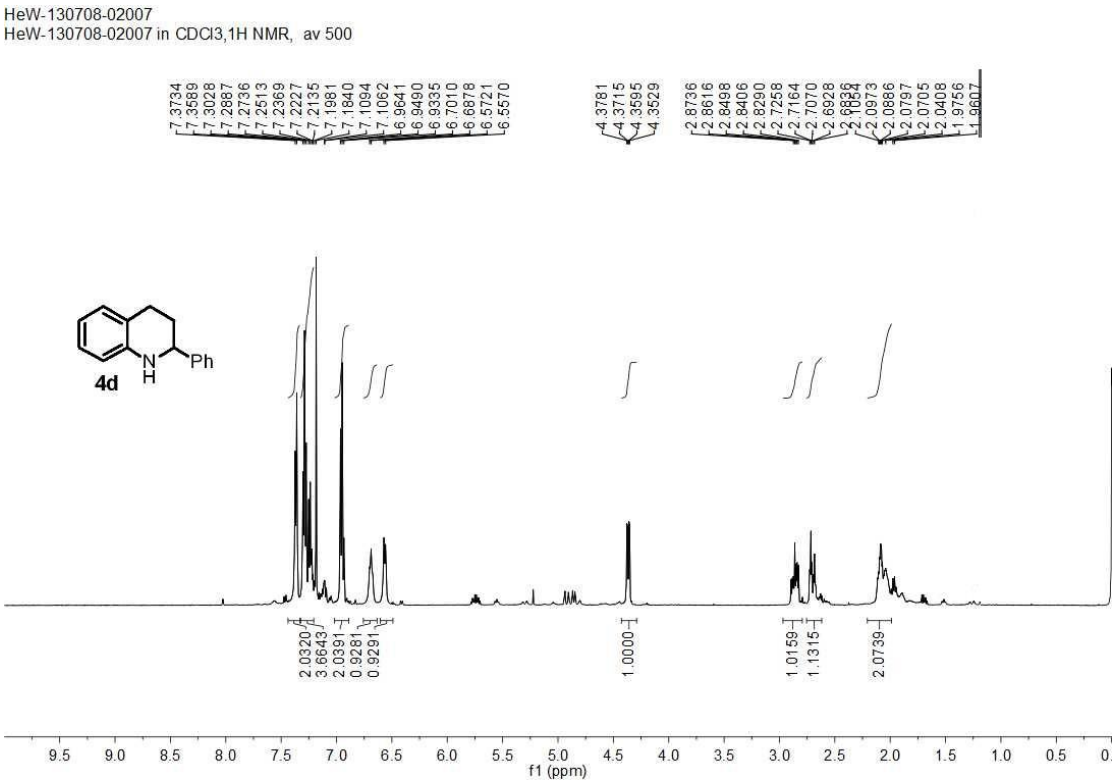

1,3,4-tetrahydro-2-(4-methoxy-phenyl)-quinoline, **4e** ^{1}H NMR

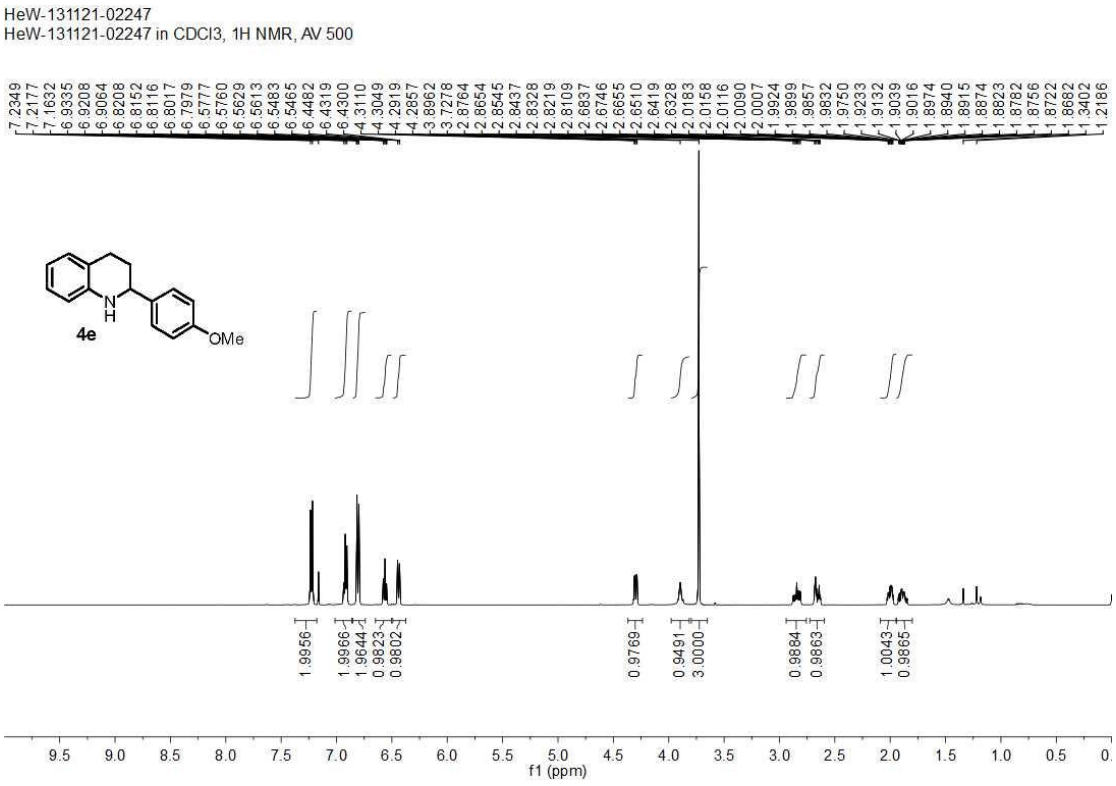

1,3,4-tetrahydro-2-phenyl-6-bromo-quinoline, **4f** ^{1}H NMR

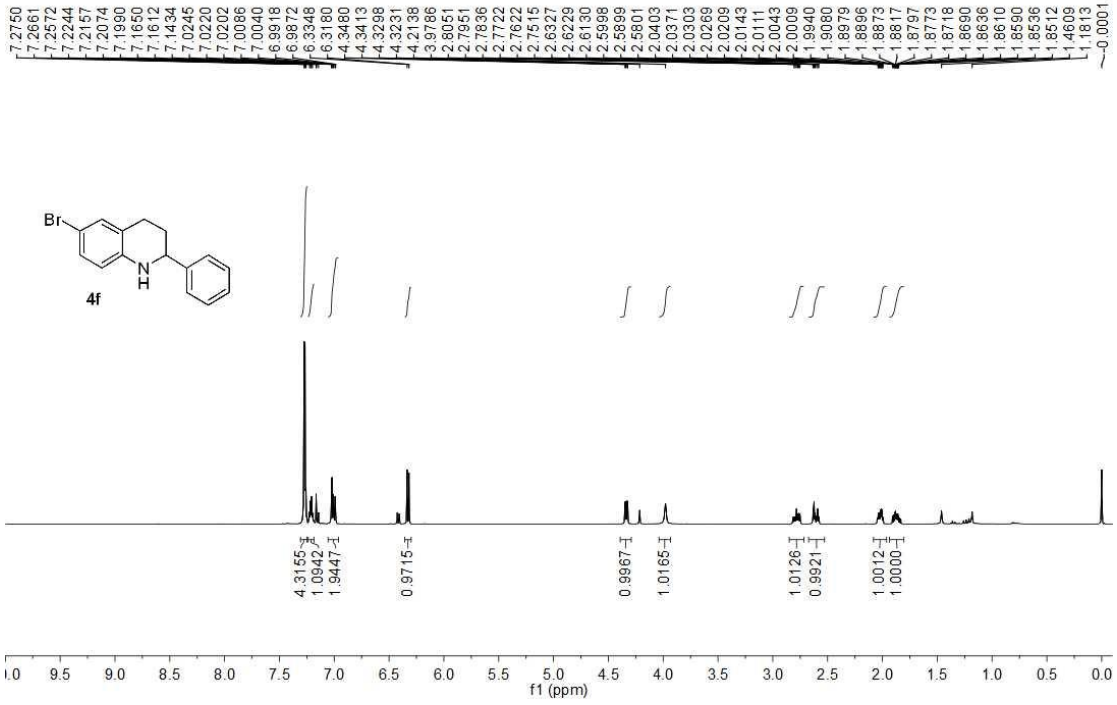

1,3,4-tetrahydro-2-phenyl-6-nitro-quinoline, **4g** ^{1}H NMR

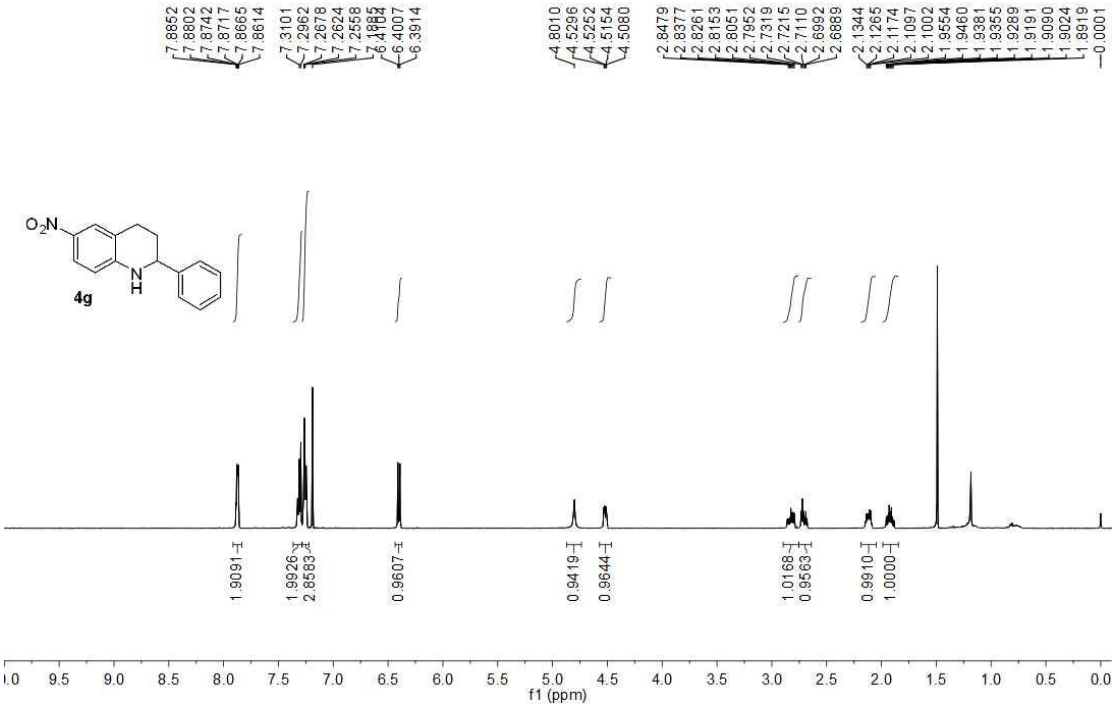

1,3,4-tetrahydro-2-phenyl-6-methyl-quinoline, **4h** ^{1}H NMR

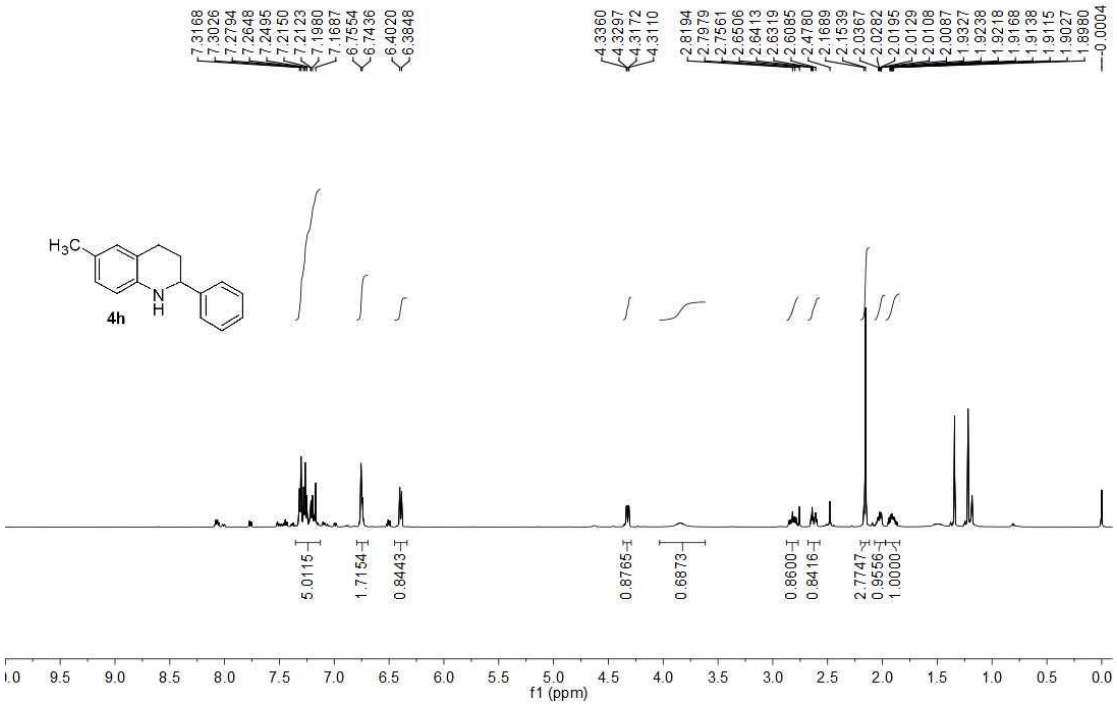

1,3,4-tetrahydro-2-methyl-8-hydroxy-quinoline, **4i** ^{1}H NMR

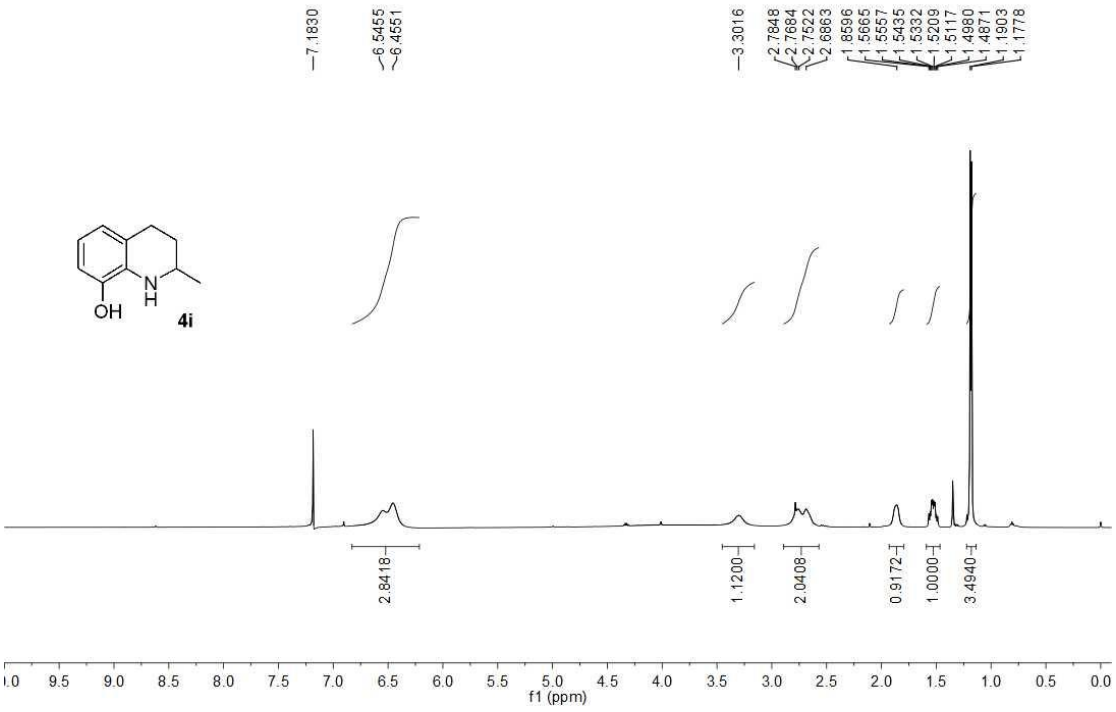

1,2,3,4-tetrahydro-1,10-phenanthroline, **4j** ^{1}H NMR

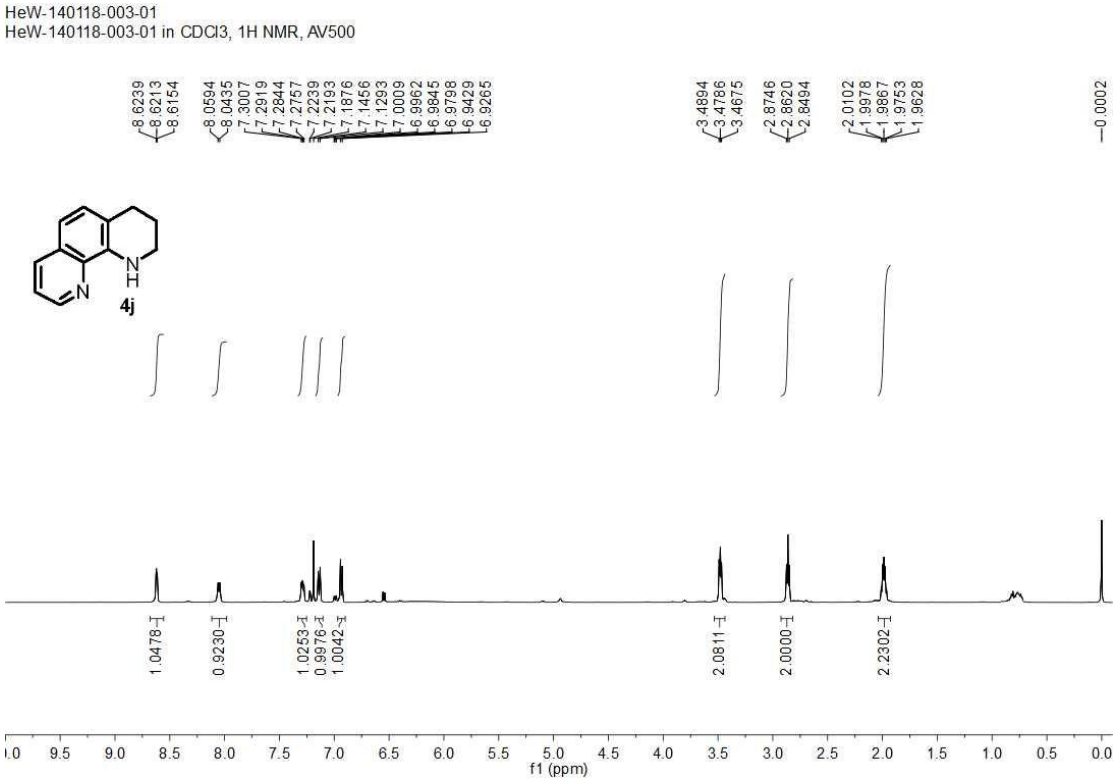

1-(1,4,5,6-tetrahydropyridin-3-yl)ethanone, **4k** ^{1}H NMR

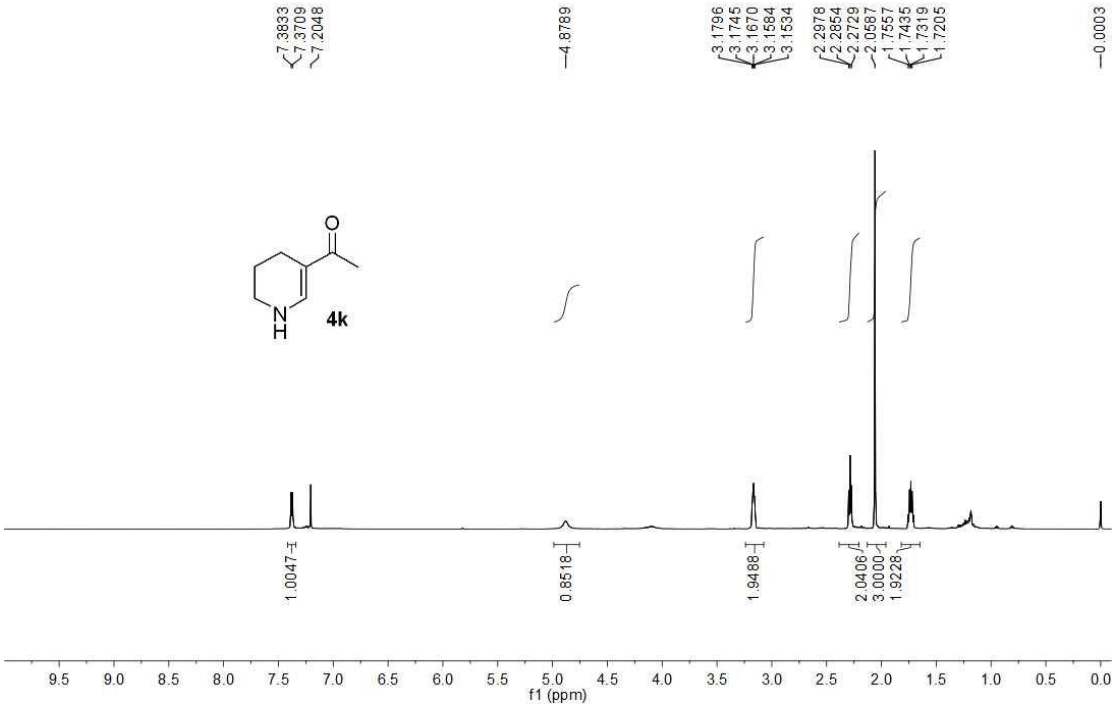

1-(1,4,5-trihydropyridin-6-methyl-3-yl)ethanone, **4l**

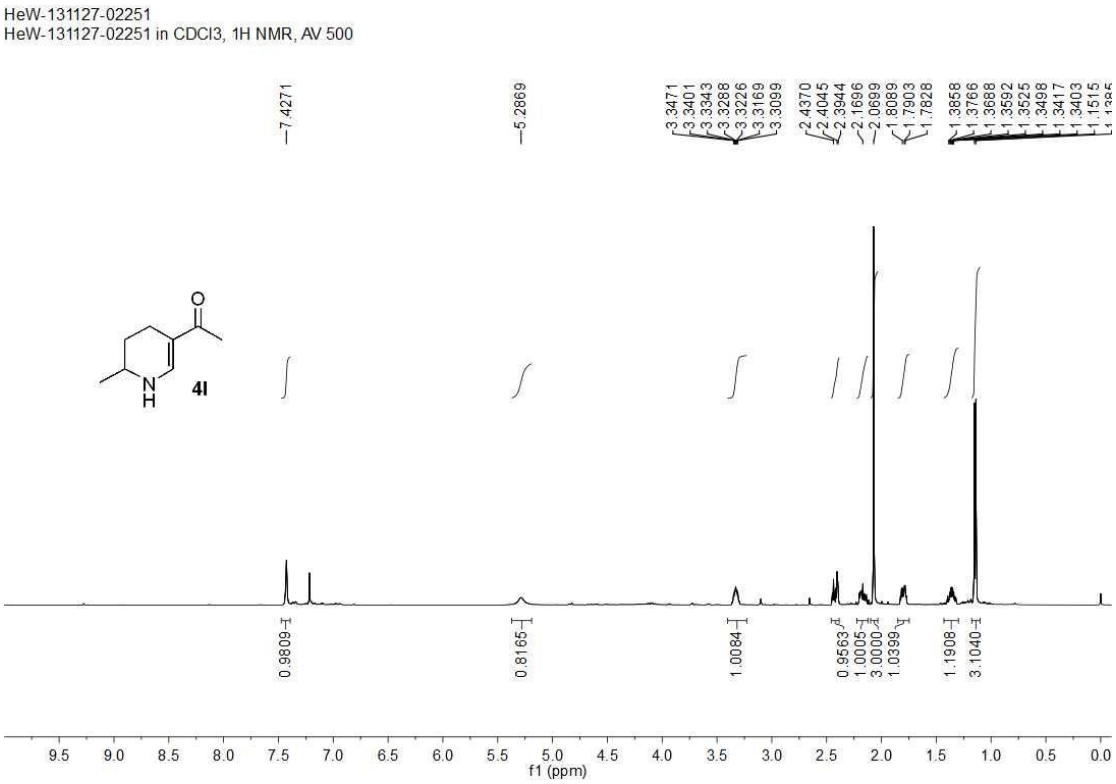

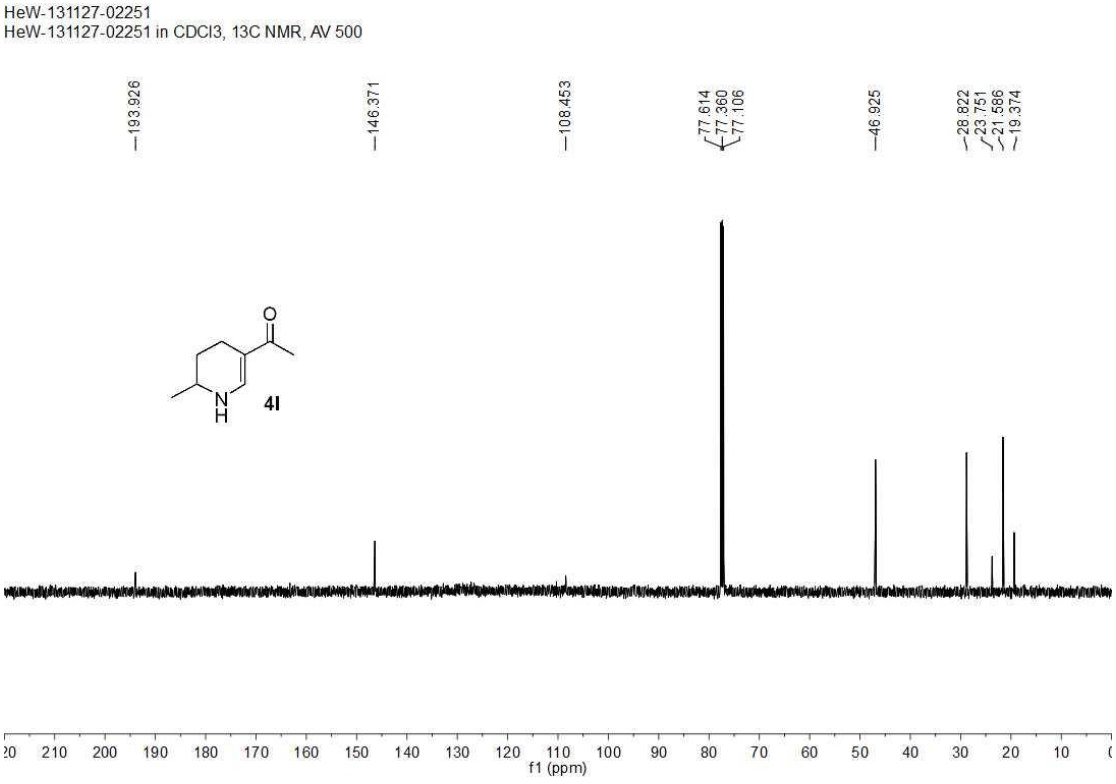

N-benzylaniline, **5a** ^{1}H NMR

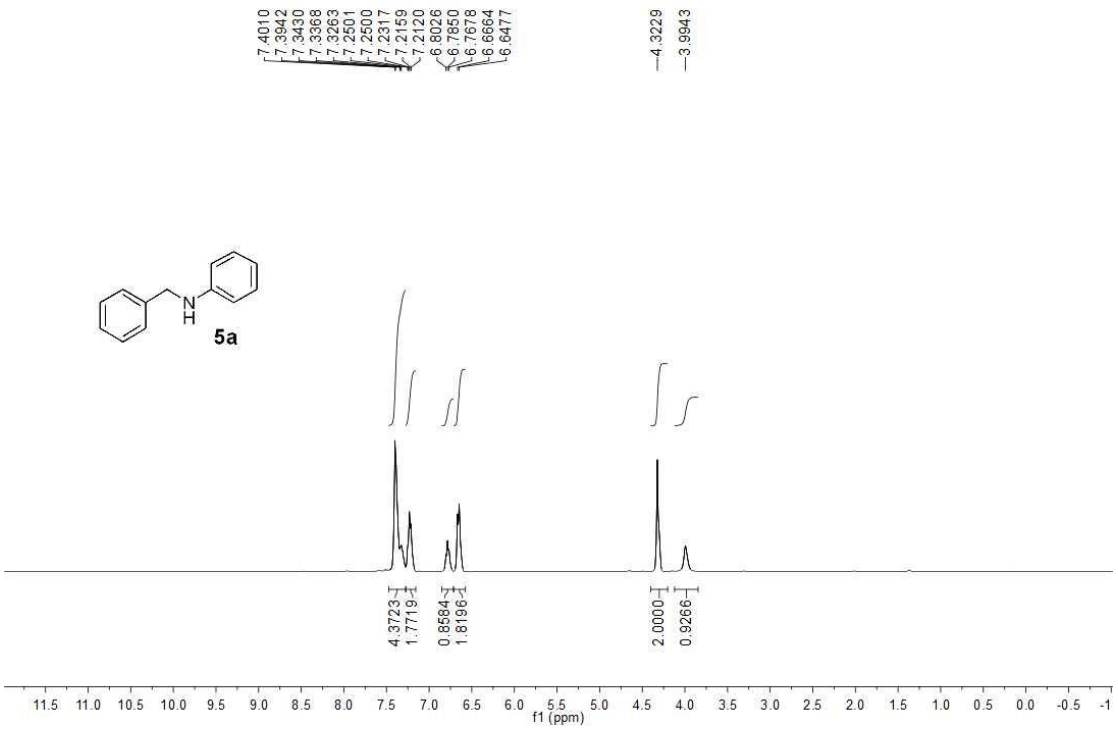

N-(4-chlorobenzyl)aniline, **5b** ^{1}H NMR

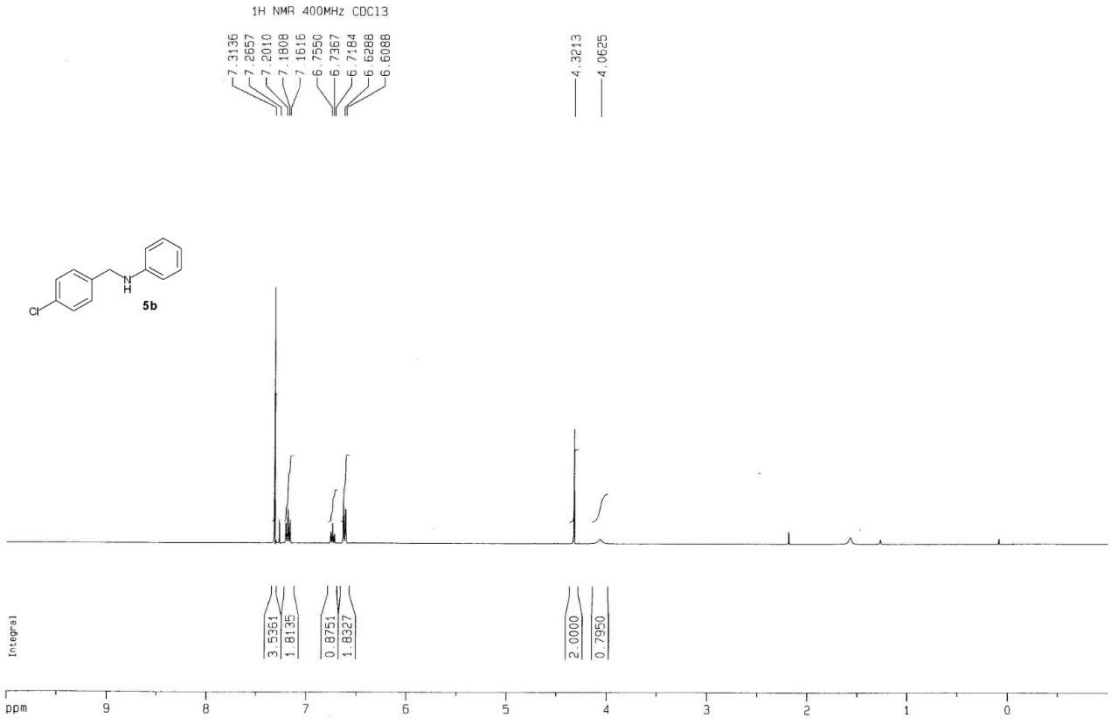

N-(4-methylbenzyl)aniline, **5c** ^{1}H NMR

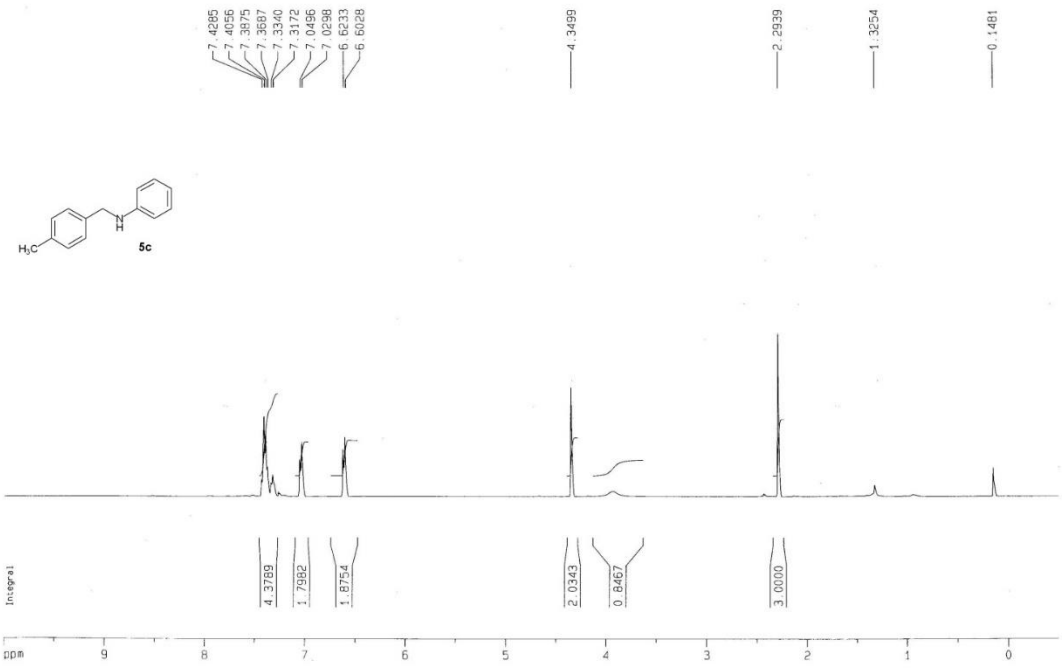

N-(naphthalen-1-ylmethyl)aniline, **5d** ^{1}H NMR

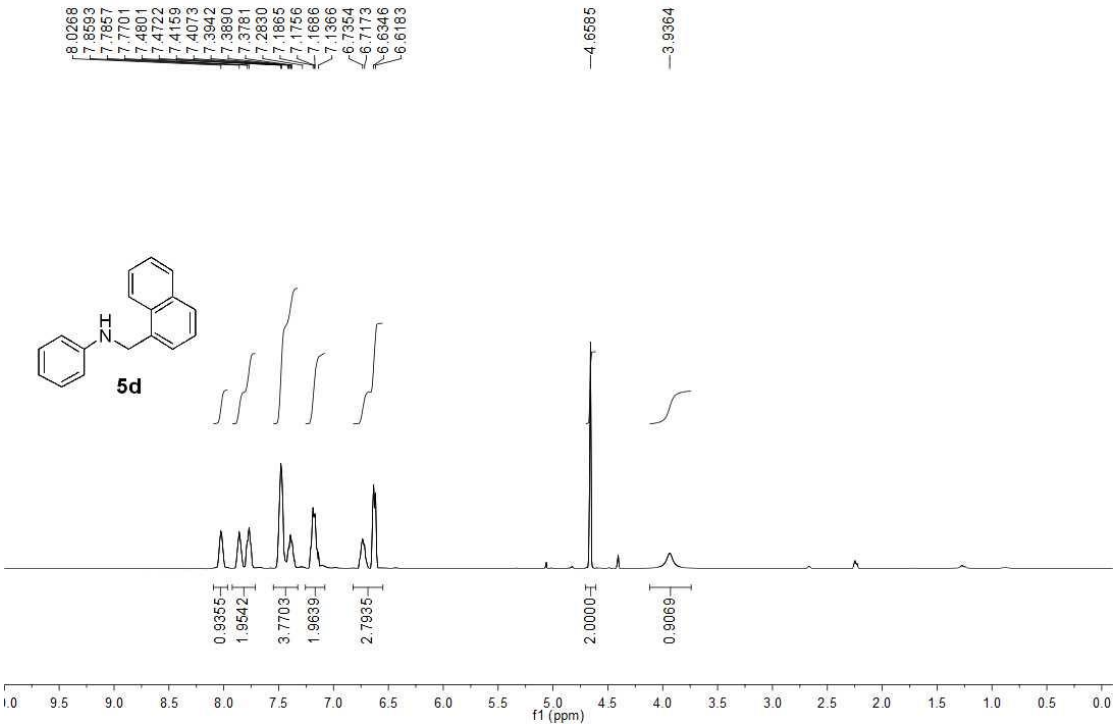

4-methyl-*N*-(4-nitrobenzyl)aniline, **5e** ^{1}H NMR

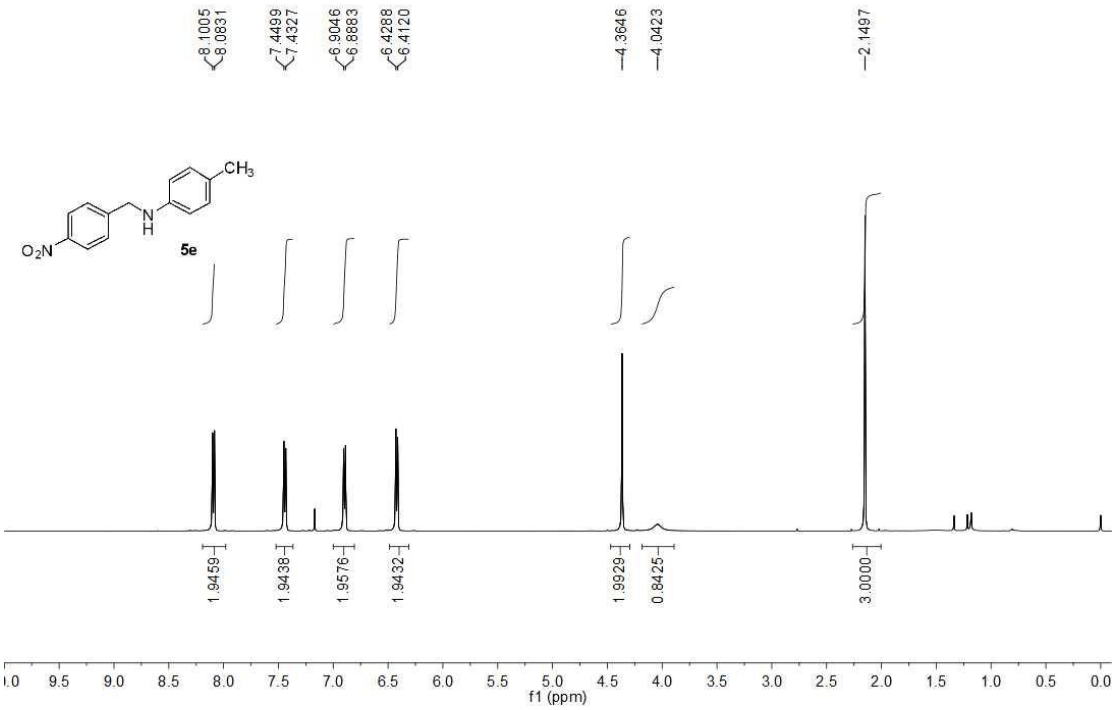

N-(1-phenylethyl)aniline, **5g** ^{1}H NMR

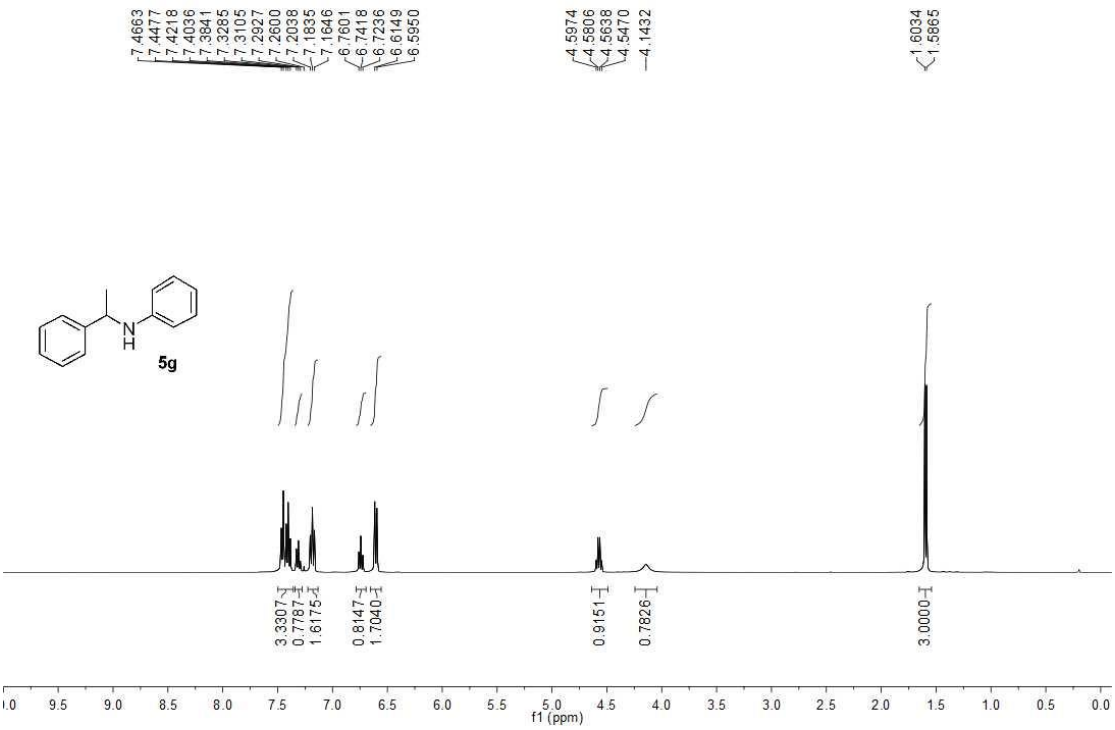

N-phenyl-*N*-[(*Z*)-phenylmethylene] amine oxide, **7a**

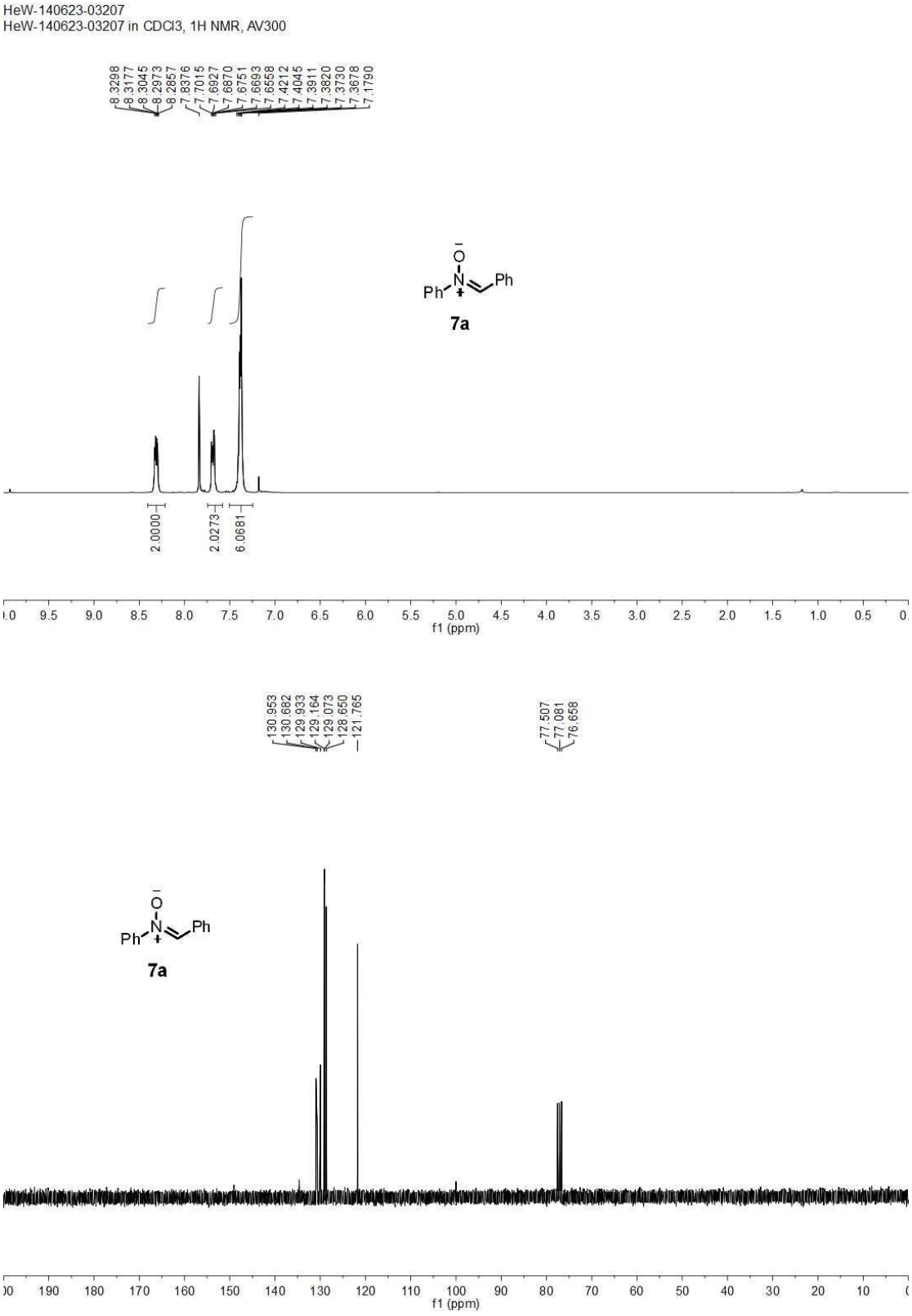

N-phenyl-*N*-[(*Z*)-4-fluoro-phenylmetgylene]amine oxide, **7b**

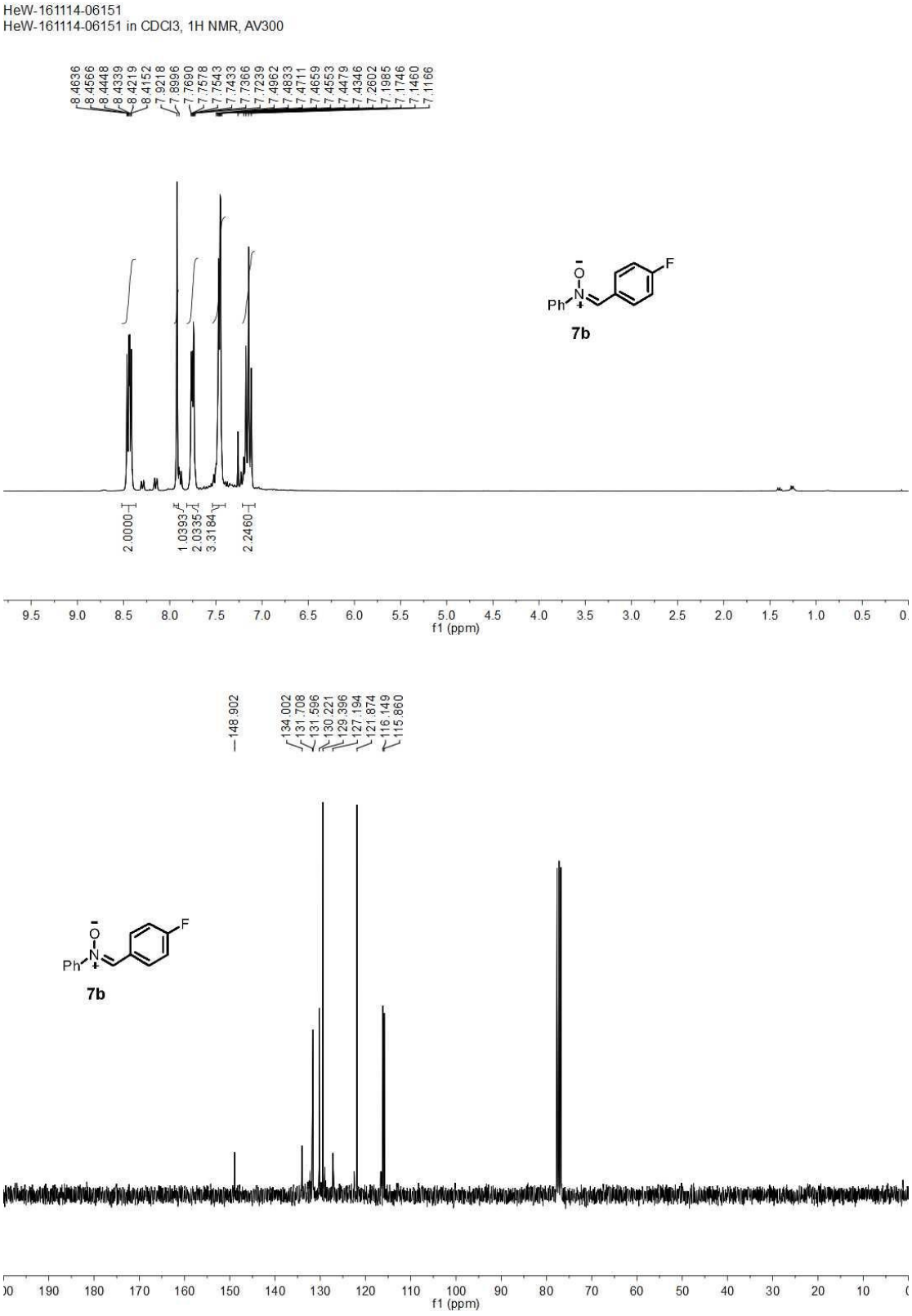

Ethyl 4-methyl-2,3-diphenylisoxazolidine-4-carboxylate, **8a**

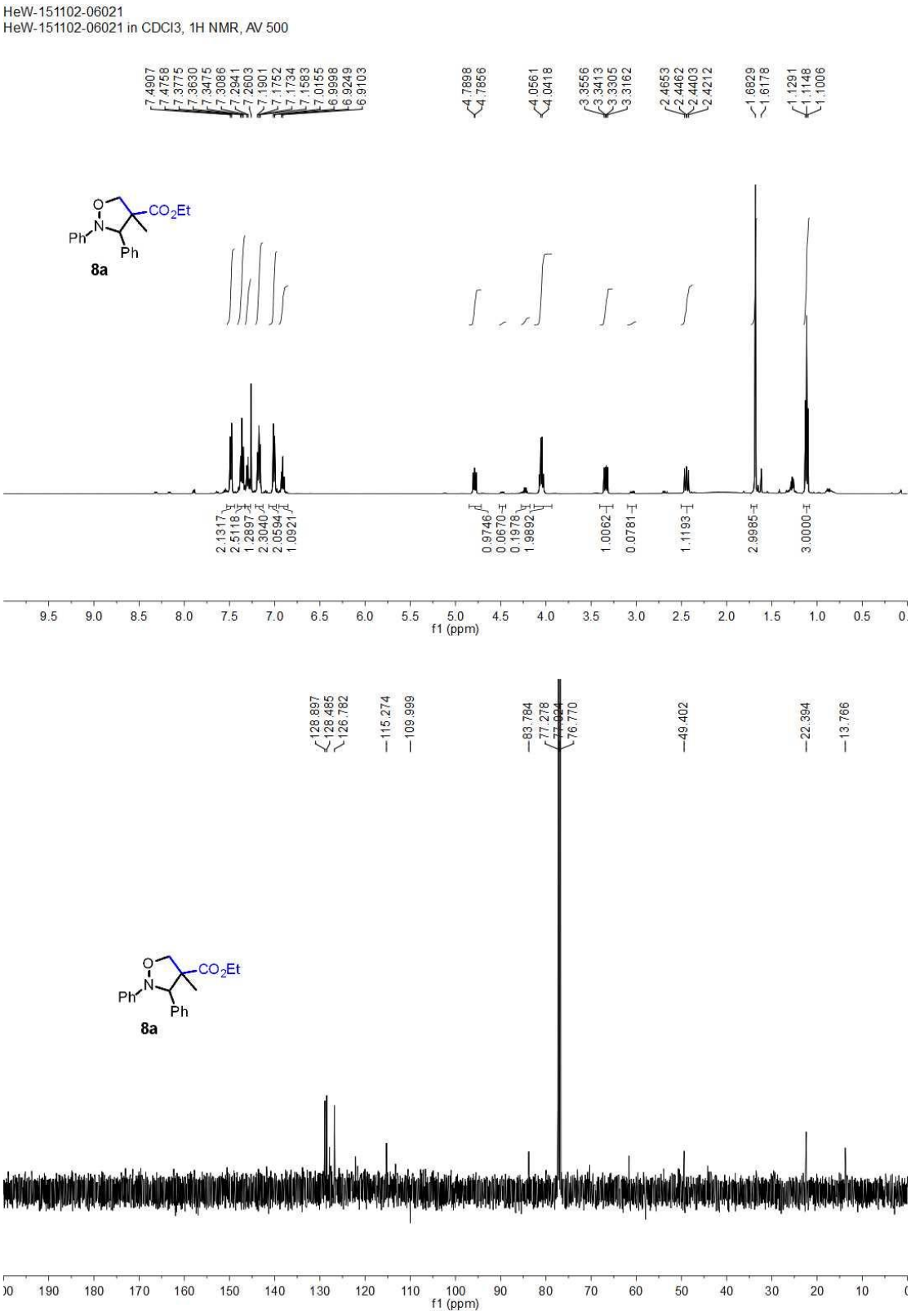

Methyl 2,3-diphenylisoxazolidine-4-carboxylate, **8b**

HeW-160408-06115
HeW-160408-06115 in CDCl3, 1H NMR AV300

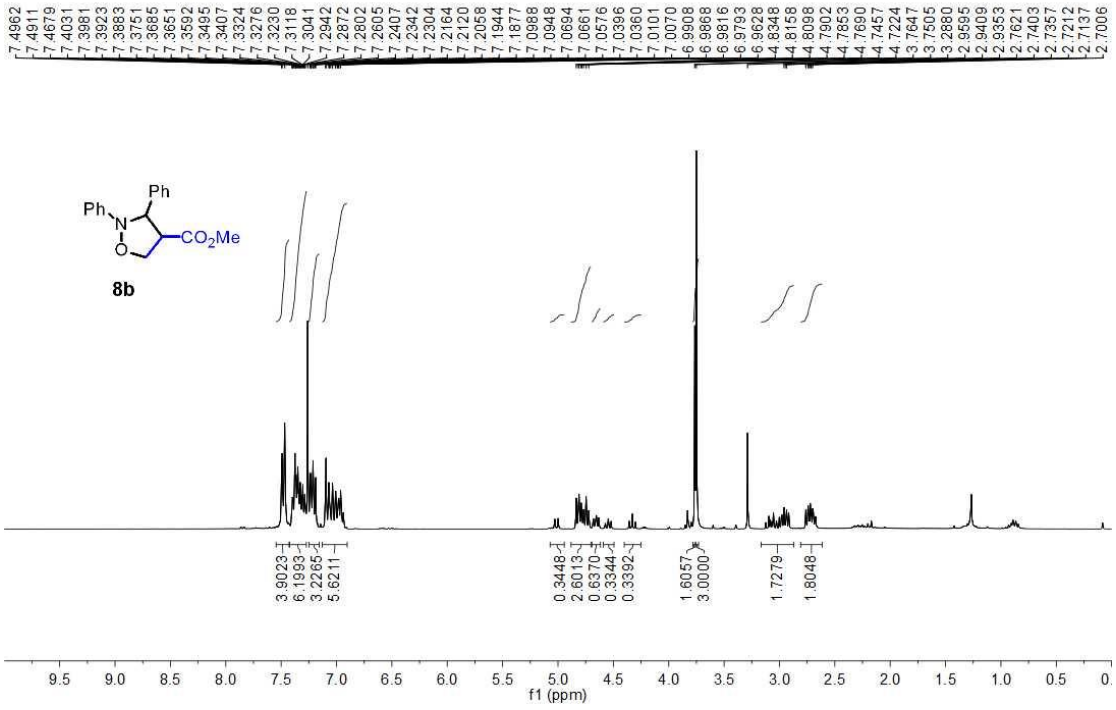

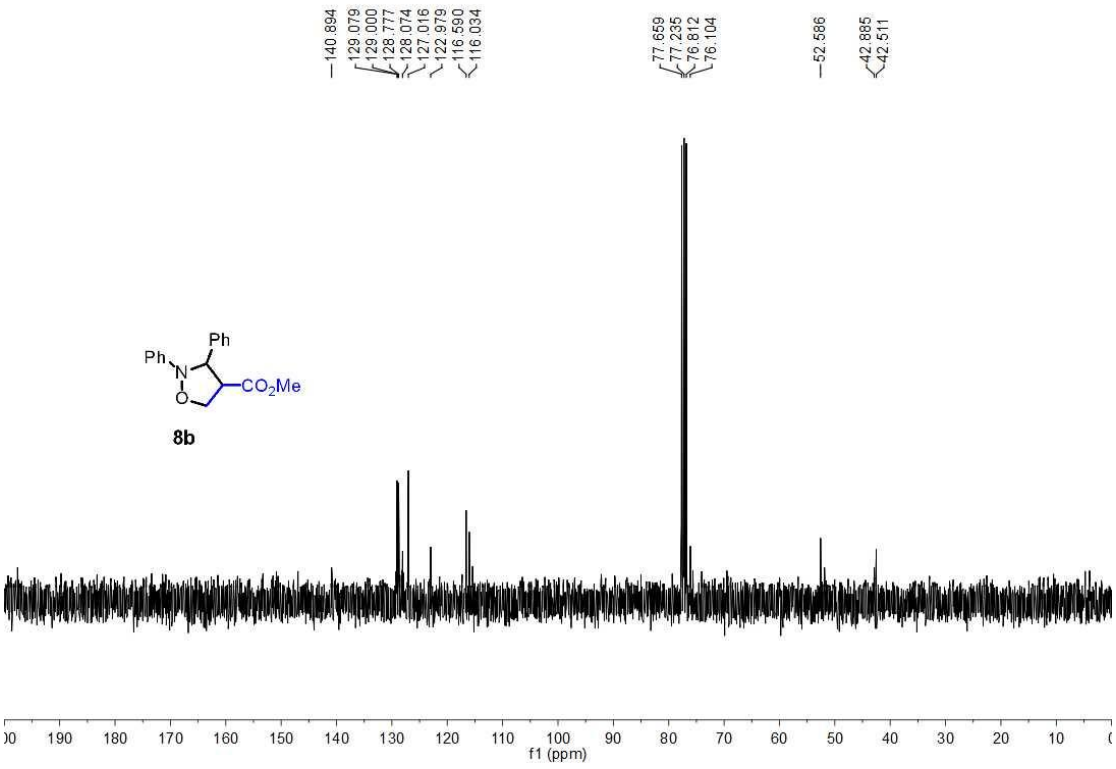

Ethyl 2,3-diphenylisoxazolidine-4-carboxylate, **8c**

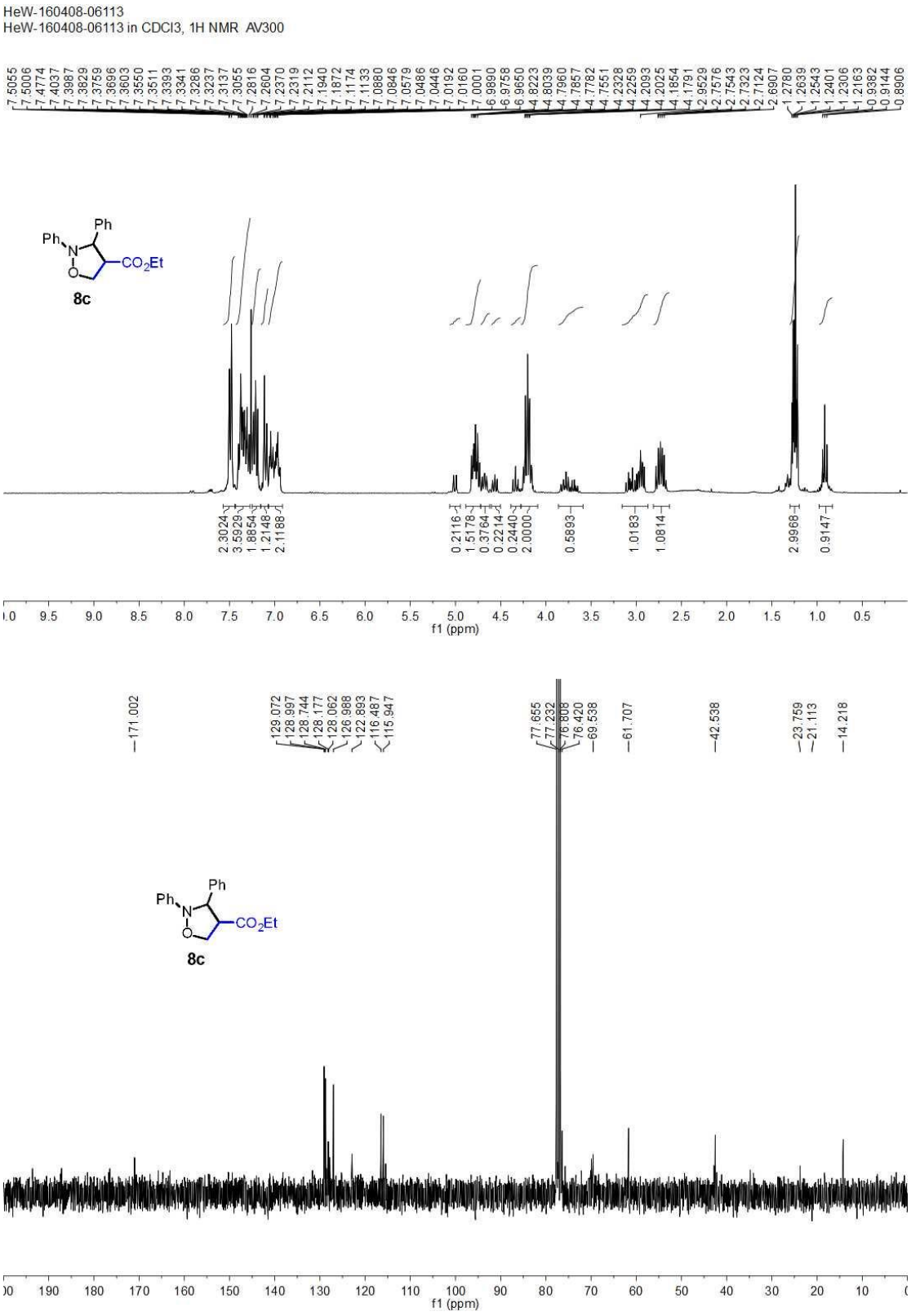

tert-butyl 2,3-diphenylisoxazolidine-4-carboxylate, **8d**

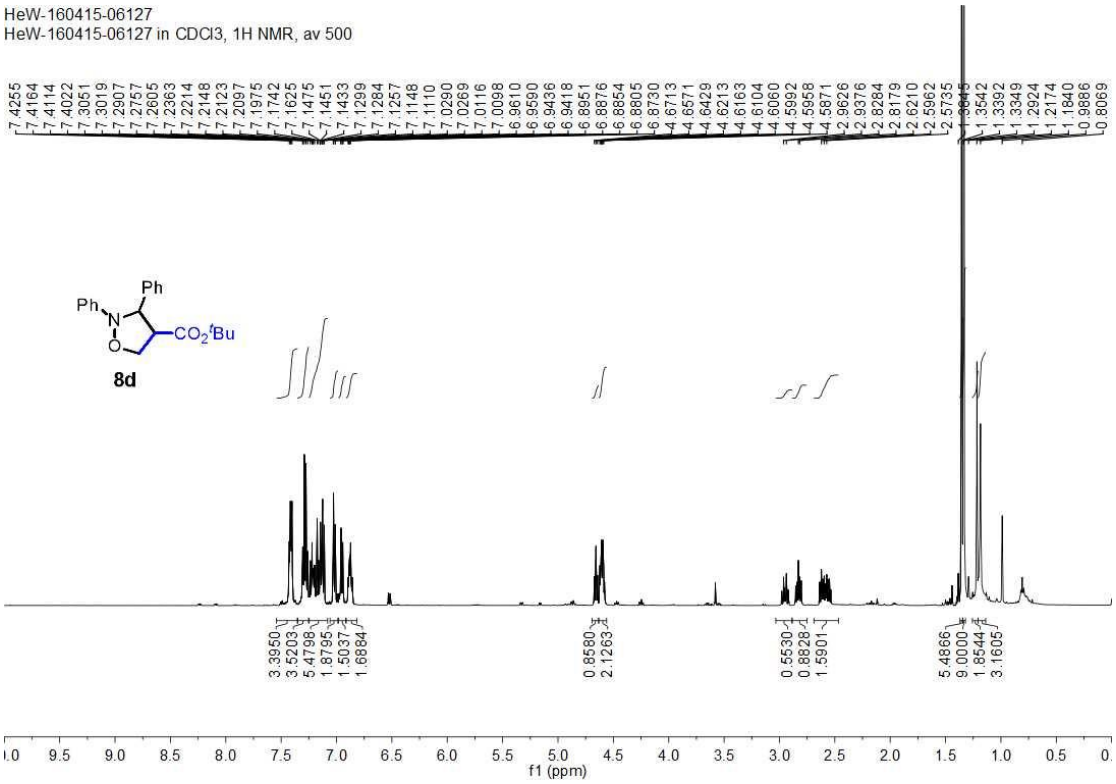

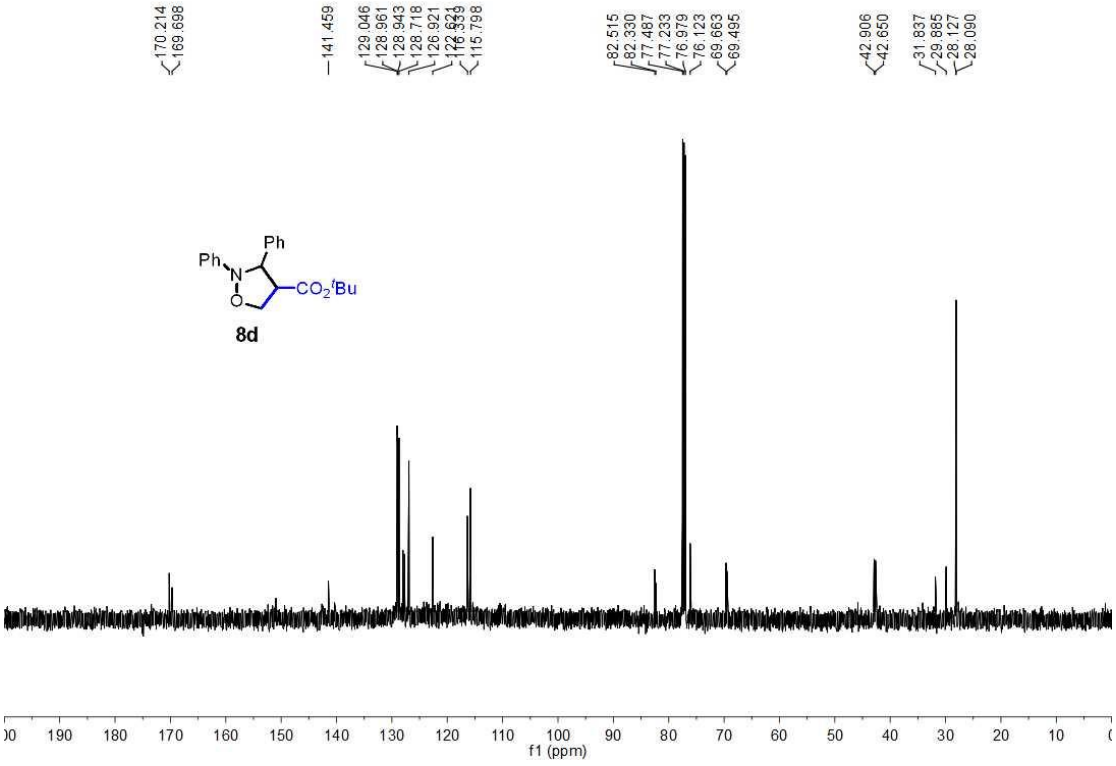

Phenyl 2,3-diphenylisoxazolidine-4-carboxylate, **8e**

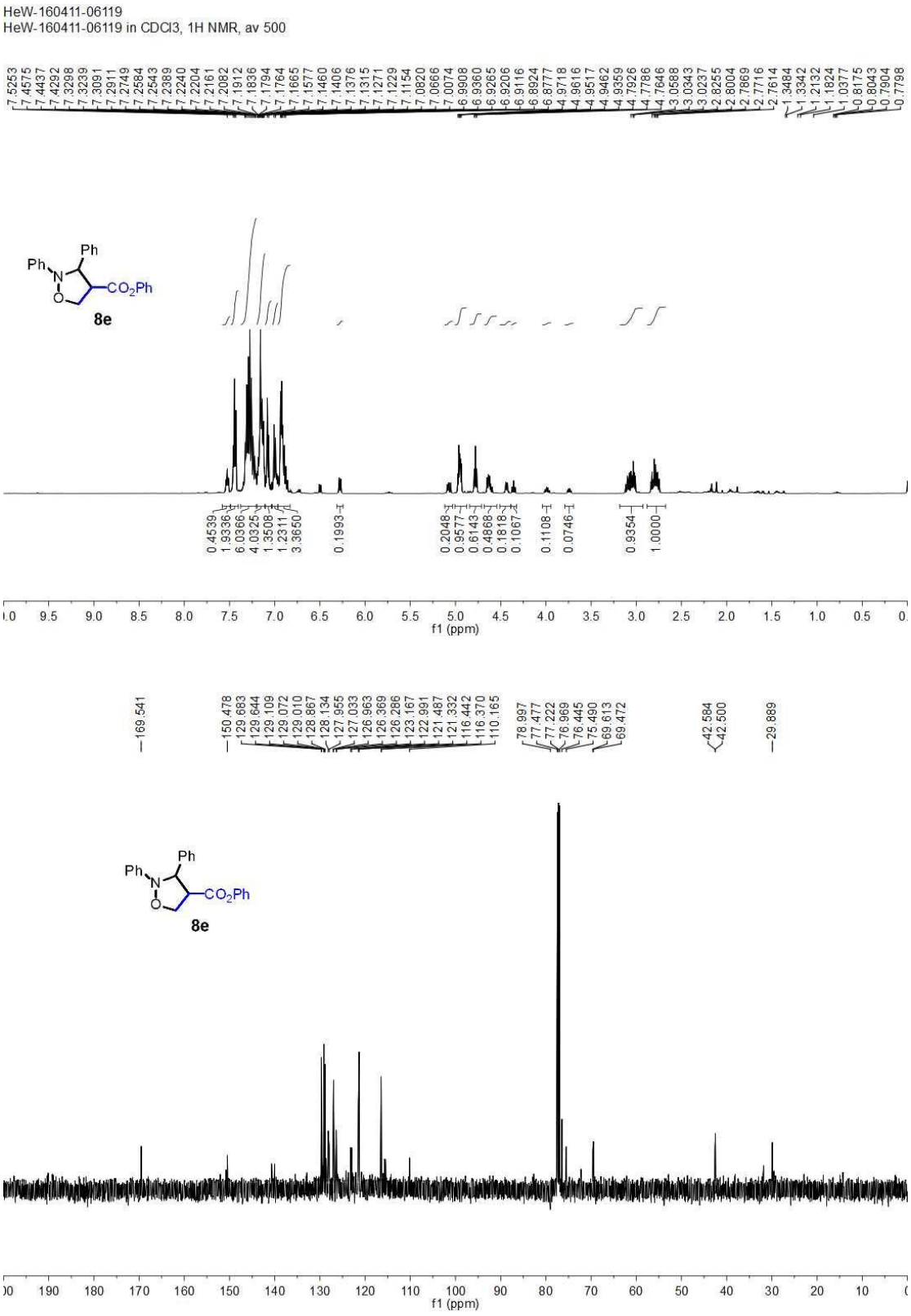

Vinyl 2,3-diphenylisoxazolidine-4-carboxylate, **8f**

HeW-160420-06143
HeW-160420-06143 in CDCl3, 1H NMR, av 500

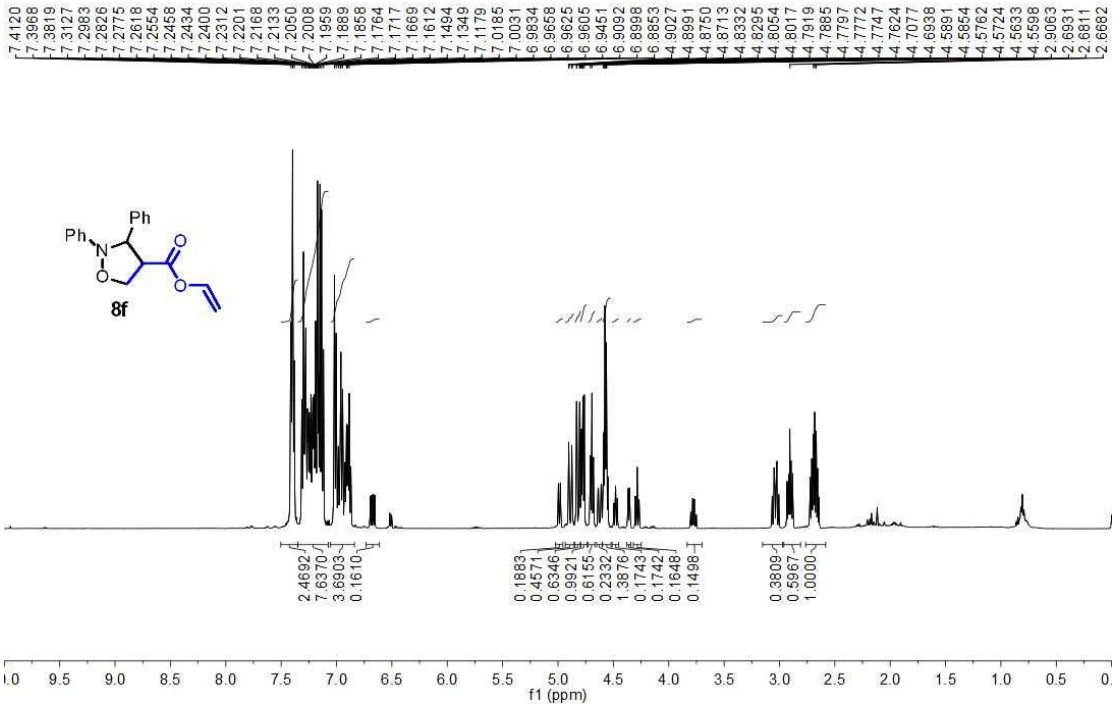

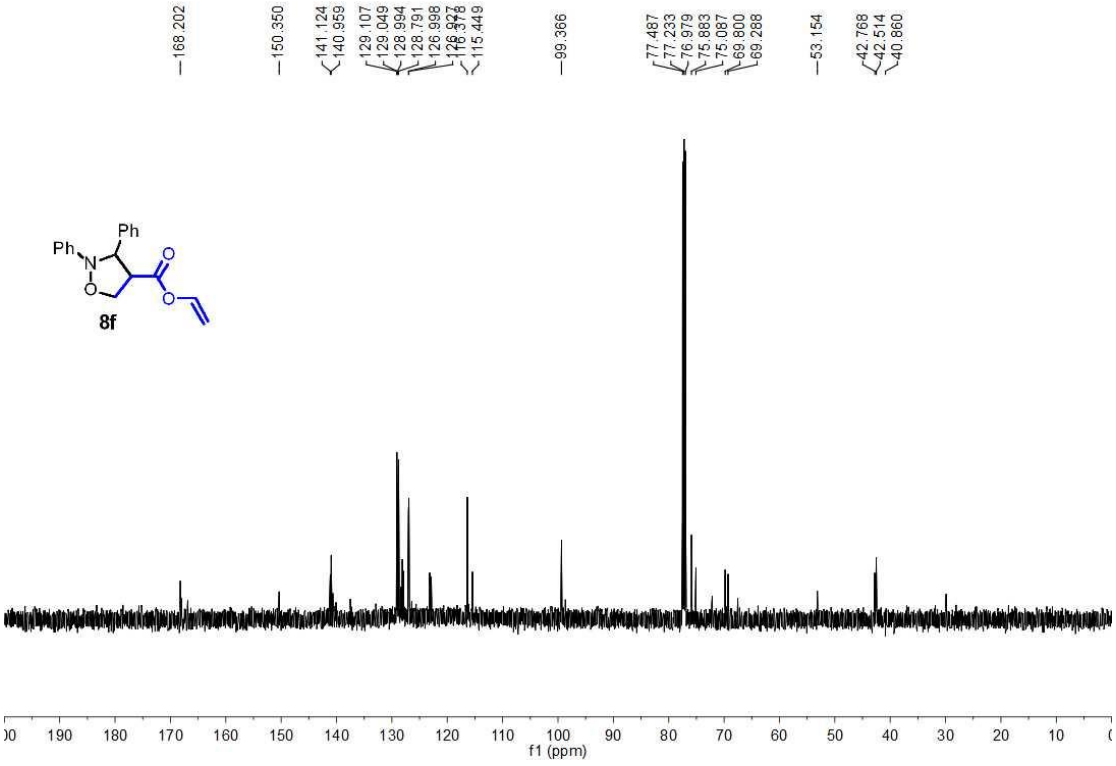

tert-butyl 5-methyl-2,3-diphenylisoxazolidine-4-carboxylate, **8g**

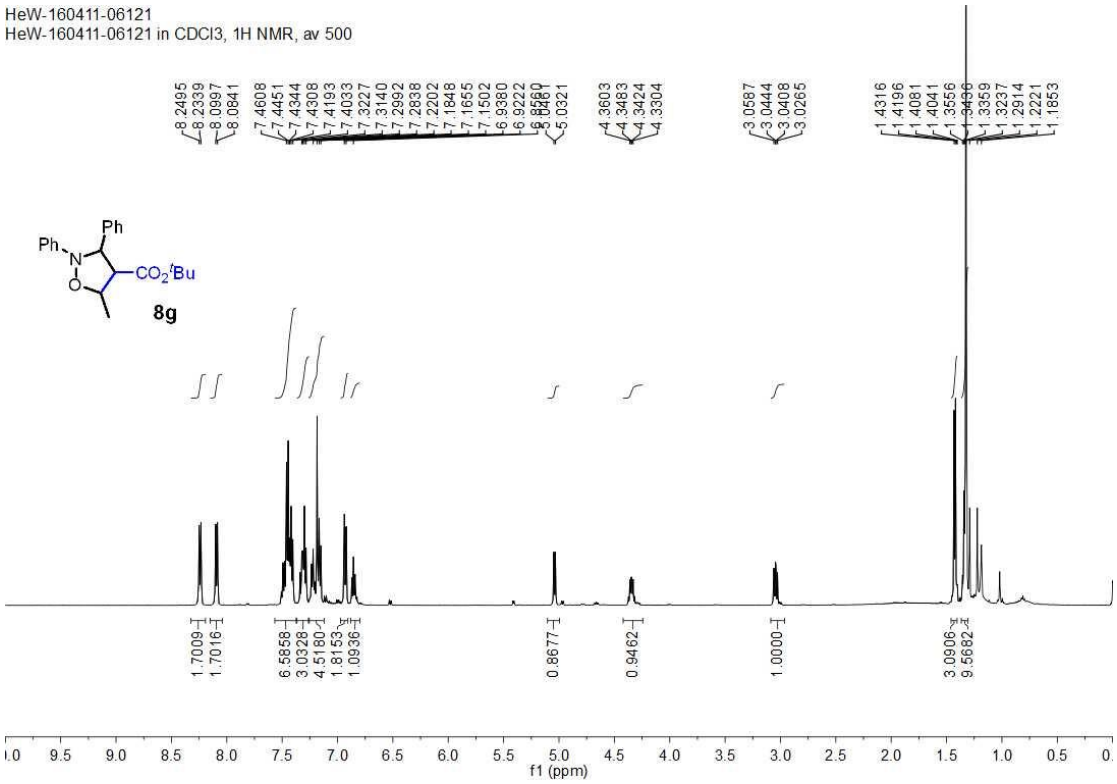

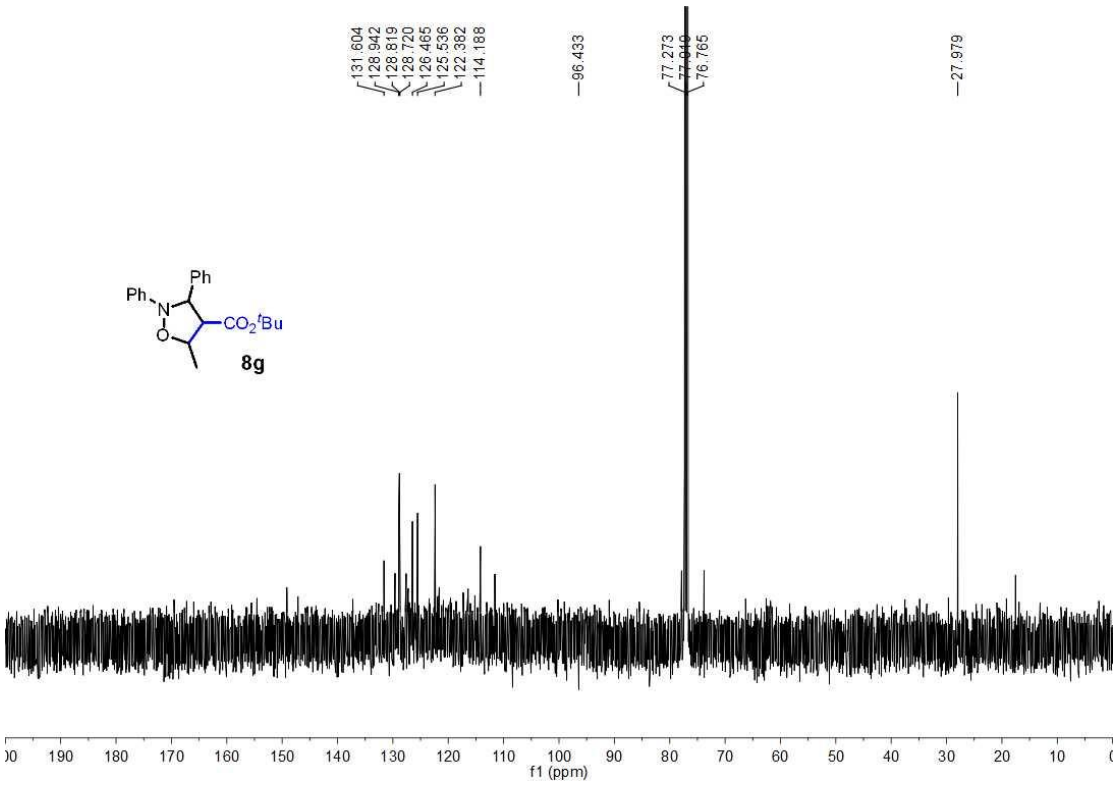

Ethyl 3-(4-fluorophenyl)-4-methyl-2-phenylisoxazolidine-4-carboxylate, **8i**

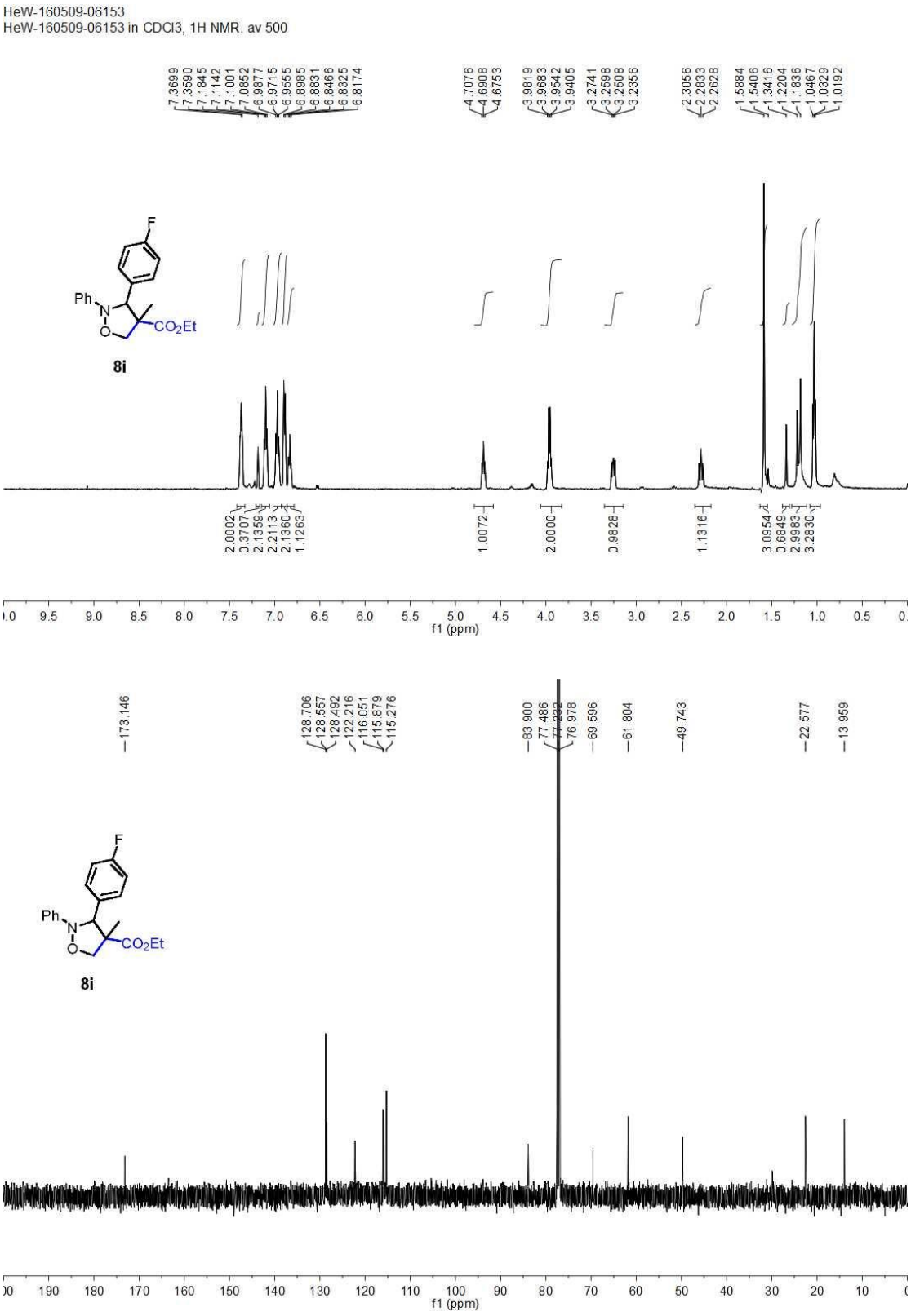

Methyl 3-(4-fluorophenyl)-2-phenylisoxazolidine-4-carboxylate, **8j**

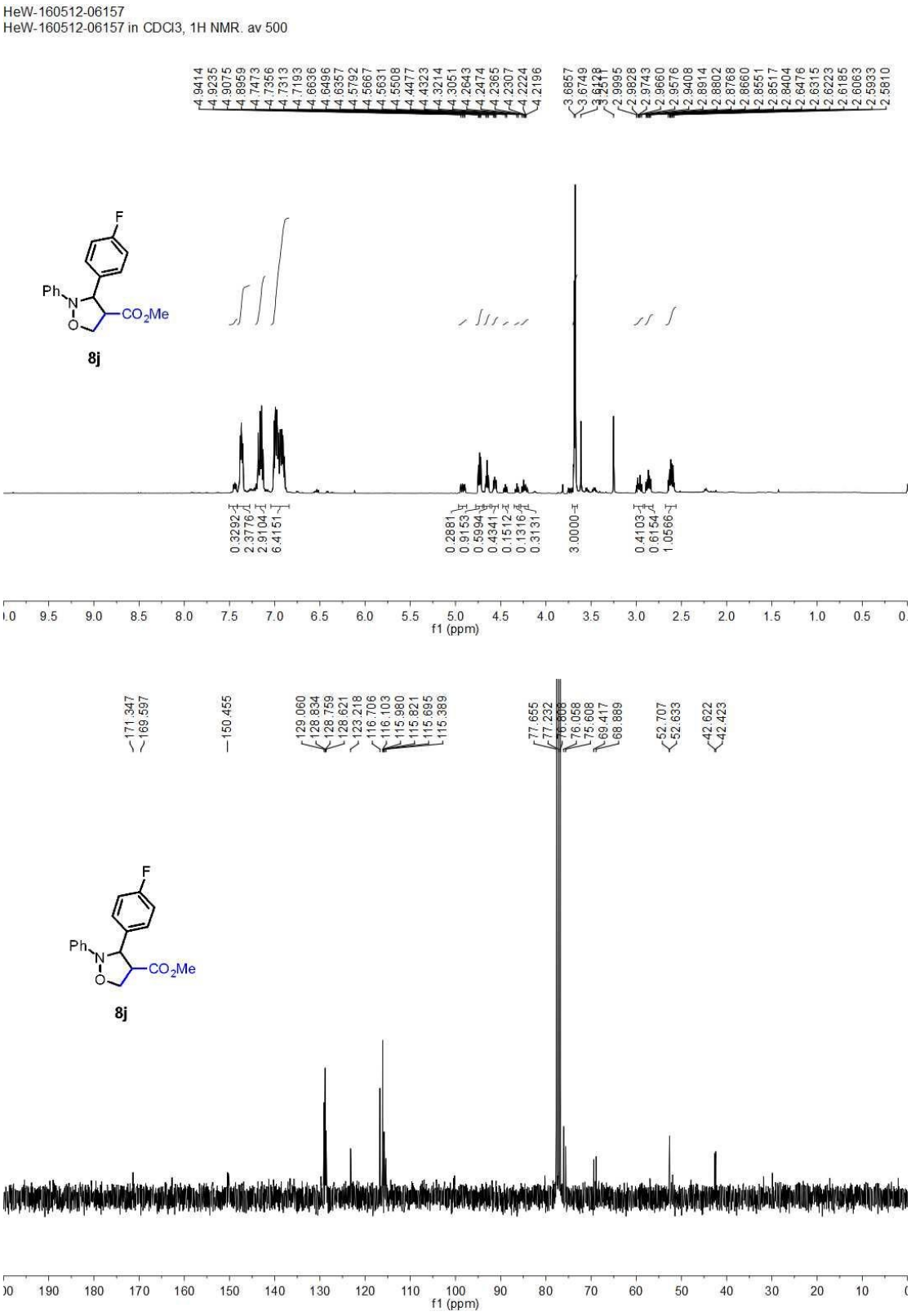

Ethyl 3-(4-fluorophenyl)-2-phenylisoxazolidine-4-carboxylate, **8k**

HeW-160509-06155
HeW-160509-06155 in CDCl3, 1H NMR. av 500

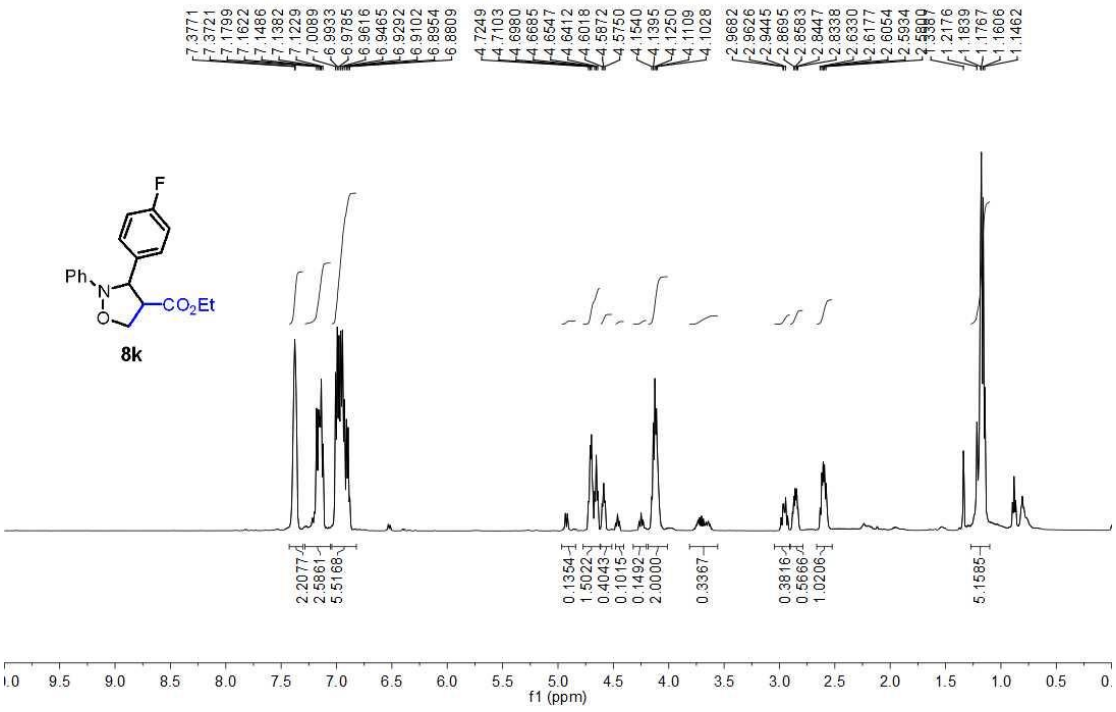

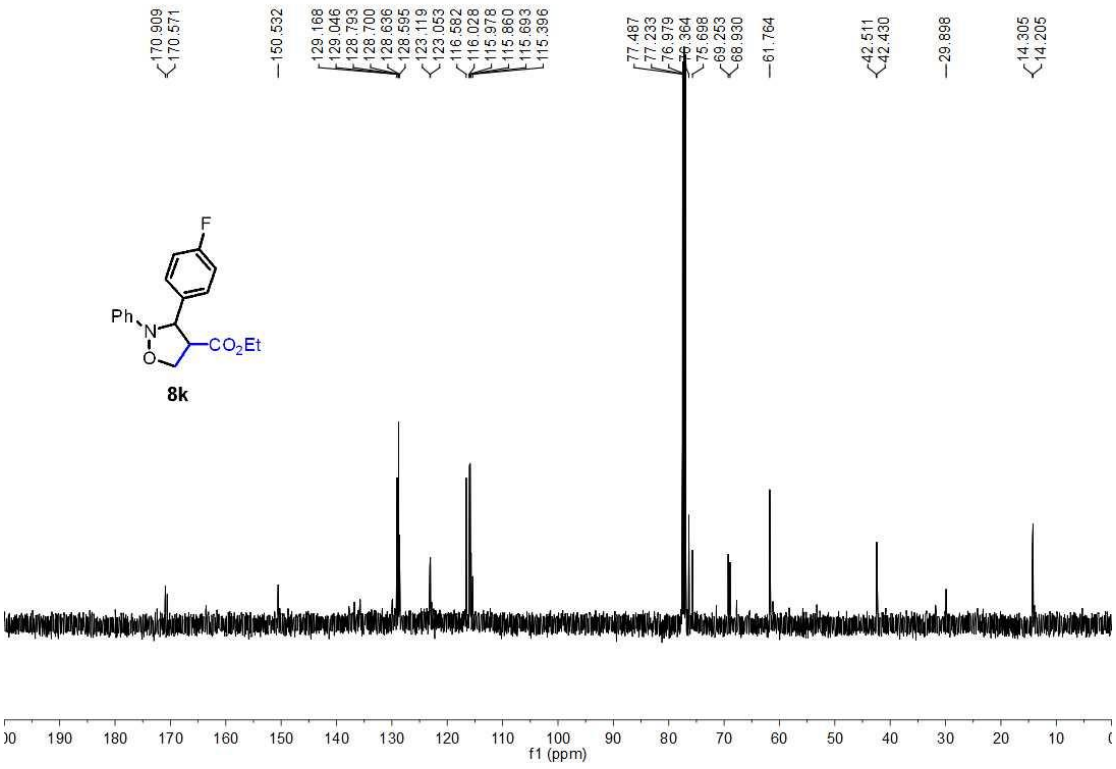

Tert-butyl 3-(4-fluorophenyl)-2-phenylisoxazolidine-4-carboxylate, **8l**

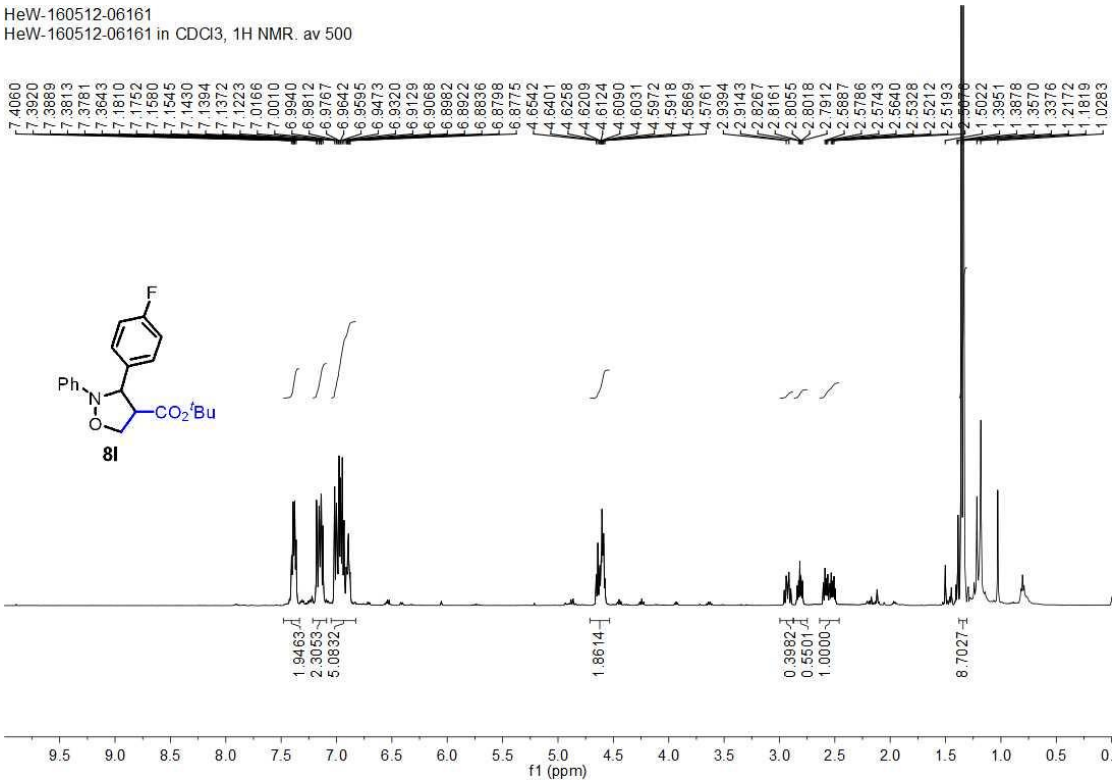

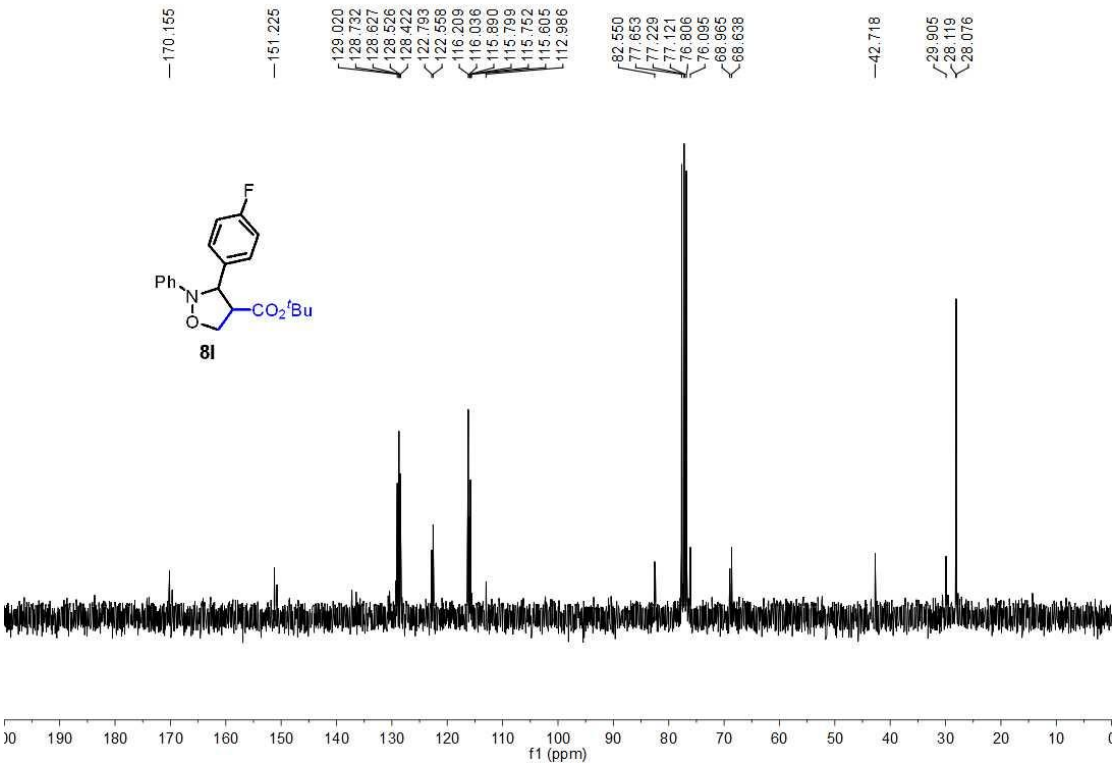

Vinyl 3-(4-fluorophenyl)-2-phenylisoxazolidine-4-carboxylate, **8l**

HeW-160512-06163
HeW-160512-06163 in CDCl3, 1H NMR. av 500

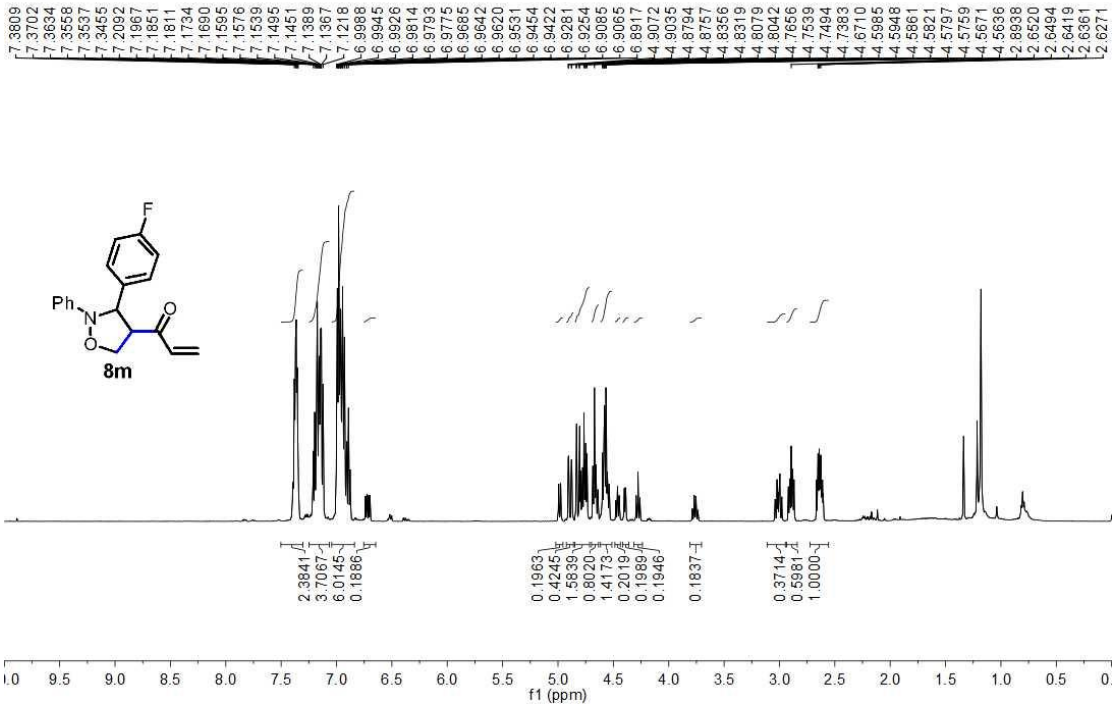

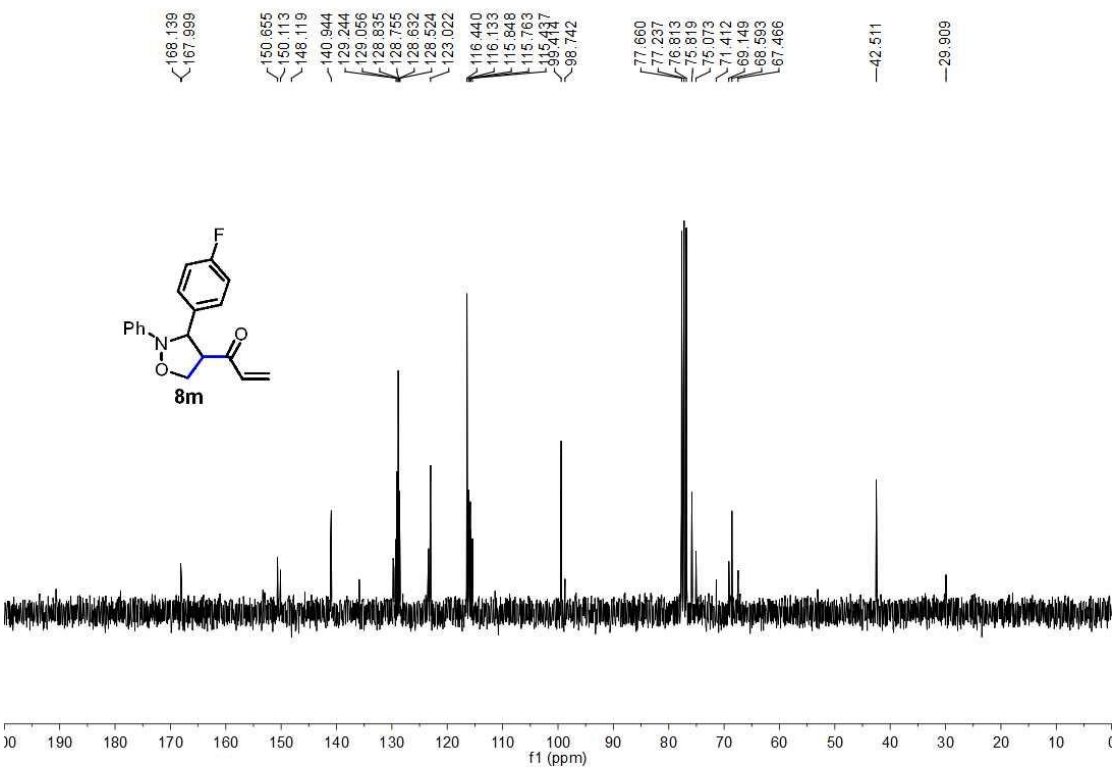

X-ray structural analysis

The X-ray structure of **C1**

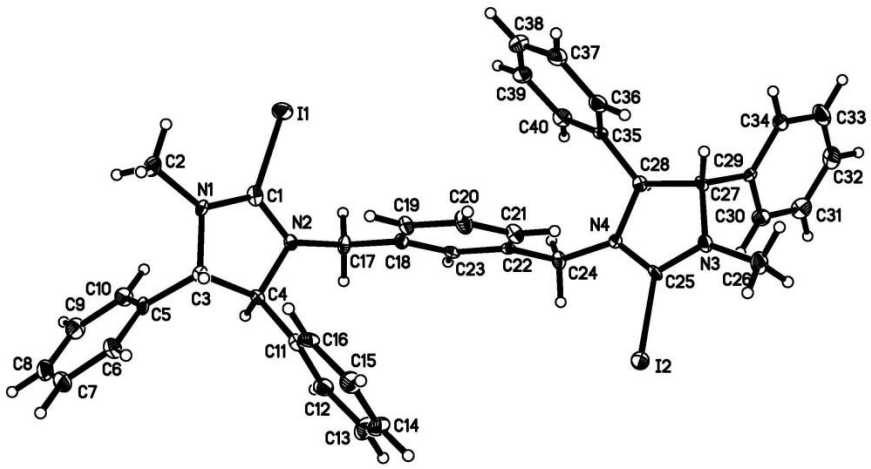

Crystal Structure Report for C1

A colorless block-like specimen of $C_{42}H_{40}F_6I_2N_4O_7S_2$, approximate dimensions 0.200 mm x 0.240 mm x 0.300 mm, was used for the X-ray crystallographic analysis. The X-ray intensity data were measured.

The total exposure time was 1.93 hours. The frames were integrated with the Bruker SAINT software package using a narrow-frame algorithm. The integration of the data using a triclinic unit cell yielded a total of 5563 reflections to a maximum θ angle of 28.40° (0.75 Å resolution), of which 5563 were independent (average redundancy 1.000, completeness = 99.4%) and 5391 (96.91%) were greater than $2\sigma(F^2)$. The final cell constants of a = 8.4586(5) Å, b = 8.5337(5) Å, c = 17.0469(9) Å, α = 77.6053(16)°, β = 80.4972(16)°, γ = 68.5488(17)°, volume = 1113.48(11) $Å^3$, are based upon the refinement of the XYZ-centroids of 9701 reflections above 20 σ(I) with 4.915° < 2θ < 56.57°. Data were corrected for absorption effects using the multi-scan method (SADABS). The ratio of minimum to maximum apparent transmission was 0.735. The calculated minimum and maximum transmission coefficients (based on crystal size) are 0.6480 and 0.7420.

The final anisotropic full-matrix least-squares refinement on F^2 with 577 variables converged at R1 = 3.02%, for the observed data and wR2 = 7.74% for all data. The goodness-of-fit was 1.117. The largest peak in the final difference electron density synthesis was 2.294 $e^-/Å^3$ and the largest hole was -0.632 $e^-/Å^3$ with an RMS deviation of 0.117 $e^-/Å^3$. On the basis of the final model, the calculated density was 1.707 g/cm^3 and F(000), 568 e^-.

Table 6.1 Sample and crystal data for tch8s.

Identification code	tch8s	
Chemical formula	$C_{42}H_{40}F_6I_2N_4O_7S_2$	
Formula weight	1144.70	
Temperature	103(2) K	
Wavelength	0.71073 Å	
Crystal size	0.200 x 0.240 x 0.300 mm	
Crystal habit	colorless block	
Crystal system	triclinic	
Space group	P 1	
Unit cell dimensions	a = 8.4586(5) Å	α = 77.6053(16)°
	b = 8.5337(5) Å	β = 80.4972(16)°
	c = 17.0469(9) Å	γ = 68.5488(17)°
Volume	1113.48(11) $Å^3$	
Z	1	
Density (calculated)	1.707 g/cm^3	
Absorption coefficient	1.585 mm^{-1}	

F(000)	568

Table 6.2 Data collection and structure refinement for tch8s.

Theta range for data collection	1.23 to 28.40°
Reflections collected	5563
Coverage of independent reflections	99.4%
Absorption correction	multi-scan
Max. and min. transmission	0.7420 and 0.6480
Refinement method	Full-matrix least-squares on F^2
Refinement program	SHELXL-2013 (Sheldrick, 2013)
Function minimized	$\Sigma\ w(F_o^2 - F_c^2)^2$
Data / restraints / parameters	5563 / 30 / 577
Goodness-of-fit on F^2	1.117
Final R indices	5391 data; $I>2\sigma(I)$ R1 = 0.0302, wR2 = 0.0754
	all data R1 = 0.0320, wR2 = 0.0774
Weighting scheme	$w=1/[\sigma^2(F_o^2)+(0.0396P)^2+1.1406P]$ where $P=(F_o^2+2F_c^2)/3$
Absolute structure parameter	0.1(0)
Largest diff. peak and hole	2.294 and -0.632 $eÅ^{-3}$
R.M.S. deviation from mean	0.117 $eÅ^{-3}$

Table 6.3 Atomic coordinates and equivalent isotropic atomic displacement

parameters (Å^2) for tch8s.

U(eq) is defined as one third of the trace of the orthogonalized U_{ij} tensor.

	x/a	y/b	z/c	U(eq)
C1	0.4658(11)	0.8905(10)	0.1436(5)	0.0133(15)
C2	0.3319(8)	0.0061(9)	0.2712(4)	0.0181(13)
C3	0.5786(8)	0.0712(8)	0.1778(3)	0.0092(10)
C4	0.6851(7)	0.9934(7)	0.1044(3)	0.0089(11)
C5	0.6852(9)	0.0541(9)	0.2439(4)	0.0116(12)
C6	0.7123(10)	0.1978(9)	0.2560(4)	0.0150(14)
C7	0.8217(12)	0.1806(11)	0.3131(4)	0.0225(14)
C8	0.8995(9)	0.0210(11)	0.3579(4)	0.0240(15)
C9	0.8710(9)	0.8789(10)	0.3460(4)	0.0212(13)
C10	0.7620(9)	0.8978(9)	0.2877(4)	0.0164(12)
C11	0.7262(12)	0.1179(12)	0.0326(5)	0.0182(18)
C12	0.8854(9)	0.0618(11)	0.9890(4)	0.0188(13)
C13	0.9251(12)	0.1678(11)	0.9180(5)	0.0280(17)
C14	0.8071(12)	0.3258(11)	0.8938(5)	0.0253(18)
C15	0.6531(11)	0.3817(11)	0.9378(4)	0.0235(15)
C16	0.6112(8)	0.2807(9)	0.0070(4)	0.0149(12)
C17	0.6459(9)	0.7994(8)	0.0191(3)	0.0133(12)
C18	0.5746(10)	0.8884(9)	0.9392(4)	0.0123(14)
C19	0.4410(11)	0.0382(10)	0.9305(4)	0.0160(16)

C20	0.3800(11)	0.1145(10)	0.8553(5)	0.0185(16)
C21	0.4518(10)	0.0348(10)	0.7891(4)	0.0165(15)
C22	0.5854(10)	0.8814(10)	0.7966(4)	0.0133(14)
C23	0.6475(9)	0.8082(9)	0.8727(4)	0.0108(13)
C24	0.6688(8)	0.7881(8)	0.7265(3)	0.0124(11)
C25	0.5821(11)	0.9673(11)	0.5945(4)	0.0124(15)
C26	0.4510(10)	0.1171(9)	0.4664(4)	0.0196(13)
C27	0.3847(8)	0.8688(8)	0.5623(3)	0.0100(10)
C28	0.4542(8)	0.7617(7)	0.6434(3)	0.0107(11)
C29	0.4147(9)	0.7599(9)	0.4982(4)	0.0088(11)
C30	0.5812(9)	0.6808(10)	0.4650(4)	0.0178(13)
C31	0.6094(10)	0.5759(9)	0.4087(4)	0.0203(13)
C32	0.4721(10)	0.5481(9)	0.3847(4)	0.0212(14)
C33	0.3088(12)	0.6244(10)	0.4185(4)	0.0236(16)
C34	0.2787(9)	0.7308(10)	0.4756(4)	0.0140(12)
C35	0.3244(10)	0.7485(10)	0.7136(4)	0.0113(15)
C36	0.1712(9)	0.8828(10)	0.7251(4)	0.0170(12)
C37	0.0585(9)	0.8665(10)	0.7934(4)	0.0208(14)
C38	0.1013(10)	0.7212(12)	0.8517(4)	0.0256(16)
C39	0.2548(12)	0.5883(12)	0.8413(4)	0.0231(16)
C40	0.3653(9)	0.6013(9)	0.7723(4)	0.0167(12)
C41	0.0474(9)	0.3582(8)	0.0933(4)	0.0182(13)

C42	0.1148(9)	0.4247(9)	0.6472(4)	0.0206(14)
F1	0.0250(9)	0.2167(6)	0.1325(3)	0.0417(14)
F2	0.9559(11)	0.4174(10)	0.0325(4)	0.059(2)
F3	0.2111(8)	0.3107(9)	0.0643(5)	0.065(2)
F4	0.0838(7)	0.5842(7)	0.6543(3)	0.0330(11)
F5	0.2760(6)	0.3635(7)	0.6149(3)	0.0316(11)
F6	0.1074(7)	0.3327(8)	0.7207(3)	0.0354(12)
I1	0.29990(5)	0.76084(5)	0.14172(3)	0.02288(13)
I2	0.74389(4)	0.10423(4)	0.58573(2)	0.02131(12)
N1	0.4571(7)	0.9742(7)	0.2011(3)	0.0138(11)
N2	0.5827(7)	0.9041(7)	0.0832(3)	0.0101(9)
N3	0.4810(7)	0.9889(7)	0.5391(3)	0.0133(10)
N4	0.5704(7)	0.8487(8)	0.6568(3)	0.0122(10)
O1	0.1204(13)	0.4326(10)	0.2181(5)	0.064(3)
O2	0.8266(9)	0.5562(8)	0.1839(4)	0.0372(14)
O3	0.0420(8)	0.6535(7)	0.1031(5)	0.0310(13)
O4	0.8067(7)	0.4622(8)	0.6350(3)	0.0280(12)
O5	0.0272(7)	0.2290(7)	0.5788(4)	0.0255(11)
O6	0.9804(7)	0.5229(7)	0.5118(3)	0.0266(12)
O1S	0.0877(14)	0.3124(15)	0.3829(6)	0.072(3)
S1	0.0048(3)	0.5172(2)	0.15702(11)	0.0223(4)
S2	0.9647(2)	0.4093(2)	0.58589(10)	0.0147(3)

Table 6.4 Bond lengths (Å) for tch8s.

C1-N1	1.309(9)	C1-N2	1.322(10)
C1-I1	2.088(10)	C2-N1	1.461(8)
C2-H2A	0.98	C2-H2B	0.98
C2-H2C	0.98	C3-N1	1.499(8)
C3-C5	1.508(8)	C3-C4	1.538(8)
C3-H3	1.0	C4-N2	1.472(7)
C4-C11	1.523(10)	C4-H4	1.0
C5-C10	1.363(10)	C5-C6	1.389(9)
C6-C7	1.401(10)	C6-H6	0.95
C7-C8	1.391(12)	C7-H7	0.95
C8-C9	1.381(11)	C8-H8	0.95
C9-C10	1.409(9)	C9-H9	0.95
C10-H10	0.95	C11-C12	1.395(11)
C11-C16	1.399(11)	C12-C13	1.419(11)
C12-H12	0.95	C13-C14	1.378(13)
C13-H13	0.95	C14-C15	1.365(12)
C14-H14	0.95	C15-C16	1.382(9)
C15-H15	0.95	C16-H16	0.95
C17-N2	1.468(7)	C17-C18	1.513(9)
C17-H17A	0.99	C17-H17B	0.99
C18-C19	1.360(10)	C18-C23	1.388(10)

C19-C20	1.396(10)	C19-H19	0.95
C20-C21	1.381(10)	C20-H20	0.95
C21-C22	1.378(11)	C21-H21	0.95
C22-C23	1.410(10)	C22-C24	1.509(9)
C23-H23	0.95	C24-N4	1.456(7)
C24-H24A	0.99	C24-H24B	0.99
C25-N3	1.317(9)	C25-N4	1.319(10)
C25-I2	2.071(9)	C26-N3	1.454(8)
C26-H26A	0.98	C26-H26B	0.98
C26-H26C	0.98	C27-N3	1.484(8)
C27-C29	1.514(9)	C27-C28	1.558(8)
C27-H27	1.0	C28-N4	1.499(8)
C28-C35	1.500(9)	C28-H28	1.0
C29-C34	1.390(9)	C29-C30	1.402(9)
C30-C31	1.383(9)	C30-H30	0.95
C31-C32	1.405(10)	C31-H31	0.95
C32-C33	1.380(12)	C32-H32	0.95
C33-C34	1.402(10)	C33-H33	0.95
C34-H34	0.95	C35-C40	1.399(10)
C35-C36	1.399(11)	C36-C37	1.395(10)
C36-H36	0.95	C37-C38	1.385(11)
C37-H37	0.95	C38-C39	1.392(13)

C38-H38	0.95	C39-C40	1.388(10)
C39-H39	0.95	C40-H40	0.95
C41-F2	1.297(9)	C41-F1	1.311(8)
C41-F3	1.333(9)	C41-S1	1.816(7)
C42-F4	1.317(9)	C42-F6	1.333(9)
C42-F5	1.338(8)	C42-S2	1.828(7)
O1-S1	1.435(7)	O2-S1	1.436(7)
O3-S1	1.418(6)	O4-S2	1.429(6)
O5-S2	1.458(5)	O6-S2	1.437(5)
O1S-H1O	0.902(11)	O1S-H2O	0.904(11)

Table 6.5 Bond angles (°) for tch8s.

N1-C1-N2	114.0(8)	N1-C1-I1	123.8(6)
N2-C1-I1	122.1(6)	N1-C2-H2A	109.5
N1-C2-H2B	109.5	H2A-C2-H2B	109.5
N1-C2-H2C	109.5	H2A-C2-H2C	109.5
H2B-C2-H2C	109.5	N1-C3-C5	114.1(5)
N1-C3-C4	101.5(4)	C5-C3-C4	113.0(5)
N1-C3-H3	109.3	C5-C3-H3	109.3
C4-C3-H3	109.3	N2-C4-C11	111.8(5)
N2-C4-C3	103.2(4)	C11-C4-C3	116.4(5)
N2-C4-H4	108.4	C11-C4-H4	108.4

C3-C4-H4	108.4	C10-C5-C6	120.7(6)
C10-C5-C3	120.2(6)	C6-C5-C3	119.0(6)
C5-C6-C7	119.4(7)	C5-C6-H6	120.3
C7-C6-H6	120.3	C8-C7-C6	119.9(7)
C8-C7-H7	120.1	C6-C7-H7	120.1
C9-C8-C7	120.4(6)	C9-C8-H8	119.8
C7-C8-H8	119.8	C8-C9-C10	119.1(7)
C8-C9-H9	120.5	C10-C9-H9	120.5
C5-C10-C9	120.6(7)	C5-C10-H10	119.7
C9-C10-H10	119.7	C12-C11-C16	119.2(8)
C12-C11-C4	117.2(7)	C16-C11-C4	123.5(7)
C11-C12-C13	119.5(8)	C11-C12-H12	120.2
C13-C12-H12	120.2	C14-C13-C12	119.6(7)
C14-C13-H13	120.2	C12-C13-H13	120.2
C15-C14-C13	120.6(7)	C15-C14-H14	119.7
C13-C14-H14	119.7	C14-C15-C16	120.9(8)
C14-C15-H15	119.5	C16-C15-H15	119.5
C15-C16-C11	120.1(7)	C15-C16-H16	119.9
C11-C16-H16	119.9	N2-C17-C18	114.1(5)
N2-C17-H17A	108.7	C18-C17-H17A	108.7
N2-C17-H17B	108.7	C18-C17-H17B	108.7
H17A-C17-H17B	107.6	C19-C18-C23	119.3(7)

C19-C18-C17	123.3(6)	C23-C18-C17	117.3(6)
C18-C19-C20	120.9(7)	C18-C19-H19	119.5
C20-C19-H19	119.5	C21-C20-C19	119.9(7)
C21-C20-H20	120.1	C19-C20-H20	120.1
C22-C21-C20	120.4(7)	C22-C21-H21	119.8
C20-C21-H21	119.8	C21-C22-C23	118.9(7)
C21-C22-C24	122.8(6)	C23-C22-C24	118.3(6)
C18-C23-C22	120.6(7)	C18-C23-H23	119.7
C22-C23-H23	119.7	N4-C24-C22	113.9(5)
N4-C24-H24A	108.8	C22-C24-H24A	108.8
N4-C24-H24B	108.8	C22-C24-H24B	108.8
H24A-C24-H24B	107.7	N3-C25-N4	113.2(7)
N3-C25-I2	123.9(6)	N4-C25-I2	122.9(5)
N3-C26-H26A	109.5	N3-C26-H26B	109.5
H26A-C26-H26B	109.5	N3-C26-H26C	109.5
H26A-C26-H26C	109.5	H26B-C26-H26C	109.5
N3-C27-C29	111.5(5)	N3-C27-C28	103.1(4)
C29-C27-C28	112.6(5)	N3-C27-H27	109.8
C29-C27-H27	109.8	C28-C27-H27	109.8
N4-C28-C35	113.3(5)	N4-C28-C27	101.6(4)
C35-C28-C27	116.7(5)	N4-C28-H28	108.3
C35-C28-H28	108.3	C27-C28-H28	108.3

C34-C29-C30	120.0(6)	C34-C29-C27	120.1(6)
C30-C29-C27	119.9(6)	C31-C30-C29	119.9(7)
C31-C30-H30	120.1	C29-C30-H30	120.1
C30-C31-C32	120.4(7)	C30-C31-H31	119.8
C32-C31-H31	119.8	C33-C32-C31	119.5(6)
C33-C32-H32	120.3	C31-C32-H32	120.3
C32-C33-C34	120.6(7)	C32-C33-H33	119.7
C34-C33-H33	119.7	C29-C34-C33	119.7(7)
C29-C34-H34	120.2	C33-C34-H34	120.2
C40-C35-C36	119.4(7)	C40-C35-C28	118.1(6)
C36-C35-C28	122.3(7)	C37-C36-C35	119.9(7)
C37-C36-H36	120.0	C35-C36-H36	120.0
C38-C37-C36	120.2(7)	C38-C37-H37	119.9
C36-C37-H37	119.9	C37-C38-C39	120.2(7)
C37-C38-H38	119.9	C39-C38-H38	119.9
C40-C39-C38	120.0(7)	C40-C39-H39	120.0
C38-C39-H39	120.0	C39-C40-C35	120.3(7)
C39-C40-H40	119.9	C35-C40-H40	119.9
F2-C41-F1	109.3(7)	F2-C41-F3	107.9(8)
F1-C41-F3	104.9(6)	F2-C41-S1	111.7(5)
F1-C41-S1	113.2(5)	F3-C41-S1	109.4(5)
F4-C42-F6	108.8(6)	F4-C42-F5	107.5(7)

F6-C42-F5	106.4(6)	F4-C42-S2	111.5(5)
F6-C42-S2	110.9(5)	F5-C42-S2	111.6(5)
C1-N1-C2	129.4(6)	C1-N1-C3	109.6(6)
C2-N1-C3	120.0(5)	C1-N2-C17	126.4(6)
C1-N2-C4	109.2(5)	C17-N2-C4	121.1(5)
C25-N3-C26	127.8(6)	C25-N3-C27	110.8(5)
C26-N3-C27	121.2(5)	C25-N4-C24	127.3(6)
C25-N4-C28	111.0(5)	C24-N4-C28	121.3(5)
H1O-O1S-H2O	93.(2)	O3-S1-O1	114.7(5)
O3-S1-O2	113.4(4)	O1-S1-O2	115.9(5)
O3-S1-C41	103.1(4)	O1-S1-C41	104.0(4)
O2-S1-C41	103.6(3)	O4-S2-O6	116.0(4)
O4-S2-O5	114.1(4)	O6-S2-O5	114.7(4)
O4-S2-C42	102.1(3)	O6-S2-C42	103.8(3)
O5-S2-C42	103.7(3)		

Table 6.6 Anisotropic atomic displacement parameters (Å^2) for tch8s.

The anisotropic atomic displacement factor exponent takes the form: $-2\pi^2[h^2 a^{*2} U_{11} + ... + 2 h k a^* b^* U_{12}]$

	U_{11}	**U_{22}**	**U_{33}**	**U_{23}**	**U_{13}**	**U_{12}**
C1	0.019(3)	0.006(3)	0.014(3)	-0.002(2)	-0.004(2)	-0.001(3)
C2	0.015(3)	0.021(3)	0.017(3)	-0.010(2)	0.003(2)	-0.003(3)

	U_{11}	U_{22}	U_{33}	U_{23}	U_{13}	U_{12}
C3	0.009(3)	0.006(3)	0.010(2)	-0.001(2)	0.000(2)	0.001(2)
C4	0.008(3)	0.006(3)	0.012(2)	-0.003(2)	-0.0035(19)	0.000(2)
C5	0.012(3)	0.014(3)	0.008(2)	-0.006(2)	0.001(2)	-0.002(2)
C6	0.020(4)	0.007(3)	0.019(3)	-0.005(2)	-0.003(2)	-0.003(3)
C7	0.032(4)	0.024(4)	0.019(3)	-0.008(3)	0.000(3)	-0.018(3)
C8	0.016(3)	0.043(5)	0.015(3)	-0.010(3)	-0.002(2)	-0.010(3)
C9	0.017(3)	0.026(3)	0.017(3)	0.001(2)	-0.006(2)	-0.004(3)
C10	0.018(3)	0.015(3)	0.016(3)	0.000(2)	-0.004(2)	-0.006(3)
C11	0.022(4)	0.026(4)	0.013(3)	-0.003(3)	-0.003(3)	-0.015(3)
C12	0.014(3)	0.022(4)	0.022(3)	-0.011(3)	0.002(2)	-0.007(3)
C13	0.036(4)	0.033(4)	0.020(3)	-0.012(3)	0.010(3)	-0.019(4)
C14	0.038(5)	0.026(4)	0.020(3)	0.001(3)	0.002(3)	-0.025(4)
C15	0.031(4)	0.023(4)	0.020(3)	0.006(3)	-0.009(3)	-0.015(3)
C16	0.008(3)	0.016(3)	0.020(3)	0.001(2)	-0.004(2)	-0.005(2)
C17	0.017(3)	0.012(3)	0.010(2)	-0.008(2)	0.001(2)	-0.001(2)
C18	0.015(3)	0.013(4)	0.010(3)	-0.001(2)	-0.002(2)	-0.007(3)
C19	0.017(4)	0.020(4)	0.012(3)	-0.002(3)	-0.005(2)	-0.008(3)
C20	0.018(4)	0.017(4)	0.018(3)	-0.005(3)	-0.007(3)	0.000(3)
C21	0.017(4)	0.017(4)	0.017(3)	-0.004(3)	-0.005(2)	-0.005(3)
C22	0.013(3)	0.020(4)	0.010(3)	0.001(2)	-0.002(2)	-0.012(3)
C23	0.007(3)	0.011(3)	0.014(3)	-0.002(2)	-0.002(2)	-0.004(3)

	U_{11}	U_{22}	U_{33}	U_{23}	U_{13}	U_{12}
C24	0.011(3)	0.012(3)	0.011(2)	-0.002(2)	-0.004(2)	0.002(2)
C25	0.014(4)	0.015(4)	0.013(3)	-0.004(3)	-0.005(3)	-0.008(3)
C26	0.028(4)	0.015(3)	0.016(3)	0.002(2)	-0.008(2)	-0.008(3)
C27	0.006(2)	0.011(2)	0.011(2)	-0.0004(18)	-0.0046(17)	0.0007(19)
C28	0.011(3)	0.008(3)	0.012(2)	-0.001(2)	-0.003(2)	-0.001(2)
C29	0.006(2)	0.006(2)	0.009(2)	0.0034(18)	-0.0010(18)	0.0007(19)
C30	0.013(3)	0.022(4)	0.018(3)	-0.007(3)	0.002(2)	-0.005(3)
C31	0.024(3)	0.014(3)	0.022(3)	-0.007(2)	0.003(3)	-0.005(3)
C32	0.032(4)	0.018(3)	0.017(3)	-0.008(2)	-0.002(3)	-0.009(3)
C33	0.031(4)	0.024(4)	0.022(3)	-0.003(3)	-0.011(3)	-0.014(4)
C34	0.012(3)	0.014(3)	0.014(3)	0.000(2)	-0.003(2)	-0.003(2)
C35	0.010(3)	0.014(3)	0.012(3)	-0.001(2)	-0.002(2)	-0.007(3)
C36	0.017(3)	0.019(3)	0.019(3)	-0.006(3)	-0.002(2)	-0.009(3)
C37	0.015(3)	0.030(4)	0.020(3)	-0.009(3)	0.001(2)	-0.008(3)
C38	0.026(4)	0.039(5)	0.018(3)	-0.004(3)	0.002(3)	-0.021(4)
C39	0.030(4)	0.028(5)	0.019(3)	0.005(3)	-0.004(3)	-0.023(3)
C40	0.020(3)	0.011(3)	0.020(3)	0.000(2)	-0.004(3)	-0.006(3)
C41	0.016(3)	0.008(3)	0.027(3)	-0.007(2)	0.002(2)	0.002(3)
C42	0.017(3)	0.019(4)	0.021(3)	-0.005(3)	-0.006(2)	0.002(3)
F1	0.061(4)	0.015(2)	0.053(3)	-0.014(2)	0.007(3)	-0.016(3)
F2	0.084(5)	0.041(4)	0.054(4)	-0.019(3)	-0.042(4)	-0.001(3)

	U_{11}	U_{22}	U_{33}	U_{23}	U_{13}	U_{12}
F3	0.036(3)	0.055(4)	0.116(6)	-0.054(4)	0.036(4)	-0.025(3)
F4	0.037(3)	0.025(3)	0.045(3)	-0.013(2)	-0.014(2)	-0.012(2)
F5	0.013(2)	0.044(3)	0.033(2)	-0.005(2)	-0.0045(17)	-0.006(2)
F6	0.032(3)	0.051(3)	0.018(2)	0.000(2)	-0.0088(18)	-0.009(2)
I1	0.0255(3)	0.0272(3)	0.0246(2)	-0.0099(2)	0.00293(19)	-0.0184(2)
I2	0.0285(3)	0.0266(3)	0.0161(2)	-0.00272(19)	-0.00188(18)	-0.0185(2)
N1	0.015(3)	0.019(3)	0.008(2)	-0.0057(19)	0.0034(18)	-0.008(2)
N2	0.011(3)	0.009(2)	0.010(2)	-0.0031(18)	-0.0017(18)	-0.002(2)
N3	0.017(3)	0.013(3)	0.011(2)	-0.0020(19)	-0.0036(19)	-0.006(2)
N4	0.011(2)	0.018(3)	0.009(2)	-0.0028(19)	-0.0001(17)	-0.007(2)
O1	0.096(7)	0.039(4)	0.062(5)	-0.011(4)	-0.057(5)	-0.009(4)
O2	0.045(4)	0.026(3)	0.041(3)	-0.014(3)	0.018(3)	-0.018(3)
O3	0.022(3)	0.014(3)	0.060(4)	-0.006(3)	-0.006(3)	-0.008(2)
O4	0.011(2)	0.036(3)	0.035(3)	-0.009(2)	-0.005(2)	-0.004(2)
O5	0.027(3)	0.014(3)	0.036(3)	-0.007(2)	-0.005(2)	-0.005(2)
O6	0.027(3)	0.029(3)	0.026(2)	0.007(2)	-0.013(2)	-0.014(2)
O1S	0.075(7)	0.084(7)	0.066(5)	-0.027(5)	-0.022(5)	-0.026(6)
S1	0.0259(10)	0.0142(9)	0.0281(8)	-0.0057(7)	-0.0098(7)	-0.0042(8)
S2	0.0113(8)	0.0094(8)	0.0213(7)	-0.0002(6)	-0.0066(6)	-0.0002(6)

Table 6.7 Hydrogen atomic coordinates and isotropic atomic displacement parameters ($Å^2$) for tch8s.

	x/a	y/b	z/c	U(eq)
H2A	0.2448	0.9565	1.2699	0.027
H2B	0.2778	1.1295	1.2701	0.027
H2C	0.3893	0.9536	1.3207	0.027
H3	0.5133	1.1948	1.1600	0.011
H4	0.7949	0.9064	1.1224	0.011
H6	0.6571	1.3068	1.2259	0.018
H7	0.8427	1.2778	1.3212	0.027
H8	0.9728	1.0097	1.3970	0.029
H9	0.9242	0.7699	1.3765	0.025
H10	0.7418	0.8008	1.2790	0.02
H12	0.9667	0.9534	1.0067	0.023
H13	1.0324	1.1299	0.8873	0.034
H14	0.8331	1.3965	0.8460	0.03
H15	0.5737	1.4916	0.9206	0.028
H16	0.5040	1.3219	1.0374	0.018
H17A	0.6168	0.6941	1.0370	0.016
H17B	0.7718	0.7650	1.0111	0.016
H19	0.3885	1.0915	0.9762	0.019
H20	0.2891	1.2210	0.8497	0.022
H21	0.4090	1.0859	0.7381	0.02
H23	0.7401	0.7030	0.8786	0.013

	x/a	y/b	z/c	U(eq)
H24A	0.7821	0.8002	0.7098	0.015
H24B	0.6872	0.6650	0.7447	0.015
H26A	0.4720	1.2178	0.4746	0.029
H26B	0.3325	1.1499	0.4546	0.029
H26C	0.5282	1.0700	0.4211	0.029
H27	0.2600	0.9340	0.5716	0.012
H28	0.5256	0.6436	0.6339	0.013
H30	0.6745	0.6991	0.4811	0.021
H31	0.7223	0.5225	0.3862	0.024
H32	0.4915	0.4772	0.3456	0.025
H33	0.2158	0.6047	0.4029	0.028
H34	0.1660	0.7828	0.4986	0.017
H36	0.1440	0.9849	0.6865	0.02
H37	-0.0480	0.9554	0.8000	0.025
H38	0.0258	0.7122	0.8990	0.031
H39	0.2838	0.4887	0.8813	0.028
H40	0.4693	0.5098	0.7649	0.02
H1O	0.07(2)	0.393(16)	0.412(8)	0.107
H2O	0.14(2)	0.363(19)	0.340(6)	0.107

The X-ray structure of **C8**

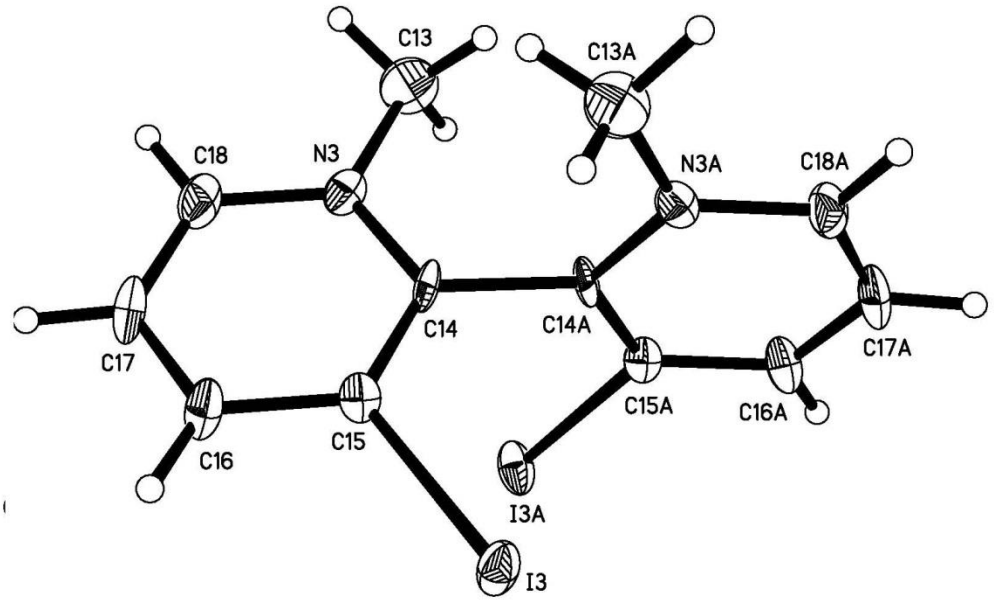

Crystal structure report for C8

A colorless needle-like specimen of $C_{14}H_{13}F_6I_2N_2O_{6.50}S_2$, approximate dimensions 0.080 mm x 0.100 mm x 0.400 mm, was used for the X-ray crystallographic analysis. The X-ray intensity data were measured.

The total exposure time was 0.43 hours. The frames were integrated with the Bruker SAINT software package using a narrow-frame algorithm. The integration of the data using a monoclinic unit cell yielded a total of 27758 reflections to a maximum θ angle of 67.87° (0.83 Å resolution), of which 7856 were independent (average redundancy 3.533, completeness = 97.4%, R_{int} = 6.12%, R_{sig} = 6.85%) and 7373 (93.85%) were greater than $2\sigma(F^2)$. The final cell constants of a = 19.2539(3) Å, b =15.2933(2) Å, c = 15.8351(2) Å, β = 101.9474(8)°, volume = 4561.73(11) $Å^3$, are based upon the refinement of the XYZ-centroids of 9803 reflections above 20 σ(I) with 8.772° < 2θ < 135.1°. Data were corrected for absorption effects using the Multi-Scan method (SADABS). The ratio of minimum to maximum apparent transmission was 0.334. The calculated minimum and

maximum transmission coefficients (based on crystal size) are 0.0370 and 0.2480.

The structure was solved and refined using the Bruker SHELXTL Software Package, using the space group C 1 2 1, with Z = 8 for the formula unit, $C_{14}H_{13}F_6I_2N_2O_{6.50}S_2$. The final anisotropic full-matrix least-squares refinement on F^2 with 735 variables converged at R1 = 4.61%, for the observed data and wR2 = 11.95% for all data. The goodness-of-fit was 1.024. The largest peak in the final difference electron density synthesis was 1.408 $e^-/Å^3$ and the largest hole was -2.162 $e^-/Å^3$ with an RMS deviation of 0.178 $e^-/Å^3$. On the basis of the final model, the calculated density was 2.170 g/cm^3 and F(000), 2840 e^-.

Table 6.8 Sample and crystal data for C8.

Identification code	tch101s	
Chemical formula	$C_{14}H_{13}F_6I_2N_2O_{6.50}S_2$	
Formula weight	745.18 g/mol	
Temperature	153(2) K	
Wavelength	1.54178 Å	
Crystal size	0.080 x 0.100 x 0.400 mm	
Crystal habit	colorless needle	
Crystal system	monoclinic	
Space group	C 1 2 1	
Unit cell dimensions	a = 19.2539(3) Å	α = 90°
	b = 15.2933(2) Å	β = 101.9474(8)°
	c = 15.8351(2) Å	γ = 90°

Volume	4561.73(11) $Å^3$
Z	8
Density (calculated)	2.170 g/cm^3
Absorption coefficient	24.187 mm^{-1}
F(000)	2840

Table 6.9 Data collection and structure refinement.

Theta range for data collection	2.85 to 67.87°
Index ranges	-21<=h<=23, -16<=k<=17, -18<=l<=18
Reflections collected	27758
Independent reflections	7856 [R(int) = 0.0612]
Coverage of independent reflections	97.4%
Absorption correction	Multi-Scan
Max. and min. transmission	0.2480 and 0.0370
Structure solution technique	direct methods
Structure solution program	XT, VERSION 2014/5
Refinement method	Full-matrix least-squares on F^2
Refinement program	SHELXL-2014/7 (Sheldrick, 2014)
Function minimized	$\Sigma\ w(F_o^2 - F_c^2)^2$
Data / restraints / parameters	7856 / 1176 / 735
Goodness-of-fit on F^2	1.024

Final R indices	7373 data; I>2σ(I)	R1 = 0.0461, wR2 = 0.1175
	all data	R1 = 0.0485, wR2 = 0.1195
Weighting scheme	$w=1/[\sigma^2(F_o^2)+(0.0832P)^2]$ where $P=(F_o^2+2F_c^2)/3$	
Absolute structure parameter	0.027(5)	
Largest diff. peak and hole	1.408 and -2.162 eÅ^{-3}	
R.M.S. deviation from mean	0.178 eÅ^{-3}	

Table 6.10 Atomic coordinates and equivalent isotropic atomic displacement parameters (Å²).

U(eq) is defined as one third of the trace of the orthogonalized U_{ij} tensor.

	x/a	y/b	z/c	U(eq)
C1	0.8047(6)	0.6043(8)	0.1183(7)	0.020(2)
C2	0.7443(8)	0.7414(9)	0.0793(9)	0.034(3)
C3	0.6862(9)	0.7958(10)	0.0699(11)	0.043(3)
C4	0.6234(8)	0.7642(10)	0.0870(9)	0.038(3)
C5	0.6190(7)	0.6798(8)	0.1140(7)	0.025(2)
C6	0.6794(5)	0.6269(8)	0.1236(6)	0.0164(17)
C7	0.6817(5)	0.5369(7)	0.1593(7)	0.0141(18)
C8	0.6992(5)	0.5194(7)	0.2459(7)	0.0159(19)

C9	0.7021(6)	0.4331(8)	0.2755(9)	0.026(2)
C10	0.6831(7)	0.3672(9)	0.2149(9)	0.033(2)
C11	0.6651(7)	0.3855(9)	0.1306(9)	0.030(2)
C12	0.6418(7)	0.4857(11)	0.0072(8)	0.037(3)
C13	0.5129(7)	0.7395(9)	0.6199(9)	0.032(3)
C14	0.5388(5)	0.6250(8)	0.5208(6)	0.0145(18)
C15	0.5855(6)	0.5672(7)	0.4953(7)	0.016(2)
C16	0.6553(6)	0.5623(8)	0.5406(7)	0.022(2)
C17	0.6754(6)	0.6131(9)	0.6115(7)	0.023(2)
C18	0.6299(6)	0.6726(8)	0.6370(7)	0.022(2)
I1	0.52660(3)	0.63139(6)	0.14631(4)	0.0284(2)
I2	0.71885(4)	0.62218(5)	0.33399(4)	0.02299(19)
I3	0.54843(3)	0.48308(5)	0.39114(4)	0.02056(19)
C19	0.4056(10)	0.2781(13)	0.4530(15)	0.033(4)
C20	0.4760(10)	0.1628(15)	0.5306(11)	0.019(3)
C21	0.4939(11)	0.1039(12)	0.6010(12)	0.024(3)
C22	0.4552(12)	0.1061(13)	0.6657(13)	0.029(3)
C23	0.3994(12)	0.1625(17)	0.6586(13)	0.026(3)
C24	0.3843(12)	0.2199(18)	0.5899(14)	0.024(3)
N4	0.4232(9)	0.2191(12)	0.5279(10)	0.020(2)
I4	0.57165(8)	0.01188(10)	0.60578(12)	0.0555(6)
C19A	0.557(2)	0.067(3)	0.631(3)	0.034(7)

C20A	0.481(2)	0.169(3)	0.540(2)	0.021(4)
C21A	0.420(2)	0.223(3)	0.521(2)	0.021(4)
C22A	0.376(3)	0.230(4)	0.579(3)	0.023(4)
C23A	0.389(3)	0.178(4)	0.651(3)	0.025(4)
C24A	0.450(3)	0.129(4)	0.670(3)	0.025(4)
N4A	0.493(2)	0.122(3)	0.612(2)	0.024(4)
I4A	0.39511(18)	0.2946(2)	0.4091(3)	0.0347(13)
N1	0.7403(5)	0.6605(6)	0.1057(6)	0.0201(18)
N2	0.6632(5)	0.4696(7)	0.1024(6)	0.0216(19)
N3	0.5612(5)	0.6771(6)	0.5911(6)	0.0169(18)
C27	0.6769(11)	0.8846(14)	0.3740(12)	0.058(4)
C28	0.5208(10)	0.3003(18)	0.8669(13)	0.074(5)
F7	0.6284(8)	0.8384(11)	0.3216(8)	0.094(4)
F8	0.7315(8)	0.8802(11)	0.3370(7)	0.091(4)
F9	0.6616(13)	0.9667(12)	0.3754(11)	0.132(6)
F10	0.4652(8)	0.2457(12)	0.8522(11)	0.097(4)
F11	0.5650(8)	0.2718(12)	0.9405(8)	0.093(4)
F12	0.4954(6)	0.3806(10)	0.8934(10)	0.088(4)
C25	0.6386(9)	0.0454(10)	0.1190(9)	0.042(3)
F1	0.6224(6)	0.0119(7)	0.0417(6)	0.058(3)
F2	0.6646(9)	0.9795(8)	0.1741(7)	0.090(4)
F3	0.5802(7)	0.0753(8)	0.1416(8)	0.074(3)

O1	0.6715(5)	0.1942(6)	0.0663(5)	0.0266(18)
O2	0.7651(5)	0.0878(8)	0.1026(7)	0.048(3)
O3	0.7164(5)	0.1574(6)	0.2168(5)	0.0283(19)
S1	0.70551(13)	0.1307(2)	0.12733(16)	0.0195(5)
C26	0.4424(10)	0.8976(14)	0.1514(13)	0.028(3)
F4	0.4570(15)	0.8884(17)	0.0722(13)	0.034(4)
F5	0.4398(10)	0.9856(11)	0.1657(12)	0.032(4)
F6	0.4962(10)	0.8668(14)	0.2099(13)	0.038(4)
O4	0.3072(13)	0.894(2)	0.1000(15)	0.024(4)
O5	0.3697(9)	0.7561(11)	0.1348(17)	0.048(4)
O6	0.3567(8)	0.8580(16)	0.2507(10)	0.039(4)
S2	0.3591(6)	0.8454(8)	0.1596(9)	0.031(2)
C26A	0.4462(15)	0.910(2)	0.152(2)	0.029(4)
F4A	0.462(3)	0.875(3)	0.081(2)	0.032(6)
F5A	0.4421(18)	0.9992(18)	0.142(2)	0.032(6)
F6A	0.5002(16)	0.897(2)	0.218(2)	0.034(6)
O4A	0.312(2)	0.893(4)	0.097(3)	0.030(7)
O5A	0.3770(15)	0.7738(19)	0.182(2)	0.040(5)
O6A	0.3569(15)	0.912(3)	0.2530(16)	0.043(6)
S2A	0.3630(11)	0.8676(15)	0.1738(12)	0.030(3)
O7	0.6328(9)	0.8395(12)	0.5117(11)	0.085(4)
O8	0.7212(9)	0.7512(9)	0.4683(7)	0.070(4)

O9	0.7558(8)	0.8888(9)	0.5249(7)	0.061(3)
O10	0.5040(10)	0.3378(11)	0.7123(10)	0.093(5)
O11	0.5890(11)	0.2291(11)	0.7677(10)	0.088(5)
O12	0.6127(10)	0.3776(13)	0.8084(12)	0.093(5)
O13	0.4069(5)	0.5711(9)	0.2053(7)	0.049(3)
S3	0.69688(18)	0.8380(2)	0.4824(2)	0.0324(7)
S4	0.5649(3)	0.3147(3)	0.7805(3)	0.0525(10)

Table 6.11 Bond lengths (Å).

C1-N1	1.488(15)	C1-H1A	0.98
C1-H1B	0.98	C1-H1C	0.98
C2-N1	1.314(18)	C2-C3	1.38(2)
C2-H2	0.95	C3-C4	1.38(2)
C3-H3	0.95	C4-C5	1.37(2)
C4-H4	0.95	C5-C6	1.399(16)
C5-I1	2.086(13)	C6-N1	1.363(14)
C6-C7	1.486(16)	C7-N2	1.365(14)
C7-C8	1.369(16)	C8-C9	1.397(17)
C8-I2	2.084(11)	C9-C10	1.39(2)
C9-H9	0.95	C10-C11	1.34(2)

C10-H10	0.95	C11-N2	1.360(18)
C11-H11	0.95	C12-N2	1.498(16)
C12-H12A	0.98	C12-H12B	0.98
C12-H12C	0.98	C13-N3	1.469(16)
C13-H13A	0.98	C13-H13B	0.98
C13-H13C	0.98	C14-N3	1.365(14)
C14-C15	1.379(16)	C14-C14	1.502(18)
C15-C16	1.388(16)	C15-I3	2.097(11)
C16-C17	1.353(17)	C16-H16	0.95
C17-C18	1.380(18)	C17-H17	0.95
C18-N3	1.373(15)	C18-H18	0.95
C19-N4	1.47(3)	C19-H19A	0.98
C19-H19B	0.98	C19-H19C	0.98
C20-N4	1.33(3)	C20-C21	1.42(3)
C20-C20	1.47(3)	C21-C22	1.39(3)
C21-I4	2.04(2)	C22-C23	1.36(3)
C22-H22	0.95	C23-C24	1.38(3)
C23-H23	0.95	C24-N4	1.35(2)
C24-H24	0.95	C19A-N4A	1.47(3)
C19A-H19D	0.98	C19A-H19E	0.98
C19A-H19F	0.98	C20A-N4A	1.33(3)
C20A-C21A	1.42(3)	C20A-C20A	1.59(6)

C21A-C22A	1.39(3)	C21A-I4A	2.04(2)
C22A-C23A	1.36(3)	C22A-H22A	0.95
C23A-C24A	1.38(3)	C23A-H23A	0.95
C24A-N4A	1.36(3)	C24A-H24A	0.95
C27-F9	1.29(3)	C27-F8	1.31(3)
C27-F7	1.32(2)	C27-S3	1.824(17)
C28-F10	1.34(3)	C28-F11	1.36(2)
C28-F12	1.42(3)	C28-S4	1.77(3)
C25-F1	1.304(17)	C25-F3	1.33(2)
C25-F2	1.36(2)	C25-S1	1.819(15)
O1-S1	1.430(9)	O2-S1	1.444(10)
O3-S1	1.448(8)	C26-F6	1.325(18)
C26-F4	1.35(2)	C26-F5	1.37(2)
C26-S2	1.820(16)	O4-S2	1.434(14)
O5-S2	1.45(2)	O6-S2	1.465(18)
C26A-F6A	1.33(2)	C26A-F4A	1.34(2)
C26A-F5A	1.38(3)	C26A-S2A	1.82(2)
O4A-S2A	1.44(2)	O5A-S2A	1.46(3)
O6A-S2A	1.45(2)	O7-S3	1.405(16)
O8-S3	1.440(15)	O9-S3	1.423(12)
O10-S4	1.464(15)	O11-S4	1.416(18)
O12-S4	1.342(18)	O13-H2O	0.8485

O13-H1O	0.8455

Table 6.12 Bond angles (°).

N1-C1-H1A	109.5	N1-C1-H1B	109.5
H1A-C1-H1B	109.5	N1-C1-H1C	109.5
H1A-C1-H1C	109.5	H1B-C1-H1C	109.5
N1-C2-C3	120.2(13)	N1-C2-H2	119.9
C3-C2-H2	119.9	C2-C3-C4	119.5(14)
C2-C3-H3	120.3	C4-C3-H3	120.3
C5-C4-C3	120.4(13)	C5-C4-H4	119.8
C3-C4-H4	119.8	C4-C5-C6	118.4(12)
C4-C5-I1	121.5(9)	C6-C5-I1	120.0(9)
N1-C6-C5	119.4(11)	N1-C6-C7	117.9(9)
C5-C6-C7	122.4(10)	N2-C7-C8	119.4(10)
N2-C7-C6	117.7(9)	C8-C7-C6	122.9(9)
C7-C8-C9	120.3(10)	C7-C8-I2	119.7(8)
C9-C8-I2	119.9(9)	C10-C9-C8	117.9(12)
C10-C9-H9	121.0	C8-C9-H9	121.0
C11-C10-C9	121.0(12)	C11-C10-H10	119.5
C9-C10-H10	119.5	C10-C11-N2	120.6(12)
C10-C11-H11	119.7	N2-C11-H11	119.7
N2-C12-H12A	109.5	N2-C12-H12B	109.5
H12A-C12-H12B	109.5	N2-C12-H12C	109.5

H12A-C12-H12C	109.5	H12B-C12-H12C	109.5
N3-C13-H13A	109.5	N3-C13-H13B	109.5
H13A-C13-H13B	109.5	N3-C13-H13C	109.5
H13A-C13-H13C	109.5	H13B-C13-H13C	109.5
N3-C14-C15	119.8(9)	N3-C14-C14	118.4(9)
C15-C14-C14	121.4(8)	C14-C15-C16	120.2(10)
C14-C15-I3	119.1(8)	C16-C15-I3	120.6(8)
C17-C16-C15	118.6(11)	C17-C16-H16	120.7
C15-C16-H16	120.7	C16-C17-C18	122.1(10)
C16-C17-H17	119.0	C18-C17-H17	119.0
N3-C18-C17	118.6(10)	N3-C18-H18	120.7
C17-C18-H18	120.7	N4-C19-H19A	109.5
N4-C19-H19B	109.5	H19A-C19-H19B	109.5
N4-C19-H19C	109.5	H19A-C19-H19C	109.5
H19B-C19-H19C	109.5	N4-C20-C21	119.8(11)
N4-C20-C20	124.1(17)	C21-C20-C20	115.7(17)
C22-C21-C20	119.0(16)	C22-C21-I4	119.4(14)
C20-C21-I4	121.5(13)	C23-C22-C21	119.2(17)
C23-C22-H22	120.4	C21-C22-H22	120.4
C22-C23-C24	120.1(13)	C22-C23-H23	119.9
C24-C23-H23	119.9	N4-C24-C23	120.5(16)
N4-C24-H24	119.7	C23-C24-H24	119.7

C20-N4-C24	121.3(16)	C20-N4-C19	118.1(16)
C24-N4-C19	120.6(16)	N4A-C19A-H19D	109.5
N4A-C19A-H19E	109.5	H19D-C19A-H19E	109.5
N4A-C19A-H19F	109.5	H19D-C19A-H19F	109.5
H19E-C19A-H19F	109.5	N4A-C20A-C21A	119.8(17)
N4A-C20A-C20A	131.(3)	C21A-C20A-C20A	109.(3)
C22A-C21A-C20A	119.(2)	C22A-C21A-I4A	119.(2)
C20A-C21A-I4A	122.(2)	C23A-C22A-C21A	119.(2)
C23A-C22A-H22A	120.4	C21A-C22A-H22A	120.4
C22A-C23A-C24A	119.8(19)	C22A-C23A-H23A	120.1
C24A-C23A-H23A	120.1	N4A-C24A-C23A	121.(2)
N4A-C24A-H24A	119.6	C23A-C24A-H24A	119.6
C20A-N4A-C24A	121.(2)	C20A-N4A-C19A	119.(2)
C24A-N4A-C19A	120.(2)	C2-N1-C6	122.1(11)
C2-N1-C1	119.0(10)	C6-N1-C1	119.0(9)
C11-N2-C7	120.7(11)	C11-N2-C12	117.9(11)
C7-N2-C12	121.3(11)	C14-N3-C18	120.6(9)
C14-N3-C13	121.3(10)	C18-N3-C13	118.1(10)
F9-C27-F8	105.4(18)	F9-C27-F7	113.4(19)
F8-C27-F7	102.8(18)	F9-C27-S3	111.5(15)
F8-C27-S3	111.7(13)	F7-C27-S3	111.5(14)
F10-C28-F11	106.(2)	F10-C28-F12	106.2(17)

F11-C28-F12	102.5(17)	F10-C28-S4	115.9(16)
F11-C28-S4	112.8(15)	F12-C28-S4	111.8(18)
F1-C25-F3	109.7(15)	F1-C25-F2	107.3(13)
F3-C25-F2	107.5(13)	F1-C25-S1	112.2(10)
F3-C25-S1	111.1(10)	F2-C25-S1	108.9(12)
O1-S1-O2	113.8(6)	O1-S1-O3	115.0(5)
O2-S1-O3	115.6(6)	O1-S1-C25	102.7(7)
O2-S1-C25	104.2(8)	O3-S1-C25	103.3(6)
F6-C26-F4	109.2(17)	F6-C26-F5	106.5(17)
F4-C26-F5	106.3(17)	F6-C26-S2	111.5(14)
F4-C26-S2	112.2(16)	F5-C26-S2	110.9(13)
O4-S2-O5	115.5(16)	O4-S2-O6	114.9(15)
O5-S2-O6	115.3(14)	O4-S2-C26	103.2(13)
O5-S2-C26	102.6(11)	O6-S2-C26	102.7(10)
F6A-C26A-F4A	109.(3)	F6A-C26A-F5A	105.(2)
F4A-C26A-F5A	108.(3)	F6A-C26A-S2A	112.(2)
F4A-C26A-S2A	112.(2)	F5A-C26A-S2A	110.(2)
O4A-S2A-O6A	116.(3)	O4A-S2A-O5A	115.(3)
O6A-S2A-O5A	116.(2)	O4A-S2A-C26A	102.(2)
O6A-S2A-C26A	103.0(17)	O5A-S2A-C26A	102.3(16)
H2O-O13-H1O	129.8	O7-S3-O9	120.2(10)
O7-S3-O8	113.7(11)	O9-S3-O8	108.8(10)

O7-S3-C27	106.0(10)	O9-S3-C27	103.0(8)
O8-S3-C27	103.1(9)	O12-S4-O11	119.1(12)
O12-S4-O10	117.4(12)	O11-S4-O10	110.7(10)
O12-S4-C28	103.9(12)	O11-S4-C28	102.7(12)
O10-S4-C28	99.3(10)		

Table 6.13 Anisotropic atomic displacement parameters (Å^2).

The anisotropic atomic displacement factor exponent takes the form: $-2\pi^2[h^2 a^{*2} U_{11} + ... + 2 h k a^* b^* U_{12}]$

	U_{11}	**U_{22}**	**U_{33}**	**U_{23}**	**U_{13}**	**U_{12}**
C1	0.014(5)	0.026(6)	0.023(5)	0.004(4)	0.008(4)	0.001(4)
C2	0.040(5)	0.034(5)	0.034(6)	0.011(4)	0.020(5)	0.001(4)
C3	0.053(6)	0.038(6)	0.046(6)	0.018(5)	0.026(5)	0.011(5)
C4	0.043(6)	0.040(5)	0.037(6)	0.017(5)	0.019(5)	0.019(5)
C5	0.028(5)	0.033(5)	0.016(5)	0.007(4)	0.009(4)	0.015(4)
C6	0.018(4)	0.029(4)	0.004(4)	0.001(3)	0.003(3)	0.002(3)
C7	0.007(4)	0.023(4)	0.015(4)	-0.003(3)	0.007(3)	0.001(3)
C8	0.014(4)	0.015(4)	0.020(4)	-0.001(3)	0.008(4)	0.003(3)
C9	0.021(5)	0.028(5)	0.033(5)	0.007(4)	0.012(4)	0.007(4)
C10	0.031(6)	0.026(5)	0.047(6)	0.004(4)	0.019(5)	0.000(4)
C11	0.021(6)	0.032(6)	0.041(6)	-0.011(4)	0.017(5)	-0.005(4)

	U_{11}	U_{22}	U_{33}	U_{23}	U_{13}	U_{12}
C12	0.036(7)	0.063(9)	0.016(5)	-0.016(5)	0.014(5)	-0.013(6)
C13	0.038(7)	0.033(7)	0.025(6)	-0.010(5)	0.005(5)	0.002(5)
C14	0.011(5)	0.024(5)	0.006(4)	0.000(4)	-0.003(3)	-0.006(4)
C15	0.014(5)	0.021(6)	0.013(5)	0.000(4)	0.003(4)	0.000(4)
C16	0.012(5)	0.032(6)	0.020(5)	-0.004(4)	0.001(4)	-0.004(4)
C17	0.011(5)	0.040(7)	0.017(5)	0.000(5)	-0.001(4)	-0.006(4)
C18	0.024(5)	0.027(6)	0.013(5)	0.002(4)	-0.004(4)	-0.005(4)
I1	0.0135(3)	0.0527(5)	0.0182(3)	0.0007(3)	0.0013(3)	0.0133(3)
I2	0.0254(4)	0.0313(4)	0.0100(3)	-0.0033(3)	-0.0016(2)	-0.0055(3)
I3	0.0141(3)	0.0284(4)	0.0186(3)	-0.0105(3)	0.0022(2)	0.0000(3)
C19	0.020(8)	0.054(10)	0.024(8)	0.012(7)	0.004(7)	0.014(7)
C20	0.017(5)	0.028(6)	0.013(5)	-0.003(4)	0.005(4)	-0.001(4)
C21	0.025(5)	0.032(7)	0.018(5)	0.003(5)	0.011(5)	0.008(5)
C22	0.029(5)	0.035(8)	0.026(5)	0.009(5)	0.012(5)	0.001(5)
C23	0.024(6)	0.034(8)	0.020(5)	0.001(5)	0.006(5)	0.000(5)
C24	0.019(6)	0.035(7)	0.021(5)	-0.001(5)	0.008(5)	0.004(5)
N4	0.016(5)	0.029(5)	0.016(5)	-0.004(4)	0.004(4)	-0.003(4)
I4	0.0487(9)	0.0533(11)	0.0721(11)	0.0345(7)	0.0303(8)	0.0235(6)
C19A	0.026(11)	0.047(14)	0.034(13)	0.010(12)	0.019(10)	0.024(11)
C20A	0.018(6)	0.030(7)	0.017(6)	-0.002(6)	0.007(6)	0.001(6)
C21A	0.017(6)	0.031(7)	0.017(6)	-0.003(6)	0.006(6)	0.001(6)

	U_{11}	U_{22}	U_{33}	U_{23}	U_{13}	U_{12}
C22A	0.019(7)	0.032(8)	0.020(7)	-0.001(6)	0.006(6)	0.002(6)
C23A	0.022(7)	0.032(9)	0.022(7)	0.000(6)	0.009(6)	0.004(7)
C24A	0.024(7)	0.032(9)	0.022(6)	0.001(6)	0.012(6)	0.005(7)
N4A	0.023(6)	0.032(8)	0.019(7)	0.000(6)	0.009(6)	0.006(6)
I4A	0.0302(19)	0.040(2)	0.028(2)	0.0032(14)	-0.0064(15)	-0.0003(13)
N1	0.022(4)	0.024(4)	0.016(4)	0.004(3)	0.008(3)	0.002(3)
N2	0.009(4)	0.029(5)	0.030(5)	-0.010(4)	0.011(4)	-0.005(3)
N3	0.019(4)	0.019(5)	0.012(4)	0.000(3)	0.003(3)	-0.004(3)
C27	0.060(10)	0.066(10)	0.040(8)	0.012(7)	-0.011(7)	-0.006(7)
C28	0.036(8)	0.122(14)	0.050(8)	-0.005(8)	-0.026(6)	0.007(8)
F7	0.087(8)	0.122(10)	0.050(6)	0.018(6)	-0.038(6)	0.000(7)
F8	0.108(9)	0.127(11)	0.033(5)	0.028(6)	0.001(5)	-0.013(7)
F9	0.219(18)	0.082(9)	0.092(10)	0.041(7)	0.027(10)	0.047(9)
F10	0.082(8)	0.103(10)	0.104(11)	-0.005(7)	0.013(7)	-0.015(7)
F11	0.076(8)	0.142(12)	0.052(6)	0.018(7)	-0.009(6)	0.027(7)
F12	0.048(6)	0.114(9)	0.099(9)	-0.019(7)	0.011(6)	0.008(6)
C25	0.066(9)	0.037(7)	0.023(6)	-0.010(5)	0.014(6)	-0.016(6)
F1	0.079(7)	0.059(6)	0.037(5)	-0.025(4)	0.014(4)	-0.031(5)
F2	0.164(11)	0.049(6)	0.054(6)	0.006(5)	0.019(7)	-0.031(7)
F3	0.073(7)	0.087(7)	0.078(7)	-0.039(6)	0.050(6)	-0.050(5)
O1	0.027(4)	0.033(5)	0.016(4)	0.001(3)	-0.004(3)	0.001(3)

	U_{11}	U_{22}	U_{33}	U_{23}	U_{13}	U_{12}
O2	0.036(5)	0.072(7)	0.034(5)	-0.020(5)	-0.001(4)	0.024(5)
O3	0.042(5)	0.035(5)	0.005(3)	-0.005(3)	-0.002(3)	0.004(4)
S1	0.0184(12)	0.0298(15)	0.0099(11)	-0.0038(10)	0.0020(9)	0.0056(11)
C26	0.015(5)	0.043(6)	0.026(6)	0.011(5)	0.004(5)	0.007(5)
F4	0.023(7)	0.052(9)	0.027(6)	0.011(6)	0.007(5)	0.010(6)
F5	0.025(6)	0.045(7)	0.027(8)	0.010(5)	0.006(6)	-0.005(5)
F6	0.019(6)	0.048(10)	0.042(7)	0.014(7)	-0.007(5)	0.007(6)
O4	0.006(7)	0.036(8)	0.026(7)	0.010(6)	-0.002(5)	0.010(6)
O5	0.028(7)	0.042(7)	0.065(11)	0.015(7)	-0.009(8)	0.009(6)
O6	0.018(6)	0.068(10)	0.030(6)	0.029(6)	0.002(5)	0.004(7)
S2	0.012(3)	0.039(5)	0.042(4)	0.022(3)	0.005(3)	0.006(3)
C26A	0.016(6)	0.045(7)	0.028(6)	0.011(6)	0.004(5)	0.006(6)
F4A	0.019(10)	0.053(12)	0.026(9)	0.009(8)	0.007(8)	0.010(9)
F5A	0.024(9)	0.052(9)	0.019(11)	0.006(7)	0.000(8)	0.005(7)
F6A	0.017(8)	0.050(12)	0.031(8)	0.009(8)	-0.002(6)	0.005(9)
O4A	0.014(10)	0.040(12)	0.032(10)	0.015(9)	-0.002(9)	0.002(9)
O5A	0.027(10)	0.052(9)	0.040(11)	0.027(8)	0.004(9)	0.002(8)
O6A	0.026(10)	0.070(13)	0.034(9)	0.012(9)	0.008(7)	0.005(10)
S2A	0.016(4)	0.049(7)	0.026(5)	0.015(5)	0.003(4)	0.003(5)
O7	0.077(9)	0.102(11)	0.083(10)	0.027(8)	0.033(8)	-0.006(8)
O8	0.122(11)	0.056(7)	0.024(6)	-0.004(5)	-0.005(6)	0.001(6)

	U_{11}	U_{22}	U_{33}	U_{23}	U_{13}	U_{12}
O9	0.074(8)	0.076(8)	0.031(6)	-0.005(5)	0.003(5)	-0.037(6)
O10	0.112(11)	0.071(10)	0.071(9)	0.027(7)	-0.036(8)	-0.001(8)
O11	0.120(13)	0.075(9)	0.059(9)	-0.006(7)	-0.007(8)	0.017(8)
O12	0.088(10)	0.096(11)	0.092(11)	-0.027(8)	0.012(8)	-0.015(8)
O13	0.022(5)	0.089(9)	0.035(6)	0.007(5)	0.004(4)	0.006(5)
S3	0.0375(18)	0.0351(18)	0.0206(14)	-0.0009(12)	-0.0033(12)	-0.0113(13)
S4	0.066(3)	0.048(2)	0.037(2)	0.0023(16)	-0.0054(18)	0.0069(19)

Table 6.14 Hydrogen atomic coordinates and isotropic atomic displacement parameters ($Å^2$).

	x/a	y/b	z/c	U(eq)
H1A	0.8425	0.6351	0.0973	0.031
H1B	0.7934	0.5497	0.0860	0.031
H1C	0.8207	0.5911	0.1798	0.031
H2	0.7875	0.7625	0.0667	0.041
H3	0.6892	0.8547	0.0518	0.052
H4	0.5830	0.8012	0.0800	0.046
H9	0.7166	0.4200	0.3352	0.032
H10	0.6829	0.3081	0.2336	0.039
H11	0.6536	0.3393	0.0900	0.036
H12A	0.5929	0.5075	-0.0066	0.055
H12B	0.6449	0.4310	-0.0239	0.055

	x/a	y/b	z/c	U(eq)
H12C	0.6736	0.5292	-0.0100	0.055
H13A	0.5406	0.7816	0.6599	0.048
H13B	0.4804	0.7078	0.6492	0.048
H13C	0.4855	0.7706	0.5698	0.048
H16	0.6882	0.5242	0.5223	0.026
H17	0.7223	0.6076	0.6447	0.028
H18	0.6458	0.7096	0.6853	0.027
H19A	0.3659	0.3158	0.4594	0.049
H19B	0.4470	0.3142	0.4498	0.049
H19C	0.3922	0.2434	0.4001	0.049
H22	0.4674	0.0687	0.7145	0.035
H23	0.3709	0.1623	0.7009	0.031
H24	0.3463	0.2603	0.5862	0.029
H19D	0.5596	0.0366	0.6863	0.051
H19E	0.5551	0.0233	0.5851	0.051
H19F	0.5997	0.1031	0.6346	0.051
H22A	0.3370	0.2690	0.5696	0.028
H23A	0.3567	0.1768	0.6889	0.03
H24A	0.4624	0.0985	0.7232	0.03
H2O	0.4196	0.5730	0.1571	0.073
H1O	0.4005	0.5275	0.2356	0.073